CARDIOVASCULAR REMODELING IN AGING AND DISEASE

EDITED BY: Lakshmi Santhanam, Jochen Steppan and Daniel Nyhan
PUBLISHED IN: Frontiers in Physiology

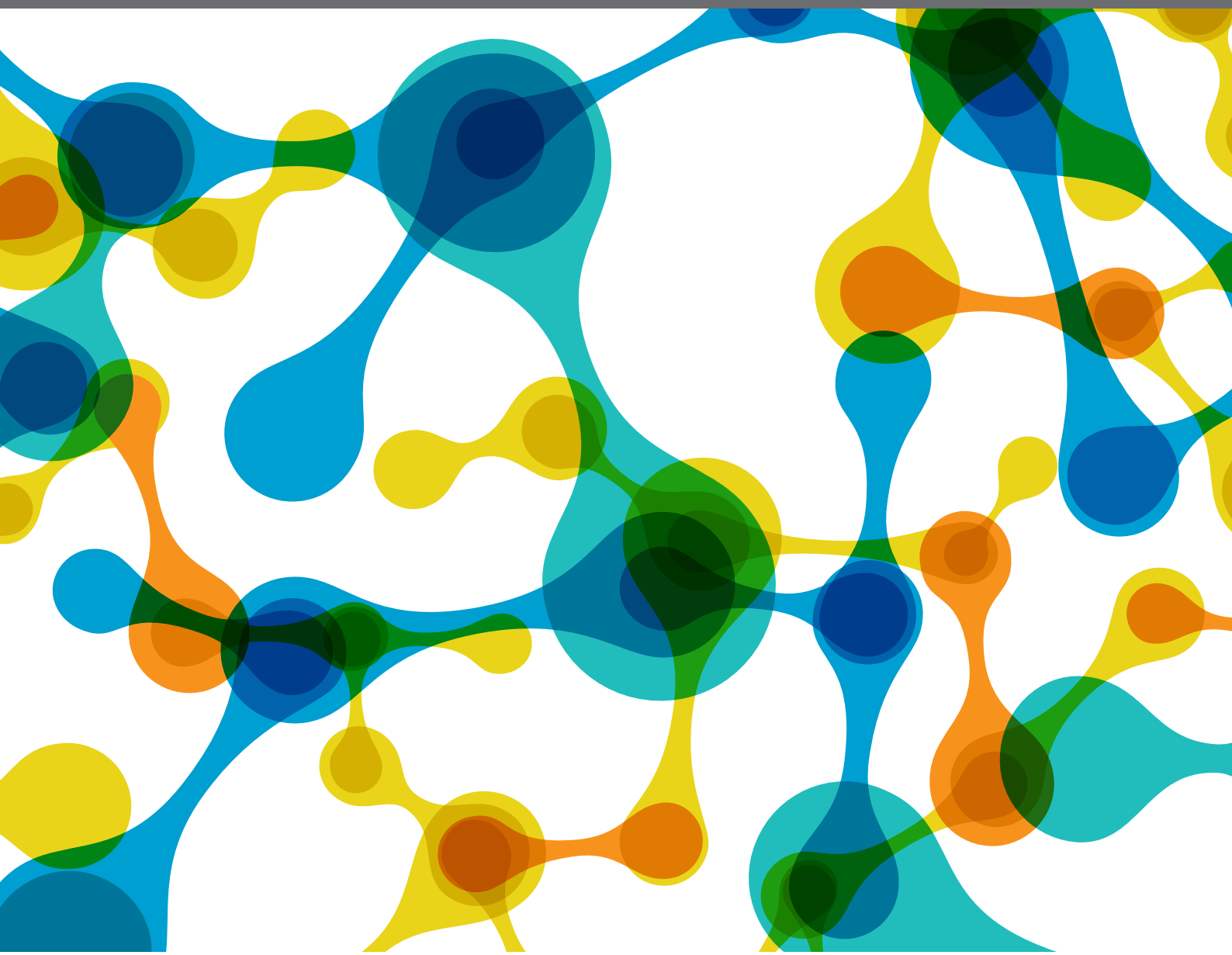

frontiers Research Topics

frontiers

ISSN 1664-8714
ISBN 978-2-88974-785-6
DOI 10.3389/978-2-88974-785-6

About Frontiers

Frontiers is more than just an open-access publisher of scholarly articles: it is a pioneering approach to the world of academia, radically improving the way scholarly research is managed. The grand vision of Frontiers is a world where all people have an equal opportunity to seek, share and generate knowledge. Frontiers provides immediate and permanent online open access to all its publications, but this alone is not enough to realize our grand goals.

Frontiers Journal Series

The Frontiers Journal Series is a multi-tier and interdisciplinary set of open-access, online journals, promising a paradigm shift from the current review, selection and dissemination processes in academic publishing. All Frontiers journals are driven by researchers for researchers; therefore, they constitute a service to the scholarly community. At the same time, the Frontiers Journal Series operates on a revolutionary invention, the tiered publishing system, initially addressing specific communities of scholars, and gradually climbing up to broader public understanding, thus serving the interests of the lay society, too.

Dedication to Quality

Each Frontiers article is a landmark of the highest quality, thanks to genuinely collaborative interactions between authors and review editors, who include some of the world's best academicians. Research must be certified by peers before entering a stream of knowledge that may eventually reach the public - and shape society; therefore, Frontiers only applies the most rigorous and unbiased reviews.
Frontiers revolutionizes research publishing by freely delivering the most outstanding research, evaluated with no bias from both the academic and social point of view. By applying the most advanced information technologies, Frontiers is catapulting scholarly publishing into a new generation.

What are Frontiers Research Topics?

Frontiers Research Topics are very popular trademarks of the Frontiers Journals Series: they are collections of at least ten articles, all centered on a particular subject. With their unique mix of varied contributions from Original Research to Review Articles, Frontiers Research Topics unify the most influential researchers, the latest key findings and historical advances in a hot research area! Find out more on how to host your own Frontiers Research Topic or contribute to one as an author by contacting the Frontiers Editorial Office: frontiersin.org/about/contact

CARDIOVASCULAR REMODELING IN AGING AND DISEASE

Topic Editors:
Lakshmi Santhanam, Johns Hopkins University, United States
Jochen Steppan, Johns Hopkins University, United States
Daniel Nyhan, Johns Hopkins University, United States

Citation: Santhanam, L., Steppan, J., Nyhan, D., eds. (2022). Cardiovascular Remodeling in Aging and Disease. Lausanne: Frontiers Media SA. doi: 10.3389/978-2-88974-785-6

Table of Contents

frontiers in Physiology

EDITORIAL
published: 07 March 2022
doi: 10.3389/fphys.2022.867185

Editorial: Cardiovascular Remodeling in Aging and Disease

Jochen Steppan[1], *Daniel Nyhan*[1] *and Lakshmi Santhanam*[1,2,3]*

[1] Department of Anesthesiology and Critical Care Medicine, Johns Hopkins University, Baltimore, MD, United States, [2] Department of Biomedical Engineering, Johns Hopkins University, Baltimore, MD, United States, [3] Department of Chemical and Biomolecular Engineering, Johns Hopkins University, Baltimore, MD, United States

Keywords: vasculature, remodeling, stiffness, aging, cardiac, hypertension, pulmonary

Editorial on the Research Topic

Cardiovascular Remodeling in Aging and Disease

Cardiovascular remodeling is a key feature of arterial aging and cardiovascular disease and a direct contributor to a shortened lifespan (van Popele et al., 2001; Vlachopoulos et al., 2010; AlGhatrif et al., 2013; Niiranen et al., 2016). Recent advances have shown that vascular stiffening affects all vascular beds, encompasses functional perturbations in resident cells, produces structural/compositional changes in the matrix, and is directly linked to cardiac remodeling and impaired ventricular-arterial coupling (Nichols et al., 1985; Qiu et al., 2010; Santhanam et al., 2010; Lacolley et al., 2018; Steppan et al., 2019; Wang et al., 2021). These changes can occur over many years, as in natural aging, or can be accelerated by factors such as hypertension, diabetes, smoking, and hyperlipidemia (Niiranen et al., 2016; Boutouyrie et al., 2021; Mitchell, 2021). In the pulmonary circulation, vascular remodeling that develops with pulmonary arterial hypertension is now an area of active investigation. In the absence of clear targetable mechanisms, diet and exercise continue to be the mainstay of therapy (Steppan et al., 2012, 2014). This Frontier's Research Topic has collated nine contributions (three reviews and six original research articles) spanning basic science and clinical research in both the systemic and pulmonary circulation.

In a comprehensive review on vascular stiffness, Vatner et al. discuss regional changes in stiffness along the aorta, the role of sex, the transferability of animal studies to the clinical setting, and global population variations. They describe extracellular matrix derangement and endothelial cell (EC) and smooth muscle cell (SMC) dysfunction at the cellular and molecular levels. In the context of molecular mechanisms, researchers increasingly recognize the contributions of the "vascular triad," comprising reactive oxygen species, inflammation, and vascular dysfunction, to the development of sustained hypertension. Ranadive et al. review these known elements and extend the discussion to include inducible nitric oxide synthase, hydrogen peroxide, hydrogen sulfide, NF-κB, and nuclear factor activated T cells as a set of "unusual suspects" potentially contributing to the pathogenesis of hypertension and the associated vascular dysfunction. The final review focuses on micro-RNAs (miR) as intriguing and important regulators of arterial stiffening. Baraban et al. review the role of miRs in stiffening of the large arteries and their potential for therapeutic intervention (Hori et al., 2017). They highlight prospective areas of research to determine regulation of miRs and their exact mechanism of action in the aging vessel.

In the systemic circulation, hyperlipidemia and atherosclerosis accelerate arterial aging. Endothelial dysfunction induced by oxidized low-density lipoprotein plays a critical role in the pathobiology of atherosclerosis and the associated vascular remodeling. A chief element of this is gene expression changes in ECs linked to histone acetylation, which is regulated by histone acetylases and histone deacetylases (HDACs). Nomura et al. demonstrate that HDAC6 inhibition with tubacin attenuates atherosclerosis in a mouse model. They further show that NEDDylation is a potential mechanism by which HDAC6 function is regulated in the atheromatous environment.

OPEN ACCESS

Edited and reviewed by:
Gerald A. Meininger,
University of Missouri, United States

Correspondence:
Lakshmi Santhanam
lsantha1@jhmi.edu

Specialty section:
This article was submitted to Vascular Physiology, a section of the journal Frontiers in Physiology

Received: *31 January 2022*
Accepted: *14 February 2022*
Published: *07 March 2022*

Citation:
Steppan J, Nyhan D and Santhanam L (2022) Editorial: Cardiovascular Remodeling in Aging and Disease. Front. Physiol. 13:867185. doi: 10.3389/fphys.2022.867185

While rodent models have clear advantages over human studies, such as feasibility of mechanistic studies and lower cost, the differences in vascular aging across species must be considered when translating the results (Vatner et al.). In novel work using fluid-structure interaction models of the human and mouse aorta, Hopper et al. demonstrate differences in the indices of vascular stiffness in the young and distinct regional differences in the aged aorta between mice and humans. Thus, results from mouse studies must be interpreted within the context of these differences. Another challenge to research in mice is that their small size and fast heart rate make echocardiographic studies particularly challenging (Rottman et al., 2007). In a human echocardiography study, Heidemann et al. evaluate the relationship between atrial septal mobility, which is related to embolic stroke, and aortic root dilation (a disease of the vessel wall). They show that increases in atrial septal mobility correlate with increases in aortic root diameter, suggesting that aortic root diameter should be evaluated in patients with increased atrial septal mobility.

Vascular stiffness measurement is also important in patients with aortic aneurysms, in particular, after endovascular repair. Using a clinical cohort of patients undergoing endovascular aortic repair, Hori et al. compared five different endovascular devices. They show, for the first time in a clinical population, that the different devices do affect aortic pulse wave velocity (PWV), the gold-standard index of *in vivo* arterial stiffness. Notably, treatment length was more important than treatment site.

Finally, pulmonary arterial remodeling is increasingly recognized as important to pulmonary hypertension and right heart failure. In an elegant study, Manning et al. evaluated the underlying role of vascular remodeling in pulmonary hypertension by using single cell RNA sequencing and multiphoton microscopy to determine microstructural features, associated changes in material stiffness, and vasoactive capacity. They show that pulmonary arteries of hypoxic mice exhibit transcriptome changes, SMC phenotype alterations, and endothelial proliferation, likely representing endothelial-to-mesenchymal transition. Interestingly, they suggest that the increased material stiffness noted in the pulmonary artery is due to collagen reorientation rather than fibrosis. Furthermore, pulmonary PWV increased. Thus, they uncovered an important positive feed-forward loop driving pulmonary hypertension. In a separate study investigating the mechanisms underlying vascular remodeling in pulmonary hypertension, Yun et al. evaluated factors modulating pulmonary arterial SMC and EC hyperplasia and migration. Using the Sugen5416/hypoxia rat model of pulmonary hypertension that recapitulates the main features of human pulmonary arterial hypertension, they show that aquaporin (AQP1) protein levels are increased in both SMCs and ECs. Using loss- and gain-of-function approaches, they establish a key role for increased AQP1 expression in the enhanced migration and proliferation of pulmonary artery SMCs and pulmonary artery ECs, both prominent features of severe pulmonary arterial hypertension.

We hope the reader finds this Research Topic to be a useful reference in understanding cardiovascular remodeling in aging and disease, in particular the underlying mechanisms, the different diseases that cause or accelerate mechanical decline of the cardiovascular system, and pitfalls in data analysis and interpretation.

AUTHOR CONTRIBUTIONS

All authors listed have made a substantial, direct, and intellectual contribution to the work and approved it for publication.

FUNDING

This work was supported by a NHLBI grant R01HL148112 (LS) and a NHLBI grant K08HL145132 (JS).

REFERENCES

AlGhatrif, M., Strait, J. B., Morrell, C. H., Canepa, M., Wright, J., Elango, P., et al. (2013). Longitudinal trajectories of arterial stiffness and the role of blood pressure: the Baltimore Longitudinal Study of Aging. *Hypertension* 62, 934–941. doi: 10.1161/HYPERTENSIONAHA.113.01445

Boutouyrie, P., Chowienczyk, P., Humphrey, J. D., and Mitchell, G. F. (2021). Arterial stiffness and cardiovascular risk in hypertension. *Circ. Res.* 128, 864–886. doi: 10.1161/CIRCRESAHA.121.318061

Hori, D., Dunkerly-Eyring, B., Nomura, Y., Biswas, D., Steppan, J., Henao-Mejia, J., et al. (2017). miR-181b regulates vascular stiffness age dependently in part by regulating TGF-beta signaling. *PLoS ONE* 12, e0174108. doi: 10.1371/journal.pone.0174108

Lacolley, P., Regnault, V., and Avolio, A. P. (2018). Smooth muscle cell and arterial aging: basic and clinical aspects. *Cardiovasc. Res.* 114, 513–528. doi: 10.1093/cvr/cvy009

Mitchell, G. F. (2021). Arterial stiffness in aging: does it have a place in clinical practice?: recent advances in hypertension. *Hypertension* 77, 768–780. doi: 10.1161/HYPERTENSIONAHA.120.14515

Nichols, W. W., O'Rourke, M. F., Avolio, A. P., Yaginuma, T., Murgo, J. P., Pepine, C. J., et al. (1985). Effects of age on ventricular-vascular coupling. *Am. J. Cardiol.* 55, 1179–1184. doi: 10.1016/0002-9149(85)90659-9

Niiranen, T. J., Kalesan, B., Hamburg, N. M., Benjamin, E. J., Mitchell, G. F., and Vasan, R. S. (2016). Relative contributions of arterial stiffness and hypertension to cardiovascular disease: the framingham heart study. *J. Am. Heart Assoc.* 5, e004271. doi: 10.1161/JAHA.116.004271

Qiu, H., Zhu, Y., Sun, Z., Trzeciakowski, J. P., Gansner, M., Depre, C., et al. (2010). Short communication: vascular smooth muscle cell stiffness as a mechanism for increased aortic stiffness with aging. *Circ. Res.* 107, 615–619. doi: 10.1161/CIRCRESAHA.110.221846

Rottman, J. N., Ni, G., and Brown, M. (2007). Echocardiographic evaluation of ventricular function in mice. *Echocardiography* 24, 83–89. doi: 10.1111/j.1540-8175.2006.00356.x

Santhanam, L., Tuday, E. C., Webb, A. K., Dowzicky, P., Kim, J. H., Oh, Y. J., et al. (2010). Decreased S-nitrosylation of tissue transglutaminase contributes to age-related increases in vascular stiffness. *Circ. Res.* 107, 117–125. doi: 10.1161/CIRCRESAHA.109.215228

Steppan, J., Sikka, G., Jandu, S., Barodka, V., Halushka, M. K., Flavahan, N. A., et al. (2014). Exercise, vascular stiffness, and tissue transglutaminase. *J. Am. Heart Assoc.* 3, e000599. doi: 10.1161/JAHA.113.000599

Steppan, J., Tran, H., Benjo, A. M., Pellakuru, L., Barodka, V., Ryoo, S., et al. (2012). Alagebrium in combination with exercise ameliorates age-associated ventricular and vascular stiffness. *Exp. Gerontol.* 47, 565–572. doi: 10.1016/j.exger.2012.04.006

Steppan, J., Wang, H., Bergman, Y., Rauer, M. J., Tan, S., Jandu, S., et al. (2019). Lysyl oxidase-like 2 depletion is protective in age-associated vascular stiffening. *Am. J. Physiol. Heart Circ. Physiol.* 317, H49–H59. doi: 10.1152/ajpheart.00670.2018

van Popele, N. M., Grobbee, D. E., Bots, M. L., Asmar, R., Topouchian, J., Reneman, R. S., et al. (2001). Association between arterial stiffness and atherosclerosis: the Rotterdam Study. *Stroke* 32, 454–460. doi: 10.1161/01.STR.32.2.454

Vlachopoulos, C., Aznaouridis, K., and Stefanadis, C. (2010). Prediction of cardiovascular events and all-cause mortality with arterial stiffness: a systematic review and meta-analysis. *J. Am. Coll. Cardiol.* 55, 1318–1327. doi: 10.1016/j.jacc.2009.10.061

Wang, H., Chen, J., Jandu, S., Melucci, S., Savage, W., Nandakumar, K., et al. (2021). Probing tissue transglutaminase mediated vascular smooth muscle cell aging using a novel transamidation-deficient Tgm2-C277S mouse model. *Cell Death Discov.* 7, 197. doi: 10.1038/s41420-021-00543-8

Conflict of Interest: The authors declare that the research was conducted in the absence of any commercial or financial relationships that could be construed as a potential conflict of interest.

Publisher's Note: All claims expressed in this article are solely those of the authors and do not necessarily represent those of their affiliated organizations, or those of the publisher, the editors and the reviewers. Any product that may be evaluated in this article, or claim that may be made by its manufacturer, is not guaranteed or endorsed by the publisher.

frontiers in Physiology

ORIGINAL RESEARCH
published: 17 June 2021
doi: 10.3389/fphys.2021.675724

Inhibition of HDAC6 Activity Protects Against Endothelial Dysfunction and Atherogenesis *in vivo*: A Role for HDAC6 Neddylation

*Yohei Nomura[1,2†], Mitsunori Nakano[1,2†], Hyun Woo Sung[3†], Mingming Han[1,4†] and Deepesh Pandey[1]**

[1] Department of Anesthesiology and Critical Care Medicine, Johns Hopkins University, Baltimore, MD, United States, [2] Department of Cardiovascular Surgery, Saitama Medical Center, Jichi Medical University, Saitama, Japan, [3] Department of Chemical and Biomolecular Engineering, Johns Hopkins University, Baltimore, MD, United States, [4] Department of Anesthesiology, The First Affiliated Hospital of USTC, University of Science and Technology of China, Hefei, China

OPEN ACCESS

Edited by:
Jochen Steppan,
Johns Hopkins University,
United States

Reviewed by:
Daiju Fukuda,
Tokushima University, Japan
Santosh Kumar,
The University of Iowa, United States

***Correspondence:**
Deepesh Pandey
Dpandey2@jhmi.edu

† These authors have contributed equally to this work

Specialty section:
This article was submitted to Vascular Physiology, a section of the journal Frontiers in Physiology

Received: 03 March 2021
Accepted: 14 May 2021
Published: 17 June 2021

Citation:
Nomura Y, Nakano M, Woo Sung H, Han M and Pandey D (2021) Inhibition of HDAC6 Activity Protects Against Endothelial Dysfunction and Atherogenesis in vivo: A Role for HDAC6 Neddylation. Front. Physiol. 12:675724. doi: 10.3389/fphys.2021.675724

We previously reported that histone deacetylase 6 (HDAC6) has an important role in endothelial cell (EC) function *in vitro*. However, whether HDAC6 plays a role in atherogenesis *in vivo* and the mechanism(s) that control HDAC6 activity/expression in response to atherogenic stimuli are unclear. The goals of this study were to determine whether HDAC6 inhibitor tubacin attenuates atherogenesis and to elucidate specific molecular mechanism(s) that regulate endothelial HDAC6 expression/activity. We evaluated whether administration of tubacin attenuated or reversed the endothelial dysfunction and atherosclerosis induced in mice by a single intraperitoneal injection of adeno-associated viruses encoding liver-target PCSK9 gain-of-function mutant followed by a high fat diet (HFD) for 18 weeks. Tubacin significantly blunted PCSK9-induced increases in pulse wave velocity (index of vascular stiffness and overall vascular health) that are also seen in atherogenic mice. Furthermore, tubacin protected vessels from defective vasorelaxation, as evaluated by acetylcholine-mediated relaxation using wire myograph. Plaque burden defined by Oil Red O staining was also found to be significantly less in mice that received tubacin than in those that received PCSK9 alone. Inhibition of the NEDDylation pathway with MLN4924, an inhibitor of NEDD8-activating enzyme 1 (NAE1), significantly increased HDAC6 activity in HAECs. Interestingly, HDAC6 expression remained unchanged. Further, HAECs exposed to the atherogenic stimulus oxidized low-density lipoprotein (OxLDL) exhibited enhanced HDAC6 activity, which was attenuated by pretreatment with MLN4924. The HDAC6 NEDDylation molecular pathway might regulate genes related to endothelial control of vasomotor tone, reactivity, and atherosclerosis. Tubacin may represent a novel pharmacologic intervention for atherogenesis and other vasculopathies.

Keywords: endothelial (dys)function, vascular biology, atherosclerosis, epigentic modifier, epigenetic regulator

INTRODUCTION

The endothelium plays a major role in the regulation of vascular homeostasis by modulating vasomotor tone, inflammation, and growth and migration of vascular smooth muscle cells. Endothelial dysfunction causes numerous abnormalities in the arterial wall (Li and Forstermann, 2009). In addition, oxidized low-density lipoprotein (OxLDL) induces pro-atherosclerotic effects in endothelial cells (ECs) by altering cell surface adhesion molecule expression (Khan et al., 1995; Liao et al., 1997), enhancing production of pro-inflammatory cytokines such as interleukin (IL)-6, TNF-α, IL-1β (Libby, 2002; Libby et al., 2002), and adhesion molecules (Khan et al., 1995); stimulating apoptosis (Dimmeler et al., 1997; Harada-Shiba et al., 1998); inducing superoxide production (Galle et al., 1995); and impairing nitric oxide (NO) production (Kugiyama et al., 1990; Simon et al., 2003). Decreases in the production and biological activity of NO lead to impaired vasodilatation and may be the earliest signs of EC dysfunction and atherogenesis (Ross, 1999).

Histone deacetylases (HDACs) have been shown to modulate atherosclerosis and EC shear stress (Choi et al., 2005; Lee et al., 2012). We have identified HDAC2 as a critical contributor to vascular homeostasis and endothelial health and shown that its inhibition leads to impaired vascular relaxation, reduced NO levels, and increased oxidative stress (Pandey et al., 2015). Conversely, increasing HDAC2 expression is endothelial-protective (Ito et al., 2002). Others have reported that SIRT1, a class III histone deacetylase, decreases acetylation of endothelial NO synthase (eNOS) post-translationally to enhance NO production (Mattagajasingh et al., 2007). Inhibition of SIRT1 increases NADPH oxidase-derived superoxide release, which leads to decreased NO bioavailability and thereby impairs aortic relaxation in rats (Mattagajasingh et al., 2007; Li et al., 2011).

HDAC6 is a structurally and functionally unique member of the HDAC family. Structurally, HDAC6 consists of two tandem deacetylase domains and a C-terminal ubiquitin binding zinc-finger domain (BUZ). Functionally, it catalyzes removal of an acetyl group from a host of cytosolic substrates other than histones, such as tubulin, HSP90, cortactin, and β-catenin (Verdel et al., 2000; Hubbert et al., 2002; Kovacs et al., 2005; Zhang et al., 2007; Li et al., 2008). Notably, unlike other HDACs, HDAC6 non-enzymatically maintains protein homeostasis by binding to ubiquitin, thereby enhancing protein clearance and degradation via the aggresome pathway (Boyault et al., 2006; Hao et al., 2013). We showed previously that increased HDAC6 activity is a major culprit in OxLDL-induced endothelial dysfunction *in vitro*. We further showed that increased activity of HDAC6 downregulates expression of endothelial cystathionine lyase γ, a major enzymatic source of the vasoactive gasotransmitter hydrogen sulfide (Kuo et al., 2016; Leucker et al., 2017). Though we have some understanding of how augmented HDAC6 activity is deleterious to cultured ECs, the role of HDAC6 in atherosclerosis *in vivo* is still unknown. In addition, it is unclear how HDAC6 activity is modulated.

Here, we show that post-translational modification of HDAC6 by small protein NEDD8 regulates its activity. Although the process of conjugation is analogous to ubiquitination, NEDDylation regulates broad range of its substrates functions such as activity, abundance, stability, and subcellular localization (Hershko and Ciechanover, 1998; Hershko, 2005; Oved et al., 2006; Enchev et al., 2015). Indeed, inhibition of NEDDylation attenuates NFκB-mediated release of proinflammatory cytokines in macrophages and human ECs (Chang et al., 2012; Ehrentraut et al., 2013). As we previously reported, inhibition of NEDDylation by MLN4924 augments HDAC2 abundance *in vitro* and *in vivo* and protects impaired endothelium-dependent vascular relaxation induced by OxLDL (Pandey et al., 2015). More importantly, a recent study has described a protective role of the DeNeddylase enzyme COPS9 in atherogenesis (Asare et al., 2017). Small molecule inhibitors of NEDDylation activating enzyme 1 (NAE1) may therefore represent a novel therapy for endothelial dysfunction and atherosclerosis.

In this study, we extend our previous findings of HDAC6 to establish its contribution to the endothelial dysfunction that underlies development of atherosclerosis *in vivo*. Notably, we investigated the use of tubacin, a small molecule inhibitor of HDAC6, in a mouse model of atherosclerosis. We then evaluated aortic stiffness and vascular relaxation—both important metrics of endothelial dysfunction—and measured atherosclerotic plaque load. Further, we identified the post-translational mechanism that regulates HDAC6 activity in human aortic endothelial cells (HAECs). Our results could shed light on the previously observed anti-atherogenic effects of MLN4924.

MATERIALS AND METHODS

Reagents

All experimental procedures involving mice were approved by the Institutional Animal Care and Use Committee (IACUC) at The Johns Hopkins University School of Medicine. Eight to ten weeks old C57BL/6 mice were purchased from Jackson Laboratory (Bar Harbor, ME). Unless otherwise stated, all reagents were obtained from Sigma (St. Louis, MO). Antibodies to hemagglutinin (HA; C29F4), HDAC6, NEDD8, p-eNOS (T495) and FLAG were purchased from Cell Signaling (Danvers, MA). NOS3 (A-9) antibody was purchased from Santa Cruz Biotechnology (Dallas, TX). Acetylated α-tubulin antibody was purchased from Abcam (ab24610; Cambridge, MA), total α-tubulin antibody was purchased from Invitrogen (62204; Waltham, MA), and Lipofectamine 2000 was purchased from Life Technologies (Waltham, MA). Tubacin was purchased from Enzo Life Sciences (Farmingdale, NY). Fresh batches of oxidized low-density lipoprotein (OxLDL) was purchased from Alfa Aesar (a Johnson Matthew company).

Cell Culture

Endothelial Cell Lines

HAECs were purchased from PromoCell and maintained in Endothelial Cell Growth Medium MV 2 (PromoCell) according to the supplier's protocol at 37°C in a humidified, 5% CO_2 atmosphere. Cells were passaged at 90% confluency. MLN4924 were purchased from Enzolifesciences and reconstituted in

DMSO. HAECs were incubated in EC growth media with either DMSO (control) or MLN4924 (0.1–1 μ M) for 24 h.

Immortal Cell Lines

Human embryonic kidney cells (HEK293A) were purchased from Life Technologies and maintained in DMEM (Gibco) supplemented with 10% fetal bovine serum (Gibco) and 1% penicillin-streptomycin (Corning). Cells were passaged at 75% confluency.

DNA Constructs

Full-length FLAG epitope-tagged HDAC6 was a kind gift from Eric Verdin (Addgene plasmid #13823). The catalytically inactive mutant of HDAC6 (H216/611A, Addgene plasmid #30483) and C-terminal zinc finger domain (binder of ubiquitin zinc finger, BUZ Addgene plasmid #30484) deleted mutant were kind gifts from Tso-Pang Yao (Kawaguchi et al., 2003). All other constructs were cloned in-house by using topo-directional cloning (Invitrogen).

Atherogenesis Model

Eight weeks old C57BL/6 wild-type (WT) male mice were administered a single tail-vein injection of 1×10^{11} vector genomes of adeno-associated virus (AAV) encoding a gain-of-function PCSK9 variant (D377Y). Then they were randomly assigned to receive vehicle or tubacin (intraperitoneal, 0.5 mg/kg daily) and fed a high-fat diet (HFD) for 18 weeks (Goettsch et al., 2016). A separate set of control mice did not receive the AAV-PCSK9 injection. Pulse wave velocity (PWV) and body weight were measured every 2 weeks in all mice. We have described this model in detail in our previous study (Hori et al., 2020).

Non-invasive Pulse Wave Velocity (PWV) Measurements

A high-frequency, high-resolution Doppler spectrum analyzer (DSPW, Indus Instruments, Houston, TX, United States) was used. Mice were anesthetized with 1.5% isoflurane and placed in a supine position on a heated pad equipped with echocardiogram (EKG) capability. The animals were allowed to stabilize to a physiologic heart rate before a 20 MHz probe was used to measure the descending aortic and abdominal aortic flow velocities. The time from the R wave of the EKG to the start of pulse waveform for each measurement location was calculated by using a real-time signal acquisition and spectrum analyzer system.

Pathological Assessment of Plaque in Aortas

Aorta, from aortic root to iliac artery bifurcation, was carefully dissected, perfused with Krebs solution, and fixed with 4% paraformaldehyde overnight. The aorta was opened longitudinally and pinned onto a wax surface by microneedles. Images of the submerged vessels were captured with a digital camera. The lipid-rich intraluminal lesions were stained with Oil red O (Sigma). Digitized images were transferred to a computer and analyzed with NIH Java Image (ImageJ, version 1.42n). The amount of aortic atheroma in each animal was measured as percent lesion area per total area of the aorta. Aortic root was embedded in OCT compound (Fisher Scientific) and cross-section was fixed with 10% formalin and stained with Oil red O.

Oil Red O Staining

Oil red O was purchased from Sigma-Aldrich (catalog no. MAK194) and the staining was performed according to manufacturer's instruction. Briefly, gross aortas or the aortic sections were fixed with 10% formalin for 30 min. After washing formalin with water twice, the samples were incubated in 60% isopropanol for 5 min. Isopropanol was discarded and the samples were further incubated in oil red o stain solution (prepared in 100% isopropanol) for 20 min. The samples were washed for 5 times with water. The gross aortas were pinned to the wax surface and the cross section of aortic root was mounted with a mounting media (FluorSave) in a coverslip and images were taken under magnifying scope using camera and phase microscope, respectively. Aortic roots were frozen using the Tissue-Tek optimum cutting temperature (O.C.T) formulation purchased from VWR, sectioned, stained with Oil Red O and image were taken using phase microscope.

Force Tension Myography

Mouse aorta was isolated and cleaned in ice-cold Krebs-Ringer-bicarbonate solution containing the following (in mM): 118.3 NaCl, 4.7 KCl, 1.6 $CaCl_2$, 1.2 KH_2PO_4, 25 $NaHCO_3$, 1.2 $MgSO_4$, and 11.1 dextrose. The aorta was immersed in a bath filled with constantly oxygenated Krebs buffer at 37°C. Equal-sized thoracic aortic rings (2 mm) were mounted under microscopy to ensure no damage to the smooth muscle or endothelium. One end of each aortic ring was connected to a transducer, and the other to a micromanipulator. The aortas were passively stretched to an optimal resting tension with the micromanipulator. Aorta was passively stretched to an optimal resting tension using the micromanipulator, after which a dose of 60 mM KCl was administered and repeated after a wash with Krebs buffer. After these washes, all vessels were allowed to equilibrate for 20–30 min in the presence of indomethacin (3 μM). Phenylephrine (1 μM) was administered to induce vasoconstriction. A dose- dependent response (1 nM–10 μM), with the muscarinic agonist, ACH or nitric oxide donor, SNP, was then performed as necessary. Relaxation responses were calculated as a percentage of tension following pre-constriction. Sigmoidal dose-response curves were fitted to data with the minimum constrained to 0. Two to four rings were isolated from each animal and the number of animals in each group (n) was 6.

Immunoprecipitation and Western Blotting

After 48 h of HEK293A cell transfection, cells were lysed in a modified ice-cold RIPA lysis buffer consisting of 20 mM Tris–HCl at pH 7.5, 150 mM NaCl, 1 mM EDTA, 1 mM EGTA, 0.3% NP40, 1% sodium deoxycholate, 1 mM Na_3VO_4, 2.5 mM sodium pyrophosphate, 1 mM β-glycerophosphate, 1 μg/mL leupeptin, and a 1:1,000 diluted protease inhibitor cocktail (Sigma). For

immunoprecipitation studies, whole cell lysates were centrifuged at 14,000 × *g* and supernatants were precleared by incubation with Protein A/G-agarose beads for 2 h at 4°C with rocking. Agarose beads were then pelleted by centrifugation at 1,000 × *g*. HA-NEDD8 in precleared lysates was immunoprecipitated by incubation overnight at 4°C with rocking after addition of anti-HA antibody (1:150). Immune complexes were eluted in sodium dodecyl sulfate (SDS) sample buffer, boiled for 5 min, and then loaded onto polyacrylamide gels for SDS–PAGE. Western blot analysis was performed by transferring proteins from the SDS gel onto a nitrocellulose membrane. Protein bands were visualized by secondary antibodies conjugated to alkaline phosphatases.

Statistical Analysis

All statistical analyses were carried out in Prism 7 for Mac (GraphPad Software Inc., San Diego, CA) and Excel version 14.1.3 (Microsoft, Redmond, WA) statistical analysis software. The results are expressed as mean ± standard error of the mean (mean ± SEM). Comparisons of all experimental data sets, groups, and pairs of data sets were analyzed with one-way ANOVA followed by the Bonferroni *post-hoc* test for multiple comparisons. A value of $p < 0.05$ was considered statistically significant. Myograph data were analyzed in STATA VERSION 15 software (STATA Corporation, College Station, TX) by using a general linear model with group as a factor and dose as a repeated measure. We applied *post-hoc* tests for each dose using linear combination based on this model.

RESULTS

Pharmacologic Inhibition of HDAC6 With Tubacin Attenuates Vascular Stiffness, Improves Relaxation, and Decreases Plaque Lesions in Atherosclerotic Mice

To determine whether HDAC6 inhibition improves vascular function, we examined the effect of HDAC6 inhibitor tubacin on vascular stiffness in atherogenic mice. Aortic PWV, a reciprocal index for vascular stiffness and overall vascular health, rose significantly in both vehicle- and tubacin-treated mice after PCSK9 transduction as compared to that in control (uninduced) mice with or without HFD (**Figure 1A**). However, PWV was significantly attenuated in the tubacin-treated group as compared to that in the vehicle-treated group (**Figure 1A**). Body weight significantly increased in PCSK9 injected and HFD fed mice as expected and interestingly these mice treated with tubacin weighed slightly but significantly more (**Figure 1B**). Further, as shown in **Figure 1C**, aortic rings from atherogenic C57BL/6 mice exhibited impaired acetylcholine-induced (endothelial-dependent) vasorelaxation after the HFD (Log EC_{50}: -7.19 ± 0.11, 95%CI -7.40 to -6.97) compared to that of uninduced controls (Log EC_{50}: -7.58 ± 0.04, 95%CI -7.67 to -7.50). However, tubacin rescued vasorelaxation (Log EC_{50}: -7.35 ± 0.06, 95%CI -7.47 to -7.22, $p < 0.001$). Sodium nitroprusside-induced (endothelial-independent) relaxation was not significantly different (**Figure 1D**). Oil Red O staining revealed a striking increase in plaque burden in WT mice subjected to the atherogenesis model and markedly lower plaque formation in tubacin-treated mice (**Figures 1E–G**). Quantification of cross-sections of Oil-Red O–stained aortic root showed significantly elevated plaque burden in atherogenic mice that was attenuated with daily tubacin toward the end of the HFD regimen. To determine whether atheroprotective effects of HDAC6 inhibition involved attenuation of inflammation, we measured whether intracellular adhesion molecules 1 (ICAM1) is attenuated in aortas isolated from control and tubacin treated atherogenic mice. As shown in **Supplementary Figure 1**, our data show decreased trend in ICAM1 expression in tubacin treated group. However, the differences was not statistically significant.

NEDDylation Pathway Inhibition Attenuates HDAC6 Activity

Previous studies have shown that MLN4924, an inhibitor that targets NAE1, provides protection against endothelial dysfunction in response to oxidative injury, halts early atherosclerosis, and inhibits inflammation in macrophages and ECs. Further, elevated HDAC6 activity has been implicated in the development of atherosclerosis, and tubacin enhances the atheroprotective effects of eNOS. Therefore, we next tested whether crosstalk occurs between the NEDDylation pathway and HDAC6. We first evaluated the effects of MLN4924 on HDAC6 activity and expression in HAECs. Because HDAC6 is a microtubule-associated deacetylase, we assessed its activity by measuring levels of acetylated α-tubulin (Hubbert et al., 2002). Interestingly, acetylated α-tubulin levels increased significantly while HDAC6 expression remained unchanged in MLN4924-exposed HAECs (**Figure 2A**). Further, MLN4924 dose-dependently increased acetylated α-tubulin (**Figure 2B**). The effectiveness of NEDDylation pathway inhibitor MLN4924 was demonstrated by immunoblotting for NEDD8. We found a marked decrease in NEDDylated substrates, suggesting that MLN4924 reduces NEDD8 conjugation (**Figures 2B,C**). Further, MLN4924 completely blocked the ectopically transfected HDAC6 (FLAG epitope-tagged) activity in HEK293 cells, as indicated by reciprocal increases in levels of acetylated tubulin (**Figure 2D**). A major component of microtubules, α-tubulin forms the cellular cytoskeletal system and plays critical role in endothelial migration, cell shape, and adhesion, all critical in the development of atherosclerotic plaques (Hubbert et al., 2002; Hashimoto-Komatsu et al., 2011). Here, immunofluorescence with α-tubulin antibody revealed quiescent ECs with more concentrated radiating α-tubulin and smaller nuclei than those of MLN4924-treated ECs, which showed reorganization of spread-out α-tubulin and enlarged round nuclei (**Figure 2E**). We also observed significantly fewer gaps between adjacent cells in MLN4924-treated ECs (**Figure 2E**).

In our study, we used the acetylation status of α-tubulin, a well-known HDAC6 substrate, to measure HDAC6 activity indirectly. To determine whether the increase in acetylation of α-tubulin that occurred when ECs were treated with MLN4924 was indeed due to decreased HDAC6 activity, we measured the effect of MLN4924 in tubacin-pretreated (HDAC6-inhibited) HAECs.

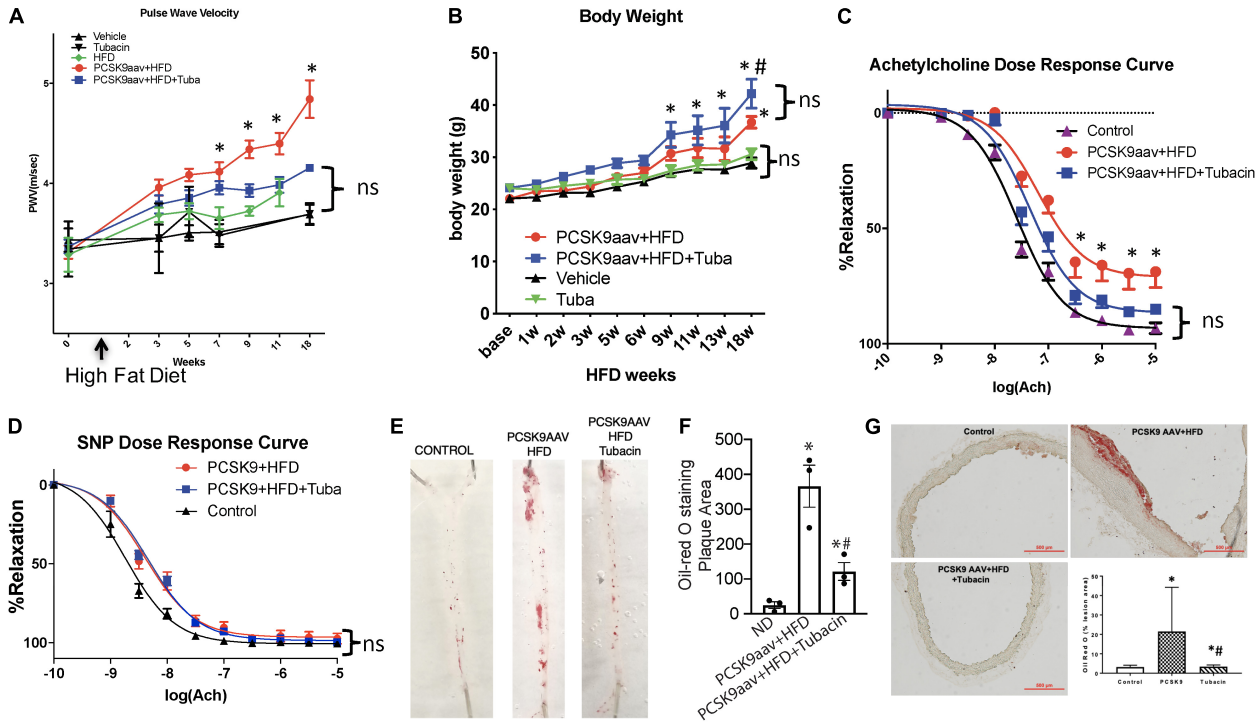

FIGURE 1 | Pharmacologic inhibition of HDAC6 attenuates elevated vascular stiffness and protects impaired endothelial-dependent vascular relaxation in atherogenic mice. Six- to eight-week-old C57BL/6 mice were injected with adeno-associated virus (AAV) encoding a PCSK9 gain-of-function mutant and then were fed a high-fat diet (HFD) for 18 weeks in the presence or absence of the HDAC6 inhibitor tubacin (0.5 mg/kg daily). **(A)** Pulse wave velocity (PWV) and **(B)** body weight was measured every 2 weeks until the end of the diet regimen (18 weeks). *$p < 0.05$ vs. vehicle group; $n = 10$–12. Vascular reactivity in response to **(C)** acetylcholine and **(D)** sodium nitroprusside (SNP) was measured by wire myography of isolated aortic rings. *$p < 0.05$ vs. control group; $n = 6$–8 mice. **(E)** Oil Red O staining was used to determine plaque burden in isolated aortas. **(F)** Quantification of plaque area presented in **(E)**. **$p < 0.05$ vs. normal diet group; #$p < 0.05$ vs. PCSK9aav + HFD group; $n = 3$. **(G)** Frozen aortic root cross sections were stained with Oil Red O. The graph in the lower right quadrant shows quantification of plaque area. *$p < 0.05$ vs. normal diet group; #$p < 0.05$ vs. PCSK9aav + HFD group; $n = 3$.

As shown in **Figures 3A,B**, MLN4924 failed to increase acetylated α-tubulin levels in tubacin-pretreated HAECs, which showed a robust increase in acetylated α-tubulin levels. HDAC6 levels remained unchanged with MLN4924, regardless of whether cells were pretreated with tubacin (**Figure 3C**). These data further confirm that MLN4924 decreases HDAC6 activity.

HDAC6 Is a NEDD8 Substrate and the Potential NEDD8 Site Is Located Within HDAC6 the BUZ Domain

Our data showed that NEDDyation pathway inhibitor MLN4924 inhibited HDAC6 activity. Next we needed to ascertain whether MLN4924 inhibited direct NEDDylation of HDAC6 or NEDDylation of an HDAC6 regulator. Therefore, we first determined whether HDAC6 is a direct substrate of NEDD8. Indeed, co-immunoprecipitation experiments showed that HDAC6 forms stable complexes with NEDD8 in HEK293 cells that co-express FLAG-tagged HDAC6 and HA-tagged NEDD8 (**Figure 4A**). UBC12, a NEDD8 E2 conjugating enzyme was transfected in all groups to enhance conjugation of NEDD8 to its substrates. We then sought to identify the specific motif within HDAC6 responsible for NEDD8 conjugation. The NEDD8 conjugation site prediction software NEDDYPREDDY predicted clusters of lysine as a potential NEDDylation site in HDAC6. Therefore, we used full-length HDAC6 (FLAGHDAC6-FL) and a C-terminal BUZ truncation mutant of HDAC6 (FLAGHDAC6 ΔBUZ) in co-immunoprecipitation experiments with HA-NEDD8. NEDD8 conjugation was nearly abolished in the HDAC6 ΔBUZ mutant suggesting that the NEDDylation site in HDAC6 is located in the ubiquitin-binding domain of HDAC6 (**Figures 4B,C**).

Atherogenic- and OxLDL-Increased HDAC6 Activity in ECs Is Abrogated by NAE1 Inhibitor MLN4924

Our previous studies showed that the atherogenic stimulus OxLDL triggers global protein NEDDylation and enhances HDAC6 deacetylation activity in HAECs (Pandey et al., 2015; Leucker et al., 2017). However, whether NEDDylation was the link between increased HDAC6 with OxLDL was unknown. Therefore, we examined whether NEDDylation plays any role in OxLDL-mediated activation of HDAC6. Indeed, MLN4924 not only blocked the stimulatory effect of OxLDL on HDAC6 activity in HAECs (as evidenced by an increase in acetylated α-tubulin)

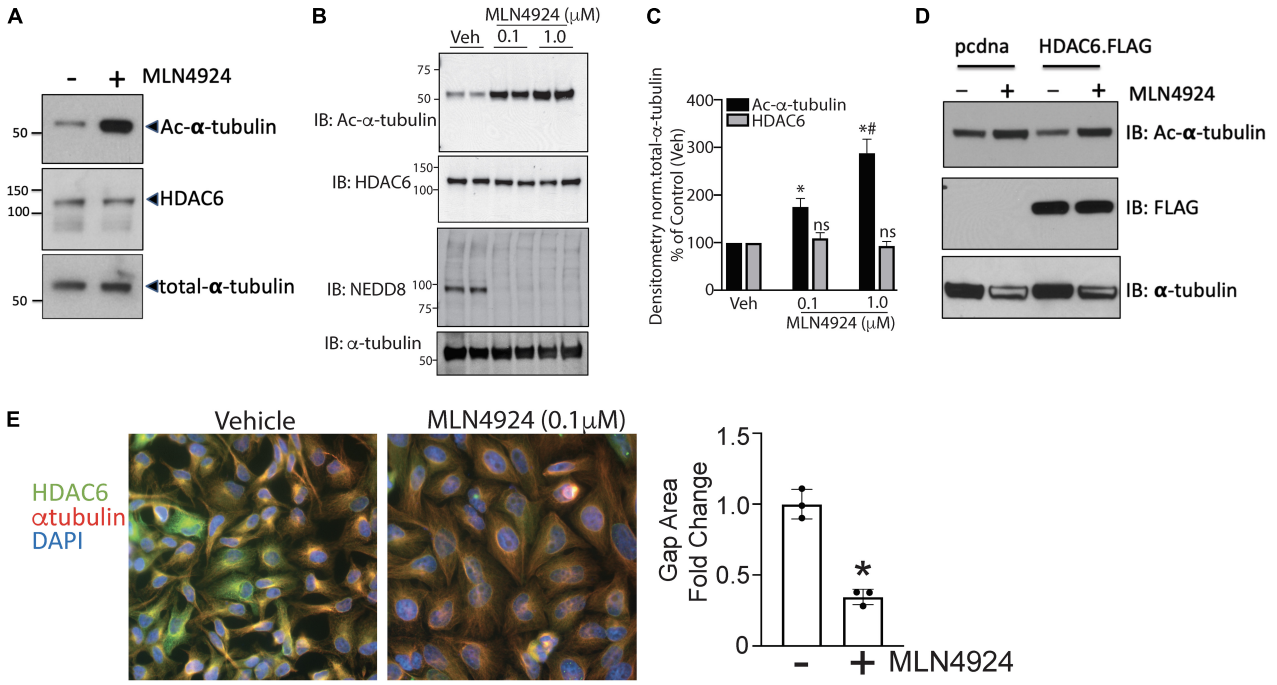

FIGURE 2 | Pharmacologic inhibition of NEDDylation pathway regulates endothelial HDAC6 activity and modulates α-tubulin organization. **(A)** Human aortic endothelial cells (HAECs) were exposed to either DMSO or MLN4924 (1 μM) for 18 h, and cell lysates were subjected to western blotting with antibodies to acetylated α-tubulin, HDAC6, or total α-tubulin. **(B)** Similar experiments were performed with two doses of MLN4924 (0.1 and 1 μM); $n = 3$. **(C)** Densitometric analysis of HDAC6 and acetylated α-tubulin levels from panels **(A,B)**. $^{*}p < 0.05$ vs. vehicle group; $^{\#}p < 0.05$ vs. MLN4925 (0.1 μM) group; $n = 3$. **(D)** HEK293 cells were transfected with empty vector (pcdna3.1) or FLAG-tagged HDAC6. After 24 h, MLN4924 or DMSO (control) was added to the media and cultured for another 18 h. Cell lysates were immunoblotted (IB) with acetylated α-tubulin and FLAG antibodies. **(E)** Left: A confluent monolayer of HAECs was exposed to DMSO or MLN4924 (1 μM) for 18 h. Cells were immunofluorescently stained for HDAC6 (green), α-tubulin (red), and DAPI (blue). Right: Quantification of gap area between adjacent cells normalized to the number of nuclei. $^{*}p < 0.05$ vs. control group; $n = 3$.

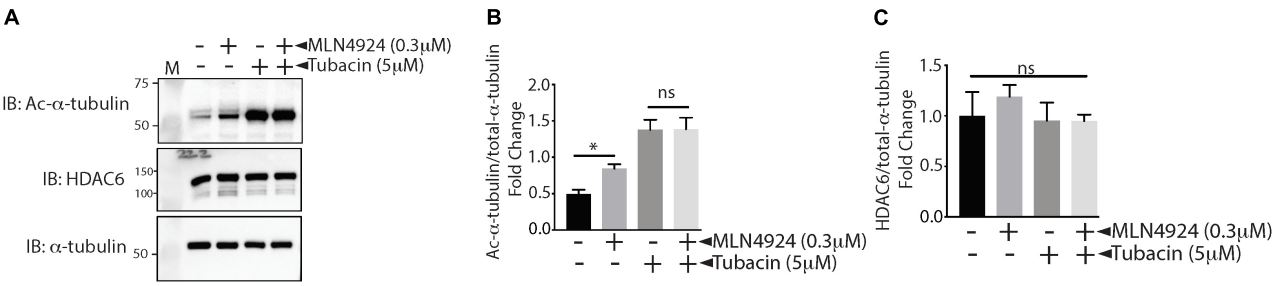

FIGURE 3 | MLN4924 fails to increase acetylated tubulin in tubacin-pretreated HAECs. **(A)** HAECs were pretreated with tubacin for 4 h before addition of MLN4924 (1 μM). After an 18 h incubation, cells were immunoblotted (IB) with antibodies to acetylated α-tubulin, HDAC6, and total α-tubulin. **(B,C)** Densitometric analysis of HDAC6 and acetylated α-tubulin levels presented in **(A)**. $^{*}p < 0.05$ vs. DMSO (control) group; $n = 3$.

but further reduced it below control levels (**Figures 5A,B**). These findings further suggest that NEDDylation of HDAC6 may be responsible for impairment of the vascular response by oxidative injury.

DISCUSSION

In this study we found that pharmacologic inhibition of HDAC6 with tubacin restores endothelial-dependent relaxation, prevents the development of vascular stiffness—one of the integrated measures of vascular health *in vivo*—and significantly reduces plaque burden in a mouse model of atherosclerosis. We also define here a novel post-translational mechanism that can control HDAC6 activity in the context of oxidative injury whereby NEDD8 is conjugated to lysine located within the C-terminal ubiquitin binding domain of HDAC6.

In our previous study we showed that the atherogenic stimulus OxLDL triggers endothelial dysfunction by downregulating expression of atheroprotective enzyme endothelial cystathionine

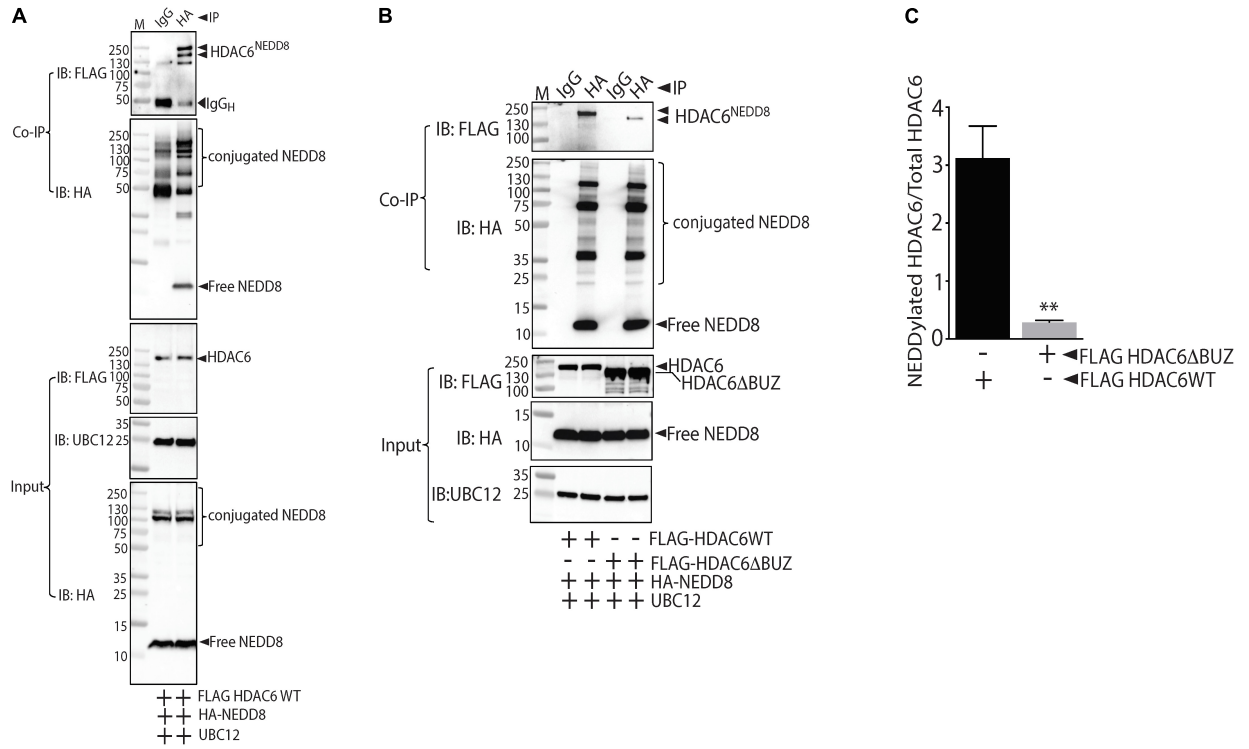

FIGURE 4 | NEDD8 binds HDAC6 within the ubiquitin binding BUZ domain. **(A)** HEK293 cells expressing FLAG-tagged full-length HDAC6 (FLAGHDAC6WT), HA-NEDD8, and UBC12 were immunoprecipitated (IP) with either isotype control IgG or HA antibodies. The purified conjugates were immunoblotted (IB) with FLAG, HA, or UBC12 antibodies. **(B)** HEK293 cells expressing FLAG-tagged full-length HDAC6 (FLAGHDAC6WT) or ubiquitin binding domain truncated HDAC6 mutant (FLAGHDAC6ΔBUZ) together with HA-NEDD8 and UBC12 were immunoprecipitated with either isotype control IgG or HA antibodies. The purified conjugates were immunoblotted with FLAG, HA, or UBC12 antibodies. **(C)** Densitometric analysis of NEDDylated FLAGHDAC6 WT and FLAGHDAC6ΔBUZ normalized to total HDAC6. $^{**}p < 0.05$ vs. FLAGHDAC6 WT group; $n = 3$.

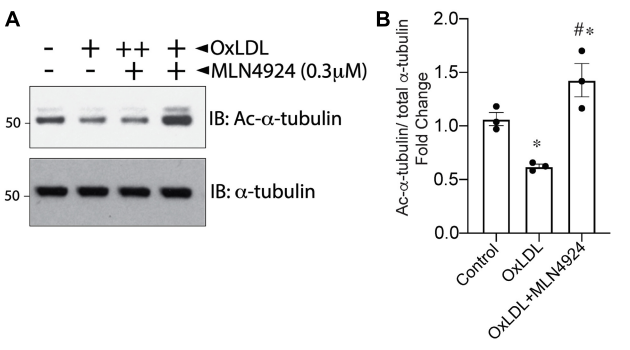

FIGURE 5 | Pharmacologic inhibition of NEDDylation pathway blocks OxLDL-induced HDAC6 activity. **(A)** HAECs pretreated with MLN4924 (1 μM) for 2 h were exposed to either phosphate-buffered saline (control) or increasing concentrations of OxLDL (50, 100 μg/mL) for 6 h. Cell lysates were immunoblotted (IB) with acetylated α-tubulin and total α-tubulin antibodies. **(B)** Densitometric analysis of acetylated α-tubulin. $^{*}p < 0.05$ vs. control group; $^{\#}p < 0.05$ vs. OxLDL group; $n = 3$.

lyase γ, which produces vasoactive hydrogen sulfide through activation of its transcriptional regulator HDAC6. Those results implicated post-translational modification via NEDDylation (covalent attachment of NEDD8 protein) and subsequent degradation of HDAC2 as causative factors (Pandey et al., 2015; Leucker et al., 2017). In contrast to its effect on HDAC2 levels, NEDDylation of HDAC6 did not alter HDAC6 levels but rather increased its activity. These effects further highlight the diverse cellular effects of NEDDylation. Our findings are consistent with a non-biased targeted proteomic study that identified HDAC2 and HDAC6 as the only two potential HDAC substrates of NEDD8 (Jones et al., 2008). One of the limitations of our current study is that we have not yet identified the specific lysine residue(s) in HDAC6 that covalently bind to NEDD8. It would be interesting to know whether mutation of the NEDD8 conjugation site in mice and in cultured HAECs using CRISPR/Cas9 would provide protection against endothelial dysfunction and atherogenesis. Using NEDDylation site predictor software and domain truncation, we have identified the C-terminal ubiquitin binding domain of HDAC6 as a potential site for NEDD8 conjugation. Future studies are warranted to understand the mechanism(s) by which NEDDylation affects HDAC6 activity in ECs.

A recent study identified tubacin as a potent inducer of eNOS expression and NO production in EC lines *in vitro*, and in mice *in vivo* (Chen et al., 2019). Interestingly, this effect was independent of tubacin's ability to inhibit HDAC6. That study

exposes a limitation of our own, in that the protective effect of tubacin against endothelial dysfunction and atherogenesis could be independent of HDAC6 inhibition. Future studies with HDAC6 knockout mice are needed to clarify this important issue. Nonetheless, these studies, which show that tubacin increases athero-protective NO and hydrogen sulfide production in ECs, and blocks atherosclerosis (current study), further strengthen the case for tubacin as a therapeutic application to prevent/reverse atherogenesis.

MLN4924, which inhibits the NEDDylation pathway, has been shown to attenuate inflammation and prevent atherosclerosis (Ehrentraut et al., 2013; Asare et al., 2017). In current study eNOS expression and phosphorylation was unaffected in HAEC treated with MLN4924 (**Supplementary Figure 2**). Studies are warranted to determine the specific effects of HDAC6 inhibition by MLN4924 on endothelial function and atherosclerosis. The identification of NEDDylation site and generation of mutant mice will facilitate to address this important question.

Endothelial barrier integrity is compromised in the process of atherosclerosis, and selective inhibition of HDAC6 in human pulmonary artery ECs has been shown to prevent TNF-α–induced EC barrier dysfunction and endotoxin-induced pulmonary edema (Yu et al., 2016). ECs are known to respond to altered fluid shear stress by altering their cellular and nuclear shape to align with the direction of flow. Microtubules are critical for this process. One of the key functions of the EC morphologic change is the transient increase in intracellular calcium that activates eNOS to release NO. In this study, we observed striking changes in EC morphology, tubulin reorganization, and nuclear shape with MLN4924 treatment. Although we did not measure the functional consequence of these changes, the shortened gaps between ECs suggest that NEDDylation could have important role in maintaining the barrier integrity of ECs. This finding is promising, given the clinical importance of endothelial barrier integrity in the regulation of inflammation and atherosclerosis. Indeed, inhibition of the deNEDDylation enzyme CSN5 has been implicated in loss of EC barrier function (Majolée et al., 2019). Further, MLN4924 increases the expression of β-catenin, which is a common substrate of cullin-ring ligases and HDAC6, and interacts with VE-cadherin at EC junctions to maintain barrier integrity, suggesting a link between NEDDylation, cell-to-cell adhesion, and barrier function (Gu et al., 2014; Tran et al., 2016).

In current study tubacin treatment significantly reduced aortic stiffness, a metric of global integrated vascular health *in vivo*, in mice that were induced to develop atherosclerosis. Our previous study shows that the elevated aortic stiffness in atherogenic mice was independent of changes in mean arterial blood pressure (Hori et al., 2020). The attenuation of aortic stiffness in tubacin treated atherogenic mice found in current study is therefore unlikely to be mediated by changes in blood pressure. The mechanism by which HDAC6 inhibition exerts protective effect on endothelial function has been shown to involve enhanced production of vasodilator gas hydrogen sulfide by cystathionine gamma lyase (Leucker et al., 2017). However, whether this holds true in atherogenesis is yet to be determined.

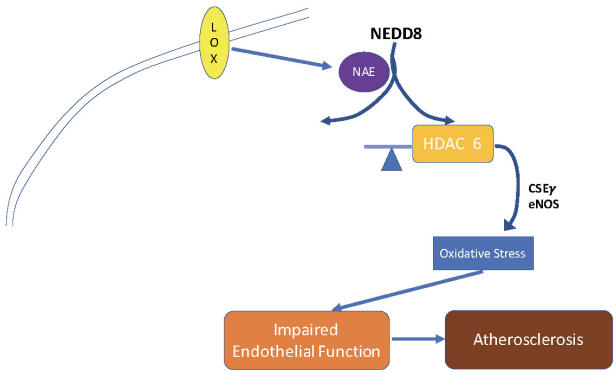

FIGURE 6 | Schematic of proposed mechanism for the role of HDAC6 in endothelial dysfunction and atherogenesis. OxLDL stimulates HDAC6 activity by enhancing HDAC6 NEDDylation. This leads to suppression of the endothelial enzymes NOS and CSEγ, thereby reducing NO and H_2S. These events result in EC dysfunction and atherosclerosis.

Taken together, our findings suggest a novel molecular pathway that influences endothelial tone, reactivity, and atherogenesis (**Figure 6**). These results provide insight that could help us to elucidate the mechanism by which genes control atherogenesis and vasculopathies. Further, blocking HDAC6 activity directly with tubacin or indirectly by blocking its post-translational modifier NEDD8 with MLN4924, provides options for new therapeutic strategies to treat or reverse endothelial dysfunction and atherosclerosis.

DATA AVAILABILITY STATEMENT

The raw data supporting the conclusions of this article will be made available by the authors, without undue reservation.

ETHICS STATEMENT

The animal study was reviewed and approved by the Johns Hopkins University Animal Care and Use Committee (ACUC).

AUTHOR CONTRIBUTIONS

DP: conception and design and drafting the manuscript for important intellectual content. YN, MN, HSW, MH, and DP: analysis and interpretation. All authors have approved it for publication.

FUNDING

This work was supported by an American Heart Association Scientist Development Grant, National Institutes of Health R56 HL139736, Gilead Sciences Research Scholars Program in Pulmonary Arterial Hypertension Award, and a Stimulating and Advancing ACCM Research (StAAR) Investigator Award from

the Johns Hopkins University Department of Anesthesiology and Critical Care Medicine to DP.

ACKNOWLEDGMENTS

We would like to thank Claire Levine, MS, ELS, Scientific Editor in the Department of Anesthesiology and Critical Care Medicine at Johns Hopkins University, for editing this manuscript. Our abstract to The Experimental Biology Meeting 2018 that contained initial findings presented in this manuscript was published in FASEB journal (https://faseb.onlinelibrary.wiley.com/doi/10.1096/fasebj.2018.32.1_supplement.568.3).

SUPPLEMENTARY MATERIAL

The Supplementary Material for this article can be found online at: https://www.frontiersin.org/articles/10.3389/fphys.2021.675724/full#supplementary-material

REFERENCES

Asare, Y., Ommer, M., Azombo, F. A., Alampour-Rajabi, S., Sternkopf, M., Sanati, M., et al. (2017). Inhibition of atherogenesis by the COP9 signalosome subunit 5 in vivo. *Proc. Natl. Acad. Sci. U.S.A.* 114, E2766–E2775. doi: 10.1073/pnas.1618411114

Boyault, C., Gilquin, B., Zhang, Y., Rybin, V., Garman, E., Meyer-Klaucke, W., et al. (2006). HDAC6-p97/VCP controlled polyubiquitin chain turnover. *EMBO J.* 25, 3357–3366. doi: 10.1038/sj.emboj.7601210

Chang, F. M., Reyna, S. M., Granados, J. C., Wei, S. J., Innis-Whitehouse, W., Maffi, S. K., et al. (2012). Inhibition of neddylation represses lipopolysaccharide-induced proinflammatory cytokine production in macrophage cells. *J. Biol. Chem.* 287, 35756–35767. doi: 10.1074/jbc.M112.397703

Chen, J., Zhang, J., Shaik, N. F., Yi, B., Wei, X., Yang, X. F., et al. (2019). The histone deacetylase inhibitor tubacin mitigates endothelial dysfunction by up-regulating the expression of endothelial nitric oxide synthase. *J. Biol. Chem.* 294, 19565–19576. doi: 10.1074/jbc.RA119.011317

Choi, J. H., Nam, K. H., Kim, J., Baek, M. W., Park, J. E., Park, H. Y., et al. (2005). Trichostatin A exacerbates atherosclerosis in low density lipoprotein receptor-deficient mice. *Arterioscler. Thromb. Vasc. Biol.* 25, 2404–2409. doi: 10.1161/01.ATV.0000184758.07257.88

Dimmeler, S., Haendeler, J., Galle, J., and Zeiher, A. M. (1997). Oxidized low-density lipoprotein induces apoptosis of human endothelial cells by activation of CPP32-like proteases. a mechanistic clue to the 'response to injury' hypothesis. *Circulation* 95, 1760–1763. doi: 10.1161/01.CIR.95.7.1760

Ehrentraut, S. F., Kominsky, D. J., Glover, L. E., Campbell, E. L., Kelly, C. J., Bowers, B. E., et al. (2013). Central role for endothelial human deneddylase-1/SENP8 in fine-tuning the vascular inflammatory response. *J. Immunol.* 190, 392–400. doi: 10.4049/jimmunol.1202041

Enchev, R. I., Schulman, B. A., and Peter, M. (2015). Protein neddylation: beyond cullin-RING ligases. *Nat. Rev. Mol. Cell Biol.* 16, 30–44. doi: 10.1038/nrm3919

Galle, J., Bengen, J., Schollmeyer, P., and Wanner, C. (1995). Impairment of endothelium-dependent dilation in rabbit renal arteries by oxidized lipoprotein(a). role of oxygen-derived radicals. *Circulation* 92, 1582–1589. doi: 10.1161/01.CIR.92.6.1582

Goettsch, C., Hutcheson, J. D., Hagita, S., Rogers, M. A., Creager, M. D., Pham, T., et al. (2016). A single injection of gain-of-function mutant PCSK9 adeno-associated virus vector induces cardiovascular calcification in mice with no genetic modification. *Atherosclerosis* 251, 109–118. doi: 10.1016/j.atherosclerosis.2016.06.011

Gu, Y., Kaufman, J. L., Bernal, L., Torre, C., Matulis, S. M., Harvey, R. D., et al. (2014). MLN4924, an NAE inhibitor, suppresses AKT and mTOR signaling via upregulation of REDD1 in human myeloma cells. *Blood* 123, 3269–3276. doi: 10.1182/blood-2013-08-521914

Hao, R., Nanduri, P., Rao, Y., Panichelli, R. S., Ito, A., Yoshida, M., et al. (2013). Proteasomes activate aggresome disassembly and clearance by producing unanchored ubiquitin chains. *Mol. Cell.* 51, 819–828. doi: 10.1016/j.molcel.2013.08.016

Harada-Shiba, M., Kinoshita, M., Kamido, H., and Shimokado, K. (1998). Oxidized low density lipoprotein induces apoptosis in cultured human umbilical vein endothelial cells by common and unique mechanisms. *J. Biol. Chem.* 273, 9681–9687. doi: 10.1074/jbc.273.16.9681

Hashimoto-Komatsu, A., Hirase, T., Asaka, M., and Node, K. (2011). Angiotensin II induces microtubule reorganization mediated by a deacetylase SIRT2 in endothelial cells. *Hypertens. Res.* 34, 949–956. doi: 10.1038/hr.2011.64

Hershko, A. (2005). The ubiquitin system for protein degradation and some of its roles in the control of the cell division cycle. *Cell Death Differ.* 12, 1191–1197. doi: 10.1038/sj.cdd.4401702

Hershko, A., and Ciechanover, A. (1998). The ubiquitin system. *Annu. Rev. Biochem.* 67, 425–479. doi: 10.1146/annurev.biochem.67.1.425

Hori, D., Nomura, Y., Nakano, M., Han, M., Bhatta, A., Chen, K., et al. (2020). Endothelial-Specific overexpression of histone deacetylase 2 protects mice against endothelial dysfunction and atherosclerosis. *Cell Physiol. Biochem.* 54, 947–958. doi: 10.33594/000000280

Hubbert, C., Guardiola, A., Shao, R., Kawaguchi, Y., Ito, A., Nixon, A., et al. (2002). HDAC6 is a microtubule-associated deacetylase. *Nature* 417, 455–458. doi: 10.1038/417455a

Ito, K., Lim, S., Caramori, G., Cosio, B., Chung, K. F., Adcock, I. M., et al. (2002). A molecular mechanism of action of theophylline: induction of histone deacetylase activity to decrease inflammatory gene expression. *Proc. Natl. Acad. Sci. U.S.A.* 99, 8921–8926. doi: 10.1073/pnas.132556899

Jones, J., Wu, K., Yang, Y., Guerrero, C., Nillegoda, N., Pan, Z. Q., et al. (2008). A targeted proteomic analysis of the ubiquitin-like modifier nedd8 and associated proteins. *J. Proteome Res.* 7, 1274–1287. doi: 10.1021/pr700749v

Kawaguchi, Y., Kovacs, J. J., McLaurin, A., Vance, J. M., Ito, A., and Yao, T. P. (2003). The deacetylase HDAC6 regulates aggresome formation and cell viability in response to misfolded protein stress. *Cell* 115, 727–738. doi: 10.1016/S0092-8674(03)00939-5

Khan, B. V., Parthasarathy, S. S., Alexander, R. W., and Medford, R. M. (1995). Modified low density lipoprotein and its constituents augment cytokine-activated vascular cell adhesion molecule-1 gene expression in human vascular endothelial cells. *J. Clin. Invest.* 95, 1262–1270. doi: 10.1172/JCI117776

Kovacs, J. J., Murphy, P. J., Gaillard, S., Zhao, X., Wu, J. T., Nicchitta, C. V., et al. (2005). HDAC6 regulates Hsp90 acetylation and chaperone-dependent activation of glucocorticoid receptor. *Mol. Cell.* 18, 601–607. doi: 10.1016/j.molcel.2005.04.021

Kugiyama, K., Kerns, S. A., Morrisett, J. D., Roberts, R., and Henry, P. D. (1990). Impairment of endothelium-dependent arterial relaxation by lysolecithin in modified low-density lipoproteins. *Nature* 344, 160–162. doi: 10.1038/344160a0

Kuo, M. M., Kim, D. H., Jandu, S., Bergman, Y., Tan, S., Wang, H., et al. (2016). MPST but not CSE is the primary regulator of hydrogen sulfide production and function in the coronary artery. *Am. J. Physiol. Heart Circ. Physiol.* 310, H71–H79. doi: 10.1152/ajpheart.00574.2014

Lee, D. Y., Lee, C. I., Lin, T. E., Lim, S. H., Zhou, J., Tseng, Y. C., et al. (2012). Role of histone deacetylases in transcription factor regulation and cell cycle modulation in endothelial cells in response to disturbed flow. *Proc. Natl. Acad. Sci. U.S.A.* 109, 1967–1972. doi: 10.1073/pnas.1121214109

Leucker, T. M., Nomura, Y., Kim, J. H., Bhatta, A., Wang, V., Wecker, A., et al. (2017). Cystathionine gamma-lyase protects vascular endothelium: a role for inhibition of histone deacetylase 6. *Am. J. Physiol. Heart Circ. Physiol.* 312, H711–H720. doi: 10.1152/ajpheart.00724.2016

Li, H., and Forstermann, U. (2009). Prevention of atherosclerosis by interference with the vascular nitric oxide system. *Curr. Pharm. Des.* 15, 3133–3145. doi: 10.2174/138161209789058002

Li, L., Gao, P., Zhang, H., Chen, H., Zheng, W., Lv, X., et al. (2011). SIRT1 inhibits angiotensin II-induced vascular smooth muscle cell hypertrophy. *Acta Biochim. Biophys. Sin.* 43, 103–109. doi: 10.1093/abbs/gmq104

Li, Y., Zhang, X., Polakiewicz, R. D., Yao, T. P., and Comb, M. J. (2008). HDAC6 is required for epidermal growth factor-induced beta-catenin nuclear localization. *J. Biol. Chem.* 283, 12686–12690. doi: 10.1074/jbc.C700185200

Liao, L., Starzyk, R. M., and Granger, D. N. (1997). Molecular determinants of oxidized low-density lipoprotein-induced leukocyte adhesion and microvascular dysfunction. *Arterioscler. Thromb. Vasc. Biol.* 17, 437–444. doi: 10.1161/01.ATV.17.3.437

Libby, P. (2002). Inflammation in atherosclerosis. *Nature* 420, 868–874. doi: 10.1038/nature01323

Libby, P., Ridker, P. M., and Maseri, A. (2002). Inflammation and atherosclerosis. *Circulation* 105, 1135–1143. doi: 10.1161/hc0902.104353

Majolée, J., Pronk, M. C. A., Jim, K. K., van Bezu, J. S. M., van der Sar, A. M., Hordijk, P. L., et al. (2019). CSN5 inhibition triggers inflammatory signaling and Rho/ROCK-dependent loss of endothelial integrity. *Sci. Rep.* 9:8131. doi: 10.1038/s41598-019-44595-4

Mattagajasingh, I., Kim, C. S., Naqvi, A., Yamamori, T., Hoffman, T. A., Jung, S. B., et al. (2007). SIRT1 promotes endothelium-dependent vascular relaxation by activating endothelial nitric oxide synthase. *Proc. Natl. Acad. Sci. U.S.A.* 104, 14855–14860. doi: 10.1073/pnas.0704329104

Oved, S., Mosesson, Y., Zwang, Y., Santonico, E., Shtiegman, K., Marmor, M. D., et al. (2006). Conjugation to Nedd8 instigates ubiquitylation and down-regulation of activated receptor tyrosine kinases. *J. Biol. Chem.* 281, 21640–21651. doi: 10.1074/jbc.M513034200

Pandey, D., Hori, D., Kim, J. H., Bergman, Y., Berkowitz, D. E., and Romer, L. H. (2015). NEDDylation promotes endothelial dysfunction: a role for HDAC2. *J. Mol. Cell Cardiol.* 81, 18–22. doi: 10.1016/j.yjmcc.2015.01.019

Ross, R. (1999). Atherosclerosis–an inflammatory disease. *N. Engl. J. Med.* 340, 115–126. doi: 10.1056/NEJM199901143400207

Simon, A., Plies, L., Habermeier, A., Martine, U., Reining, M., and Closs, E. I. (2003). Role of neutral amino acid transport and protein breakdown for substrate supply of nitric oxide synthase in human endothelial cells. *Circ. Res.* 93, 813–820. doi: 10.1161/01.RES.0000097761.19223.0D

Tran, K. A., Zhang, X., Predescu, D., Huang, X., Machado, R. F., Göthert, J. R., et al. (2016). Endothelial β-catenin signaling is required for maintaining adult blood-brain barrier integrity and central nervous system homeostasis. *Circulation* 133, 177–186. doi: 10.1161/CIRCULATIONAHA.115.015982

Verdel, A., Curtet, S., Brocard, M. P., Rousseaux, S., Lemercier, C., Yoshida, M., et al. (2000). Active maintenance of mHDA2/mHDAC6 histone-deacetylase in the cytoplasm. *Curr. Biol.* 10, 747–749. doi: 10.1016/S0960-9822(00)00542-X

Yu, J., Ma, Z., Shetty, S., Ma, M., and Fu, J. (2016). Selective HDAC6 inhibition prevents TNF-α-induced lung endothelial cell barrier disruption and endotoxin-induced pulmonary edema. *Am. J. Physiol. Lung. Cell Mol. Physiol.* 311, L39–L47. doi: 10.1152/ajplung.00051.2016

Zhang, X., Yuan, Z., Zhang, Y., Yong, S., Salas-Burgos, A., Koomen, J., et al. (2007). HDAC6 modulates cell motility by altering the acetylation level of cortactin. *Mol. Cell.* 27, 197–213. doi: 10.1016/j.molcel.2007.05.033

Conflict of Interest: The authors declare that the research was conducted in the absence of any commercial or financial relationships that could be construed as a potential conflict of interest.

The handling editor declared a shared affiliation with one of the author DP.

frontiers in Physiology

BRIEF RESEARCH REPORT
published: 24 August 2021
doi: 10.3389/fphys.2021.701399

Increased Mobility of the Atrial Septum in Aortic Root Dilation: An Observational Study on Transesophageal Echocardiography

Altair Heidemann Jr.[1,2,3], *Lorença Dall'Oglio*[3,4], *Eduardo Gehling Bertoldi*[1,5] *and Murilo Foppa*[1,2,3]*

[1] Graduate Studies Program in Cardiology, Universidade Federal do Rio Grande do Sul, Porto Alegre, Brazil, [2] Cardiology Division, Hospital de Clínicas de Porto Alegre, Porto Alegre, Brazil, [3] NUPIC (Núcleo de Pesquisa em Imagem Cardiovascular), Hospital de Clínicas de Porto Alegre, Porto Alegre, Brazil, [4] School of Medicine, Universidade Luterana do Brasil, Porto Alegre, Brazil, [5] School of Medicine, Universidade Federal de Pelotas, Pelotas, Brazil

Background: There is a growing interest in the relationship between atrial septal anatomy and cardioembolic stroke. Anecdotal reports suggest that the enlargement of the aortic root could interfere with atrial septal mobility (ASM). We sought to investigate the association between ASM and aortic root dilation.

Methods and Findings: From all consecutive clinically requested transesophageal echocardiogram (TEE) studies performed during the study period in a single institution, we were able to review and evaluate the ASM and anteroposterior length, aortic root diameter, and the prevalence of atrial septal aneurysm (ASA) and of patent foramen ovale (PFO) in 336 studies. Additional variables, such as left ventricular ejection fraction, left atrial diameter, diastolic dysfunction, age, sex, weight, height, previous stroke, atrial fibrillation, and TEE indication, were extracted from patient medical records and echocardiographic clinical reports. In 336 patients, we found a mean ASM of 3.4 mm, ranging from 0 to 21 mm; 15% had ASA and 14% had PFO. There was a 1.0 mm increase in ASM for every 10-mm increase in aortic root diameter adjusted for age, sex, weight, height, ejection fraction, and left atrial size ($B = 0.1$; $P = 0.04$). Aortic diameter was not associated with a smaller septal length ($B = 0.03$; $P = 0.7$).

Conclusion: An increased motion of the atrial septum can occur in association with aortic dilation. These findings deserve attention for the relevance of aortic root anatomy in future studies involving atrial septal characteristics and embolic stroke risk.

Keywords: atrial septal aneurysm, aortic dilation, atherosclerosis, transesophageal echocardiography, stroke

OPEN ACCESS

Edited by:
Jochen Steppan, Johns Hopkins University, United States

Reviewed by:
Jie Li, Augusta University, United States
Erik Josef Behringer, Loma Linda University, United States

***Correspondence:**
Murilo Foppa
mufoppa@hcpa.edu.br

Specialty section:
This article was submitted to Vascular Physiology, a section of the journal Frontiers in Physiology

Received: *27 April 2021*
Accepted: *20 July 2021*
Published: *24 August 2021*

Citation:
Heidemann A Jr, Dall'Oglio L, Bertoldi EG and Foppa M (2021) Increased Mobility of the Atrial Septum in Aortic Root Dilation: An Observational Study on Transesophageal Echocardiography. Front. Physiol. 12:701399. doi: 10.3389/fphys.2021.701399

INTRODUCTION

Embolic stroke has multiple causes, and more than one disease is frequently detected during the assessment of patients (Chatzikonstantinou et al., 2012; Amarenco et al., 2013). There is a growing knowledge regarding the roles of patent foramen ovale (PFO) and atrial septal aneurysm (ASA) as sources of embolism in ischemic stroke (Pearson et al., 1991; Lamy et al., 2002; Ward et al., 2006; Mas et al., 2017; Saver et al., 2017; Søndergaard et al., 2017). Other phenotypic expressions

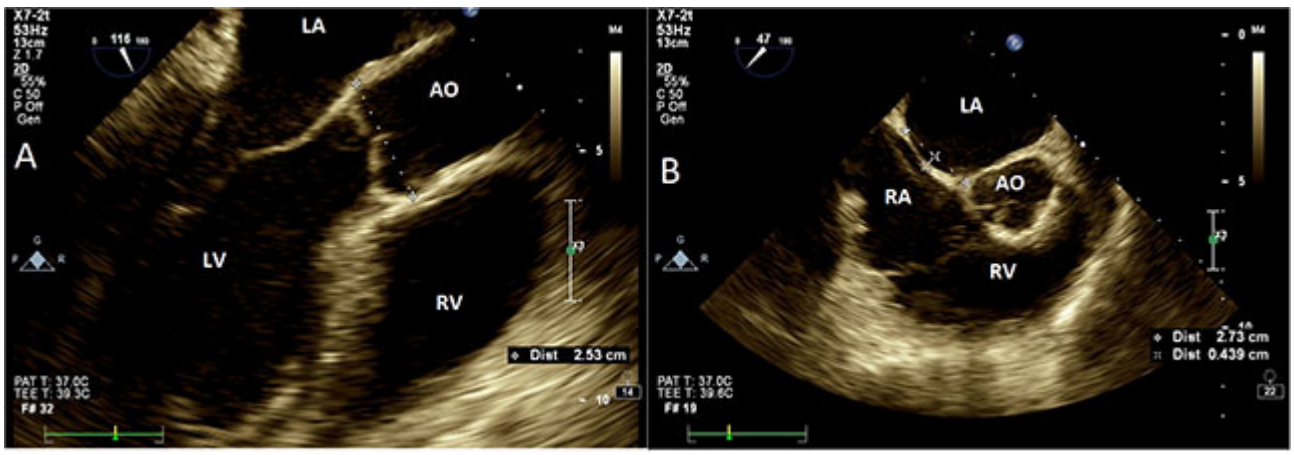

FIGURE 1 | Transesophageal echocardiography. **(A)** Aortic measurements at Valsalva sinus plane (120°, mid-esophageal view). Aorta measured at leading edge echo signal of posterior wall to the leading edge of anterior wall. **(B)** Interatrial septal size and oscillation (25–45°, mid-esophageal view) measured as the maximal perpendicular distance from an imaginary line drawn between atrial septal insertion points (dashed line). AO, aorta; LA, left atrium; RA, right atrium; LV, left ventricle; RV, right ventricle.

of large vessel atherosclerotic diseases, such as aortic enlargement and atherosclerotic plaques, are also frequently present in these patients, and they increase with aging (Reed et al., 1992). However, the causal role of diffuse advanced atherosclerosis and senile aortic dilation in stroke as well as their interconnections with other stroke risk factors is less understood.

The anatomic relation between the aortic root and atrial septum first appeared on case reports of patients with platypnea–orthodeoxia syndrome (Medina et al., 2001; Chopard and Meneveau, 2013; Hasegawa et al., 2020). An enlarged aorta could geometrically impinge a shortening in the anteroposterior atrial septal length, consequently augmenting the atrial septal mobility (ASM) (**Supplementary Video**). This effect, added to the presence of atrial septal defects or PFO, is part of the mechanism of hypoxia in this syndrome (Eicher, 2005). Moreover, differences in the left and right atrial filling pressures may influence the interatrial septum (IAS) movement dynamics.

The potential of aortic root enlargement to increase ASM has been previously suggested (Bertaux et al., 2007). This hypothesis deserves to be tested. Transesophageal echocardiogram (TEE) has high spatial and temporal resolutions, with high sensitivity for detecting PFO with the use of agitated saline solution (Di Tullio, 2010), and allows evaluation of the anatomic relationships between IAS and aortic root. In this study, we aimed to investigate the associations between aortic root and atrial septal morphological and functional characteristics in patients subjected to TEE for clinical indications.

METHODS

We identified 508 consecutive TEEs performed for clinical indications from January 2014 to December 2015 in the Hospital de Clínicas de Porto Alegre, a tertiary care teaching hospital in Brazil. The institutional review board approved this study and individual informed consent was waived due to the retrospective analysis of data.

Clinical variables, extracted from electronic medical records, were age, sex, weight, height, clinical indication for TEE, medical history of previous stroke, and atrial fibrillation. Additional echocardiographic data were extracted from transthoracic reports (performed regularly in all patients who had TEE), including left ventricular ejection fraction (LVEF), left atrial diameter, diastolic dysfunction, and central venous pressure estimate.

A single investigator (AH) reviewed all archived TEE images, and study-specific measurements were performed, which were blinded to the TEE clinical reports. Aortic root size was measured from leading-to-leading edge at mid-esophageal view 120–140° at end diastole (**Figure 1A**). Cine loops at mid-esophageal view 25–45° at the plane of Valsalva sinus, showing both the thin component of atrial septum and the aortic root, were used to quantify atrial septal length and oscillation. ASM was defined as the distance between the maximal leftward and rightward atrial positions during spontaneous breathing (**Figure 1B**). Aortic plaques were computed as simple (<4 mm) or complex. Contrast study with a saline–air solution was routinely performed to identify PFO. All measurements were performed with QLab software, version 3.3.2 (Philips Healthcare, Andover, MA) and images were acquired with commercially available equipment (EPIQ7 and IE33, Philips Ultrasound, Bothell, WA) with a multiplane 7.5 MHz transducer.

Sample size was estimated in 300 cases, considering the correlation ($r = 0.3$) between aortic size and ASM as described by Bertaux (Bertaux et al., 2007), from which we estimated the period length for retrospective data collection. Quantitative variables are presented as number of cases and prevalence or mean ± standard deviation. The Student's *t*-test and chi-square-test were used to compare group means and categorical

variables, respectively. Continuous variables were compared with Pearson's correlation coefficients. The impact of clinically relevant covariates in the main association was investigated in unadjusted and multivariable linear regression models. Intra-reader reproducibility of the study-specific measurements was tested from repeated readings in a randomly selected sample of 20 TEE studies using intraclass correlation coefficients (ICC) and Bland–Altman graphs. All tests were two-tailed and *P*-values < 0.05 were considered statistically significant. The Statistical Package for the Social Sciences (SPSS) software program, IBM, Corp., Armonk, NY, version 23.0 and STATA version 12.0 were used for analysis.

RESULTS

From the initial 508 studies, we excluded 33 repeated TEE studies performed in the same patients and 14 patients with congenital atrial septal defects, resulting in 461 patients. We also excluded 64 TEE studies without archived images and 61 studies in which images measurements could not be performed in accordance to study protocol, resulting in a final sample of 336 patients. It was noted that 336 patients included in the analysis did not differ from the excluded 125 patients who had TEE during the same study period regarding their age, sex, weight, height, prevalence of atrial fibrillation, or exam indication.

Included patients were 55 ± 16 years old, 49% were women, and 25% were obese (body mass index > 30 kg/m^2). LVEF < 40% was present in 10% of the sample. Previous stroke occurred in 124 (37%) patients and 48 (14.3%) of them had atrial fibrillation. The main indications for TEE were infective endocarditis in 142 (42.2%), stroke in 103 (30.6%) and pre-cardioversion in 44 (13%) patients.

Table 1 shows the echocardiographic measurements and relevant findings. The average diameter of the aortic root was larger in men (35 ± 5 vs. 31 ± 4 mm; $P < 0.001$) and was positively associated with age ($r = 0.16$; $P = 0.004$), height ($r = 0.35$; $P < 0.001$), and weight ($r = 0.25$; $P < 0.001$). Sixty (17.9%) patients had aortic root enlargement (≥38 mm), and three of them had aortic aneurysm (>50 mm). Forty-four percent of the sample had atherosclerotic plaques in the aorta and 50% had some degree of aortic valve fibrocalcific degeneration. The prevalences of ASA and of PFO were 15 and 14%, respectively.

The mean atrial septal anteroposterior length was 24 ± 7 mm and ASM was measured as 3.4 ± 3.7 mm, ranging from 0 to 21 mm. A significant positive correlation was observed between ASM and aortic root diameter (**Figure 2**). In multivariable analysis (**Table 2**), the linear association between ASM and aortic root diameter remained significant when adjusted for age, sex, LV ejection fraction, and left atrial diameter (adjusted *B* coefficient = 0.1; $P = 0.04$). In summary, there was a mean 1 mm increase in ASM for each 10 mm increase in aortic root diameter. No significant linear association was found between aortic size and septal length ($P = 0.7$).

In addition, we were not able to identify significant associations between ASM and the presence of aortic plaques ($P = 0.61$), diastolic dysfunction ($P = 0.17$), or elevated central venous pressure ($P = 0.37$). As expected, patients with ASA had a higher prevalence of PFO (43 vs. 10%; $P < 0.001$). The prevalence of PFO was thrice as frequent among patients with leftward bulging of the atrial septum compared with those with rightward shift (24 vs. 8%; $P < 0.001$).

The reproducibility analysis showed an ICC of 0.91 for aortic diameter, with 95% limits of agreement of −0.9–1.5 mm, and an ICC of 0.87 for ASM, with 95% limits of agreement of −0.2–0.6 mm.

TABLE 1 | Transesophageal echocardiographic measurements and findings of patients with clinically indicated studies.

	Studied sample (*n* = 336)
Transesophageal images	
Aortic root diameter (mm)	33.4 ± 5.1
Aortic plaques	
Absent	189 (56)
Simple	99 (30)
Complex	48 (14)
Aortic valve morphology	
Normal	178 (49)
Aortic valve sclerosis	145 (40)
Aortic stenosis	38 (10)
Bicuspid aortic valve	5 (1)
Atrial septal diameter (mm)	24.1 ± 7.2
Atrial septal mobility (mm)	3.4 ± 3.7
Atrial septal aneurysm	49 (15)
Patent foramen ovale	46 (14)
Transthoracic images	
Left atrial diameter (mm)	42.2 ± 8.0
Left ventricular ejection fraction	
<40%	32 (10)
40–50%	26 (7)
>50%	278 (83)
Diastolic function	
Normal	118 (35)
Mild dysfunction	113 (34)
Moderate or severe	25 (7)
Indeterminate/non-measurable	80 (24)
Dilated inferior vena cava	64 (19)

N (%) or mean ± SD.

DISCUSSION

We were able to demonstrate a positive linear association between the aortic root diameter and interatrial septal mobility. Determinants of IAS mobility are less understood, but our findings may suggest new connections between two different well-known ischemic stroke mechanisms. Bertaux et al. demonstrated this same association but in a smaller and stricter sample (Bertaux et al., 2007). Our findings reinforce the hypothesis that, due to their geometry and anatomic proximity, the aortic root dilation could increase ASM. This

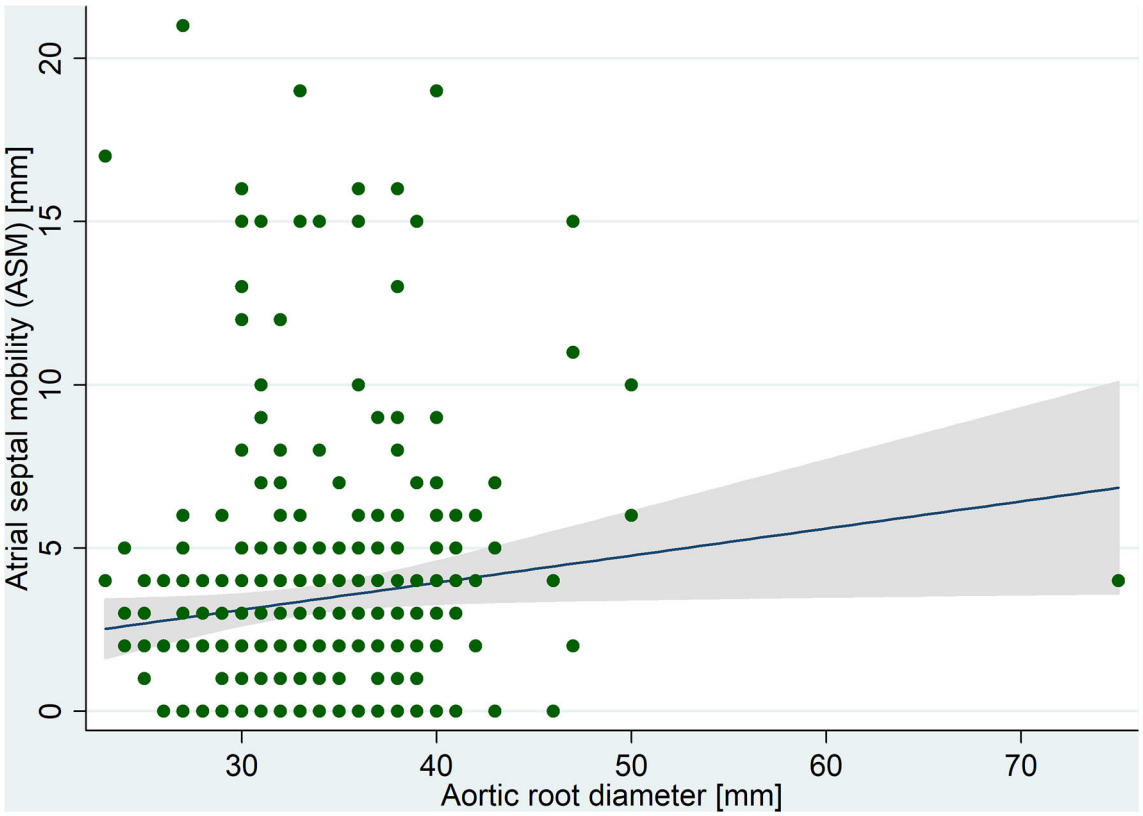

FIGURE 2 | Correlation between atrial septal mobility and aortic root diameter measured in transesophageal echocardiography images.

TABLE 2 | Crude and adjusted linear regression coefficients between aortic root diameter and atrial septal mobility (ASM).

	B coefficient	CI (95%)	*P*
Aortic root diameter			
Crude	0.08	0.01–0.16	0.03
Adjusted for:			
Age	0.08	0.002–0.16	0.04
Sex	0.11	0.03–0.19	0.01
Weight	0.07	−0.01–0.16	0.10
Height	0.08	−0.01–0.17	0.08
LVEF	0.09	0.01–0.17	0.02
Left atrial diameter	0.10	0.02–0.18	0.01
Multivariable adjusted*	0.10	0.002–0.2	0.04

** Adjusted for age, sex, weight, height, left ventricular ejection fraction (LVEF), and left atrial diameter.*

mechanism was already postulated in case reports of patients with platypnea–orthodeoxia syndrome (Kazawa et al., 2017).

Aortic atherosclerosis and dilation are also associated with cardiovascular risk factors and vascular clinical events (Gardin et al., 2006). Similar to population-based studies, we found a positive linear correlation of aortic diameter with sex, age, weight, and height. Noteworthy, the association between aortic dimension and IAS mobility persisted significant after adjusting for the main determinants of aortic size, reinforcing the independent association between them.

Although patients with aortic plaques had, in average, a larger aorta, we could not find a significant direct association between aortic plaques and augmented ASM. It is worth to say that we found the triple prevalence of PFO in patients with leftward IAS mobility, suggesting that the movement of IAS toward the left atrium could favor the opening of the foramen ovale, probably by increasing the distance between septum primum and secundum.

Methodological limitations of this study design should be considered while evaluating our findings. First, causality could not be inferred due to the cross-sectional design. We acknowledge that our indirect echocardiographic tools are inaccurate compared with invasive measurements to estimate the pressure gradients between atria. The echocardiographic images were analyzed retrospectively and, although the aorta can be easily measured, the widest ASM movement might have been occasionally missed due to the limited set of cine recording. Missing relevant clinical information from retrospectively collected data could mislead associations. It must also be noted that our sample was based on patients of a tertiary hospital, where the prevalence of illness is greater than in population-based studies.

CONCLUSION

Our results support the idea that an increased motion of atrial septum can occur due to aortic dilation. There may be a geometric relationship, in which the aortic root manifestations of systemic atherosclerotic disease may partially affect the ASM. These findings raise attention to consider the relevance of aortic root anatomy in the associations between atrial septal characteristics and embolic stroke risk in future clinical studies.

DATA AVAILABILITY STATEMENT

The raw data supporting the conclusions of this article will be made available by the authors, without undue reservation.

ETHICS STATEMENT

The studies involving human participants were reviewed and approved by GPPG HCPA. Written informed consent for participation was not required for this study in accordance with the national legislation and the institutional requirements.

AUTHOR CONTRIBUTIONS

AH contributed to the concept/design, data collection, data analysis/interpretation, drafting of the article. LD'O contributed to the data collection and data analysis/interpretation. EB contributed to the data analysis/interpretation and drafting of the article. MF contributed to the concept/design, data analysis/interpretation and drafting of the article. All authors listed have made a substantial, direct, intellectual contribution to the work, and approved it for publication.

FUNDING

This work was supported by the Coordenação de Aperfeiçoamento de Pessoal de Nível Superior—Brasil (CAPES, Coordination of Superior Level Staff Improvement)—Finance Code 001, and Hospital de Clinicas de Porto Alegre (No. FIPE-GPPG: 10-0133). The sponsors had no participation in the design and conduct of the study; collection, management, analysis, and interpretation of the data; and preparation, review, or approval of the manuscript.

SUPPLEMENTARY MATERIAL

The Supplementary Material for this article can be found online at: https://www.frontiersin.org/articles/10.3389/fphys.2021.701399/full#supplementary-material

Supplementary Video 1 | A 3D transesophageal echocardiography focused in the aortic valve, illustrating the relationship between the dilated aortic root and the oscillation of the interatrial septum (superior part of the video) during the cardiac cycle.

REFERENCES

Amarenco, P., Bogousslavsky, J., Caplan, L. R., Donnan, G. A., Wolf, M. E., and Hennerici, M. G. (2013). The ASCOD phenotyping of ischemic stroke (updated ASCO phenotyping). *Cerebrovasc. Dis.* 36, 1–5. doi: 10.1159/000352050

Bertaux, G., Eicher, J.-C., Petit, A., Dobšák, P., and Wolf, J.-E. (2007). Anatomic interaction between the aortic root and the atrial septum: a prospective echocardiographic study. *J. Am. Soc. Echocardiogr.* 20, 409–414. doi: 10.1016/j.echo.2006.09.008

Chatzikonstantinou, A., Krissak, R., Schaefer, A., Schoenberg, S. O., Fink, C., and Hennerici, M. G. (2012). Coexisting large and small vessel disease in patients with ischemic stroke of undetermined cause. *Eur. Neurol.* 68, 162–165. doi: 10.1159/000339945

Chopard, R., and Meneveau, N. (2013). Right-to-left atrial shunting associated with aortic root aneurysm: a case report of a rare cause of platypnea–orthodeoxia syndrome. *Heart Lung Circ.* 22, 71–75. doi: 10.1016/j.hlc.2012.08.007

Di Tullio, M. R. (2010). Patent foramen ovale: echocardiographic detection and clinical relevance in stroke. *J. Am. Soc. Echocardiogr.* 23, 144–155; quiz 220. doi: 10.1016/j.echo.2009.12.008

Eicher, J.-C. (2005). Hypoxaemia associated with an enlarged aortic root: a new syndrome? *Heart* 91, 1030–1035. doi: 10.1136/hrt.2003.027839

Gardin, J. M., Arnold, A. M., Polak, J., Jackson, S., Smith, V., and Gottdiener, J. (2006). Usefulness of aortic root dimension in persons ≥65 years of age in predicting heart failure, stroke, cardiovascular mortality, all-cause mortality and acute myocardial infarction (from the cardiovascular health study). *Am. J. Cardiol.* 97, 270–275. doi: 10.1016/j.amjcard.2005.08.039

Hasegawa, M., Nagai, T., Murakami, T., and Ikari, Y. (2020). Platypnoea–orthodeoxia syndrome due to deformation of the patent foramen ovale caused by a dilated ascending aorta: a case report. *Eur. Heart J. Case Rep.* 4, 1–4. doi: 10.1093/ehjcr/ytaa045

Kazawa, S., Enomoto, T., Suzuki, N., Koshikawa, T., Okubo, Y., Yoshii, S., et al. (2017). Platypnea-orthodeoxia syndrome in a patient with an atrial septal defect: the diagnosis and choice of treatment. *Intern. Med.* 56, 169–173. doi: 10.2169/internalmedicine.56.7728

Lamy, C., Giannesini, C., Zuber, M., Arquizan, C., Meder, J. F., Trystram, D., et al. (2002). Clinical and imaging findings in cryptogenic stroke patients with and without patent foramen ovale: the PFO-ASA Study. *Stroke* 33, 706–711. doi: 10.1161/hs0302.104543

Mas, J.-L., Derumeaux, G., Guillon, B., Massardier, E., Hosseini, H., Mechtouff, L., et al. (2017). Patent foramen ovale closure or anticoagulation vs. antiplatelets after stroke. *N. Engl. J. Med.* 377, 1011–1021. doi: 10.1056/NEJMoa1705915

Medina, A., de Lezo, J. S., Caballero, E., and Ortega, J. R. (2001). Platypnea-orthodeoxia due to aortic elongation. *Circulation* 104, 741–741. doi: 10.1161/hc3101.093603

Pearson, A. C., Nagelhout, D., Castello, R., Gomez, C. R., and Labovitz, A. J. (1991). Atrial septal aneurysm and stroke: a transesophageal echocardiographic study. *J. Am. Coll. Cardiol.* 18, 1223–1229. doi: 10.1016/0735-1097(91)90539-l

Reed, D., Reed, C., Stemmermann, G., and Hayashi, T. (1992). Are aortic aneurysms caused by atherosclerosis? *Circulation* 85, 205–211. doi: 10.1161/01.cir.85.1.205

Saver, J. L., Carroll, J. D., Thaler, D. E., Smalling, R. W., MacDonald, L. A., Marks, D. S., et al. (2017). Long-term outcomes of patent foramen ovale closure or medical therapy after stroke. *N. Engl. J. Med.* 377, 1022–1032. doi: 10.1056/NEJMoa1610057

Søndergaard, L., Kasner, S. E., Rhodes, J. F., Andersen, G., Iversen, H. K., Nielsen-Kudsk, J. E., et al. (2017). Patent foramen ovale closure or antiplatelet therapy for cryptogenic stroke. *N. Engl. J. Med.* 377, 1033–1042. doi: 10.1056/NEJMoa1707404

Ward, R. P., Don, C. W., Furlong, K. T., and Lang, R. M. (2006). Predictors of long-term mortality in patients with ischemic stroke referred for transesophageal echocardiography. *Stroke* 37, 204–208. doi: 10.1161/01.STR.0000196939.12313.16

Conflict of Interest: The authors declare that the research was conducted in the absence of any commercial or financial relationships that could be construed as a potential conflict of interest.

Publisher's Note: All claims expressed in this article are solely those of the authors and do not necessarily represent those of their affiliated organizations, or those of the publisher, the editors and the reviewers. Any product that may be evaluated in this article, or claim that may be made by its manufacturer, is not guaranteed or endorsed by the publisher.

frontiers in Physiology

ORIGINAL RESEARCH
published: 14 September 2021
doi: 10.3389/fphys.2021.726253

Mechanisms of Hypoxia-Induced Pulmonary Arterial Stiffening in Mice Revealed by a Functional Genetics Assay of Structural, Functional, and Transcriptomic Data

Edward P. Manning[1,2], Abhay B. Ramachandra[3], Jonas C. Schupp[1,4], Cristina Cavinato[3], Micha Sam Brickman Raredon[3,5,6], Thomas Bärnthaler[1,7], Carlos Cosme Jr.[1], Inderjit Singh[1], George Tellides[2,5,8], Naftali Kaminski[1] and Jay D. Humphrey[3,5]*

[1] Pulmonary, Critical Care and Sleep Medicine, Yale School of Medicine, New Haven, CT, United States, [2] VA Connecticut Healthcare System, West Haven, CT, United States, [3] Department of Biomedical Engineering, Yale University, New Haven, CT, United States, [4] Respiratory Medicine, Hannover Medical School, Hannover, Germany, [5] Vascular Biology and Therapeutics Program, Yale University, New Haven, CT, United States, [6] Department of Anesthesiology, Yale School of Medicine, New Haven, CT, United States, [7] Division of Pharmacology, Otto Loewi Research Center, Medical University of Graz, Graz, Austria, [8] Department of Surgery, Yale School of Medicine, New Haven, CT, United States

OPEN ACCESS

Edited by:
Lakshmi Santhanam, Johns Hopkins University, United States

Reviewed by:
Larissa Shimoda, Johns Hopkins Medicine, United States
Michael S. Wolin, New York Medical College, United States

***Correspondence:**
Edward P. Manning
edward.manning@yale.edu

Specialty section:
This article was submitted to Vascular Physiology, a section of the journal Frontiers in Physiology

Received: *16 June 2021*
Accepted: *19 August 2021*
Published: *14 September 2021*

Citation:
Manning EP, Ramachandra AB, Schupp JC, Cavinato C, Raredon MSB, Bärnthaler T, Cosme C Jr, Singh I, Tellides G, Kaminski N and Humphrey JD (2021) Mechanisms of Hypoxia-Induced Pulmonary Arterial Stiffening in Mice Revealed by a Functional Genetics Assay of Structural, Functional, and Transcriptomic Data. Front. Physiol. 12:726253. doi: 10.3389/fphys.2021.726253

Hypoxia adversely affects the pulmonary circulation of mammals, including vasoconstriction leading to elevated pulmonary arterial pressures. The clinical importance of changes in the structure and function of the large, elastic pulmonary arteries is gaining increased attention, particularly regarding impact in multiple chronic cardiopulmonary conditions. We establish a multi-disciplinary workflow to understand better transcriptional, microstructural, and functional changes of the pulmonary artery in response to sustained hypoxia and how these changes inter-relate. We exposed adult male C57BL/6J mice to normoxic or hypoxic (FiO_2 10%) conditions. Excised pulmonary arteries were profiled transcriptionally using single cell RNA sequencing, imaged with multiphoton microscopy to determine microstructural features under *in vivo* relevant multiaxial loading, and phenotyped biomechanically to quantify associated changes in material stiffness and vasoactive capacity. Pulmonary arteries of hypoxic mice exhibited an increased material stiffness that was likely due to collagen remodeling rather than excessive deposition (fibrosis), a change in smooth muscle cell phenotype reflected by decreased contractility and altered orientation aligning these cells in the same direction as the remodeled collagen fibers, endothelial proliferation likely representing endothelial-to-mesenchymal transitioning, and a network of cell-type specific transcriptomic changes that drove these changes. These many changes resulted in a system-level increase in pulmonary arterial pulse wave velocity, which may drive a positive feedback loop exacerbating all changes. These findings demonstrate the power of a multi-scale genetic-functional assay. They also highlight the need for systems-level analyses to determine which of the many changes are clinically significant and may be potential therapeutic targets.

Keywords: pulmonary artery, hypoxia, mouse, vascular, remodeling

INTRODUCTION

The main pulmonary artery and associated first branch right and left pulmonary arteries are classified as elastic conduit vessels whose function is to facilitate blood flow from the right ventricle to the small pulmonary arteries, arterioles, and eventually capillaries where gas exchange occurs. This complex network of vessels regulates the ventilation:perfusion ratio by directing blood to regions of the lung where it can be best oxygenated. Medium-sized and small pulmonary arteries within the lung parenchyma can vasoconstrict to divert blood flow from alveoli that are not well-aerated or vasodilate to direct greater amounts of blood to alveoli that are well-aerated. The response of the pulmonary circulation to hypoxia is well-described in mammals. Hypoxia often results in acute and sustained narrowing leading to elevated intraluminal pressures in the pulmonary vasculature primarily of the small, muscular arteries (Chan and Vanhoutte, 2013). Chronic hypoxia entrenches structural and functional changes in the muscular pulmonary arteries that associate with smooth muscle cell (SMC) and endothelial cell (EC) proliferation and possible thrombosis. These changes are believed to be mediated by EC dysfunction or insult resulting in altered homeostasis between vasodilators and vasoconstrictors, growth inhibitors and mitogenic factors, and antithrombotic and prothrombotic factors (Farber and Loscalzo, 2004). That is, hypoxia alters the transcriptome of vascular cells altering extracellular matrix within evolving states defined by the relative changes in vasodilatation and vasoconstriction (Chan and Vanhoutte, 2013).

Arterial stiffening has gained attention as clinically relevant to changes in vascular biology that drive chronic conditions (Triposkiadis et al., 2019). It can be estimated by the so-called pulse wave velocity (PWV), that is, the speed of propagation of a wave of pressure and flow (pulse) of blood that travels along the pulmonary arteries with each beat of the right ventricle. As the wave travels distally (forward), a portion is reflected proximally (backward) due to interactions with the tapering and branching vessels through which the pulse travels. More elastic arteries distend and absorb the energy of the distally traveling wave, resulting in decreased PWV in the distal direction and less wave reflection in the proximal direction toward the right ventricle. Typically, reflected pulse waves in the pulmonary artery return to the right ventricle in late systole or early diastole. Stiffer arteries distend less and result in greater PWV distally and an increased reflection of the pulse wave proximally toward the right ventricle (Castelain et al., 2001; Lau et al., 2014). This results in greater magnitude pressure waves reaching smaller arteries and arterioles and thus distal tissues, which are not accustomed to high pulse pressures (Castelain et al., 2001). Increased PWV as produced by large arterial stiffening has been shown to induce pro-inflammatory and pro-proliferative responses in pulmonary arterial EC *in vitro* and in patients with pulmonary arterial hypertension (Li et al., 2009; Tan et al., 2014). Reflected waves also tend to arrive back to the right ventricle earlier and with greater magnitude due to pulmonary arterial stiffening. This results in an increased afterload against which the right ventricle must contract and to which the right ventricle will adapt and remodel (Castelain et al., 2001; Silva et al., 2017). Although it is axiomatic that many changes in the pulmonary vasculature that manifest at a clinical scale and determine particular therapeutic strategies result from underlying microstructural changes that in turn result from transcriptional changes that define changing vascular cell phenotypes, prior studies have focused primarily on changes at individual scales rather than integrative changes across scales. The goal of this paper, therefore, is to propose a different strategy, one that exploits recent advances in *in vivo* measurements in mice, *ex vivo* biomechanical phenotyping, microstructural assessments under *in vivo* relevant multiaxial loads, standard histology, and single cell RNA sequencing (scRNA-seq) to identify the transcriptional changes in individual cell types that drive adverse pulmonary vascular remodeling during periods of hypoxia. We submit that this multi-scale approach will not only advance the utility of diverse mouse models, but also facilitate translation of multiple methods and data analysis to investigation of the human pulmonary artery in health and diverse cardiopulmonary diseases, including pulmonary arterial hypertension, congenital heart defects, and COPD.

MATERIALS AND METHODS

The overall design of this study is summarized in **Figure 1**. Following surgical removal of the right pulmonary artery from mice, vessels were subjected either to *ex vivo* biomechanical measurements that maintained cell viability, followed by multiphoton microscopy and standard histology, or to isolation of cells for scRNA-seq to identify transcriptional changes. Data were collected and quantified separately for mice exposed to normoxic or hypoxic conditions. The study was approved by Yale University Institutional Animal Care and Use Committee.

Hypoxic Exposure

Thirteen adult male mice (C57BL/6J; 14–20 weeks old, Jackson Laboratory, Bar Harbor, ME, United States) were housed in an antigen-free and virus-free animal care facility under a 12-h light and dark cycle. Six mice were exposed to hypoxic conditions by placing them in a plexiglass chamber connected to OxyCycler Models A420OC and AT42CO gas controllers and analyzers (BioSpherix, NY, United States). This gas control delivery system regulated the flow of room air, N_2, and O_2 into the chamber to create and maintain prescribed fraction inspired O2 (FiO_2) levels. Persistent hypoxia defined by a FiO_2 of 10% was maintained for 3–6 weeks at 24 h/day. Seven age matched C57BL6J mice were kept in similar conditions but exposed to room air ($\sim FiO_2$ 20%) as controls. Both groups of mice were fed a standard rodent chow and had free access to water. Animals were euthanized with overdose of urethane by intraperitoneal injection followed by exsanguination, followed by harvest of the hearts, lungs, and pulmonary arteries.

Biomechanical Testing

Specimens were excised from the main pulmonary artery to the first branch of the right pulmonary artery (RPA) and prepared as previously described (Ramachandra and Humphrey, 2019). After flushing of blood with a Hanks buffered physiologic

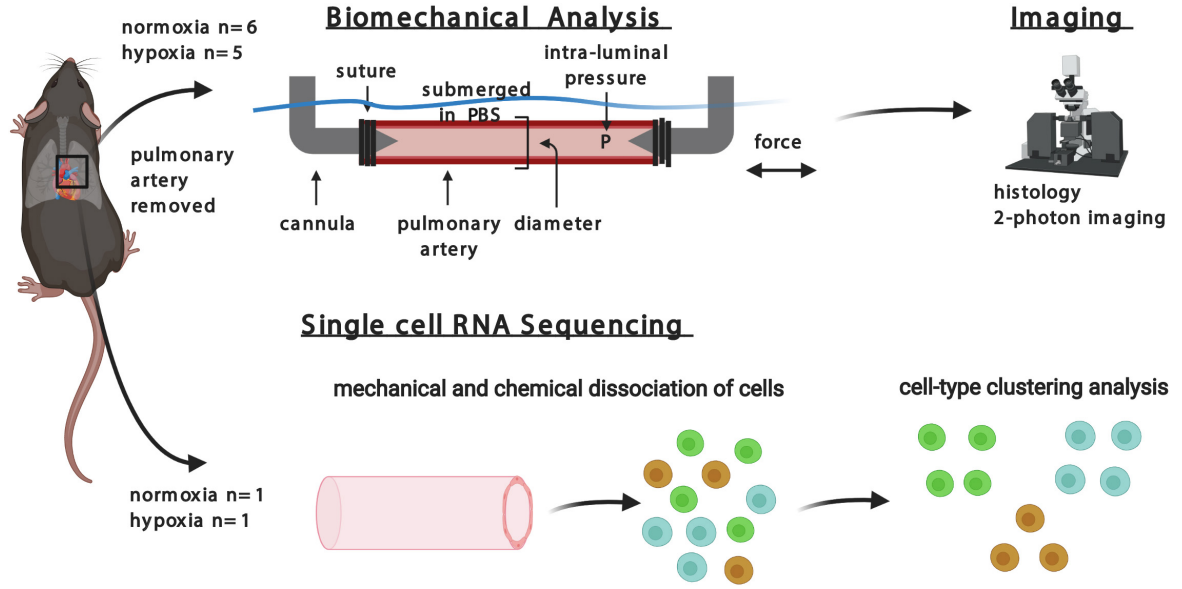

FIGURE 1 | Multi-disciplinary approach to investigating hypoxia in pulmonary artery of mice.

solution (Hanks and Wallace, 1949), perivascular tissue and fat were gently removed, and the left pulmonary artery and small branch vessels were ligated with suture. The RPA was cannulated on custom glass micropipettes and secured beyond the main pulmonary artery with ligature on one end and the first branch of the pulmonary at the other end. The specimen was submerged in a 37°C bath of Krebs-Ringer solution perfused with 95% O_2/5% CO_2. The specimens were tested using a custom computer-controlled testing device (Gleason and Humphrey, 2004), with an active protocol followed by a passive protocol (n = 5 for hypoxia, n = 6 for normoxia). Active testing focused primarily on SMC contractile responses near *in vivo* conditions, that is, a mean distending pressure of 15 mmHg and the specimen-specific value of *in vivo* axial stretch as previously described (Murtada et al., 2016; Caulk et al., 2019; Ramachandra and Humphrey, 2019). Such protocols are much more relevant physiologically than the standard "ring-tests" performed with uniaxial myographs. First, however, the SMCs were conditioned at 10 mmHg and an axial stretch of 1.1 (relative to the unloaded length) by contracting the vessel with 100 mM KCl. Axial stretch was subsequently increased in steps of 0.01 and pressure in steps of 1 mmHg to avoid sudden large deformations, which could compromise the viability of the SMCs and ECs. Following conditioning, the vessels were contracted with 100 mM KCl and then 1 mM phenylephrine (PE), both at 15 mmHg and the *in vivo* axial stretch. This protocol consisted of 5 min of equilibration, 15 min of contraction, and 10 min relaxation following washout of the vaso-stimulant with a fresh Krebs-Ringer solution. EC testing immediately followed maximal SMC contraction with PE without vaso-stimulant washout. Specimens were exposed to 10 μM acetylcholine (ACh) followed by inhibition of eNOS release by 1 mM N(gamma)-nitro-L-arginine methyl ester (L-NAME). Arterial diameter is regulated by the combined activities of EC and SMC; therefore, inhibition of EC secretion of vasodilatory molecules such as nitric oxide enables determination of maximal SMC contractility (Murtada and Humphrey, 2018).

Multiphoton Microscopy

A Titanium-Sapphire Laser (Chameleon Vision II, Coherent) was used to image representative regions of pulmonary arteries at *in vivo* relevant loading conditions (*in vivo* stretches and pressures identical to those used during passive mechanical testing, described below). A LaVision Biotec TriMScope microscope was tuned at 840 nm and equipped with a water immersion 20× objective lens (NA. 0.95). The backward scattering second harmonic generation signal from fibrillar collagens was detected within the wavelength range 390–425 nm; the autofluorescent signal arising from elastin was detected at 500–550 nm, and the fluorescent signal of cell nuclei labeled with Syto red stain was detected above 550 nm. An in-plane field of view (axial-circumferential plane) of 500 μm × 500 μm and a volume of about 0.05 mm^3 were used; this provides a much greater volume of tissue for imaging than via standard histology and hence averaging over significantly greater numbers of cells and extracellular matrix. The in-plane resolution was 0.48 μm/pixel and the out-of-plane (radial direction) step size was 1 μm/pixel. 3D images acquired concurrently for the three signals (collagen, elastin, and cell nuclei) were post-processed using MATLAB R2019b and ImageJ 1.53a. The first processing step relied on the near cylindrical shape of the samples to fit a circle to the two-dimensional mid-thickness profile of the arterial wall and transform each circumferential-radial slice of the 3D images from Cartesian to polar coordinates (angle and radius). This allowed a layer-specific microstructural analysis to focus on collagen fiber alignment and cell volume density analyses, as described in previously (Cavinato et al., 2020, 2021).

Histology

Following biaxial testing and multiphoton imaging, the specimens were fixed in 10% neutral buffered formalin and stored in 70% ethanol at 4°C for histology. After embedding in paraffin, they were sectioned (5 μm thickness) and radial-circumferential cross-sections (planes) were stained with Verhoeff Van Giesen (VVG), Masson's Trichrome (MTC) or Movat pentachrome. Details of image quantification can be found elsewhere (Bersi et al., 2017). Briefly, each section was imaged with an Olympus BX/51 microscope using an Olympus DP70 digital camera under a 20× magnification objective. Complete cross-sections were obtained by stitching together sub-images with Image Composite Editor software (Microsoft Research). The stitched images were subsequently analyzed using custom MATLAB scripts. Briefly, following background subtraction and pixel-based thresholding, area fractions for elastin (from VVG) and cytoplasm (from MTC) were computed as the ratio of pixels corresponding to a stain divided by the total number of pixels in the image. Because MTC can overstain collagen, its area fraction was computed as 1 - area fraction of elastin plus cytoplasm, with GAG content assumed negligible (Ferruzzi et al., 2015, 2018) as confirmed with Movat Pentachrome staining (data not shown). Three sections were analyzed per vessel per stain.

Material Characterization

We used a 2-D formulation to model the passive mechanical behavior since residual stresses tend to homogenize the stress field, thereby rendering mean values as good estimates of overall wall stress (Humphrey, 2013). Mean stresses along the circumferential (θ) and axial (z) directions are,

$$\sigma_\theta = \frac{Pr_i}{r_o - r_i}, \text{ and } \sigma_z = \frac{f_T + P\pi r_i^2}{\pi(r_o^2 - r_i^2)},$$

where P is the transmural pressure, r_i internal radius, r_o outer radius, and f_T the transducer measured axial force. Under the assumption of incompressibility, inner radius $r_i = \sqrt{r_o^2 - \overline{V}/\pi l}$, where l is the instantaneous length between the ligatures securing the vessel to the micropipettes and $\overline{V}$ is the volume of the vessel in the unloaded state; $\overline{V} = \pi L(OD^2 - ID^2)/4$ where L is the unloaded length, OD the unloaded outer diameter, and $ID = OD - 2H$, the unloaded inner diameter.

A pseudoelastic constitutive formulation, which has successfully described passive biaxial behaviors of pulmonary arteries (Ramachandra and Humphrey, 2019), modeled the passive mechanical behavior in terms of a stored energy function, W. Associated wall stress and material stiffness can be computed from first and second derivatives of W with respect to an appropriate deformation metric. Based on success of prior work, we let

$$W = \frac{c}{2}(I_c - 3) + \sum_{i=1}^{4} \frac{c_1^i}{4c_2^i}\left\{exp\left[c_2^i\left(IV_c^i - 1\right)^2\right] - 1\right\},$$

where c, c_1^i and c_2^i are material parameters; i=1,2,3,4 represent four collagen-dominated families of fibers along axial, circumferential, and two symmetric diagonal directions, respectively. I_c is the first invariant of right Cauchy-Green tensor ($= \lambda_\theta^2 + \lambda_z^2 + 1/\lambda_\theta^2\lambda_z^2$) and IV_c^i is the square of the stretch of the i^{th} fiber family ($= \lambda_\theta^2 sin^2\alpha_0^i + \lambda_z^2 cos^2\alpha_0^i$); α_0^i is the fiber angle relative to axial direction in the reference configuration. $\lambda_\theta = (r_i + r_o)/\ 2\rho_{mid}$, $\lambda_z = l/L$ are the mean circumferential and axial stretch, and ρ_{mid} is the unloaded mid-wall radius. The best-fit values of the material parameters and the fiber angle were determined via nonlinear regression of biaxial data from all seven passive protocols. More details on parameter estimation can be found elsewhere (Ramachandra and Humphrey, 2019).

Pulse wave velocity depends on both the geometry and mechanical properties of the arteries and can be well-approximated based on the material stiffness or distensibility of the arterial walls, namely

$$\text{PWV} = \sqrt{\frac{1}{\rho \cdot D}}(Bramwell - Hill\ equation),$$

where ρ is the mass density of the contained fluid (approximately 1,050 kg/m^3) and D is the distensibility coefficient (in Pa^{-1}or kg^{-1}m·s^2) determined by the normalized change in arterial diameter from end-diastole to end-systole divided by the change in end-diastolic and end-systolic pressures (Bramwell and Hill, 1922). PWV in the pulmonary artery and its effects on right ventricular hemodynamics can thus be measured non-invasively using the aforementioned variables (Peng et al., 2006; Sanz et al., 2008; Gupta et al., 2018).

Statistics

For variables with only two categories, differences between hypoxic and normoxic groups in morphological, histological, mechanical, and contractile properties were determined by a two-tailed, unpaired t test. For categorical variables with more than two categories, levels of stretch or pressure were compared using a two-factor analysis of variance (ANOVA). A global test across all levels was performed and then pair-wise comparisons were conducted with post-hoc tests using Bonferroni adjustment. A $p < 0.05$ level of significance was used, with data reported as mean ± standard error from the mean (SEM).

Single Cell RNA Sequencing

Viable cells from the main pulmonary arteries of one mouse exposed to hypoxic conditions for six weeks and one age-matched normoxic mouse were analyzed. Following euthanasia, the heart, lungs, and pulmonary arteries were excised with surrounding tissue. The pulmonary arteries were chopped mechanically and placed in 1 mg/ml collagenase (Roche) and 3 U/ml elastase (Worthington). Following cellular dissociation, we barcoded unique mRNA molecules of each cell using our 10× Genomics Chromium platform (3' v3.1 kit), a droplet-based microfluidic system, and performed reverse transcription, cDNA amplification, fragmentation, adaptor ligation, and sample index PCR according to the manufacturer's protocol. High sensitivity DNA bioanalyzer traces of cDNA after barcoding and of the final cDNA library were evaluated for quality control. The final cDNA libraries were sequenced on a HiSeq 4000 Illumina platform in our core facility aiming for 150 million reads per

library. Raw sequencing reads were demultiplexed based on sample index adaptors, which were added during the last step of cDNA library preparation. Possible adaptor and/or primer contamination were removed using Cutadapt. We processed the RNA-sequence data using the scRNA-seq implementation of STAR (STARsolo), where reads were mapped to the murine reference genome GRCm38 release M22 (GRCm38.p6), collapsed and counted, and summarized to a gene expression matrix. Data were analyzed and visualized using the R packages Seurat (Stuart et al., 2019). Specifically, we clustered the cellular transcriptomes and visualized them in a uniform manifold approximation and projection (UMAP) space to delineate cell types. To identify aberrant gene expression profiles in cellular subpopulations, we established differentially expressed genes between normoxic and hypoxic cells using the non-parametric Wilcoxon rank sum test with Bonferroni adjustment of multiple testing. We used connectomic analyses (R package "Connectome") (Raredon et al., 2019) to identify conserved patterns of cell-cell cross-talk between the ECs, SMCs and fibroblasts in the pulmonary artery (Raredon et al., 2019; Browaeys et al., 2020). Connectomtic analysis uses an algorithm to visualize intercellular signaling using ligand-receptor mapping. It filters single-cell data to identify the distribution of ligand and receptor z-scores and percent expression to identify cell-type specific communication patterns (edges) with increased statistical confidence. The thickness of the edges corresponds to the z-score (Raredon et al., 2019). Enriched terms analyses of phenotype (using MGI Mammalian Phenotype Level 4 2019 database) and signaling pathways (using WikiPathways 2019 Mouse database) were based on differentially expressed genes when comparing hypoxic with normoxic genetic expression (Chen et al., 2013; Kuleshov et al., 2016). The top results of the gene-set libraries of the collective functions of gene lists generated from the gene list of our single cell sequencing experiments were displayed and plotted as bar charts to show the top enriched terms in the chosen library based on their p-value (plotted as $-\log_{10}p$-value).

RESULTS

Hypoxia Alters Tissue-Level Properties

Biomechanical phenotyping of normoxic (n = 6) and hypoxic (n = 5) RPAs revealed a general structural stiffening in hypoxia despite modest changes in wall thickness (**Figure 2**). The mean pressure-diameter findings are shown at the vessel-specific optimal, or *in vivo*, axial stretch and similarly for the circumferential stress-stretch findings; the axial stress-stretch findings are shown at a common pressure of 15 mmHg. The increased structural stiffness was reflected further by a significant decrease in distensibility and associated increase in the calculated PWV. The modest decrease in wall thickness in hypoxia (inferred during *ex vivo* testing and confirmed via multiphoton microscopy; **Supplementary Figure 1**) implicated an increase in material stiffness in hypoxia, which in turn suggested a change in extracellular matrix. Material stiffness and elastically stored energy were computed using the four-fiber family constitutive relation, with associated best-fit material parameters (**Supplementary Table 1**). Calculated values of biaxial material stiffness (circumferential and axial) were greater for hypoxic than for normoxic vessels in the axial direction alone at diastolic, mean, and systolic pressures (5, 15, 25 mmHg, respectively), as shown in **Figure 2**. Hypoxia did not change the elastically stored energy at diastolic or mean pressures but did decrease it at systolic pressures (**Supplementary Figure 2**).

Hypoxia Induces Microstructural Changes, Notably Collagen Remodeling

Wall composition and characteristics of intramural collagen are shown in **Figure 3** for representative RPAs from normoxic and hypoxic mice. Movat-stained cross-sections of normoxic and hypoxic vessels suggested no major changes in composition (**Figures 3A–C**). Area fractions for normoxic and hypoxic RPAs were computed for elastin (37 ± 3.5% vs. 41 ± 4.4%, respectively, p = 0.43), collagen (42 ± 8.0% vs. 32 ± 7.8%, p = 0.40), cytoplasm (12% fraction ± 2.9% vs. 17 ± 3.3%, p = 0.27), ground substance (7% fraction ± 0.9% vs. 6 ± 0.8%, p = 0.20), and fibrin (2% fraction ± 0.3 vs. 4 ± 1%, p = 0.14). Pico-sirius red stained sections imaged with polarized light (**Figure 3D**) revealed, however, that medial collagen was reduced in hypoxic compared to normoxic vessels ($p < 0.05$). Alignment and orientation of collagen was assessed using multiphoton imaging, with characteristic images shown at 15 mmHg for both groups (**Figures 3E–H**); additional images are included in **Supplementary Figure 3** and **Supplementary Material**. The mean orientation of collagen fibers (primarily adventitial) was less axially directed for the hypoxic (10.8° ± 5.3°) than the normoxic (2.0° ± 2.1°) vessels (p = 0.20). Collagen fiber alignment was significantly greater for the hypoxic (κ = 14.3 ± 1.9) than the normoxic (κ = 7.0 ± 1.0) vessels (p = 0.02), where the parameter κ and width of distribution are inversely related (i.e., lower κ equals greater width of distribution and *vice versa*). To the author's knowledge, these are the first published measurements of collagen fiber alignment in pulmonary arteries of mice. Note, too, that immunohistochemistry delineated changes in these fibrillar collagens by type, I versus III, revealing a decrease in the former and increase in the latter with hypoxia (**Supplementary Figure 4**).

Pearson correlation analysis revealed that collagen fiber orientations correlated inversely with distensibility (R^2 = 0.88), but not wall thickness (R^2 = 0.07), as shown in **Figure 3I**. Collagen fiber orientation also correlated directly with axial material stiffness (R^2 = 0.77) but less so with circumferential stiffness (R^2 = 0.48), as shown in **Figure 3J**. Multiphoton imaging also revealed an increase in the density of adventitial cells in the hypoxic compared with the normoxic arteries (**Figure 3K**). Similar results were found in H&E-stained paraffin samples (**Supplementary Figure 5**), noting that the ratio of the medial : adventitial cross-sectional areas did not change (**Supplementary Figure 6**). Immunohistochemistry and immunofluorescence were used to confirm that the layers and morphology of cells of the intimal, medial, and adventitial layers were not co-located (**Supplementary Figure 5**). Recall that paraffin-embedded

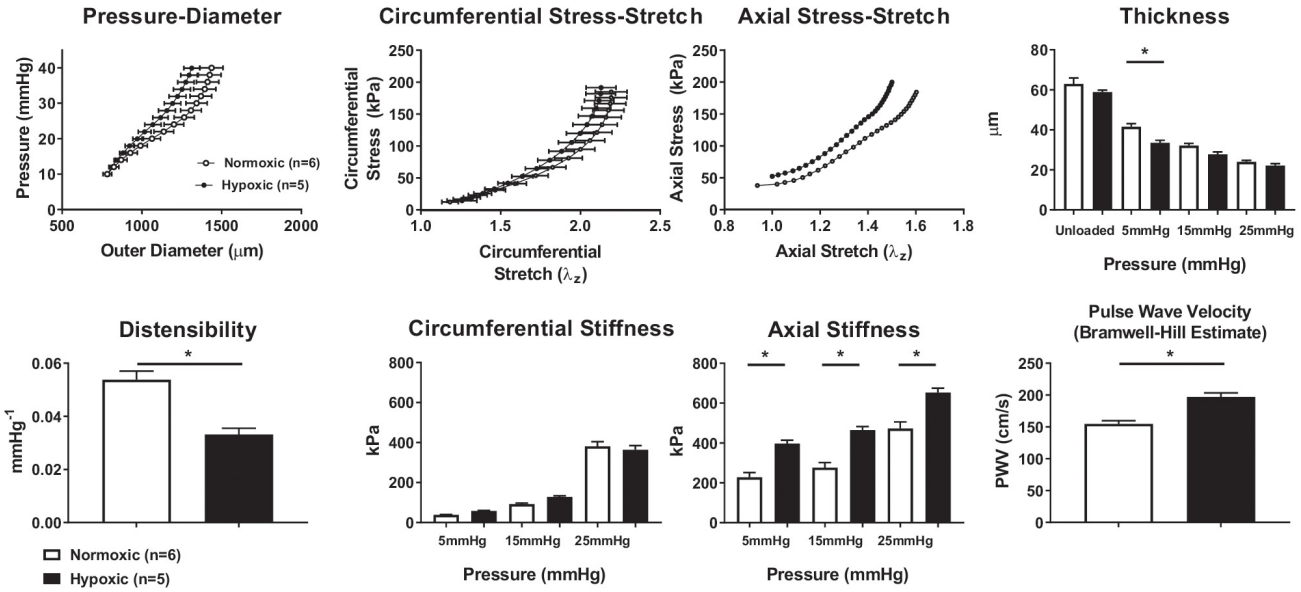

FIGURE 2 | Mechanical properties of normoxic and hypoxic mouse pulmonary arteries. **(Top row)** Data collected (pressure, arterial diameter, stretch) or calculated (stress) from cannulated normoxic (n = 6) and hypoxic (n = 5) right pulmonary arteries of C57BL6J mice using a computer-controlled testing device. Pressure-diameter measurements were at vessel-specific optimized axial stretch (mean ± SEM). Stress-stretch measurements were taken with the vessel at 15 mmHg. Wall thickness measurements for normoxic (n = 6) and hypoxic (n = 5) right pulmonary artery vessels at various pressures. Unloaded (zero mmHg intraluminal pressure) wall thickness was measured by histologic analysis and MatLab. Loaded (5, 15, 25 mmHg) wall thickness measurements were calculated based on mechanical measurements. Despite some differences at individual pressures, there is no overall difference in thickness of normoxic and hypoxic vessels. **(Bottom row)** Mechanical properties calculated from mechanical testing and fit to the four-fiber constitutive relation, including distensibility, circumferential stiffness, axial stiffness, and PWV. There is a significant decrease in distensibility observed in hypoxic vessels. The circumferential stiffness of hypoxic and normoxic pulmonary arteries is similar at lower pressures; however, at 25 mmHg, the circumferential wall stress in hypoxic pulmonary arteries tends to decrease. The axial stiffness calculated for hypoxic vessels is greater than normoxic vessels at diastolic, mean, or systolic pressures (5, 15, 25 mmHg, respectively). The changes in structural and mechanical properties of the arterial wall and distensibility due to hypoxic exposure result in a significant increase ($p < 0.05$) in PWV of the right pulmonary artery of mice at 15 mmHg. *$p < 0.05$.

histological cross-sections are sampled at ∼5 μm increments along the length of the artery, whereas multiphoton imaging is along an entire 500 μm length. Noting that most of the collagen fibers were in the adventitia, enriched terms analysis of phenotype and signaling pathways are shown for fibroblasts in **Figure 3L**. The bar chart shows the top enriched term search results based on their p-value (plotted as $-\log_{10}p$-value). Differential gene expression in fibroblasts due to hypoxia associated with phenotypic changes in extracellular matrix previously associated with inflammation and endovascular morphology. Pathways associated with the differentially expressed genes observed due to hypoxia included PI3K-Akt-mTOR, TGFβ, and p38-MAPK, as highlighted in **Figure 3M**. Differentially expressed genes associated with NF-kB, TLR signaling, and IL-3 signaling were also observed. There was a large increase in the number of ribosomal genes expressed in response to hypoxic exposure.

Hypoxia Alters Vasoactive Function

SMCs endow the pulmonary artery with the ability to vasoconstrict and vasodilate, which were assessed as responses to vasoactive substances at a fixed pressure (15 mmHg) and optimized specimen-specific axial stretch (**Figure 4**), both over time (panels A and B) and as a percent change based on normalized outer diameter at the end of 15 minutes (C and D). The normalized reduction in outer diameter during vasoconstriction (KCl and PE) of control mice (normoxia) was 31 and 35%, respectively, at 15 min, similar to previous findings (Ramachandra and Humphrey, 2019), while hypoxic exposure (10% FiO_2 for 3–6 weeks) resulted in a statistically significant decrease ($p < 0.05$) in this measure of contractility *ex vivo* for both KCl (14%) and PE (28%). Multiphoton imaging of the SMCs yet revealed that their mean orientation was more circumferential (θ–90°) in hypoxic (84°–88°) than in normoxic (63°–86°) vessels (panel E). SMC alignment was also greater in hypoxic (κ = 14.12–20.79) than in normoxic (κ = 7.59–9.03) vessels (panel F). Enriched terms analysis of phenotype and signaling pathways are shown for SMC cells (panel G). SMC differential gene expression due to hypoxic exposure associated with phenotypic changes in morphology, matrix, and cell cycle. Pathways associated with the differentially expressed genes observed due to hypoxia include selenoproteins, proteins of myocontractility, and oxidative stress. Differentially expressed genes associated with PI3K-Akt-mTOR and Ras-MAPK intracellular pathways, as highlighted in **Figure 4G**. There was a large increase in the number of ribosomal genes expressed in response to hypoxic exposure.

Endothelial cell-dependent vaso-dilatation was measured in response to acetylcholine (Ach), with further functional

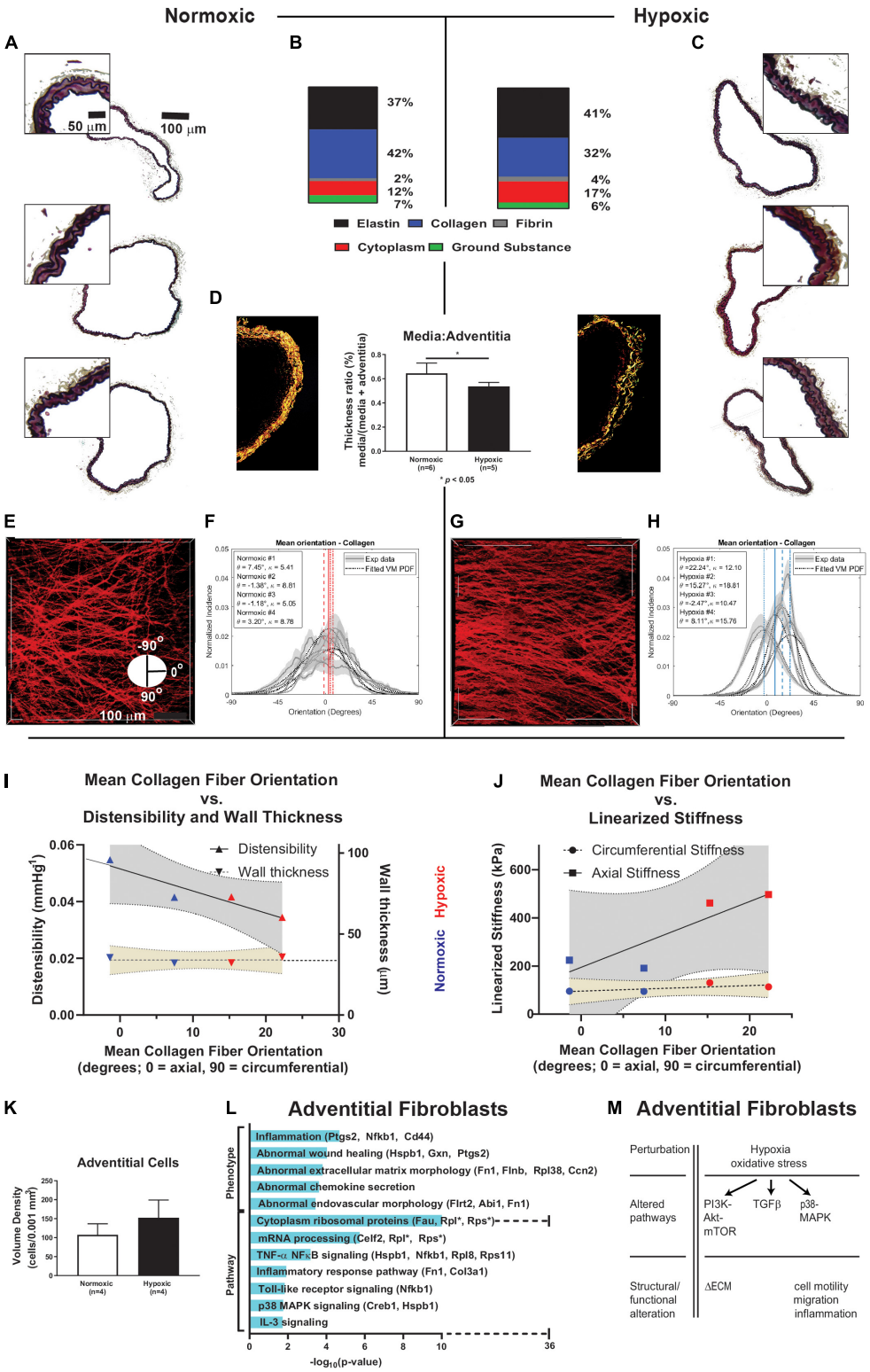

FIGURE 3 | Composition analyses, collagen orientation correlation with stiffness. **(A,C)** Paraffin embedded, Movat-stained cross-sectional imaging of representative pulmonary arteries from normoxic mice (n = 3) and hypoxic mice (n = 3). The complete pulmonary arteries are composite images of 20× magnification stitched together using Microsoft Image Editor. Small portions of the wall for these samples were enlarged with equal proportion for closer visual examination and comparison. **(B)** The area fractions for elastin (from VVG), cytoplasm (from MTC), and ground substance and fibrin (from Movat) were computed based on n = 5 samples for

(Continued)

FIGURE 3 | (Continued)
each stain. Area fraction of collagen was computed as 1 - area fraction of elastin plus cytoplasm plus ground substance. **(D)** The media to adventitia thickness ratio was calculated using picosirius red staining and imaged using polarized light to identify media and adventitial collagen components, revealing significant decrease in medial collagen in hypoxic samples ($n = 5$) compared to normoxic samples ($n = 6$), $p < 0.05$. **(E–H)** Representative 2-photon images of collagen fibers (red) at 15 mmHg for a normoxic and hypoxic vessel. Collagen fiber alignment (κ) and orientation (θ) analyses for normoxic ($n = 4$) and hypoxic ($n = 4$) vessels at 15 mmHg. Collagen fiber alignment is represented by the width of the collagen fiber orientation distribution, κ, where κ and width of distribution are inversely related. Collagen fiber orientation shows distribution of collagen fiber alignment ranging from the axial direction (0 degrees, running the length of the pulmonary artery) to the circumferential direction (-90 or 90 degrees, running around the circumference of the pulmonary artery and orthogonal the axial direction). Hypoxic exposure causes a circumferential shift in collagen fibers. **(I,J)** Linear least squares fit of data with 95% confidence bands for distensibility ($R^2 = 0.88$), arterial wall thickness ($R^2 = 0.07$), and linearized axial stiffness ($R^2 = 0.77$) and circumferential stiffness ($R^2 = 0.48$) with respect to mean collagen fiber orientation. Material stiffness of pulmonary arteries correlates with collagen fiber alignment, arterial wall thickness does not. Circumferential orientation of collagen fibers directly correlates with axial stiffness. **(K)** 2-photon imaging revealed an increase in the cell density of adventitial cells of hypoxic pulmonary arteries ($n = 4$) compared to normoxic ($n = 4$). Cell numbers were then normalized by a volume of 0.001 mm^3 to allow consistent comparisons. We found similar results in H&E-stained paraffin samples (normoxic $n = 6$, and hypoxic $n = 5$) as shown in **Supplementary Figure 5**. **(L)** Enriched terms analysis of phenotype (using MGI Mammalian Phenotype Level 4 2019 database) and signaling pathways (using WikiPathways 2019 Mouse database). The bar chart shows the top enriched terms in the chosen library based on their p-value (plotted as $-\log_{10}p$-value). Fibroblast differential gene expression due to hypoxic exposure is associated with phenotypic changes in extracellular matrix previously associated with inflammation and endovascular morphology. Pathways associated with the differentially expressed genes observed due to hypoxia include TNF-kB, TLR signaling, p38-MAPK, and IL-3. There is a large increase in the number of ribosomal genes expressed in response to hypoxic exposure. **(M)** Schematic summary of hypoxia-induced alterations of cellular pathways and function in fibroblasts based on transcriptomic and functional data. ECM = extracellular matrix.

assessment following eNOS inhibition with L-NAME, the latter shown in panel H. The normalized baseline outer diameter in this case (1.0) is the vessel-specific outer diameter following maximal contraction with PE and after 10 minutes exposure to 10 μM Ach. Panel I reveals no significant hypoxia-induced change in EC induced vasodilatation *ex vivo*. The authors are not aware of previously published data regarding EC function in the *ex vivo* mouse pulmonary artery. Multiphoton imaging further revealed an increase in the density of intimal cells of hypoxic compared with normoxic vessels (Panel J, images, and panel K, quantitative). Results from H&E-stained paraffin-embedded sections were consistent (**Supplementary Figure 5**). Enriched terms analysis of phenotype and signaling pathways for ECs (panel L) revealed that differential gene expression due to hypoxic exposure associated with phenotypic changes in focal adhesion, endovascular morphology, thrombosis, neovascularization, and protection against ischemia. Pathways associated with the differentially expressed genes observed due to hypoxia include TGFβ and PI3K-Akt-mTOR signaling and endothelial processes such as thrombosis (prostaglandins and thromboxane), oxidative phosphorylation, and vasoactivity. These changes and associated structural or functional alterations are summarized in **Figure 4L**. There was a large increase in the number of ribosomal genes expressed in response to hypoxic exposure.

Hypoxia Resulted in Hundreds of Differentially Expressed Genes in Resident Cell Types

We identified 3,142 resident cells from a segment of the pulmonary artery from one mouse exposed to hypoxic conditions (FiO_2 10%) for six weeks and one age-matched control mouse exposed to normoxic conditions (FiO_2 21%). These cells were represented on a uniformed manifold approximation and projection (UMAP) of cells clustered by genetic markers and cellular origin for normoxia versus hypoxia (**Figure 5**). Identification of resident cell types was based on their expression of marker genes as shown in **Figure 5B**: endothelial cells (*Dkk2, Gja5, Cxcl12, Bmx, Efnb2, Fbln2, Gja4, Dll4, Hey1, Htra1, Cldn5, Cdh5,* and *Bmp6*), smooth muscle cells (*Tagln, Acta2, Myh11, Mustn1*), and fibroblasts (*Tshz2, Vcan, Col1a1, Col1a2, Col14a1, Fbln1, Dcn, Lum, Aspn, Pi16, Serpinf1, Cygb,* and *Htra3*). There was a decreased proportion of SMCs and increased proportion of ECs in the hypoxic sample, as shown in the inset of **Figure 5A**. **Figure 5C** shows heat maps for differentially expressed genes in ECs, SMCs, and fibroblasts. There were 331 differentially expressed genes in hypoxic ECs, with higher expression associated with hypoxia-induced proteins for cellular differentiation and proliferation and angiogenesis such as *Igfb7, Ifg1r, Igf2r, Myc, Sox5, Lgals1* and lower expression of genes associated with oxidative respiration metabolism such as *Atp5mpl, mt-Atp6Atp5e*, and *Cox7c*. Hypoxic ECs also had lower expressions of intercellular junction proteins such as *Icam2, Gja5, Cdh11*, and *Cldn5* with higher expression of cytoskeletal and extracellular proteins such as *Fbln5, Actn1, Eln, and Ccn2*, and *Csgalnact1*. There is higher expression of genes associated with endothelial-mesenchymal transitioning, such as *Klf2, Fn1, Bmp6, Smad6, Tcf4*, and *Eng* (Medici and Kalluri, 2012; Chen et al., 2016). Finally ECs had a higher expression of chemotactic proteins such *Vwf* and *Hbegf* in hypoxia as well as *Edn1*, which encodes endothelin-1, a potent vaso-constrictor. There were 107 differentially expressed genes in hypoxic SMCs, including a higher expression of genes associated with cytoskeletal rearrangement such as *Tgfb3, Vim, Actn4, Tnnt2, Col18a1, Ecm1*, and *Smtn* (van der Loop et al., 1996; Worth et al., 2001; Chen et al., 2016; Pedroza Albert et al., 2020) and cell signaling such as *Gne, Pde10a*, and *Map3k19*. Finally, there were 113 differentially expressed genes in hypoxic fibroblasts, with higher expression of genes associated with cellular adhesion and migration such as *Cd44, Rock2* and *Fn1* and the degradation of extracellular matrix and the ubiquitination-proteosome system such as *Smurf2, Tnfaip3, and Ntn4*. This is the first single cell RNA sequencing of mouse pulmonary arteries of which the authors are aware, noting that the induced hypoxia resulted in an increase in right ventricular pressure and cavity volume (**Supplementary Figure 7**).

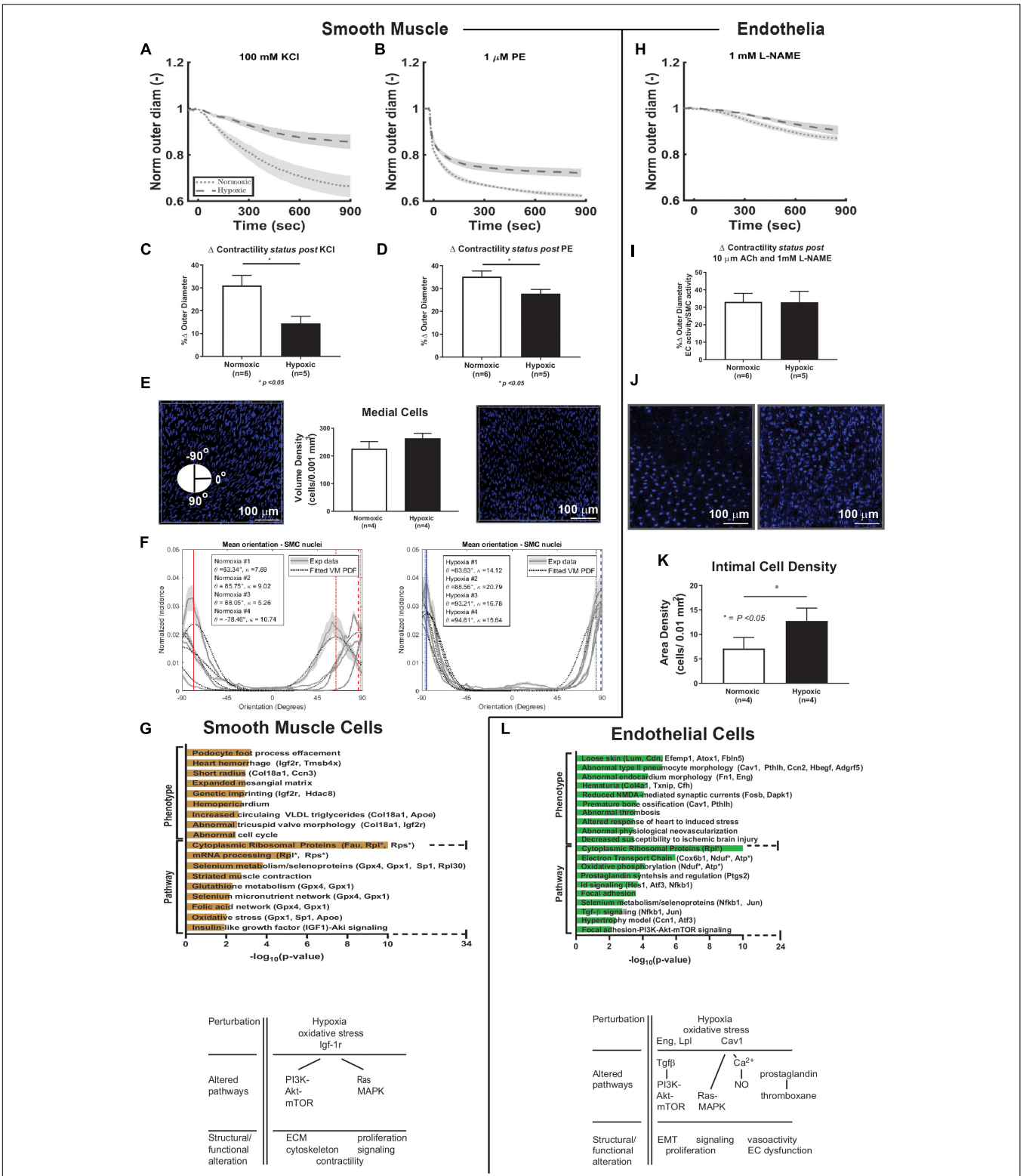

FIGURE 4 | Smooth muscle cell and endothelial cell functional-transcriptomics. **(A,B)** Vaso-constriction response to vasoactive substances, potassium chloride (KCl) and phenylephrine (PE), as a function of time plotted as mean (dashed and dotted lines) ± standard error from the mean (shade) for normoxic (dotted, $n = 6$) and hypoxic (dashed, $n = 5$) samples. Vessels were maintained at a fixed pressure (15 mmHg) and specimen-specific optimized axial stretch. **(C,D)** Percent change in contractility based on normalized outer diameter change at the end of 15 min exposure to KCl and PE. There is a significant decrease in contractility of hypoxic

(Continued)

FIGURE 4 | (Continued)
vessels compared to normoxic vessels for both vasoactive substances ($p < 0.05$). **(E)** Cell quantification in medial layers. Cellular density measurements were made using 2-photon imaging of normoxic ($n = 4$) and hypoxic ($n = 4$) vessels and normalized by a volume of 0.001 mm^3. Representative images from 2-photon imaging are shown. Similar measurements were made on the number of cells per layer based on counting nuclei using H&E stained paraffin-embedded cross-sections of right pulmonary arteries using light microscopy at 20× magnification as shown in **Supplementary Figure 5**. An advantage of 2-photon imaging is its ability to samples larger regions of the vessel than histology, which only samples one cross-section of the artery at a time. **(F)** Analysis of SMC orientation based on 2-photon imaging reveals increased alignment of these cells following hypoxic exposure and a shift in orientation toward the circumferential direction similar to the phenomenon that we observed in collagen fibers in hypoxic pulmonary arteries. **(G)** Enriched terms analysis of phenotype (using MGI Mammalian Phenotype Level 4 2019 database) and signaling pathways (using WikiPathways 2019 Mouse database). The bar chart shows the top enriched terms in the chosen library based on their p-value (plotted as $-\log_{10}p$-value). SMC differential gene expression due to hypoxic exposure is associated with phenotypic changes in morphology, matrix, and cell cycle. Pathways associated with the differentially expressed genes observed due to hypoxia include selenoproteins, proteins of myocontractility, and oxidative stress. There is a large increase in the number of ribosomal genes expressed in response to hypoxic exposure. Hypoxia-induced alterations of cellular pathways and function in SMC are summarized in the schematic diagram. **(H)** Vaso-dilatation measured following exposure to acetylcholine (Ach) followed by inhibition of eNOS release by L-NAME. Effects of L-NAME on vessel outer diameter over time plotted as mean (dashed and dotted lines) ± standard error from the mean (shade) for normoxic (dotted, $n = 6$) and hypoxic (dashed, $n = 5$) samples. Vessels were maintained at a fixed pressure (15 mmHg) and specimen-specific optimized axial stretch. **(I)** Percent change in vasoactivity based on normalized outer diameter change at the end of 15 min exposure to L-NAME. There was no significant change when comparing hypoxic and normoxic vessels. **(J)** Representative images from 2-photon imaging of the intimal layer. **(K)** Cell quantification of intimal layer. Cellular density was computed as number of cells per surface area and normalized by an area of 0.01 mm^2 from 2-photon images. **(L)** Enriched terms analysis of phenotype (using MGI Mammalian Phenotype Level 4 2019 database) and signaling pathways (using WikiPathways 2019 Mouse database). The bar chart shows the top enriched terms in the chosen library based on their p-value (plotted as $-\log_{10}p$-value). EC differential gene expression due to hypoxic exposure is associated with phenotypic changes in focal adhesion, endovascular morphology, thrombosis, neovascularization, and protection against ischemia. Pathways associated with the differentially expressed genes observed due to hypoxia include oxidative phosphorylation, prostaglandins, NFkB, TGFb, and PI3K-Akt-mTOR signaling. There is a large increase in the number of ribosomal genes expressed in response to hypoxic exposure. Hypoxia-induced alterations of cellular pathways and function in EC are summarized in the schematic diagram. ECM = extracelluluar matrix. EMT = endothelial-mesenchymal transitioning. $^*p < 0.05$.

Differential connectomic analysis identifies changes in cell-type-specific molecular communications that occur among ECs, SMCs, and fibroblasts when comparing hypoxic and normoxic conditions based on previously described protein interactions (**Figure 6**). These results demonstrate how differentially expressed genes within one cell type may affect gene expression in another cell type, ultimately altering structure and function at the tissue level. *Fn1/Vim-Cd44* connections between ECs and fibroblasts in the RPA involves a pathway that has been associated with ECM-cell receptor interactions (Geng et al., 2019) and endothelial-to-mesenchymal transition (Endo-MT) (Goveia et al., 2020). The *Tgfb3-Eng* connection between SMCs and ECs is associated with EC adhesion and regulation of ECM formation (Cheifetz et al., 1992; Kaartinen et al., 1995). *Hbegf-Cd9* signaling seen in the connections between ECs and fibroblasts has previously been associated with preservation of membrane barrier function (Schenk et al., 2013) and enhancing cell viability (Takemura et al., 1999). Enriched terms analysis of phenotype and signaling pathways based on genes identified through differential connectome analysis revealed associations with abnormal lung vasculature, altered collagen deposition, alterations of cell cycle, regulation of actin cytoskeleton, TGF-beta signaling, and alterations in focal adhesion. This captures phenomena and pathways of importance that we observed in this study. These are the first time that these communications between the resident cell types of the mouse pulmonary arteries resulting from hypoxic exposure have been described in this manner.

DISCUSSION

This study reports previously undescribed changes in the orientation of collagen fibers and similarly SMCs in the mouse RPA following 3-6 weeks of hypoxic exposure, with associated structural stiffening and decreased contractility. Cell-specific differentially expressed genes suggested potential molecular mechanisms and pathways driving these changes.

That the pulmonary artery stiffening in hypoxia observed herein appears to result more from collagen remodeling than increased accumulation is in contrast to hypertension-induced stiffening of the aorta, the largest elastic artery of the systemic circulation, which results from increased collagen largely in the adventitia (Bersi et al., 2016, 2017; Oh Young et al., 2017). This finding has multiple implications, including differential species-dependent responses. Previous reports detail thickening of the branched pulmonary arteries from increased adventitial collagen in rats due to acute hypoxic exposure ranging from hours to 30 days (Fung and Liu, 1991). That the collagen fiber reorientation toward the circumferential direction correlated herein with the increased material stiffness suggests that remodeling is a dominant mechanism of pulmonary artery stiffening in mice in the setting of periods of hypoxia for greater than 3 weeks. Association of collagen disorientation with arterial stiffening is relatively new (Cavinato et al., 2020, 2021; Pursell and Valdez-Jasso, 2020). Increased material stiffness due to extracellular remodeling has been proposed as an underlying mechanism of disease in humans with pulmonary hypertension, thus this may have broad clinical importance (Milnor et al., 1969; Lammers et al., 2008; Westerhof et al., 2009; Saouti et al., 2010; Stevens et al., 2012; Pagnamenta et al., 2013; Dragu et al., 2015; Ghio et al., 2015; Hadinnapola et al., 2015). Increased pulmonary arterial stiffness has been shown to negatively affect right ventricular cardiac function, which is the primary predictor of survival in humans with pulmonary hypertension (Dupont et al., 2012; Stevens et al., 2012; Douwes et al., 2013; Pellegrini et al., 2014; Al-Naamani et al., 2015; Blyth et al., 2017). Increased collagen deposition has been speculated to result from chronic hypoxic

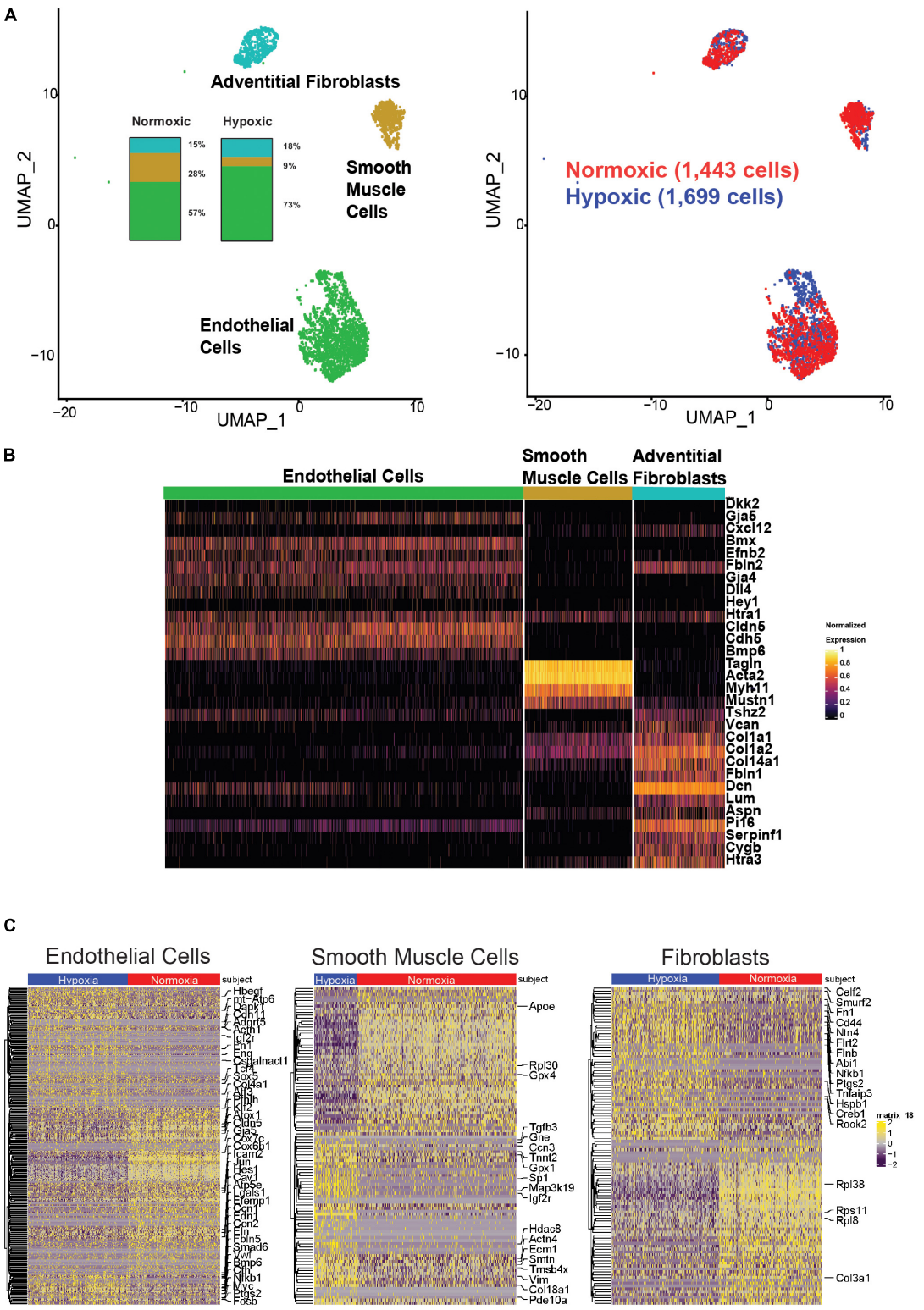

FIGURE 5 | Single cell RNA sequencing of mouse pulmonary artery resident cells. **(A)** Uniform Manifold Approximation and Projection (UMAP) representation of cells clustered by expressed genes. About 1,443 cells from hypoxic PA [1,053 endothelial cells (EC), 127 smooth muscle cells (SMC), 263 adventitial fibroblasts (FB)]. About 1,699 cells from normoxic PA (967 EC, 479 SMC, 253 FB). Although there are similar number of cells overall between normoxia and hypoxia samples, there is a decrease in the proportion of SMC in the hypoxia sample and an increase in the proportion of EC. **(B)** Heatmap identifies cell markers used to identify PA resident

(Continued)

FIGURE 5 | (Continued)
cell types. **(C)** Heat maps of differentially expressed genes by cell-type. EC: 331 differentially expressed genes in were found in hypoxic EC. Hypoxic arterial EC show higher expression of genes associated with hypoxia-induced proteins, cellular differentiation, proliferation and angiogenesis and lower expression of genes associated with oxidative respiration metabolism. Hypoxic EC are associated with lower expressions of intercellular junction proteins with higher expression of cytoskeletal and extracellular genes. There is higher expression of genes associated with endothelial-mesenchymal transitioning (Medici and Kalluri, 2012; Chen et al., 2016) and a higher expression of genes associated with chemotaxis and vasodilators. SMC: 107 differentially expressed genes were found in hypoxic SMC. Hypoxic SMCs show a higher expression of genes associated with cytoskeletal rearrangement (van der Loop et al., 1996; Worth et al., 2001; Chen et al., 2016; Pedroza Albert et al., 2020) and cell signaling. Fibroblasts: 113 differentially expressed genes were found in hypoxic fibroblasts. Fibroblasts show a higher expression of genes associated with cellular adhesion and migration, degradation of extracellular matrix and the ubiquitination-proteosome system.

exposure (Morrell et al., 1995a,b, 1997), though others have suggested that variable degradation and deposition of collagen associates with pulmonary arterial remodeling in animal hypoxia models and humans with pulmonary arterial hypertension (Zhang et al., 2020). Regardless, changes in the extracellular matrix influences changes in SMC phenotype (Safdar et al., 2014; Žaloudíková et al., 2019; Chen et al., 2020). The need to identify parameters to assess the stiffness of the pulmonary artery has been emphasized further due to the important role that stiffening of the pulmonary artery plays in diseases of the lungs such as pulmonary hypertension and chronic obstructive pulmonary disease (Sanz et al., 2008; Vivodtzev et al., 2013; Schäfer et al., 2016; Weir-McCall et al., 2018). Studies to validate the correlation of altered collagen orientation and pulmonary arterial stiffness in human tissue are underway. This study reveals further that intercellular communications between the resident cells of the pulmonary arteries play an important role in this remodeling. Further investigation is needed to better understand the underlying mechanism of the collagen disorientation and how to mitigate it under hypoxic conditions.

We confirmed that pulmonary arteries from mice have impaired contractility due to hypoxic exposure. In general, such impairment could result from dysfunctional EC signaling and/or changes in SMC phenotype (Chan and Vanhoutte, 2013). Interestingly, however, hypoxic exposure has been reported to result in EC-mediated augmentation of pulmonary and systemic arterial vasoconstriction (Chan and Vanhoutte, 2013) with sustained SMC contractility assumed to drive pulmonary vascular remodeling (Song et al., 2014). Yet, precise quantification of vasoconstriction of the pulmonary artery due to acute or chronic hypoxia has remained wanting. In the current study, we observed greater than 10% impairment of contractility of the large, elastic pulmonary artery due to chronic hypoxia. Intimal cell proliferation suggested EC proliferation in response to the hypoxic exposure, while the number of SMCs within the tunica media remained relatively unchanged. The net decreased vasocontractility despite no decrease in cell number thus suggests that there is altered function in the ECs, the SMCs, or the interaction between these cells. Further investigation is necessary to determine which of these is occurring as a result of hypoxic exposure.

Despite the increased number of intimal cells and increased expression of the endothelial-secreted vaso-constrictor peptide endothelin-1 in our study, there was no change in vasodilatory ability of the pulmonary arteries exposed to hypoxia. The decreased expression of cell adhesion genes and increased expression of Endo-MT markers suggest that ECs changed their phenotypes in response to the hypoxia (Marsboom and Rehman, 2018). There are conflicting data regarding EC proliferation due to hypoxia, some reporting EC proliferation (Fung and Liu, 1991; Porter et al., 2014), some reporting decreased ECs (Junhui et al., 2008), and some no change (Yu and Hales, 2011). It should be noted that these studies were performed with isolated ECs, separated from their natural milieu. ECs are normally juxtaposed with the innermost layer of SMCs though separated by the basement membrane and internal elastic lamina. The results herein likely reflect EC-SMC-ECM interactions that are difficult to replicate with *in vitro* experiments (Ochoa et al., 2008). Our findings may also be due to our focus on the proximal pulmonary arteries rather than more distal smaller pulmonary arteries. Regional differences of vascular biomechanics are well-described in the systemic circulation (Murtada and Humphrey, 2018). There has been an emphasis on muscular arteries and small vessels in pulmonary hemodynamics and wall mechanics, with less attention to the large elastic pulmonary artery. Previous studies have identified increased cellular density of endothelial cells in rat pulmonary arteries during the first weeks of hypoxic exposure without explanation of the cause (Fung and Liu, 1991). This study suggests that this intimal cell proliferation may reflect Endo-MT transitioning, which is supported by our observation of differentially expressed genes such as *Klf2, Fn1, Bmp6, Smad6, Tcf4*, and *Eng* (Medici and Kalluri, 2012; Chen et al., 2016). Signs of transdifferentiation also include the loss of cytoskeletal cell-cell contacts and increased transcripts for factors such as *Icam2, Gja5, Cdh11*, and *Cldn5* (Frid et al., 2002). Epigenetic changes are largely involved with Endo-MT; therefore, RNA expression may not be the optimal measure of Endo-MT. In ECs, TGF-Smad signaling pathways help bring about Endo-MT (Kovacic et al., 2019). *In vivo* studies have also shown that dysregulation of BMPR2-Wnt interactions in response to serum starvation impairs proliferation of pulmonary arterial ECs lost to apoptosis (de Jesus Perez et al., 2009). Dysregulated MAPK and Wnt signaling, as observed in our study, has been associated with a pro-proliferative, anti-apoptotic EC phenotype resulting in vascular remodeling (Awad et al., 2016). MAPK pathways comprise evolutionarily conserved kinases such as extracellular signal–regulated kinase (ERK1/2), p38 MAPK, and c-Jun NH2-terminal kinase (JNK). They receive and integrate extracellular or intracellular stimuli, regulating important cellular processes including proliferation, differentiation, metabolism, migration, survival, and apoptosis (Roux and Blenis, 2004).

Our study found decreased vaso-contractility of the pulmonary artery despite little change in SMC quantity. We hypothesized that this represented a change in SMC phenotype. The combination of decreased contractility coupled with altered gene expression of cytoskeletal proteins and increased differential

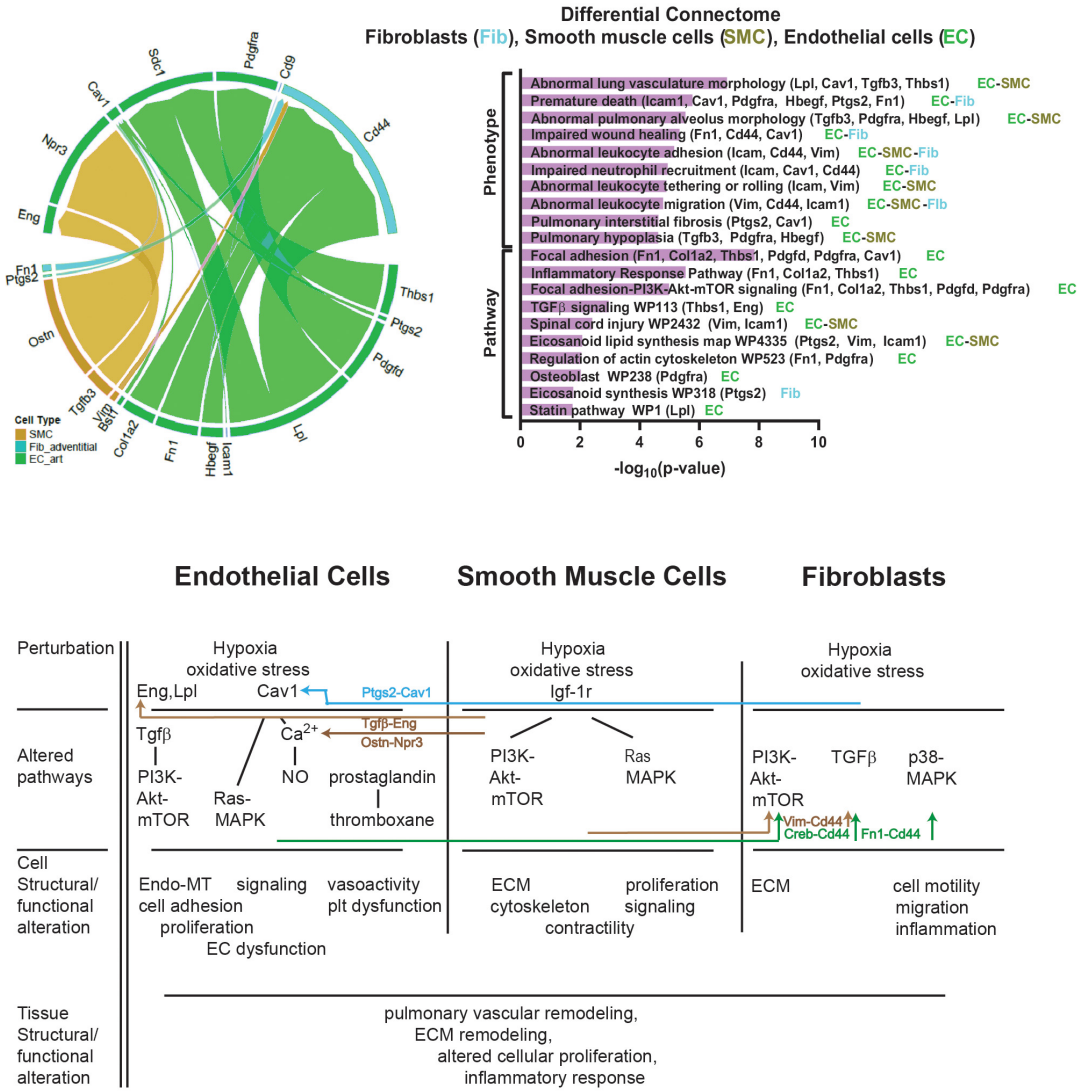

FIGURE 6 | Hypoxia-normoxia differential connectome of mouse pulmonary artery resident cells. **(Left)** Differential connectome mapping comparing hypoxic and normoxic communication based on scRNAseq data to identify differences between hypoxic and normoxic cell-cell signaling. Differential connectomic analysis identifies and visualizes the major perturbed cell–cell communication pathways between single cell data from similar cell types under two different conditions, in this case hypoxia versus normoxia, using ligand-receptor connectomic analysis (Raredon et al., 2019). Connecomtic analysis is an algorithm to visualize intercellular signaling using ligand-receptor mapping. It filters single-cell data to identify the distribution of ligand and receptor z-scores and percentage expression to identify cell-type specific communication patterns (edges) with increased statistical confidence. The thickness of the edges is proportional to the ligand and receptor z-scores. The bottom half of the circle identifies the ligand gene and "sender" cell-type, the top half of the circle identifies the receptor gene and "receiver" cell-type. **(Right)** Enriched terms analysis of phenotype (using MGI Mammalian Phenotype Level 4 2019 database) and signaling pathways (using WikiPathways 2019 Mouse database) based on genes identified through differential connectome analysis. The bar chart shows the top enriched terms in the chosen library based on their *p*-value (plotted as $-\log_{10}p$-value). Genes associated with the identified phenotype or pathway are listed along with the cell-type in which these genes were found to be expressed. The differential connectome cell-cell signaling genes identified accurately represent observed phenomena and pathways associated with phenomena observed in our experiments including abnormal lung vasculature, fibrosis, alterations of cell cycle, regulation of actin cytoskeleton, TGF-beta signaling, and alterations in focal adhesion. Whether this type of analysis hold predictive abilities requires further investigation. **(Bottom)** Potential cell–cell interactions between based on the differential connectome demonstrating how differentially expressed genes from one cell type may influence gene expression and cellular pathways in another cell type. ECM = ECM = extracellular matrix. Endo-MT = endothelial-mesenchymal transitioning. EC = endothelial cell.

expression of genes associated with cytoskeletal rearrangement (*Tgfb3, Vim, Actn4, Tnnt2, Col18a1, Ecm1*, and *Smtn*) (van der Loop et al., 1996; Worth et al., 2001; Chen et al., 2016; Pedroza Albert et al., 2020) and cell signaling (*Gne, Pde10a*, and *Map3k19*) suggests a shift from contractile to synthetic SMC phenotype (Worth et al., 2001; Rensen et al., 2007; Branchetti et al., 2013; Frismantiene et al., 2018). The differentially expressed genes associated with cytoskeletal rearrangement and the observed change of SMC orientation and alignment suggest further that the medial SMCs may have changed their

orientation to align better with the stress field resulting from newly deposited or realigned adventitial collagen fibers having more of a circumferential orientation. The mechanism of this non-local phenomenon remains unclear, but contraction of SMCs reduces overall wall stress by reducing stretch in the extracellular matrix, including collagen fibers, as we observed in our mechanical measurements of this study. Therefore, (re)alignment of SMCs and collagen fibers may serve as a compensatory mechanism within pulmonary arteries to optimize the reduction of wall stress resulting from greater distension. Numerous studies have demonstrated SMC proliferation following hypoxic exposure; however, the majority of these studies have focused on medium-to-small arteries within the lungs rather than the large, elastic pulmonary arteries and many were performed *in vitro* (Minamino et al., 2001; Sodhi et al., 2001; Frid et al., 2002; Chan and Vanhoutte, 2013).

A unique aspect to this study is that scRNA sequencing and connectomic analyses allowed us to observe intercellular communication among ECs, SMCs, and fibroblasts while they remain juxtaposed in their native milieu of the pulmonary artery and exposed to hypoxia. This is the first scRNA sequencing analysis and the first connectome of pulmonary arteries in mice. Our results validate previously described differential gene expression due to hypoxic exposure, including increases in HIF, Wnt, TGFβ, and BMP related genes in ECs as well as tyrosine-kinase receptors, fibroblast growth factors, and cytoskeletal protein RNA in SMCs that have been associated with hypoxic animal models and humans with chronic hypoxia due to pulmonary arterial hypertension (Chan and Vanhoutte, 2013; Lei et al., 2016; Tao et al., 2018). We hypothesize that endothelial sensing of hypoxia triggers altered collagen orientation toward the circumferential direction, thus increasing arterial wall stiffness. We suspect that SMCs alter their orientation to better align with newly deposited or realigned collagen fibers to reduce increased overall wall stress in the pulmonary artery resulting from hypoxia. We also suspect that these changes constitute positive feedback driving continued changes due to chronic hypoxic exposures. It is unclear if these changes would continue after hypoxic exposure ceases or if these changes are reversible.

This study demonstrates the potential benefit of combining mechanical testing and imaging with cell-specific differentially expressed gene mapping and applying it to the pulmonary circulation in conjunction with transcriptomic analysis. For example, our ability to use this method to associate stiffening of the pulmonary artery with PWV may prove beneficial. Increased PWV resulting from large arterial stiffening has been associated with proinflammatory responses (increased TLR2, NF-kB activation) in pulmonary arterial ECs *in vitro* and in intralobar pulmonary arterial ECs from humans with idiopathic pulmonary arterial hypertension (Tan et al., 2014). *In vitro* studies have also demonstrated that increased flow pulsatility increased signals of inflammation and pulmonary vascular EC proliferation (*VEGF, ICAM, E-selectin, MCP-1, Flt-1*) (Li et al., 2009). We observed similar increases in gene expression of transcription factors (*Nfkb1*) and EC proliferation (*Icam1, Icam2, Flt1*) in hypoxic mice. However, we also observe how these and other changes in gene expression in ECs affect the SMCs and fibroblasts in the pulmonary arterial environment. This demonstrates that our current method of mechanical testing combined with scRNA sequencing is capable of identifying underlying mechanisms associated with increased PWV in mice following hypoxic mice. Recent evidence has suggested that failures of therapies to reduce pulsatile flow associated with arterial stiffening in patients with pulmonary arterial hypertension predicts poor clinical outcomes but the mechanisms underlying this phenomenon remain unclear (Malhotra et al., 2016; Ghio et al., 2017). A functional genetics approach as presented here applied to pulmonary arterial stiffening in humans may reveal potential mechanisms of disease or therapeutic targets. Next steps in the evolution of this method will need to include systems-level approaches to discern which of the large number of differentially expressed genes and signaling pathways have the greatest impact on functional changes and whether those impacts are protective or maladaptive. Additional methods of analysis, such as proteomics, will also be necessary to bridge transcriptomics and tissue dynamics to help identify future targets for interventions to reduce deleterious changes in pulmonary arterial structure and function while promoting compensatory changes.

Our study is limited by its small sample sizes and failure to evaluate the effects of sex on these findings; the primary goal here, however, was to establish a novel workflow. We intend to apply this method in larger studies to provide the necessary statistical power in the future. Our results are also limited by a lack of protein level analysis to validate the genetic expressions we observed. We also intend to augment our gene discovery to tissue multi-disciplinary approach with protein level investigation in future studies. Finally, despite the changes in gene expression and pathways that we observed, our study is limited in its ability to differentiate which genes or pathways are compensatory and which are maladaptive. We suspect that some of the changes we observed, such as differential gene expression of SMC cytoskeletal proteins associated with alignment of SMCs with collagen fibers, are compensatory since a decrease in arterial wall stress would be favored with SMC and collagen alignment. However, detailed gene regulatory network analysis and computational modeling of molecular and pathway interactions would be necessary to correlate changes in proteins and pathways and functional consequences. It is important to recognize that our conclusions are limited by the sample size of the sequencing data in this study. Though sufficient numbers of cells were extracted and our results revealed similar differentially expressed genes as other tissues exposed to hypoxia, more detailed analyses require a larger sample size. We intend to expand our sample size and incorporate these analyses in future work.

In summary, we observed numerous functional, structural, and transcriptomic changes in the pulmonary arteries of mice due to chronic hypoxic exposure: increased material stiffness is likely due to collagen reorientation rather than excessive collagen accumulation (fibrosis); a change in SMC phenotype resulting in decreased contractility and an alignment of the SMCs with collagen fibers; EC proliferation likely representing Endo-MT; increased pulmonary arterial PWV; and a network of cell-type specific transcriptomic changes that influence these changes. The strength of using an *ex vivo* method as described here is the complexity of the cell-cell communications

is maintained. EC-SMC-ECM communication is captured because these cells were juxtaposed *in situ* up until the moment that the tissue was excised and the cells dissociated. Cellular functional and structural analyses were performed with *in situ* conditions to allow the same communications to maximize genotype:phenotype correlation. We believe that this method demonstrates the power of functional genetics which elucidates causative molecular pathways and potential genotype:phenotype correlations to justify further exploration (Maron, 2020). This multi-dimensional approach (structure, function, transcriptomics) to assessing the pulmonary artery sheds insight into its normal properties and changes due to insult. It holds great potential to investigate the pulmonary arteries in health and disease and identify potential therapeutic pathways.

DATA AVAILABILITY STATEMENT

The datasets presented in this study can be found in the GEO repository under accession number GSE182564.

ETHICS STATEMENT

The animal study was reviewed and approved by Yale Institutional Animal Care and Use Committee.

AUTHOR CONTRIBUTIONS

EM performed the experiments and analyses and wrote the manuscript. AR performed the mechanical measurements and analyses and edited the manuscript. JS performed the single cell experiments and analyses and edited manuscript. CCa performed the 2-photon imaging and analyses and edited the manuscript. MR performed the differential connectome analysis and edited the manuscript. TB performed histologic experiments and analyses. CCo analyzed the single cell data. IS and GT edited the manuscript. NK supervised the single cell experiments and analyses and edited manuscript. JH supervised the biomechanical and imaging experiments and analyses and edited manuscript. All authors contributed to the article and approved the submitted version.

FUNDING

This work was supported, in part, by Additional Ventures via the Single Ventricle Research Fund. MSBR's contribution was funded, in part, by NIH grant F30 HL143906. TB is a recipient of the FWF Schoedinger Fellowship (J4547).

ACKNOWLEDGMENTS

EM is a Pepper Scholar with support from the Claude D. Pepper Older American Independence Center at Yale School of Medicine (P30AG021342).

SUPPLEMENTARY MATERIAL

The Supplementary Material for this article can be found online at: https://www.frontiersin.org/articles/10.3389/fphys.2021.726253/full#supplementary-material; 10.6084/m9.figshare.16451466

REFERENCES

Al-Naamani, N., Preston, I. R., Paulus, J. K., Hill, N. S., and Roberts, K. E. (2015). Pulmonary arterial capacitance is an important predictor of mortality in heart failure with a preserved ejection fraction. *JACC Heart Fail.* 3, 467–474. doi: 10.1016/j.jchf.2015.01.013

Awad, K. S., West, J. D., de Jesus Perez, V., and MacLean, M. (2016). Novel signaling pathways in pulmonary arterial hypertension (2015 Grover Conference Series). *Pulm. Circ.* 6, 285–294. doi: 10.1086/688034

Bersi, M., Khosravi, R., Wujciak, A., Harrison, D., and Humphrey, J. (2017). Differential cell-matrix mechanoadaptations and inflammation drive regional propensities to aortic fibrosis, aneurysm or dissection in hypertension. *J. R. Soc. Interf.* 14:20170327. doi: 10.1098/rsif.2017.0327

Bersi, M. R., Bellini, C., Wu, J., Montaniel, K. R., Harrison, D. G., and Humphrey, J. D. (2016). Excessive adventitial remodeling leads to early aortic maladaptation in angiotensin-induced hypertension. *Hypertension.* 67, 890–896. doi: 10.1161/hypertensionaha.115.06262

Blyth, K. G., Bellofiore, A., Jayasekera, G., Foster, J. E., Steedman, T., Chesler, N. C., et al. (2017). Dobutamine stress MRI in pulmonary hypertension: relationships between stress pulmonary artery relative area change, RV performance, and 10-year survival. *Pulm. Circ.* 7, 465–475. doi: 10.1177/2045893217704838

Bramwell, J. C., and Hill, A. V. (1922). The velocity of pulse wave in man. *Proc. R. Soc. London B Contain. Biol. Char.* 93, 298–306. doi: 10.1098/rspb.1922.0022

Branchetti, E., Poggio, P., Sainger, R., Shang, E., Grau, J. B., Jackson, B. M., et al. (2013). Oxidative stress modulates vascular smooth muscle cell phenotype via CTGF in thoracic aortic aneurysm. *Cardiovasc. Res.* 100, 316–324. doi: 10.1093/cvr/cvt205

Browaeys, R., Saelens, W., and Saeys, Y. (2020). NicheNet: modeling intercellular communication by linking ligands to target genes. *Nat. Methods* 17, 159–162. doi: 10.1038/s41592-019-0667-5

Castelain, V., Hervé, P., Lecarpentier, Y., Duroux, P., Simonneau, G., and Chemla, D. (2001). Pulmonary artery pulse pressure and wave reflection in chronic pulmonary thromboembolism and primary pulmonary hypertension. *J. Am. Coll. Cardiol.* 37, 1085–1092. doi: 10.1016/S0735-1097(00)01212-2

Caulk, A. W., Humphrey, J. D., and Murtada, S.-I. (2019). Fundamental roles of axial stretch in isometric and isobaric evaluations of vascular contractility. *J. Biomech. Eng.* 141, 0310081–03100810. doi: 10.1115/1.4042171

Cavinato, C., Badel, P., Krasny, W., Avril, S., and Morin, C. (2020). "Experimental characterization of adventitial collagen fiber kinematics using second-harmonic generation imaging microscopy: similarities and differences across arteries, species and testing conditions," in *Multi-scale Extracellular Matrix Mechanics and Mechanobiology*, ed. Y. Zhang (Cham: Springer International Publishing). doi: 10.1007/978-3-030-20182-1_5

Cavinato, C., Murtada, S. I., Rojas, A., and Humphrey, J. D. (2021). Evolving structure-function relations during aortic maturation and aging revealed by multiphoton microscopy. *Mech. Ageing Dev.* 196:111471. doi: 10.1016/j.mad.2021.111471

Chan, C. K., and Vanhoutte, P. M. (2013). Hypoxia, vascular smooth muscles and endothelium. *Acta Pharm. Sinica B* 3, 1–7. doi: 10.1016/j.apsb.2012.12.007

Cheifetz, S., Bellón, T., Calés, C., Vera, S., Bernabeu, C., Massagué, J., et al. (1992). Endoglin is a component of the transforming growth factor-beta receptor system in human endothelial cells. *J. Biol. Chem.* 267, 19027–19030. doi: 10.1016/S0021-9258(18)41732-2

Chen, E. Y., Tan, C. M., Kou, Y., Duan, Q., Wang, Z., Meirelles, G. V., et al. (2013). Enrichr: interactive and collaborative HTML5 gene list enrichment analysis tool. *BMC Bioinform.* 14:128. doi: 10.1186/1471-2105-14-128

Chen, J., Zhang, H., Yu, W., Chen, L., Wang, Z., and Zhang, T. (2020). Expression of pulmonary arterial elastin in rats with hypoxic pulmonary hypertension using H2S. *J. Recept. Signal. Transduct. Res.* 40, 383–387. doi: 10.1080/10799893.2020.1738482

Chen, P. Y., Qin, L., Li, G., Tellides, G., and Simons, M. (2016). Smooth muscle FGF/TGF β cross talk regulates atherosclerosis progression. *EMBO Mol. Med.* 8, 712–728. doi: 10.15252/emmm.201506181

de Jesus Perez, V. A., Alastalo, T.-P., Wu, J. C., Axelrod, J. D., Cooke, J. P., Amieva, M., et al. (2009). Bone morphogenetic protein 2 induces pulmonary angiogenesis via Wnt–β-catenin and Wnt–RhoA–Rac1 pathways. *J. Cell Biol.* 184, 83–99. doi: 10.1083/jcb.200806049

Douwes, J. M., Roofthooft, M. T., Bartelds, B., Talsma, M. D., Hillege, H. L., and Berger, R. M. (2013). Pulsatile haemodynamic parameters are predictors of survival in paediatric pulmonary arterial hypertension. *Int. J. Cardiol.* 168, 1370–1377. doi: 10.1016/j.ijcard.2012.12.080

Dragu, R., Rispler, S., Habib, M., Sholy, H., Hammerman, H., Galie, N., et al. (2015). Pulmonary arterial capacitance in patients with heart failure and reactive pulmonary hypertension. *Eur. J. Heart Fail.* 17, 74–80. doi: 10.1002/ejhf.192

Dupont, M., Mullens, W., Skouri, H. N., Abrahams, Z., Taylor, D. O., Wu, Y., et al. (2012). Prognostic role of pulmonary arterial capacitance in advanced heart failure. *Circ. Heart Fail.* 5, 778–785. doi: 10.1161/CIRCHEARTFAILURE.112.968511

Farber, H. W., and Loscalzo, J. (2004). Pulmonary arterial hypertension. *N. Engl. J. Med.* 351, 1655–1665. doi: 10.1161/CIRCHEARTFAILURE.112.968511

Ferruzzi, J., Bersi, M., Uman, S., Yanagisawa, H., and Humphrey, J. (2015). Decreased elastic energy storage, not increased material stiffness, characterizes central artery dysfunction in fibulin-5 deficiency independent of sex. *J. Biomech. Eng.* 137, 0310071–03100714. doi: 10.1115/1.4029431

Ferruzzi, J., Di Achille, P., Tellides, G., and Humphrey, J. D. (2018). Combining *in vivo* and *in vitro* biomechanical data reveals key roles of perivascular tethering in central artery function. *PLoS One.* 13:e0201379. doi: 10.1371/journal.pone.0201379

Frid, M. G., Kale, V. A., and Stenmark, K. R. (2002). Mature vascular endothelium can give rise to smooth muscle cells via endothelial-mesenchymal transdifferentiation: *in vitro* analysis. *Circ. Res.* 90, 1189–1196. doi: 10.1161/01.RES.0000021432.70309.28

Frismantiene, A., Philippova, M., Erne, P., and Resink, T. J. (2018). Smooth muscle cell-driven vascular diseases and molecular mechanisms of VSMC plasticity. *Cell. Signal.* 52, 48–64. doi: 10.1016/j.cellsig.2018.08.019

Fung, Y., and Liu, S. (1991). Changes of zero-stress state of rat pulmonary arteries in hypoxic hypertension. *J. Appl. Physiol.* 70, 2455–2470. doi: 10.1152/jappl.1991.70.6.2455

Geng, X-d, Wang, W-w, Feng, Z., Liu, R., Cheng, X. L., Shen, W. J., et al. (2019). Identification of key genes and pathways in diabetic nephropathy by bioinformatics analysis. *J. Diabetes Investig.* 10, 972–984. doi: 10.1111/jdi.12986

Ghio, S., D'Alto, M., Badagliacca, R., Vitulo, P., Argiento, P., Mulè, M., et al. (2017). Prognostic relevance of pulmonary arterial compliance after therapy initiation or escalation in patients with pulmonary arterial hypertension. *Int. J. Cardiol.* 230, 53–58. doi: 10.1016/j.ijcard.2016.12.099

Ghio, S., Schirinzi, S., and Pica, S. (2015). Pulmonary arterial compliance: how and why should we measure it? *Global Cardiol. Sci. Prac.* 2015:58. doi: 10.5339/gcsp.2015.58

Gleason, R., and Humphrey, J. (2004). A mixture model of arterial growth and remodeling in hypertension: altered muscle tone and tissue turnover. *J. Vasc. Res.* 41, 352–363. doi: 10.1159/000080699

Goveia, J., Rohlenova, K., Taverna, F., Treps, L., Conradi, L. C., Pircher, A., et al. (2020). An integrated gene expression landscape profiling approach to identify lung tumor endothelial cell heterogeneity and angiogenic candidates. *Cancer Cell* 37, 21–36.e13. doi: 10.1159/00008069910.1016/j.ccell.2019.12.001

Gupta, A., Sharifov, O. F., Lloyd, S. G., Tallaj, J. A., Aban, I., Dell'italia, L. J., et al. (2018). Novel noninvasive assessment of pulmonary arterial stiffness using velocity transfer function. *J. Am. Heart Assoc.* 7:e009459. doi: 10.1161/JAHA.118.009459

Hadinnapola, C., Li, Q., Su, L., Pepke-Zaba, J., and Toshner, M. (2015). The resistance-compliance product of the pulmonary circulation varies in health and pulmonary vascular disease. *Physiol. Rep.* 3:e12363. doi: 10.14814/phy2.12363

Hanks, J. H., and Wallace, R. E. (1949). Relation of oxygen and temperature in the preservation of tissues by refrigeration. *Proc. Soc. Exp. Biol. Med.* 71, 196–200.

Humphrey, J. D. (2013). *Cardiovascular Solid Mechanics: Cells, Tissues, and Organs*. Berlin: Springer Science & Business Media.

Junhui, Z., Xingxiang, W., Guosheng, F., Yunpeng, S., Furong, Z., and Junzhu, C. (2008). Reduced number and activity of circulating endothelial progenitor cells in patients with idiopathic pulmonary arterial hypertension. *Respir. Med.* 102, 1073–1079. doi: 10.1016/j.rmed.2007.12.030

Kaartinen, V., Voncken, J. W., Shuler, C., Warburton, D., Bu, D., Heisterkamp, N., et al. (1995). Abnormal lung development and cleft palate in mice lacking TGF–β3 indicates defects of epithelial–mesenchymal interaction. *Nat. Genet.* 11, 415–421. doi: 10.1038/ng1295-415

Kovacic, J. C., Dimmeler, S., Harvey, R. P., Finkel, T., Aikawa, E., Krenning, G., et al. (2019). Endothelial to mesenchymal transition in cardiovascular disease. *J. Am. Coll. Cardiol.* 73:190. doi: 10.1016/j.jacc.2018.09.089

Kuleshov, M. V., Jones, M. R., Rouillard, A. D., Fernandez, N. F., Duan, Q., Wang, Z., et al. (2016). Enrichr: a comprehensive gene set enrichment analysis web server 2016 update. *Nucleic Acids Res.* 44(W1), W90–W97. doi: 10.1093/nar/gkw377

Lammers, S. R., Kao, P. H., Qi, H. J., Hunter, K., Lanning, C., Albietz, J., et al. (2008). Changes in the structure-function relationship of elastin and its impact on the proximal pulmonary arterial mechanics of hypertensive calves. *Am. J. Physiol.Heart Circ. Physiol.* 295, H1451–H1459. doi: 10.1152/ajpheart.00127.2008

Lau, E. M. T., Abelson, D., Dwyer, N., Yu, Y., Ng, M. K., and Celermajer, D. S. (2014). Assessment of ventriculo-arterial interaction in pulmonary arterial hypertension using wave intensity analysis. *Eur. Respir. J.* 43:1804. doi: 10.1183/09031936.00148313

Lei, W., He, Y., Shui, X., Li, G., Yan, G., Zhang, Y., et al. (2016). Expression and analyses of the HIF-1 pathway in the lungs of humans with pulmonary arterial hypertension. *Mol. Med. Rep.* 14, 4383–4390. doi: 10.3892/mmr.2016.5752

Li, M., Scott, D. E., Shandas, R., Stenmark, K. R., and Tan, W. (2009). High pulsatility flow induces adhesion molecule and cytokine mRNA expression in distal pulmonary artery endothelial cells. *Ann. Biomed. Eng.* 37, 1082–1092. doi: 10.1007/s10439-009-9684-3

Malhotra, R., Dhakal, B. P., Eisman, A. S., Pappagianopoulos, P. P., Dress, A., Weiner, R. B., et al. (2016). Pulmonary vascular distensibility predicts pulmonary hypertension severity, exercise capacity, and survival in heart failure. *Circ. Heart Fail.* 9:e003011. doi: 10.1161/CIRCHEARTFAILURE.115.003011

Maron, B. A. (2020). Clarifying the pulmonary arterial hypertension molecular landscape using functional genetics. *Am. J. Respir. Crit. Care Med.* 202, 488–490. doi: 10.1164/rccm.202004-1411ED

Marsboom, G., and Rehman, J. (2018). Hypoxia signaling in vascular homeostasis. *Physiology.* 33, 328–337. doi: 10.1152/physiol.00018.2018

Medici, D., and Kalluri, R. (2012). Endothelial-mesenchymal transition and its contribution to the emergence of stem cell phenotype. *Semin Cancer Biol.* 22, 379–384. doi: 10.1016/j.semcancer.2012.04.004

Milnor, W. R., Conti, C. R., Lewis, K. B., and O'Rourke, M. F. (1969). Pulmonary arterial pulse wave velocity and impedance in man. *Circ. Res.* 25, 637–649. doi: 10.1161/01.RES.25.6.637

Minamino, T., Mitsialis, S. A., and Kourembanas, S. (2001). Hypoxia extends the life span of vascular smooth muscle cells through telomerase activation. *Mol. Cell Biol.* 21, 3336–3342. doi: 10.1128/MCB.21.10.3336-3342.2001

Morrell, N. W., Atochina, E. N., Morris, K. G., Danilov, S. M., and Stenmark, K. R. (1995a). Angiotensin converting enzyme expression is increased in small pulmonary arteries of rats with hypoxia-induced pulmonary hypertension. *J. Clin. Invest.* 96, 1823–1833. doi: 10.1172/JCI118228

Morrell, N. W., Morris, K. G., and Stenmark, K. R. (1995b). Role of angiotensin-converting enzyme and angiotensin II in development of hypoxic pulmonary hypertension. *Am. J. Physiol. Heart Circ. Physiol.* 269, H1186–H1194. doi: 10.1152/ajpheart.1995.269.4.H1186

Morrell, N. W., Danilov, S. M., Satyan, K. B., Morris, K. G., and Stenmark, K. R. (1997). Right ventricular angiotensin converting enzyme activity and expression is increased during hypoxic pulmonary hypertension. *Cardiovasc. Res.* 34, 393–403. doi: 10.1016/S0008-6363(97)00049-7

Murtada, S.-I., Ferruzzi, J., Yanagisawa, H., and Humphrey, J. (2016). Reduced biaxial contractility in the descending thoracic aorta of fibulin-5 deficient mice. *J. Biomech. Eng.* 138:051008. doi: 10.1115/1.4032938

Murtada, S.-I., and Humphrey, J. D. (2018). Regional heterogeneity in the regulation of vasoconstriction in arteries and its role in vascular mechanics. *Adv. Exp. Med. Biol.* 1097, 105–128. doi: 10.1007/978-3-319-96445-4_6

Ochoa, C. D., Baker, H., Hasak, S., Matyal, R., Salam, A., Hales, C. A., et al. (2008). Cyclic stretch affects pulmonary endothelial cell control of pulmonary smooth muscle cell growth. *Am. J. Respir. Cell Mol. Biol.* 39, 105–112. doi: 10.1165/rcmb.2007-0283OC

Oh Young, S., Berkowitz Dan, E., Cohen Richard, A., Figueroa, C. A., Harrison, D. G., Humphrey, J. D., et al. (2017). A special report on the nhlbi initiative to study cellular and molecular mechanisms of arterial stiffness and its association with hypertension. *Circ. Res.* 121, 1216–1218. doi: 10.1161/CIRCRESAHA.117.311703

Pagnamenta, A., Vanderpool, R., Brimioulle, S., and Naeije, R. (2013). Proximal pulmonary arterial obstruction decreases the time constant of the pulmonary circulation and increases right ventricular afterload. *J. Appl. Physiol.* 114, 1586–1592. doi: 10.1152/japplphysiol.00033.2013

Pedroza Albert, J., Tashima, Y., Shad, R., Cheng, P., Wirka, R., Churovich, S., et al. (2020). Single-Cell transcriptomic profiling of vascular smooth muscle cell phenotype modulation in marfan syndrome aortic aneurysm. *Arterioscler. Thromb. Vasc. Biol.* 40, 2195–2211. doi: 10.1161/ATVBAHA.120.314670

Pellegrini, P., Rossi, A., Pasotti, M., Raineri, C., Cicoira, M., Bonapace, S., et al. (2014). Prognostic relevance of pulmonary arterial compliance in patients with chronic heart failure. *Chest* 145, 1064–1070. doi: 10.1161/ATVBAHA.120.31467010.1378/chest.13-1510

Peng, H. H., Chung, H. W., Yu, H. Y., and Tseng, W. Y. (2006). Estimation of pulse wave velocity in main pulmonary artery with phase contrast MRI: preliminary investigation. *J. Magn. Reson. Imaging.* 24, 1303–1310. doi: 10.1002/jmri.20782

Porter, K. M., Kang, B.-Y., Adesina, S. E., Murphy, T. C., Hart, C. M., and Sutliff, R. L. (2014). Chronic hypoxia promotes pulmonary artery endothelial cell proliferation through H 2 O 2-induced 5-lipoxygenase. *PLoS One.* 9:e98532. doi: 10.1371/journal.pone.0098532

Pursell, E., and Valdez-Jasso, D. (2020). Transmural variation of collagen orientation and structure distributions in the right pulmonary arterial wall. *FASEB J.* 34(S1), 1–1. doi: 10.1096/fasebj.2020.34.s1.06659

Ramachandra, A. B., and Humphrey, J. D. (2019). Biomechanical characterization of murine pulmonary arteries. *J. Biomech.* 84, 18–26. doi: 10.1016/j.jbiomech.2018.12.012

Raredon, M. S. B., Adams, T. S., Suhail, Y., Schupp, J. C., Poli, S., Neumark, N., et al. (2019). Single-cell connectomic analysis of adult mammalian lungs. *Sci. Adv.* 5:eaaw3851. doi: 10.1126/sciadv.aaw3851

Rensen, S. S., Doevendans, P. A., and van Eys, G. J. (2007). Regulation and characteristics of vascular smooth muscle cell phenotypic diversity. *Neth. Heart J.* 15, 100–108. doi: 10.1007/BF03085963

Roux, P. P., and Blenis, J. (2004). ERK and p38 MAPK-activated protein kinases: a family of protein kinases with diverse biological functions. *Microbiol. Mol. Biol. Rev.* 68, 320–344. doi: 10.1128/MMBR.68.2.320-344.2004

Safdar, Z., Tamez, E., Chan, W., Arya, B., Ge, Y., Deswal, A., et al. (2014). Circulating collagen biomarkers as indicators of disease severity in pulmonary arterial hypertension. *JACC Heart Fail.* 2, 412–421. doi: 10.1016/j.jchf.2014.03.013

Sanz, J., Prat-Gonzalez, S., Macaluso, F., Fuster, V., and Garcia, M. (2008). 155 Quantification of pulse wave velocity in the pulmonary artery in patients with pulmonary hypertension. *J. Cardiovasc. Mag. Reson.* 10:A56. doi: 10.1186/1532-429X-10-S1-A56

Saouti, N., Westerhof, N., Postmus, P., and Vonk-Noordegraaf, A. (2010). The arterial load in pulmonary hypertension. *Eur. Respir. Rev.* 19, 197–203. doi: 10.1183/09059180.00002210

Schäfer, M., Myers, C., Brown, R. D., Frid, M. G., Tan, W., Hunter, K., et al. (2016). Pulmonary arterial stiffness: toward a new paradigm in pulmonary arterial hypertension pathophysiology and assessment. *Curr. Hypertens. Rep.* 18:4. doi: 10.1007/s11906-015-0609-2

Schenk, G. J., Dijkstra, S., van het Hof, A. J., van der Pol, S. M., Drexhage, J. A., van der Valk, P., et al. (2013). Roles for HB-EGF and CD9 in multiple sclerosis. *Glia* 61, 1890–1905. doi: 10.1002/glia.22565

Silva, GTdA, Guest, B. B., Gomez, D. E., McGregor, M., Viel, L., O'Sullivan, M. L., et al. (2017). Development of a technique for determination of pulmonary artery pulse wave velocity in horses. *J. Appl. Physiol.* 122, 1088–1094. doi: 10.1152/japplphysiol.00962.2016

Sodhi, C. P., Phadke, S. A., Batlle, D., and Sahai, A. (2001). Hypoxia stimulates osteopontin expression and proliferation of cultured vascular smooth muscle cells: potentiation by high glucose. *Diabetes.* 50, 1482–1490. doi: 10.2337/diabetes.50.6.1482

Song, S., Yamamura, A., Yamamura, H., Ayon, R. J., Smith, K. A., Tang, H., et al. (2014). Flow shear stress enhances intracellular Ca2+ signaling in pulmonary artery smooth muscle cells from patients with pulmonary arterial hypertension. *Am. J. Physiol. Cell Physiol.* 307, C373–C383. doi: 10.1152/ajpcell.00115.2014

Stevens, G. R., Garcia-Alvarez, A., Sahni, S., Garcia, M. J., Fuster, V., and Sanz, J. (2012). RV dysfunction in pulmonary hypertension is independently related to pulmonary artery stiffness. *JACC Cardiovasc. Imaging.* 5, 378–387. doi: 10.1016/j.jcmg.2011.11.020

Stuart, T., Butler, A., Hoffman, P., Hafemeister, C., Papalexi, E., Mauck, W. M., et al. (2019). Comprehensive integration of single-cell data. *Cell* 177, 1888–1902.e21. doi: 10.1016/j.cell.2019.05.031

Takemura, T., Hino, S., Murata, Y., Yanagida, H., Okada, M., Yoshioka, K., et al. (1999). Coexpression of CD9 augments the ability of membrane-bound heparin-binding epidermal growth factor-like growth factor (proHB-EGF) to preserve renal epithelial cell viability. *Kidney Int.* 55, 71–81. doi: 10.1046/j.1523-1755.1999.00259.x

Tan, Y., Tseng, P.-O., Wang, D., Zhang, H., Hunter, K., Hertzberg, J., et al. (2014). Stiffening-induced high pulsatility flow activates endothelial inflammation via a TLR2/NF-κB pathway. *PLoS one.* 9:e102195. doi: 10.1371/journal.pone.0102195

Tao, J., Barnett, J. V., Watanabe, M., and Ramírez-Bergeron, D. (2018). Hypoxia supports epicardial cell differentiation in vascular smooth muscle cells through the activation of the TGFβ Pathway. *J. Cardiovasc. Dev. Dis.* 5:19. doi: 10.3390/jcdd5020019

Triposkiadis, F., Xanthopoulos, A., and Butler, J. (2019). Cardiovascular aging and heart failure: JACC review topic of the week. *J. Am. Coll. Cardiol.* 74, 804–813. doi: 10.1016/j.jacc.2019.06.053

van der Loop, F. T., Schaart, G., Timmer, E. D., Ramaekers, F. C., and van Eys, G. J. (1996). Smoothelin, a novel cytoskeletal protein specific for smooth muscle cells. *J. Cell Biol.* 134, 401–411. doi: 10.1083/jcb.134.2.401h

Vivodtzev, I., Minet, C., Tamisier, R., Arbib, F., Borel, J. C., Baguet, J. P., et al. (2013). Arterial stiffness by pulse wave velocity in COPD: reliability and reproducibility. *Eur. Respir. J.* 42, 1140–1142. doi: 10.1183/09031936.00014813

Weir-McCall, J. R., Liu-Shiu-Cheong, P. S., Struthers, A. D., Lipworth, B. J., and Houston, J. G. (2018). Pulmonary arterial stiffening in COPD and its implications for right ventricular remodelling. *Eur. Radiol.* 28, 3464–3472. doi: 10.1007/s00330-018-5346-x

Westerhof, N., Lankhaar, J.-W., and Westerhof, B. E. (2009). The arterial windkessel. *Med. Biol. Eng. Comput.* 47, 131–141. doi: 10.1007/s11517-008-0359-2

Worth, N. F., Rolfe, B. E., Song, J., and Campbell, G. R. (2001). Vascular smooth muscle cell phenotypic modulation in culture is associated with reorganisation

of contractile and cytoskeletal proteins. *Cell Motility* 49, 130–145. doi: 10.1002/cm.1027

Yu, L., and Hales, C. A. (2011). Hypoxia does neither stimulate pulmonary artery endothelial cell proliferation in mice and rats with pulmonary hypertension and vascular remodeling nor in human pulmonary artery endothelial cells. *J. Vasc. Res.* 48, 465–475. doi: 10.1159/000327005

Žaloudíková, M., Eckhardt, A., Vytášek, R., Uhlík, J., Novotný, T., Bačáková, L., et al. (2019). Decreased collagen VI in the tunica media of pulmonary vessels during exposure to hypoxia: a novel step in pulmonary arterial remodeling. *Pulm. Circ.* 9:2045894019860747. doi: 10.1177/2045894019860747

Zhang, H., Huang, W., Liu, H., Zheng, Y., and Liao, L. (2020). Mechanical stretching of pulmonary vein stimulates matrix metalloproteinase-9 and transforming growth factor-β1 through stretch-activated channel/MAPK pathways in pulmonary hypertension due to left heart disease model rats. *PLoS One.* 15:e0235824. doi: 10.1371/journal.pone.0235824

Conflict of Interest: The authors declare that the research was conducted in the absence of any commercial or financial relationships that could be construed as a potential conflict of interest.

frontiers in Physiology

REVIEW
published: 27 September 2021
doi: 10.3389/fphys.2021.747789

Deciphering the Role of microRNAs in Large-Artery Stiffness Associated With Aging: Focus on miR-181b

Jay M. Baraban[1], *Eric Tuday*[2,3], *Dan E. Berkowitz*[4] *and Sam Das*[5,6]*

[1] Department of Neuroscience, School of Medicine, Johns Hopkins University, Baltimore, ML, United States, [2] Division of Cardiovascular Medicine, Department of Internal Medicine, School of Medicine, University of Utah, Salt Lake City, UT, United States, [3] Geriatric Research, Education and Clinical Center, VA Salt Lake City Health Care System, Salt Lake City, UT, United States, [4] Department of Anesthesiology and Perioperative Medicine, School of Medicine, University of Alabama at Birmingham, Birmingham, AL, United States, [5] Department of Pathology, School of Medicine, Johns Hopkins University, Baltimore, ML, United States, [6] Department of Anesthesiology and Critical Care Medicine, Johns Hopkins Medicine, Baltimore, ML, United States

Large artery stiffness (LAS) is a major, independent risk factor underlying cardiovascular disease that increases with aging. The emergence of microRNA signaling as a key regulator of vascular structure and function has stimulated interest in assessing its role in the pathophysiology of LAS. Identification of several microRNAs that display age-associated changes in expression in aorta has focused attention on defining their molecular targets and deciphering their role in age-associated arterial stiffening. Inactivation of the microRNA-degrading enzyme, translin/trax, which reverses the age-dependent decline in miR-181b, confers protection from aging-associated arterial stiffening, suggesting that inhibitors targeting this enzyme may have translational potential. As LAS poses a major public health challenge, we anticipate that future studies based on these advances will yield innovative strategies to combat aging-associated arterial stiffening.

Keywords: miR-181b, translin/trax, microRNA degradation, arterial stiffness, aging

OPEN ACCESS

Edited by:
Lakshmi Santhanam, Johns Hopkins University, United States

Reviewed by:
Mingyi Wang, National Institutes of Health (NIH), United States
Patrick Osei-Owusu, Case Western Reserve University, United States

***Correspondence:**
Sam Das
sdas11@jhmi.edu

Specialty section:
This article was submitted to Vascular Physiology, a section of the journal Frontiers in Physiology

Received: *26 July 2021*
Accepted: *30 August 2021*
Published: *27 September 2021*

Citation:
Baraban JM, Tuday E, Berkowitz DE and Das S (2021) Deciphering the Role of microRNAs in Large-Artery Stiffness Associated With Aging: Focus on miR-181b. Front. Physiol. 12:747789. doi: 10.3389/fphys.2021.747789

INTRODUCTION

The emergence of Large-Artery Stiffness (LAS) as a major risk factor for cardiovascular morbidity has stimulated interest in developing strategies to combat this endemic public health challenge (O'Rourke, 1990; Mitchell et al., 2010; Boutouyrie et al., 2011; O'Rourke et al., 2016; Chirinos et al., 2019). Under normal conditions, the elasticity of the aorta and other major arteries absorbs and dampens the pressure pulsation generated during systole. However, the increased stiffness of these vessels in patients with LAS disrupts the normal hemodynamics of the cardiac cycle, allowing conduction of waves with abnormally high pressure into the vascular beds of target organs, such as kidney and brain, that contribute to tissue damage.

IDENTIFICATION OF CANDIDATE MICRORNAS IMPLICATED IN LAS

Arterial stiffness is determined by the composition and organization of the extracellular matrix, as well as the cytoskeletal properties of vascular smooth muscle cells (VSMCs;

Qiu et al., 2010; Sehgel et al., 2015; Chirinos et al., 2019). Therefore, investigators have concentrated on defining the biochemical and associated structural changes responsible for increased arterial stiffness, as well as the upstream regulatory pathways driving these changes. From this perspective, the microRNA system has emerged as a potential culprit, since this highly versatile signaling pathway can coordinate cellular adaptations in response to developmental and environmental signals (Bartel, 2004) and has been found to play key roles in vascular smooth muscle development and function (Albinsson et al., 2010; Kang and Hata, 2012). However, since each cell contains hundreds of distinct microRNAs, and these microRNA profiles differ across cell types, identifying candidate microRNAs involved in regulating arterial stiffness poses a difficult challenge.

Initial clues implicating dysregulation of specific microRNAs in LAS emerged from two approaches. As patients with LAS can be identified by measuring pulse wave velocity (PWV) using non-invasive techniques, investigators looked for alterations in microRNA signaling associated with elevated PWV. This approach yielded identification of two microRNAs linked to elevated PWV: miR-765 and (Liao et al., 2015), miR-1185 (Deng et al., 2017). The second approach was based on the epidemiological observation that the prevalence of LAS increases markedly with aging (O'Rourke and Nichols, 2005; Mitchell et al., 2007; Chirinos et al., 2019). Furthermore, mice also display aging-associated increases in PWV that model LAS (Nicholson et al., 2017; Steppan et al., 2019). Thus, investigators checked for microRNAs that show altered expression with aging in blood samples from humans and in mouse aorta. This approach led to the identification of several candidate microRNAs that show altered expression with aging: mir-29, miR-34a, miR-92a, miR-137, miR-181b, miR-203, and miR-222. Mir-29, miR-34a, miR-137, miR-203, and miR-222 increase with aging in mouse aorta (Boon et al., 2011; Badi et al., 2015; Nicholson et al., 2017) and miR-34a has been shown, very recently, to be associated, along with miR-34c, with aortic stiffening in human subjects (Gatsiou et al., 2021). Conversely, miR-92a and miR-181b decrease in mouse aorta with aging (Hazra et al., 2016; Hori et al., 2017) and miR-92a is also decreased in human blood with aging (Hazra et al., 2016).

Based on these initial observations, investigators examined whether mimicking these changes is sufficient to produce stiffening. Using a transfection-based approach *in vivo*, Nicholson et al. (2017) found that elevating miR-203 leads to arterial stiffening. Furthermore, administering an antagonist of miR-92a to mice increases PWV (Hazra et al., 2016). To examine the effect of decreased miR-181b on aortic stiffness, Hori et al. (2017) used mice carrying a deletion of the locus (miR-181a1/b1) that blocks expression of both miR-181a and miR-181b in aorta. These mice showed a premature onset of arterial stiffness as young adults. Thus, these findings indicate that aging-associated changes in expression of these candidate microRNAs play a causal role in eliciting arterial stiffness.

ORGANIZATION OF THE MICRORNA SIGNALING SYSTEM CONFERS VERSATILITY

Prior to discussing how altered expression of these microRNAs might contribute to LAS, we will first provide a brief overview of the operating principles of the microRNA signaling pathway (Bartel, 2004; Friedman et al., 2009; McGeary et al., 2019). MicroRNAs are ∼20–22 nucleotide fragments that are generated from larger RNA transcripts that undergo two processing steps. The primary transcript is cleaved into one or more hairpin-shaped fragments in the nucleus. These hairpin-shaped fragments, called pre-microRNAs, are then exported from the nucleus into the cytoplasm, where they are cleaved by Dicer, an RNA endonuclease, into mature microRNAs, double-stranded oligomers with 3' overhangs. One of these strands, called the guide strand, binds to Ago, a protein component of the RNA-induced silencing complex (RISC). The guide strand targets the RISC complex to mRNAs that contains its complementary sequence in its 3'UTR, where it acts to prevent its translation or trigger its degradation. By using guide microRNAs to target specific mRNAs, this system has tremendous versatility. Each species of microRNA can target multiple mRNAs to regulate their translation; conversely, each mRNA can be regulated by multiple microRNAs.

While the architecture of the microRNA signaling pathway appears to be designed to maximize versatility, it is also important that it have the capacity for selectivity, the ability of the cell to enhance or dampen the impact of individual or a small cohort of microRNAs. Since Dicer plays an essential role in generating virtually all microRNAs, regulating its activity would not provide a mechanism to generate selectivity as it would produce a global change in microRNA production. Instead, two alternative mechanisms are used to achieve selectivity. One depends on selective transcription of the primary transcripts. Like mRNAs, microRNAs are also transcribed by Pol II. Thus, their expression is regulated by the same cohort of promoters used to regulate coding transcripts. This promoter system enables each cell type to express a different profile of microRNAs and alter their levels in response to changes in cellular conditions. The other depends on selective degradation of microRNAs, which is achieved by two distinct mechanisms: one involves conventional RNase enzymes (Fu et al., 2016; Baraban et al., 2018) while the other involves a novel RNA-guided mechanism.

MICRORNA DEGRADATION PATHWAYS CONFER SELECTIVITY

The best characterized microRNA-degrading pathway is mediated by Lin28, which targets the let-7 group of pre-microRNAs (Heo et al., 2008, 2009; Hagan et al., 2009). These pre-microRNAs contain a common motif in their loop that is recognized by Lin28. Binding of Lin28 to let-7 pre-miRNAs triggers addition of uridine residues to its 3'terminal, which targets these pre-miRNAs for degradation.

The translin (TN)/trax (TX) microRNA-degrading enzyme is another RNase that targets a subset of pre-microRNAs (Asada et al., 2014). The target specificity of the TN/TX RNase has not been as well characterized as that of Lin28. However, limited characterization of its substrate specificity indicates that it acts at mismatches in base pairing located in the stem, as mutations that eliminate selected mismatches abolish cleavage. Comparison of microRNA profiles from wild type tissues or cells with those that are devoid of TN/TX activity has yielded identification of a small subset of microRNAs that are elevated by this manipulation and hence considered candidate substrates.

A third microRNA-degrading enzyme, called monocyte chemotactic protein-induced protein (MCPIP), has been identified in studies on immune cells (Suzuki et al., 2011). Initial characterization of its substrate specificity has demonstrated that it, like Lin28, recognizes a motif in the loop of pre-microRNAs. Further studies are needed to define its role in regulating microRNA signaling.

One of the potential advantages of using RNases with a high degree of selectivity to regulate microRNA levels is that they can cause rapid decreases in the levels of a small subset of target microRNAs. Elegant studies from the Meffert lab have demonstrated that rapid activation of the Lin28 degradation pathway is used by BDNF and other growth factors to trigger rapid increases in translation of mRNAs that mediate cellular plasticity changes mediated by these growth factors (Huang et al., 2012; Amen et al., 2017). At the same time, these growth factors also increase Dicer activity to produce a global increase in generation of microRNAs and subsequent translational silencing of mRNAs that are not targeted by the Lin28/let-7 pathway. In a similar vein, several forms of synaptic plasticity in hippocampal slices are dependent on TN/TX-mediated degradation of a few microRNAs, which triggers *de novo* translation of plasticity transcripts (Park et al., 2017, 2020). Thus, activation of these microRNA-degrading enzymes provides a mechanism to trigger selective increases in protein translation by reversing microRNA-mediated silencing.

Based on these findings with Lin28, TN/TX, and MCPIP, we and others have speculated that there may be many other microRNA-degrading enzymes that remain to be discovered that target discrete subsets of microRNAs. However, this may not be the case because recent studies have uncovered a novel RNA-based mechanism for selective degradation of microRNAs (Sheu-Gruttadauria et al., 2019). This process was initially discovered as a means by which a viral encoded mRNA triggers degradation of a specific host cell microRNA (Cazalla et al., 2010). In this process, called target-mediated degradation of microRNAs (TMDM), the viral transcript binds with a high degree of complementarity to the target microRNA. At first glance, it is unclear how this initial step in the degradation process differs from what occurs in the silencing process. However, a more detailed analysis of the degree of complementarity between the guide microRNA and its target sequence has revealed a critical difference. In the silencing process, a microRNA guides Ago to a target mRNA by a region of complementarity in the 5' portion of the microRNA. However, in TMDM, the mRNA transcript co-opts this process by binding to the guide microRNA at both its 5' and 3' ends. This fairly subtle difference in the degree of complementarity between microRNA and its target mRNA has a huge impact on the outcome of this interaction. Rather than the microRNA silencing the mRNA, the mRNA triggers degradation of the microRNA. Thus, by using RNA-mediated recognition of microRNAs, cells can produce degradation of selected microRNAs without the need for additional RNase enzymes (Han et al., 2020; Shi et al., 2020).

TABLE 1 | MicroRNAs that show altered expression in aorta with aging.

miRNA	Δ with aging	Candidate targets
miR-29	Up	Elastin, fibrillin, collagen 1A1/3A1
miR-34a	Up	SIRT1, Src, FAK, paxillin, vinculin
miR-137	Up	Src, paxillin
miR-203	Up	Src, Crk, paxillin, talin
miR-222	Up	Crk, FAK
miR-92a	Down	Collagen 1, TNFalpha R1
miR-181b	Down	Elastin, TIMP-3, TGF-βi

MOLECULAR TARGETS OF CANDIDATE MICRORNAS

As microRNAs act by suppressing translation of target mRNAs, identification of microRNAs implicated in LAS has stimulated interest in identifying their direct mRNA targets (**Table 1**). Using bioinformatic approaches, candidate target mRNAs for these microRNAs were identified by the presence of complementary binding sites in their 3'UTR. Using this search strategy, elastin, fibrillin, and collagens 1A1 and 3A1 have been identified as targets of miR-29 (van Rooij et al., 2008; Boon et al., 2011). Since miR-29 levels increase with aging, expression of these target proteins decline, as expected. Furthermore, administration of an miR-29 antagonist *in vivo* has the opposite effect. Using a similar approach, sirtuin 1 (SIRT1), which has been linked to preventing cellular senescence, was identified as a target of miR-34a in VSMCs (Badi et al., 2015). According to this scenario, the elevation in miR-34a inhibits SIRT1 expression, thereby enhancing cellular senescence, which contributes to stiffening. Conversely, miR-92a which decreases with aging has been shown to target collagen 1 and TNF-alpha receptor 1 (Hazra et al., 2016). Direct targets identified for miR-181b, which decreases with aging, are elastin and tissue inhibitor of metalloproteinase-3 (TIMP-3) (Di Gregoli et al., 2017), as well as TGF-βi, an uncharacterized gene product that is induced by TGF-β (Hori et al., 2017). Lastly, miR-34a, miR-137, miR-203 and miR-222, which increase with aging, have been shown to target components of the pathway that mediate Src-dependent cytoskeletal remodeling in VSMCs, a process that can reduce agonist-induced VSMC stiffness *in vitro*. Therefore, heightened expression of these microRNAs could contribute to increased VSMC stiffness in aging by impairing this signaling pathway which promotes aortic plasticity (Nicholson et al., 2017).

TESTING THE ROLE OF miR-181b IN LAS

An important goal of deciphering the pathophysiology of LAS is to identify potential therapeutic strategies that can be used to prevent or reverse this disorder. Accordingly, a critical step in evaluating the role of candidate microRNAs in LAS is testing whether manipulations that normalize levels of a candidate microRNA during aging decrease arterial stiffness in an animal model of LAS. Although several studies have demonstrated that mimicking the alteration of a candidate microRNA is sufficient to elicit arterial stiffness, to our knowledge, miR-181b is the only candidate microRNA that has been subjected to this rigorous test.

Our strategy for normalizing miR-181b levels in aorta emerged from our observation that this microRNA is one of those elevated in a cell line that had been subjected to knockdown of TN/TX, suggesting that it was targeted by this microRNA-degrading enzyme (Asada et al., 2014). To confirm this inference, we first checked whether miR-181b levels are elevated in aorta harvested from TN KO mice and found this to be the case (Tuday et al., 2019). Therefore, we reasoned that if a decrease in miR-181b levels plays a key role in driving LAS, then TN KO mice might be resistant to developing arterial stiffness. As C57BL6 mice display aging-associated arterial stiffening, they provide a suitable animal model of this disorder (Nicholson et al., 2017). However, since that would require waiting until the mice are close to 18 months old, we first tested this hypothesis in a paradigm that elicits increased aortic stiffness in just a few weeks. In this streamlined paradigm, mice are switched from regular water to high salt water (HSW; 4% w/v), and their PWV measured on a weekly basis. Remarkably, we found that TN KO mice are resistant to developing increased PWV induced by this paradigm. Furthermore, exposure to HSW decreases levels of miR-181b in WT mice, but not in TN KO mice, consistent with the view that TN deletion confers protection from increased stiffness by blocking degradation of miR-181b. However, it is important to emphasize that this *in vivo* study leaves open a variety of alternative possibilities. For example, it is possible that the protective effect of TN deletion is due to blocking degradation of other miRNAs during the HSW paradigm.

To test our hypothesis that miR-181b plays a key role in regulating arterial stiffness, we have, more recently, examined the impact of manipulating miR-181b in an *in vitro* model of VSMC stiffness (Tuday et al., 2021). In this paradigm, exposure of VSMCs to arginine vasopressin (AVP) for several hours elevates their stiffness, as determined by magnetic twist cytometry, and reduces miR-181b levels in a TN/TX-dependent fashion. Thus, this model provided an excellent opportunity to test whether the increased stiffness produced by AVP is mediated by its ability to reduce miR-181b levels. To check this key point, we found that transfecting cells with exogenous miR-181b blocked the ability of AVP to increase stiffness. Furthermore, we found that the AVP-induced reductions in miR-181b trigger increased VSMC stiffness by increasing levels of TGF-β in the media, as neutralizing antibodies to TGF-β block AVP-induced increases in VSMC stiffness in this paradigm (**Figure 1**).

To assess whether TN/TX inactivation can also confer protection against arterial stiffness associated with aging, we checked whether mice containing a point mutation in TX, E126A, which abolishes the RNase activity of the TN/TX RNase (Fu et al., 2020), display protection in this paradigm. As expected, we found that that these mutant mice are protected from developing arterial stiffness with aging. As aging-induced arterial stiffness is associated with increased vessel wall thickness, it is also noteworthy that aorta wall thickness in aged TX(E126A) mice is thinner than in aged WT mice. Thus, these studies strongly indicate that deletion or inactivation of the TN/TX microRNA degrading enzyme confers protection against arterial stiffening *in vivo*, and that it does so by blocking the reduction in miR-181b observed with aging.

ROLE OF miR-181b IN OTHER VASCULAR PATHOLOGY PARADIGMS

MiR-181b has also been studied in other paradigms of vascular pathology. Whereas the studies outlined above indicate that reduced levels of miR-181b contribute to arterial stiffness and that reversing that decrease has therapeutic effects, Di Gregoli et al. (2017) report that miR-181b levels are elevated in human atherosclerotic plaques and abdominal aortic aneurysms and that *in vivo* administration of miR-181b inhibitors has beneficial effects in mouse models of both these pathologies. These investigators provide compelling evidence that tissue inhibitor of metalloproteinase-3 (TIMP-3) is a direct target of miR-181b in macrophages present in atherosclerotic plaques and in abdominal aortic aneurysms that mediates its deleterious effects. Furthermore, administration of an miR-181b inhibitor *in vivo* to ApoE KO mice, which are prone to developing aneurysms, alters the composition of the extracellular matrix by decreasing the presence of new collagen and increasing the amount of elastin. As bioinformatic analysis indicates that elastin is a direct target of miR-181b, these findings would fit with the predicted effects of miR-181b inhibition.

On the surface, the findings of Di Gregoli et al. (2017) appear to be at odds with those of Tuday et al. (2021). The latter indicates that elevation of miR-181b by inhibiting its degradation via TN/TX protects against age-associated arterial stiffness; the former suggests that miR-181b inhibition protects against development of atherosclerotic plaques and aortic aneurysms. However, one straightforward way of integrating these findings is that normalizing the levels of miR-181b in each of these paradigms leads to a beneficial result. In aging, when miR-181b levels are low, increasing them by inhibiting TN/TX is beneficial. In models of atherosclerotic plaque and aortic aneurysms which display marked elevations of miR-181b, then selective inhibition of this microRNA is protective. Another common feature of these results is that manipulating miR-181b has striking effects on key components of the extracellular matrix, reinforcing the view that strategies aimed at regulating its expression provide an effective means of influencing arterial stiffness.

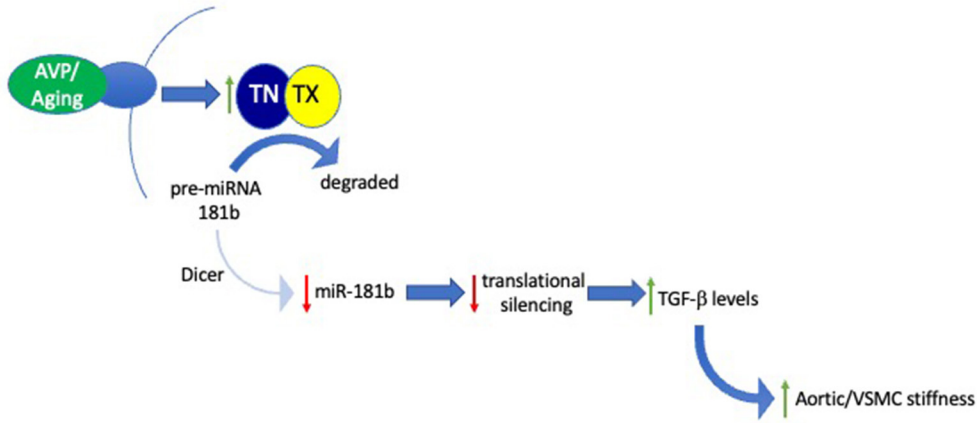

FIGURE 1 | Signaling pathway mediating role of the TN/TX microRNA-degrading enzyme in regulating aortic stiffness. Schematic diagram integrates results obtained in both *in vitro* and *in vivo* studies examining the role of TN/TX and miR-181b in mediating VSMC and aortic stiffness. In this model, aging or AVP stimulation elicit activation of TN/TX which cleaves pre-miR-181b, the precursor of mature miR-181b. Degradation of pre-miR-181b prevents Dicer from generating mature miR-181b. The subsequent decrease in levels of mature miR-181b blocks its ability to silence translation of its mRNA targets. Although the identity of these mRNA targets remains to be identified, we hypothesize that allowing them to be translated by reducing miR-181b levels leads to increased extracellular levels of TGF-β. According to this model, excess TGF-β signaling drives the increase in VSMC and ECM stiffness underlying LAS.

SUMMARY AND FUTURE DIRECTIONS

Taken together, the studies summarized above provide compelling evidence that alterations in microRNA signaling in aorta play a key role in the development of LAS. In this review, we have focused on their role in VSMCs. However, there is also a large body of literature documenting their important roles in regulating endothelial cell function (Wei et al., 2013; Cao et al., 2020). Thus, an important next step in this field will be to assess whether manipulating miRNA levels in VSMCs selectively is sufficient to induce or prevent arterial stiffening or whether parallel processes in endothelial cells or other cells present in large vessels, such as immune cells or fibroblasts, also play a key role in the pathophysiology of LAS.

Comparison of the longitudinal development of arterial stiffness with aging in males and females has revealed a prominent increase in post-menopausal women (Coutinho, 2014; DuPont et al., 2019), suggesting that estrogen has a protective effect. The exact mechanism in human pathophysiology is not fully understood; however, animal studies suggest significant effects of estrogen on the extracellular matrix as a primary contributor (Ogola et al., 2018). The growing evidence for a role of microRNA dysregulation in the etiology of this disorder provides a strong rationale for assessing whether these epidemiological findings reflect hormonal effects on microRNA signaling. Furthermore, since aging male mice develop increased PWV (Nicholson et al., 2017), we now emphasize the need for a comprehensive female animal longitudinal study as it would be interesting to check whether female aging mice might provide a useful model to investigate mechanisms underlying increased LAS in post-menopausal women.

As inhibiting the activity of the TN/TX microRNA-degrading enzyme confers protection from the development of aging-associated arterial stiffening, inhibitors of this enzyme may have translational potential. However, since the observed protection occurred in mice with a constitutive inactivation of TN/TX, it will be important to check if inhibition of this enzyme after the initial onset of aging-associated arterial stiffening can prevent the progression or even reverse this process. In addition, as TN/TX inhibition may also elevate other microRNAs, it might be more advantageous to explore other strategies to increase miR-181b levels selectively. For example, recent studies have demonstrated that methotrexate increases transcription of miR-181b since its metabolite, adenosine, stimulates the adenosine A3 receptor (Yang et al., 2021). Focusing on strategies able to selectively elevate miR-181b seems particularly attractive since, in addition to its ability to decrease stiffness in VSMCs, this microRNA also exerts anti-inflammatory effects in endothelial cells (Sun et al., 2014). However, since extremely high elevations of miR-181b have been implicated in the development of atherosclerotic plaques, (Di Gregoli et al., 2017), it may be important to identify strategies that reverse the age-associated decline in miR-181b levels without elevating them further into the range associated with pathological effects.

In summary, the hypothesis that microRNAs play a key role in the pathophysiology of LAS has stimulated important progress in identifying specific microRNAs implicated in this process. These advances provide a firm foundation for further studies aimed at deciphering: (1) how these microRNAs are regulated, and (2) how they impact arterial stiffness, information that will be essential to identifying strategies capable of combatting the enormous public health challenge presented by LAS.

AUTHOR CONTRIBUTIONS

JB, ET, DB, and SD discussed the scope of the review. JB wrote the initial draft and revised it based on comments made by

ET. All authors contributed to the article and approved the submitted version.

FUNDING

This study was supported by NIH, Stimulating and Advancing ACCM Research, Western Institute for Veterans Research.

ACKNOWLEDGMENTS

We would like to acknowledge support from Stimulating and Advancing ACCM Research, as well as the following NIH grants: U54AG062333 (SD), U18TR003780 (SD), T32HL007227 (ET), Western Institute for Veterans Research (WIVR) 831 (ET), and DA044123 (JB).

REFERENCES

Albinsson, S., Suarez, Y., Skoura, A., Offermanns, S., Miano, J. M., and Sessa, W. C. (2010). MicroRNAs are necessary for vascular smooth muscle growth, differentiation, and function. *Arterioscler. Thromb. Vas. Biol.* 230,1118–1126. doi: 10.1161/ATVBAHA.109.200873

Amen, A. M., Ruiz-Garzon, C. R., Shi, J., Subramanian, M., Pham, D. L., and Meffert, M. K. (2017). A rapid induction mechanism for Lin28a in trophic responses. *Mol. Cell* 65, 490–503. doi: 10.1016/j.molcel.2016.12.025

Asada, K., Canestrari, E., Fu, X., Li, Z., Makowski, E., Wu, Y. C., et al. (2014). Rescuing Dicer defects via inhibition of an anti-dicing nuclease. *Cell Rep.* 9, 1471–1481. doi: 10.1016/j.celrep.2014.10.021

Badi, I., Burba, I., Ruggeri, C., Zeni, F., Bertolotti, M., Scopece, A., et al. (2015). MicroRNA-34a induces vascular smooth muscle cells senescence by SIRT1 downregulation and promotes the expression of age-associated pro-inflammatory secretory factors. *J. Gerontol. A Biol. Sci. Med. Sci.* 70, 1304–1311. doi: 10.1093/gerona/glu180

Baraban, J. M., Shah, A., and Fu, X. (2018). Multiple pathways mediated microrna degradation: focus on the Translin/Trax RNase complex. *Adv. Pharmacol.* 82, 1–20. doi: 10.1016/bs.apha.2017.08.003

Bartel, D. P. (2004). MicroRNAs: genomics, biogenesis, mechanism, and function. *Cell* 116, 281–297. doi: 10.1016/S0092-8674(04)00045-5

Boon, R. A., Seeger, T., Heydt, S., Fischer, A., Hergenreider, E., Horrevoets, A. J. G., et al. (2011). MicroRNA-29 in aortic dilation: implications for aneurysm formation. *Circul. Res.* 109, 1115–1119. doi: 10.1161/CIRCRESAHA.111.255737

Boutouyrie, P., Lacolley, P., Briet, M., Regnault, V., Stanton, A., Laurent, S., et al. (2011). Pharmacological modulation of arterial stiffness. *Drugs* 71, 1689–1701. doi: 10.2165/11593790-000000000-00000

Cao, Q., Wu, J., Wang, X., and Song, C. (2020). Noncoding RNAs in vascular aging. *Oxidat. Med. Cell. Longev.* 7914957. doi: 10.1155/2020/7914957

Cazalla, D., Yario, T., and Steitz, J. A. (2010). Down-regulation of a host microRNA by a Herpesvirus saimiri noncoding RNA. *Science* 328, 1563–1566. doi: 10.1126/science.1187197

Chirinos, J. A., Segers, P., Hughes, T., and Townsend, R. (2019). Large-artery stiffness: in health and disease: JACC state-of-the-art review. *Jam. Coll. Cardiol.* 74, 1237–1263. doi: 10.1016/j.jacc.2019.07.012

Coutinho, T. (2014). Arterial stiffness and its clinical implications in women. *Can. J. Cardiol.* 30, 756–764. doi: 10.1016/j.cjca.2014.03.020

Deng, H., Song, Z., Xu, H., Deng, X., Zhang, Q., Chen, H., et al. (2017). MicroRNA-1185 promotes arterial stiffness through modulating VCAM-1 and E-selectin expression. *Cell. Physiol. Biochem.* 41, 2183–2193. doi: 10.1159/000475576

Di Gregoli, K., Anuar, N. N. M., Bianco, R., White, S. J., Newby, A. C., George, S. J., et al. (2017). MicroRNA-181b controls atherosclerosis and aneurysms through regulation of TIMP-3 and elastin. *Circul. Res.* 120, 49–65. doi: 10.1161/CIRCRESAHA.116.309321

DuPont, J. J., Kenney, R. M., Patel, A. R., and Jaffe, I. Z. (2019). Sex differences in mechanisms of arterial stiffness. *Br. J. Pharmacol.* 176, 4208–4225. doi: 10.1111/bph.14624

Friedman, R. C., Farh, K. K., Burge, C. B., and Bartel, D. P. (2009). Most mammalian mRNAs are conserved targets of microRNAs. *Genome Res.* 19, 92–105. doi: 10.1101/gr.082701.108

Fu, X., Shah, A., and Baraban, J. M. (2016). Rapid reversal of translational silencing: emerging role of microRNA degradation pathways in neuronal plasticity. *Neurobiol. Learn. Mem.* 133, 225–232. doi: 10.1016/j.nlm.2016.04.006

Fu, X., Shah, A. P., Li, Z., Li, M., Tamashiro, K. L., and Baraban, J. M. (2020). Genetic inactivation of the translin/trax microRNA-degrading enzyme phenocopies the robust adiposity induced by Translin (Tsn) deletion. *Mol. Metab.* 40:101013. doi: 10.1016/j.molmet.2020.101013

Gatsiou, A., Georgiopoulos, G., Vlachogiannis, N. I., Pfisterer, L., Fischer, A., Sachse, M., Laina, A., Bonini, F., and Delialis, D., et al. (2021). Additive contribution of microRNA-34a/b/c to human arterial ageing and atherosclerosis. *Atherosclerosis* 327, 49–58. doi: 10.1016/j.atherosclerosis.2021.05.005

Hagan, J., Piskounova, E., and Gregory, R. (2009). Lin28 recruits the TUTase Zcchc11 to inhibit let-7 maturation in mouse embryonic stem cells. *Nat. Struct. Mol. Biol.* 16:1021–1025. doi: 10.1038/nsmb.1676

Han, J., LaVigne, C. A., Jones, B. T., Zhang, H., Gillett, F., and Mendell, J. T. (2020). A ubiquitin ligase mediates target-directed microRNA decay independently of tailing and trimming. *Science* 370:1432. doi: 10.1126/science.abc9546

Hazra, S., Henson, G. D., Morgan, R. G., Breevoort, S. R., Ives, S. J., Richardson, R. S., et al. (2016). Experiimental reduction of miR-92a mimics arterial aging. *Exp. Gerontol.* 83, 165–170. doi: 10.1016/j.exger.2016.08.007

Heo, I., Joo, C., Cho, J., Ha, M., Han, J., and Kim, V. (2008). Lin28 Mediates the Terminal Uridylation of let-7 Precursor MicroRNA. *Mol. Cell* 32:276–284. doi: 10.1016/j.molcel.2008.09.014

Heo, I., Joo, C., Kim, Y., Ha, M., Yoon, M., Cho, J., et al. (2009). TUT4 in concert with Lin28 suppresses MicroRNA biogenesis through Pre-MicroRNA uridylation. *Cell* 138, 696–708. doi: 10.1016/j.cell.2009.08.002

Hori, D., Dunkerly-Eyring, B., Nomura, Y., Biswas, D., Steppan, J., Henar-Mejia, J., et al. (2017). miR-181b regulates vascular stiffness age dependently in part by regulating TGF-β signaling. *PLoS ONE* 12:e0174108. doi: 10.1371/journal.pone.0174108

Huang, Y. W., Ruiz, C. R., Eyler, E. C., Lin, K., and Meffert, M. K. (2012). Dual regulation of miRNA biogenesis generates target specificity in neurotrophin-induced protein synthesis. *Cell* 148, 933–946. doi: 10.1016/j.cell.2012.01.036

Kang, H., and Hata, A. (2012). MicroRNA regulation of smooth muscle gene expression and phenotype. *Curr. Opin. Hematol.* 19, 224–231. doi: 10.1097/MOH.0b013e3283523e57

Liao, Y.-C., Wang, Y.-S., His, E., Chang, M.-H., You, Y.-Z., and Juo, S.-H. H. (2015). MicroRNA-765 influences areterial stiffness through modulating apelin expression. *Mol. Cell. Endocrin.* 411, 11–19. doi: 10.1016/j.mce.2015.04.006

McGeary, S. E., Lin, K. S., Shi, C. Y., Pham, T. M., Bisaria, N., Kelley, G. M., et al. (2019). The biochemical basis of microRNA targeting efficacy. *Science* 366:eaav1741. doi: 10.1126/science.aav1741

Mitchell, G. F., Guo, C. Y., Benjamin, E. J., Larson, M. G., Keyes, M. J., Vita, J. A., et al. (2007). Cross-sectional correlates of increased aortic stiffness in the community: the Framingham Heart Study. *Circulation* 115, 2628–2636. doi: 10.1161/CIRCULATIONAHA.106.667733

Mitchell, G. F., Hwang, S. J., Vasan, R. S., Larson, M. G., Pencina, M. J., Hamburg, N. M., et al. (2010). Arterial stiffness and cardiovascular events: the Framingham Heart Study. *Circulation* 121, 505–511. doi: 10.1161/CIRCULATIONAHA.109.886655

Nicholson, C. J., Seta, F., Lee, S., and Morgan, K. G. (2017). MicroRNA-203 mimics age-related aortic smooth muscle dysfunction of cytoskeletal pathways. *J. Cell. Mol. Med.* 1, 81–95. doi: 10.1111/jcmm.12940

Ogola, B. O., Zimmerman, M. A., Clark, G. L., Abshire, C. M., Gentry, K. M., Miller, K. S., et al. (2018). New insights into arterial stiffening: does sex matter? *Am. J. Physiol. Heart Circ. Physiol.* 315, H1073–H1087. doi: 10.1152/ajpheart.00132.2018

O'Rourke, M. (1990). Arterial stiffness, systolic blood pressure, and logical treatment of arterial hypertension. *Hypertension* 15, 339–347. doi: 10.1161/01.HYP.15.4.339

O'Rourke, M. F., and Nichols, W. W. (2005). Aortic diameter, aortic stiffness, and wave reflection increase with age and isolated systolic hypertension. *Hypertension* 45, 652–656. doi: 10.1161/01.HYP.0000153793.84859.b8

O'Rourke, M. F., O'Brien, C., and Edelman, E. R. (2016). Arterial stiffening in perspective: advances in physical and physiological science over centuries. *Am. J. Hypertens.* 29, 785–791. doi: 10.1093/ajh/hpw019

Park, A. J., Havekes, R., Fu, X., Hansen, R., Tudor, J. C., Peixoto, L., et al. (2017). Learning induces the translin/trax RNase complex to express activin receptors for persistent memory. *Elife* 6:e27872. doi: 10.7554/eLife.27872.018

Park, A. J., Shetty, M. S., Baraban, J. M., and Abel, T. (2020). Selective role of the translin/trax RNase complex in hippocampal synaptic plasticity. *Mol. Brain* 13:145. doi: 10.1186/s13041-020-00691-5

Qiu, H., Zhu, Y., Sun, Z., Trzeciakowki, J. P., Gansner, M., Depre, C., et al. (2010). Vascular smooth muscle cell stiffness as a mechanism for increased aortic stiffness with aging. *Circ. Res.* 107, 615–619. doi: 10.1161/CIRCRESAHA.110.221846

Sehgel, N. L., Vatner, S. F., and Meininger, G. A. (2015). "Smooth muscle cell stiffness syndrome"—revisiting the structural basis of arterial stiffness. *Front. Physiol.* 6:335. doi: 10.3389/fphys.2015.00335

Sheu-Gruttadauria, J., Pawlica, P., Klum, S. M., Wang, S., Yario, T. A., Schirle Oakdale, N. T., et al. (2019). Structural basis for target-directed microrna degradation. *Mol. Cell* 75, 1243–1255. doi: 10.1016/j.molcel.2019.06.019

Shi, C. Y., Kingston, E. R., Kleaveland, B., Lin, D. H., Stubna, M. W., and Bartel, D. P. (2020). The ZSWIM8 ubiquitin ligase mediates target-directed microRNA degradation. *Science* 370:eabc9359. doi: 10.1126/science.abc9359

Steppan, J., Wang, H., Bergman, Y., Rauer, M. J., Tan, S., Jandu, S., et al. (2019). Lysyl oxidase-like 2 depletion is protective in age-associated vascular stiffening. *Am. J. Physiol. Heart Circ. Physiol.* 317, H49–H59. doi: 10.1152/ajpheart.00670.2018

Sun, X., Sit, A., and Feinberg, M. W. (2014). Role of miR-181 family in regulating vascular inflammation and immunity. *Trends Cardiovasc. Med.* 24, 105–112. doi: 10.1016/j.tcm.2013.09.002

Suzuki, H., Arase, M., Matsuyama, H., Choi, Y., Ueno, T., Mano, H., et al. (2011). MCPIP1 ribonuclease antagonizes dicer and terminates MicroRNA biogenesis through precursor MicroRNA degradation. *Mol. Cell.* 44, 424–436. doi: 10.1016/j.molcel.2011.09.012

Tuday, E., Nakano, M., Akiyoshi, K., Fu, X., Shah, A. P., Yamaguchi, A., et al. (2021). *Degradation of Premature-miR-181b by the translin/trax RNase Increases Vascular Smooth Muscle Stiffness*. Hypertension, in press.

Tuday, E., Nomura, Y., Ruhela, D., Nakano, M., Fu, X., Shah, A., et al. (2019). Deletion of the microRNA-degrading nuclease, translin/trax, prevents pathogenic vascular stiffness. *Am. J. Physiol. Heart Circ. Physiol.* 317, H1116–H1124. doi: 10.1152/ajpheart.00153.2019

van Rooij, E., Sutherland, L. B., Thatcher, J. E., DiMaio, J. M., Naseem, R. H., Marshall, W. S., et al. (2008). Dysregulation of microRNAs after myocardial infarction reveals a role of mir-29 in cardiac fibrosis. *Proc. Nat. Acad. Sci.* 105, 13027–13032. doi: 10.1073/pnas.0805038105

Wei, Y., Schober, A., and Weber, C. (2013). Pathogenic arterial remodeling: the good and bad of microRNAs. *Am. J. Physiol. Heart Circ. Physiol.* 304, H1050–1059. doi: 10.1152/ajpheart.00267.2012

Yang, D., Haemmig, S., Zhou, H., Perez-Cremades, D., Sun, X., Chen, L., et al. (2021). Methotrexate attenuates vascular inflammation through an adenosine-microRNA-dependent pathway. *Elife* 10:e58064. doi: 10.7554/eLife.58064

Conflict of Interest: The authors declare that the research was conducted in the absence of any commercial or financial relationships that could be construed as a potential conflict of interest.

Publisher's Note: All claims expressed in this article are solely those of the authors and do not necessarily represent those of their affiliated organizations, or those of the publisher, the editors and the reviewers. Any product that may be evaluated in this article, or claim that may be made by its manufacturer, is not guaranteed or endorsed by the publisher.

frontiers in Physiology

MINI REVIEW
published: 01 October 2021
doi: 10.3389/fphys.2021.746278

Vascular Health Triad in Humans With Hypertension—Not the Usual Suspects

Sushant M. Ranadive[1], Gabrielle A. Dillon[2,3], Sara E. Mascone[1] and Lacy M. Alexander[2,3]*

[1] Department of Kinesiology, University of Maryland, College Park, College Park, MD, United States, [2] Department of Kinesiology, The Pennsylvania State University, University Park, PA, United States, [3] Center for Healthy Aging, The Pennsylvania State University, University Park, PA, United States

OPEN ACCESS

Edited by:
Jochen Steppan, Johns Hopkins University, United States

Reviewed by:
Eduardo Damasceno Costa, Federal University of Minas Gerais, Brazil
Yu Huang, China University of Geosciences Wuhan, China
Deepesh Pandey, Johns Hopkins University, United States

***Correspondence:**
Sushant M. Ranadive
ranadive@umd.edu

Specialty section:
This article was submitted to Vascular Physiology, a section of the journal Frontiers in Physiology

Received: *23 July 2021*
Accepted: *25 August 2021*
Published: *01 October 2021*

Citation:
Ranadive SM, Dillon GA, Mascone SE and Alexander LM (2021) Vascular Health Triad in Humans With Hypertension—Not the Usual Suspects. Front. Physiol. 12:746278. doi: 10.3389/fphys.2021.746278

Hypertension (HTN) affects more than one-third of the US population and remains the top risk factor for the development of cardiovascular disease (CVD). Identifying the underlying mechanisms for developing HTN are of critical importance because the risk of developing CVD doubles with ∼20 mmHg increase in systolic blood pressure (BP). Endothelial dysfunction, especially in the resistance arteries, is the primary site for initiation of sub-clinical HTN. Furthermore, inflammation and reactive oxygen and nitrogen species (ROS/RNS) not only influence the endothelium independently, but also have a synergistic influence on each other. Together, the interplay between inflammation, ROS and vascular dysfunction is referred to as the vascular health triad, and affects BP regulation in humans. While the interplay of the vascular health triad is well established, new underlying mechanistic targets are under investigation, including: Inducible nitric oxide synthase, hydrogen peroxide, hydrogen sulfide, nuclear factor kappa-light-chain-enhancer of activated B cells (NF-κB) and nuclear factor activated T cells. This review outlines the role of these *unusual suspects* in vascular health and function in humans. This review connects the dots using these *unusual suspects* underlying inflammation, ROS and vascular dysfunction especially in individuals at risk of or with diagnosed HTN based on novel studies performed in humans.

Keywords: blood pressure, endothelium, inflammation, oxidative stress, reactive oxygen species

INTRODUCTION

Cardiovascular disease (CVD) is the leading cause of morbidity and mortality worldwide, and the prevalence of CVD increases with aging (Virani et al., 2021). The increase in blood pressure (BP) or diagnosed hypertension (HTN) is widely accepted as the primary precursor to CVD; the risk of CVD is assumed to increase in a linear fashion as BP increases. In general, the risk of CVD doubles when there is an approximately 20 mmHg increase in systolic BP and 10 mmHg increase

in diastolic BP (Lewington et al., 2002). Further, BP rises substantially as humans age (Guzik and Touyz, 2017); however, the rise in BP with age is linear among men but rises in a differential pattern among women. Sex differences in HTN and their underlying mechanisms have been reviewed in detail previously (Ji et al., 2020).

In 2017, the American College of Cardiology (ACC) and American Heart Association (AHA) redefined the classifications of HTN diagnosis (Whelton et al., 2018). In the revised categorizations, the BP threshold has been lowered for stage 1 HTN and prehypertension (now elevated BP). Stage 1 HTN is defined as resting systolic BP between 130 and 139 mmHg or diastolic BP between 80 and 89 mmHg, and elevated BP is now defined as systolic BP between 120 and 129 mmHg and diastolic BP below 80 mmHg. Elevated BP is a strong predictor of late life HTN and CVD (Whelton et al., 2018). The revised categorizations have drastically increased the prevalence of HTN to about 46% of Americans (Virani et al., 2021), and have highlighted the importance of preclinical and clinical research in humans to identify therapeutic targets for interventions that extend the health of aging humans (Whelton et al., 2018). Moreover, identification of novel drug treatment based targets is important as medication adherence with traditional antihypertensives (diuretics, angiotensin converting enzyme inhibitors, calcium channel blockers, etc.) remains a significant issue.

The main site for vascular resistance, and thus a critical component of BP regulation, are the arterioles in the microcirculation (Nowroozpoor et al., 2021). The arterioles have similar anatomical layers as larger arteries; however, the lumen size of the arterioles (10–150 μm diameter) creates a substantial resistance to the blood flow and thus BP responses. In addition to the lumen size, the smooth muscle tone being normally in a state of contraction makes the resistance vessels an important site for BP control. Vascular resistance within the arteries is controlled by a complex interplay between local vasodilators, sympathetic modulation, and endocrine (paracrine) driven changes. Not only is the microvascular bed the first site to present with dysfunction, but it can also experience dysfunction without displaying any evidence in the macrovasculature or feed arteries (Nowroozpoor et al., 2021). Well established causes of endothelial dysfunction include imbalances in inflammation and/or reactive oxygen species (ROS). This is of particular importance because endothelial dysfunction can further potentiate imbalances in inflammation and ROS, leading to a "never ending cycle (or triad)" (**Figure 1**). The cumulative effects of these minor insults on the vasculature lead to a pro-hypertensive environment. In this mini-review we will first present aspects of the vascular health triad and then novel mechanisms that induce imbalances within the system, leading to HTN in humans. **Table 1** summarizes the methods utilized to elucidate mechanisms underlying hypertension-associated vascular dysfunction A comprehensive discussion of the renal and sympathetic contributions to HTN is beyond the scope of this review, but have been recently reviewed (Grassi et al., 2018, 2019; Fonkoue et al., 2019; Holwerda et al., 2019; Keir et al., 2020).

VASCULAR HEALTH—ROLE OF INFLAMMATION AND REACTIVE OXYGEN AND NITROGEN SPECIES—*"THE USUAL SUSPECTS"*

In young, healthy adults, inflammation and reactive oxygen and nitrogen species (ROS/RNS) serve a critical, positive physiological role in vascular homeostasis. The maintenance of vascular health is the complex relationship between vasoprotective factors, such as the nitric oxide system, and other pathways that impair these mechanisms, including both inflammation and ROS. "Normal" vascular function is often characterized by the ability to efficiently vasodilate or vasoconstrict in response to a stimulus. On the contrary, vascular dysfunction is characterized by the loss of efficiency in the vasodilatory component even in the presence of a stimulus. *Inflammation* is one such stimulus (and a cornerstone of the vascular health triad) which influences vascular function acutely and chronically—in a temporal fashion. Inflammation is heightened as a natural defense mechanism to tissue injury, infection, or pathogen infiltration. The initial inflammatory cascade is characterized by heightened pro-inflammatory cytokine release, immune cell movement to the site of invasion or injury, and the release of local chemoattractants, notably, adhesion molecules (Wadley et al., 2013). This acute inflammation (influx of inflammatory cytokines) can transiently impair vascular function (8–32 h), through an acute impairment in nitric oxide (NO) bioavailability, even in young otherwise healthy individuals (Hingorani et al., 2000). The second component of the vascular health triad is ROS, which are free radicals, such as superoxide or peroxynitrite, that are integral to cellular signaling (El Assar et al., 2013; Wadley et al., 2013). ROS are produced via oxidative metabolism and proteins, such as NADPH oxidase, xanthine oxidase and via endothelial nitric oxide synthase (eNOS) uncoupling (Jacobi et al., 2005; Ding et al., 2007; El Assar et al., 2013; Wadley et al., 2013). Endogenous antioxidants, such as superoxide dismutase (SOD), glutathione, and NO, clear ROS enzymatically, or through direct chemical reaction (Selemidis et al., 2007; El Assar et al., 2013; Wadley et al., 2013). The aspect of mitochondrial ROS is covered in detail in an excellent review by Kirkman et al. (2021).

In young, otherwise healthy adults, there is ***(I)*** redundancy in the vasodilatory pathways with abundant bioavailability of endothelium-derived vasodilating substances (e.g., NO, prostaglandins, EDHF) ***(II)*** low basal concentrations of vasoconstrictive substances and ***(III)*** low basal concentrations of inflammatory cytokines and ROS. However, while there is ample data indicating impaired endothelial function in human subject cohorts who are at risk for the development of HTN later in life, including those with a family history of HTN (Greaney et al., 2015; Matthews et al., 2017), and non-traditional CVD risk factors (Martens et al., 2016; Greaney et al., 2019; Katulka et al., 2019), there is lack of data in individuals who are young and otherwise healthy but have undiagnosed HTN. Moreover, due to this redundancy it is difficult to unravel these interrelated

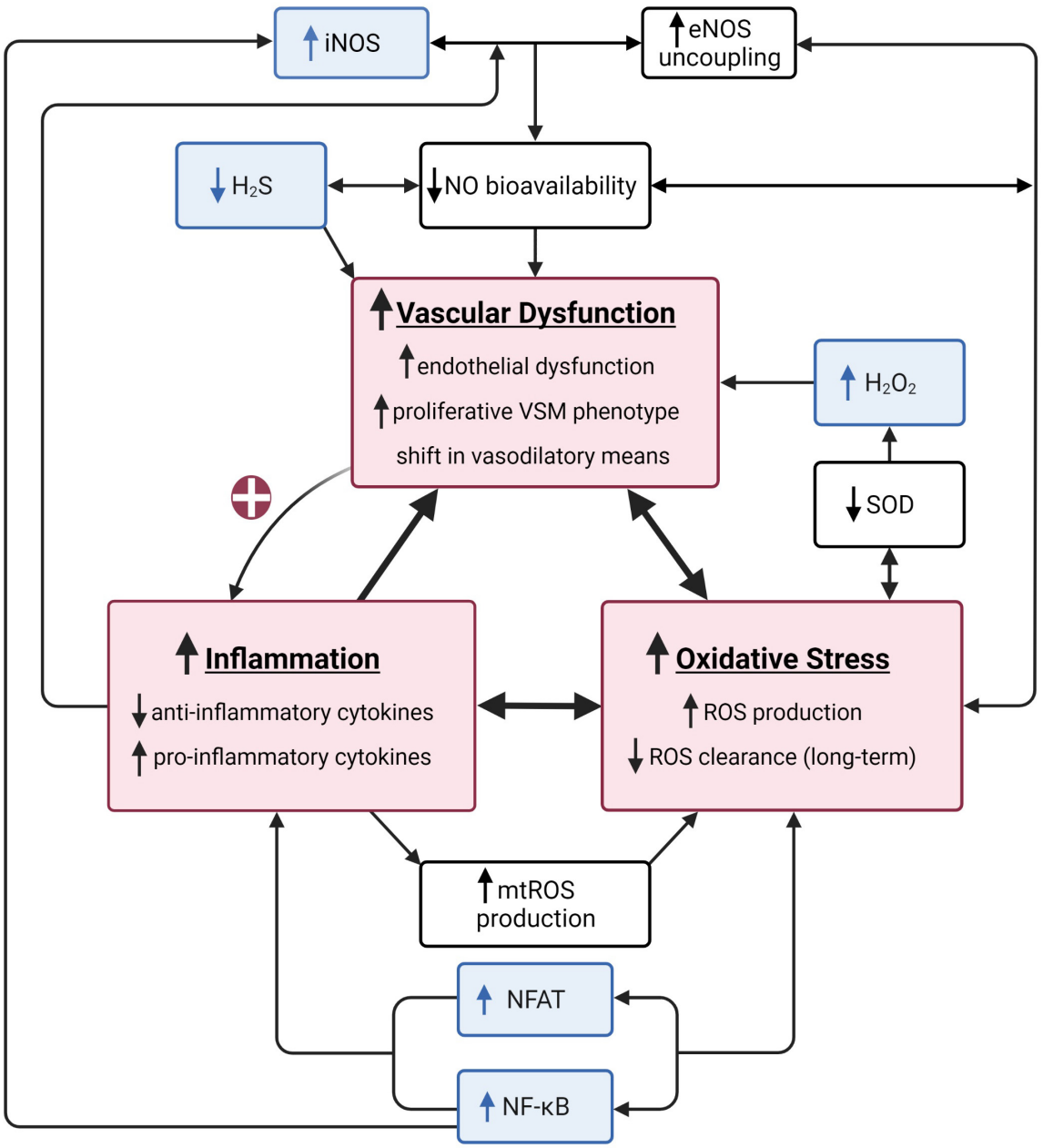

FIGURE 1 | A summary of the vascular health triad. The vascular health triad is composed of oxidative stress, inflammation, and vascular dysfunction (red boxes). These outcomes are synergistically interdependent as their underlying mechanisms directly (e.g., high inflammatory state causes a decrease in nitric oxide (NO) bioavailability resulting in increased vascular dysfunction) or indirectly [e.g., vascular dysfunction increasing inflammation via positive feedback loop (red plus sign)] interact, resulting in a vicious cycle of increased cardiovascular disease risk. Well-established underlying mechanisms of the triad include decreased NO bioavailability via increased endothelial nitric oxide synthase (eNOS) uncoupling, decreased superoxide dismutase (SOD), and increased mitochondrial reactive oxygen species (mtROS) production (white boxes). The unusual suspects include inducible nitric oxide synthase (iNOS), hydrogen sulfide (H2S), hydrogen peroxide (H2O2), nuclear factor kappa-light-chain-enhancer of active B cells (NF-κB), and nuclear factor of activated T cells (NFAT; blue boxes). Created with BioRender.com.

mechanisms using gross measures of endothelial function in conduit arteries.

Our laboratory recently induced acute inflammation using an influenza vaccine *in vivo* and *in vitro* in young, healthy African American and Caucasian American individuals (Sapp et al., 2021). Although the vaccine stimulus did not impact conduit artery function (as measured by flow-mediated dilation), there were decreases in eNOS messenger RNA in the African American group, coinciding with race-specific changes in intracellular and extracellular microRNAs (miR) related to inflammation (miR-221-3p, 222-3p, and 150-5p) (Sapp et al., 2021). Circulating miRs are novel biomarkers of acute and chronic inflammation

TABLE 1 | Summary of methodology for mechanisms mediating vascular function in hypertensive adults.

Method	References	Pathway
In vivo		
Flow-mediated Dilation + Doppler Ultrasound		
	Gokce et al., 2001; Benjamin et al., 2004; Juonala et al., 2004; McGowan et al., 2006; Buus et al., 2007; Yang et al., 2010; Broxterman et al., 2019; Figueiredo et al., 2012	Endothelium-dependent dilation
	Ratchford et al., 2019a	Endothelium-dependent dilation Oxidative stress (acute antioxidant cocktail)
	Sapp et al., 2021	Endothelium-dependent dilation Inflammation (influenza vaccine)
	Craighead et al., 2020	Endothelium-dependent dilation, Endothelium in-dependent dilation (sublingual NTG), Oxidative stress (Vitamin C)
Venous Occlusion Plethysmography		
	On et al., 2002	Endothelium-dependent (ACh)
	Bottino et al., 2015	Endothelium-dependent dilation, Endothelium in-dependent (sublingual NTG) Endothelium-dependent (ACh, Bradykinin)
	Hingorani et al., 2000	Endothelium in-dependent (NTG, verapamil) Inflammation (salmonella typhi vaccine)
Arterial Infusions + Doppler Ultrasound		
	Takase et al., 2006; Broxterman et al., 2019	Endothelium-dependent dilation (ACh)
	Gokce et al., 2001; McGowan et al., 2006; Buus et al., 2007	Endothelium in-dependent dilation (NTG)
Iontophoresis + Laser Doppler Flowmetry		
	Cupisti et al., 2000	Endothelium-dependent dilation (ACh) Endothelium-independent dilation (SNP)
	Farkas et al., 2004	
	Lindstedt et al., 2006	Endothelium-dependent dilation (ACh; local heating) Endothelium in-dependent dilation (SNP)
Intradermal Microdialysis + Laser Doppler Flowmetry		
	Smith et al., 2011	Endothelium-dependent dilation (ACh, local heating) NO (L-NAME) iNOS (1400W) nNOS (NPLA)
	Smith et al., 2013	Vasoconstriction (local cooling, yohimbine + propranolol), Rho/Rho-Kinase (fasudil)
	Bruning et al., 2015	Endothelium-dependent dilation (local heating), NO (L-NAME)
	Craighead et al., 2017	Endothelium-dependent dilation (ACh, local heating), NO (L-NAME), iNOS (1400w)
	HTN Greaney et al., 2017	Endothelium-dependent dilation (ACh), NO (L-NAME), H_2S (Na2S, AOAA)
	Craighead et al., 2018	Endothelium independent dilation (SNP), NE-induced vasoconstriction, Lysyl Oxidation (BAPN)
	Dillon et al., 2020	Endothelium-dependent (ACh), NO (L-NAME)
Sublingual NTG + Doppler Ultrasound		
	McGowan et al., 2006	Endothelium in-dependent dilation
Non-invasive Single Limb Exercise + Doppler Ultrasound		
	Ratchford et al., 2019b	BF response to exercise (IHG)
	McGowan et al., 2006	BF response to exercise (static IHG, dynamic knee extension)
Single Limb Exercise + NIRS-derived TSI		
	Sprick et al., 2019	BF response to exercise (IHG)

TABLE 1 | (Continued)

Method	References	Pathway
In vivo		
***Ex vivo* / *in vitro* Circulating concentrations**		
	Hingorani et al., 2000	IL-1β, IL-1Ra IL-6, TNF-α
	Bottino et al., 2015	IL-1, IL-6, OxLDL, sICAM, sVCAM, sE-Selectin, TNF-α
	Junqueira et al., 2018	Adiponectin, CRP, endothelin, ICAM, VCAM
	Craighead et al., 2020	IL-6, OxLDL, TNF-α, total antioxidant status, hsCRP
PBMCs		
	Huang et al., 2016	IL-6, NFAT, TNF-α
Arterial Biopsy		
	Phillips et al., 2007	NO (L-NAME)
		Oxidative stress (H_2O_2)
	Donato et al., 2007	Oxidative stress (nitrotyrosine, NFκB)
	Migrino et al., 2011	Endothelial-dependent dilation (ACh), Endothelial in-dependent dilation (papaverine), Oxidative stress (SOD, BH4, mitoquinone, gp91ds-tat)
	Beyer et al., 2014	Oxidative stress (H_2O_2,mtROS, tempol)
	Beyer et al., 2017	Oxidative stress (H_2O_2,mtROS)
	Kadlec et al., 2017	H_2O_2, NO, PGC-1α
	Hughes et al., 2021b	NO (L-NAME, c-PTIO), H_2O_2(peg-cat) Oxidative stress (rotenone)
	Hader et al., 2019	
	Hughes et al., 2021a	H_2O_2
Venous Endothelial Cell Biopsy		
	Donato et al., 2007	Oxidative stress (NADPH oxidase p47phox, SOD, NFκB)
	Pierce et al., 2009	Inflammation (NFκB, TNF-α)
		Oxidative stress (NADPH oxidase p47phox)
	Craighead et al., 2020	Oxidative stress (NADPH, MnSOD), Inflammation (NFkB)
Cutaneous Biopsies		
	Smith et al., 2011	eNOS, iNOS, nNOS, pVASP
	Smith et al., 2013	ROCK activity and expression
	HTN Greaney et al., 2017	H_2S (CSE, 3-MPST)
Myograph		
	Buus et al., 2007	"small artery relaxation with ACh"

3-MPST, 3-mercaptopyruvate sulfurtransferase; ACh, acetylcholine; BAPN, β-aminopropionitrile; CRP, C-reactive protein; CSE, cystathionine gamma-lyase; H_2S, hydrogen sulfide; hsCRP, high-sensitivity C-reactive protein; IHG, intermittent handgrip; IL, interleukin; iNOS, inducible nitric oxide synthase; L-NAME, N^G-nitro-l-arginine methyl ester; MnSOD, manganese superoxide dismutase; NADPH, nicotinamide adenine dinucleotide phosphate; NE, norepinephrine; NFkB, nuclear factor kappa-light-chain-enhancer of activated B cells; nNOS, neuronal nitric oxide synthase; NO, nitric oxide; NPLA, N(ω)-propyl-L-arginine; NTG, nitroglycerin; oxLDL, oxidized low-density lipoprotein; PBMCs, peripheral blood mononuclear cells; ROCK, rho-associated protein kinase; ROS, reactive oxygen species; sICAM, soluble inter-cellular adhesion molecule; SNP, sodium nitroprusside; sVCAM, soluble vascular cell adhesion molecule; TNF-α, tumor necrosis factor alpha.

(Mi et al., 2013; Benz et al., 2016). miRs play mechanistic roles in endothelial activation, inflammation, and dysfunction; thus, initiating events in HTN (Cheng et al., 2014; Shi et al., 2015; Fernández-Hernando and Suárez, 2018). Furthermore, certain miRs [miR-146-protective (Wang et al., 2017); miR-34a- pro-inflammatory (Badi et al., 2018); miR-570-3p- pro-senescence (Baker et al., 2019); miR-217- pro-inflammatory (Zhang et al., 2019)] regulate ROS mechanisms via sirtuin-1 (Yamakuchi, 2012; Yamakuchi and Hashiguchi, 2018). Circulating miRs are taken up by endothelial cells, where they affect endothelial cell function, promote inflammation, and increase ROS (Njock and Fish, 2017; Zhong et al., 2018). Furthermore, the flow patterns within the arterial tree, i.e., turbulent flow near bifurcations or atherosclerotic lesions which can accentuate endothelial permeability or in contrast laminar flow which can exert beneficial effects on the vessel wall tend to trigger a number of miRs (Marin et al., 2013; Schmitz et al., 2019). Case in point, laminar shear stress (could be exercise induced) can upregulate miR-126 which is generally accepted as an anti-inflammatory and anti-atherogenic miR (Sapp et al., 2017). Therefore, in recent years circulating miRs have emerged as novel molecules mediating cell-to-cell communication in physiological processes (Njock and Fish, 2017; Bär et al., 2019). Mechanistically, emerging data in humans indicates significant cross-talk between inflammation and ROS within the endothelial cells in young, otherwise healthy adults, even before measurable conduit artery or macrovascular dysfunction plausibly through miRs (Sapp et al., 2021).

VASCULAR HEALTH TRIAD—AGING OR DISEASED STATES

In aging and diseased states, the vascular health triad becomes a positive feedback loop of heightened inflammation, oxidative stress, and vascular dysfunction. Chronic overproduction of inflammatory mediators, such as inflammatory cytokines, adhesion molecules, and inflammatory proteins, result in systemic low-grade inflammation initiating the complex cascade of heightened NADPH oxidase activity, eNOS uncoupling, and mitochondrial dysfunction, all of which result in heightened ROS production. Early in aging or disease pathogenesis, heightened antioxidant concentrations accommodate excessive ROS production. Following long-term exposure to increased ROS and inflammation, antioxidant defense mechanisms are reduced. Previous studies have interrogated these mechanisms with the acute administration of antioxidant cocktails (including ascorbic acid and alpha-tocopherol) in older adults (Eskurza et al., 2004a,b; Crecelius et al., 2010; Wray et al., 2012; Richards et al., 2015; Trinity et al., 2016), post-menopausal females (Ozemek et al., 2016), and individuals with heart failure with preserved ejection fraction (Ratchford et al., 2019a). However, more recent studies have focused on targeted pharmacological agents to identify specific ROS molecules within the triad (Alexander et al., 2013; Hurr et al., 2018; Martens et al., 2018; Park et al., 2018; Rossman et al., 2018). One emerging link in this triad is through the inducible nitric oxide synthase (iNOS) pathway. iNOS activity is increased during inflammation and NO is produced in toxic concentrations to prevent cell death by clearing excessive ROS (Aktan, 2004). NO reacts with superoxide (O_2^-), a main type of ROS produced during heightened inflammation, to form peroxynitrite ($ONOO^-$). Concurrently, superoxide dismutase (SOD) reacts with superoxide (O_2^-) to form hydrogen peroxide (H_2O_2). Interestingly H_2O_2 becomes the main contributing vasodilatory substance when NO bioavailability is decreased (Phillips et al., 2007; Beyer et al., 2014; Kadlec et al., 2017). Initially with acute inflammatory/ROS stimuli, other vasodilatory substances, such as prostaglandins and H_2O_2, can compensate for the impairment in NO-mediated vasodilation (Beyer et al., 2017). However, if the allostatic load presented by inflammation and ROS persists, not only do the compensatory mechanisms fail, but eventually deleterious vascular remodeling occurs. Therefore, with aging and/or disease progression the healthy functioning of the vasculature is disrupted due to ***(I)*** loss of redundant vasodilatory pathways, with limited bioavailability of vasodilating substances (especially NO), ***(II)*** increased circulating vasoconstrictive substances and ***(III)*** increased concentrations of inflammatory cytokines and ROS.

Typically, when considering vascular dysfunction, the role of NO bioavailability/scavenging due to eNOS uncoupling, decreased superoxide dismutase (SOD), and increased mitochondrial reactive oxygen species (mtROS) production are of significant importance (**Figure 1**). Therefore, in the following sections we have presented some of the newer and not widely discussed factors which can also have role in decreased NO bioavailability and/or increased NO scavenging, leading to vascular dysfunction.

VASCULAR HEALTH TRIAD—"*THE UNUSUAL SUSPECTS*"

Role of Inducible Nitric Oxide Synthase

During heightened inflammation and oxidative stress, there are various intersecting pathways that contribute to impaired NO bioavailability and, eventually, vascular dysfunction. Increased iNOS expression is stimulated by nuclear factor kappa-light-chain-enhancer of activated B cells (NF-κB), interleukin-6 (IL-6), and ROS producers, such as the $p47^{phox}$ subunit of NADPH oxidases (Hemmrich et al., 2003; Wu et al., 2008; Li et al., 2015). With chronic low-grade inflammation, iNOS activity increases, resulting in increased iNOS-derived NO production. To pharmacodissect the NOS balance in humans and prominent role of iNOS, we performed a unique *bed to bench* experiment evaluating endothelial-dependent microvascular function in individuals with HTN during iNOS, neuronal NOS (nNOS) and non-selective-NOS inhibition (Smith et al., 2011). Interestingly, the attenuated endothelial-dependent vasodilation in hypertensive adults was restored with iNOS inhibition, suggesting a prominent role of iNOS in hypertension-induced microvascular dysfunction. Even though the eNOS expression was similar between normotensives and hypertensives adults, iNOS expression in biopsy samples from hypertensive subjects was significantly greater as compared to age-matched normotensives (Smith et al., 2011). Thus, the NO produced during inflammation with HTN adopts a scavenging and cell-preserving role, as opposed to an active vasodilatory role.

Hydrogen Peroxide (H_2O_2) and H_2O_2-Mediated Primary Vasodilatory Mechanism

SOD is a primary antioxidant defense system with three known forms: SOD1 (cytosolic), SOD2 (mitochondrial), and SOD3 (circulating) (Zelko et al., 2002). SOD scavenges O_2^- radicals to form H_2O_2. During states of heightened inflammation and ROS, NADPH oxidase activity and eNOS uncoupling subsequently increase, resulting in increased O_2^- production (El Assar et al., 2013; Risbano and Gladwin, 2013; Wadley et al., 2013). In early disease initiation and progression, SOD activity increases to clear excessively produced O_2^-, subsequently increasing the production of H_2O_2 during both acute and chronic increases in inflammation and oxidative stress (El Assar et al., 2013). Recent studies from the Gutterman laboratory have suggested a novel theory of shifts in vasodilatory pathways during vascular inflammatory conditions, especially HTN (Migrino et al., 2011; Beyer et al., 2014, 2017; Kadlec et al., 2017). The NO-mediated vasodilatory pathway is vasoprotective, as it helps maintain normal BP in young, healthy individuals. However, with increased intraluminal pressure, as seen in HTN and reduced bioavailability of NO, there is a shift in microvascular vasodilatory pathways toward H_2O_2-dependent mechanisms, even though the total magnitude of the vasodilation to a given shear stimulus remains the same (Beyer et al., 2014). Hughes et al. (2021b) examined the effect of transient increases in intraluminal

pressure in resistance arterioles of hypertensive individuals with and without coronary artery disease were evaluated. In this model, there was a compensatory switch to the H_2O_2-mediated vasodilatory pathway following increased intraluminal pressure, suggesting diseased and healthy aged adults have similar shifts in primary vasodilatory mechanisms, but along a different time course (Hughes et al., 2021b). Furthermore, in the presence of transient increases in intraluminal pressure, even in isolated arterioles of healthy individuals, H_2O_2 is typically mitochondria derived (Beyer et al., 2014). These *ex-vivo* studies have also led to potential targets, such as autophagy and extranuclear telomerase (Hughes et al., 2021a). Taken together, these studies suggests an important switch in the physiological mechanism of vasodilation and heightened ROS production, specifically production of O_2^-, H_2O_2, and $ONOO^-$ as propagating a positive feedback loop that promotes vascular dysfunction.

Nuclear Factor Kappa-Light-Chain-Enhancer of Activated B Cells and Nuclear Factor From Activated T Cells

Investigating upstream transcriptional molecular targets underlying endothelial and vascular smooth muscle cell dysfunction in humans has yielded significant understanding of the complexity of these signaling mechanisms. Despite the complexity and multiple downstream effects, these studies are necessary for the development of targeted treatment and prevention strategies for HTN in humans. It is well established that NF-κB are an important intracellular mediator of inflammation and vascular dysfunction (specifically, NO-mediated mechanisms) (Donato et al., 2007, 2009; Pierce et al., 2009; Lee et al., 2014). In an elegant series of preclinical and clinical studies, Donato et al. (2009) established that activation of NF-κB mediates age-related vascular dysfunction. These studies interrogated NF-κB functionality in human subjects using a short-term (4 days) high-dose oral salsalate approach (Pierce et al., 2009). Salsalate, a non-acytlated salicylate, inhibits NF-κB translocation to the nucleus, reducing ROS synthesis through NADPH oxidases (Kopp and Ghosh, 1994; Pierce et al., 1996). They demonstrated that oral salsalate reduces endothelial cell NF-κ p65 expression by ∼25%, total nitrotrysine, a global marker of oxidative stress, and NADPH oxidase $p47^{phox}$ expression by 25 and 30%, respectively. Importantly, inhibition of NF-κB functionally resulted in improved NO-dependent vasodilation. Additionally, when comparing inactive to habitually active older adults, active adults had reduced NF-κB p65 expression, reduced nitrotyrosine, and endothelial function similar to their younger counterparts (Walker et al., 2014).

A growing body of literature suggests that the family of Ca^{2+}/calcineurin-sensitive transcriptional factors of nuclear factor from activated T-cells (NFAT) may play an essential role as a molecular switch that initiates dysfunction in both the endothelium (Cockerill et al., 1995; Boss et al., 1998; Armesilla et al., 1999; Bochkov et al., 2002; Gonzalez Bosc et al., 2004; Zetterqvist et al., 2015; Huang et al., 2016) and vascular smooth muscle (Suzuki et al., 2002; Lipskaia et al., 2003; Amberg et al., 2004; Nilsson et al., 2006; Nieves-Cintrón et al., 2007; Orr et al., 2009; Pang and Sun, 2009; Nilsson-Berglund et al., 2010; Berglund et al., 2012; Shiny et al., 2016; Soudani et al., 2016; Govatati et al., 2019). NFATs regulate multiple downstream mechanisms that initiate vascular dysfunction. Specifically, NFATs ***(I)*** impair endothelial function through NO-dependent mechanisms (Armesilla et al., 1999; Bochkov et al., 2002; Johnson et al., 2003; Norata et al., 2007; Garcia-Vaz et al., 2020; Wang et al., 2020), ***(II)*** increase the expression of inflammatory mediators in the arterial wall promoting atherosclerosis (Pierce et al., 1996; Pang and Sun, 2009; Nilsson-Berglund et al., 2010; Berglund et al., 2012; Zetterqvist et al., 2014; Weng et al., 2017), and ***(III)*** initiate pathogenic VSM proliferation (Suzuki et al., 2002; Lipskaia et al., 2003; Nilsson et al., 2006; Nieves-Cintrón et al., 2007; Donato et al., 2009; Orr et al., 2009; Pang and Sun, 2009; Nilsson-Berglund et al., 2010; Yan et al., 2015; Shiny et al., 2016; Soudani et al., 2016; Govatati et al., 2019). In preclinical models, inhibition of NFAT has prevented the activation of inflammatory cytokines (Kiani et al., 2000; Zetterqvist et al., 2014; Bretz et al., 2015; Huang et al., 2016), enhanced eNOS expression (Smith et al., 2011), increased NO bioavailability (Friedman et al., 2014; Zetterqvist et al., 2014, 2015; Garcia-Vaz et al., 2020), prevented VSM proliferation (Lipskaia et al., 2003; Berglund et al., 2012; Shiny et al., 2016), lowered BP (Garcia-Vaz et al., 2020), and reduced total atherosclerotic load (Norata et al., 2007; Nilsson-Berglund et al., 2010; Zetterqvist et al., 2014). Currently, these investigations/findings are limited to cellular and animal models. There are promising approaches, including examining NFATs in the skin microcirculation and in peripheral blood mononuclear cells, for investigating the role of NFATs in humans (Huang et al., 2016). Elucidation of the role of NFATs and their putative upstream contributions to the vascular health triad in humans is still needed.

Hydrogen Sulfide

As one of the three gasotransmitters ubiquitously synthesized in mammalian systems, hydrogen sulfide (H_2S) is emerging as a critical component of vascular homeostasis (Polhemus and Lefer, 2014). HTN-associated microvascular dysfunction is characterized by a loss of endothelium-dependent signaling pathways, including hydrogen sulfide (H_2S) (Cupisti et al., 2000; Lindstedt et al., 2006; Smith et al., 2011; Craighead et al., 2017; Greaney et al., 2017). Similar to NO, H_2S exerts several beneficial physiological effects, including inhibiting inflammatory markers and leukocyte adhesion molecules, enhancing anti-inflammatory markers, and acting as an antioxidant (Polhemus and Lefer, 2014). NO and H_2S vasodilatory pathways are synergistically interdependent. Both exogenous and endogenous enzymatic H_2S synthesis helps to maintain NO bioavailability by stabilizing the eNOS dimer and improving tetrahydrobiopterin (BH_4) bioavailability (Zhao et al., 2001; Coletta et al., 2012;

Altaany et al., 2013; Polhemus and Lefer, 2014; Greaney et al., 2017). Exogenous administration of H_2S improves NO-dependent vasodilation, while blockade of the H_2S producing enzyme, cystahionine γ-layase (CSE), impairs NO-dependent vasodilation (Coletta et al., 2012; Altaany et al., 2013). Reciprocally, blockade of NO synthesis also reduces H_2S-dependent vasodilation (Zhao et al., 2001; Coletta et al., 2012). We reported that the H_2S-dependent contribution to endothelium-dependent vasodilation is functionally absent in naïve-to-therapy hypertensive adults (Greaney et al., 2017). This was partially due to reduced endogenous enzymatic synthesis of H_2S, as expression and activity of H_2S producing enzymes, including cystathione-γ-lyase and 3-mercaptopyruvate transulferase, were reduced in hypertensive compared to normotensive adults (Greaney et al., 2017). However, vascular responsiveness to exogenous H_2S donors remained intact in hypertensive adults. In preclinical models, treatment with an H_2S donating antihypertensive agents improves endothelial function and normalizes BP (Bucci et al., 2014; Ji et al., 2014; Al-Magableh et al., 2015; Xue et al., 2015). These improvements were partially mediated by increased NO bioavailability (Bucci et al., 2014; Ji et al., 2014; Al-Magableh et al., 2015; Xue et al., 2015), demonstrating the synergistic nature of these gasotransmitter pathways. Various nutraceutical intervention studies suggest that allicin, the bioactive component of garlic, improves vascular function, specifically through the H_2S enzymatic pathway (Cui et al., 2020). Due to the ubiquitous nature of H_2S, there are several clinical trials evaluating the impact of H_2S donating pharmacologics in a variety of disease states. At present, the H_2S synthetic pathway remains an underexplored therapeutic target in human HTN and other CVDs, including heart failure.

Potential Targets

In humans, the potential targets to mitigate the vascular health triad and improve the vascular function have been pursued from a global, holistic approach of exercise training to more specific, targeted treatments. In humans, ascorbic acid and folic acid supplementation have been shown to improve vascular function in populations with inflammatory diseases (Alexander et al., 2013; Karbach et al., 2014; Stanhewicz et al., 2015; Stanhewicz and Kenney, 2017). BH_4 precursors and antioxidants are the main therapeutic targets facilitating eNOS coupling and reducing eNOS-derived ROS production. BH_4 in the form of saproterin is an orphan drug used in the treatment of certain genetic variants of phenylketonuria. Saproterin has improved eNOS function and NO-dependent vasodilation in aged and hypercholesterolemic human subjects in both acute and interventional studies. Specifically, saproterin (or, BH_4) supplementation works through eNOS coupling mechanisms and not simply through its moderate antioxidant capacity. Folic acid (and its active metabolite 5-MTHF) is a cost-effective strategy for improving BH_4 bioavailability through BH2 recycling. Thus, reducing eNOS uncoupling is an attractive, accessible, and affordable intervention for improving the vascular health triad in aging and diseased states.

Similarly, mitochondrial ROS targeted interventions have shown promise in the past decade. Nicotinamide riboside (NR) is a sirtuin-1 (SIRT-1) precursor that has gained recent popularity in vascular intervention treatment research. NR is a precursor to NAD^+, and SIRT1 is a NAD^+-dependent deacetylase. Similar to resveratrol and Mito Q, NR supplementation has had vastly positive impacts on vascular function and oxidative stress in pre-clinical animal models (Yoshino et al., 2011; Mills et al., 2016). NR has been shown to improve vascular function and reduce oxidative stress in aged mice. However, in humans, these findings have not been replicated. NR has shown small impacts on various measures of vascular function (Martens et al., 2018). Thus, there is a knowledge gap in the positive benefits of long-term NR supplementation.

CONCLUSION

In summary, there is ample evidence that the shift from healthy endothelial function to dysfunction, typically preceding HTN and CVD, is driven by a cross-talk between inflammation and ROS. There are numerous "players" that have been recently identified to be responsible for this abnormal shift toward dysfunction. Therefore, it is crucial to investigate these key players in human experimental models to further understand and improve human vascular function with the ultimate goal of preventing CVD risk.

AUTHOR CONTRIBUTIONS

SR and LA conceived the research review. SR, GD, SM, and LA designed the research review, drafted, revised, and approved the final version of the manuscript. GD and SM prepared figure and table. All authors contributed to the article and approved the submitted version.

FUNDING

Support for this work was provided by National Institute of Health (NIH) grant T32-5T32-AG049676 to GD, NIH grant R01-HL-093238 to LA, and University of Maryland (UMD) Tier 1 (pilot grant) to SR.

REFERENCES

Aktan, F. (2004). iNOS-mediated nitric oxide production and its regulation. *Life Sci.* 75, 639–653. doi: 10.1016/j.lfs.2003.10.042

Alexander, L. M., Kutz, J. L., and Kenney, W. L. (2013). Tetrahydrobiopterin increases NO-dependent vasodilation in hypercholesterolemic human skin through eNOS-coupling mechanisms. *Am. J. Physiol. Regul. Integr. Comp. Physiol.* 304, R164–R169. doi: 10.1152/ajpregu.00448.2012

Al-Magableh, M. R., Kemp-Harper, B. K., and Hart, J. L. (2015). Hydrogen sulfide treatment reduces blood pressure and oxidative stress in angiotensin II-induced hypertensive mice. *Hypertens. Res.* 38, 13–20. doi: 10.1038/hr.2014.125

Altaany, Z., Yang, G., and Wang, R. (2013). Crosstalk between hydrogen sulfide and nitric oxide in endothelial cells. *J. Cell. Mol. Med.* 17, 879–888. doi: 10.1111/jcmm.12077

Amberg, G. C., Rossow, C. F., Navedo, M. F., and Santana, L. F. (2004). NFATc3 regulates Kv2.1 expression in arterial smooth muscle. *J. Biol. Chem.* 279, 47326–47334. doi: 10.1074/jbc.M408789200

Armesilla, A. L., Lorenzo, E., Gomez del Arco, P., Martinez-Martinez, S., Alfranca, A., and Redondo, J. M. (1999). Vascular endothelial growth factor activates nuclear factor of activated T cells in human endothelial cells: a role for tissue factor gene expression. *Mol. Cell Biol.* 19, 2032–2043. doi: 10.1128/MCB.19.3.2032

Badi, I., Mancinelli, L., Polizzotto, A., Ferri, D., Zeni, F., Burba, I., et al. (2018). miR-34a Promotes Vascular Smooth Muscle Cell Calcification by Downregulating SIRT1 (Sirtuin 1) and Axl (AXL Receptor Tyrosine Kinase). *Arterioscler. Thromb. Vascul. Biol.* 38, 2079–2090. doi: 10.1161/ATVBAHA.118.311298

Baker, J. R., Vuppusetty, C., Colley, T., Hassibi, S., Fenwick, P. S., Donnelly, L. E., et al. (2019). MicroRNA-570 is a novel regulator of cellular senescence and inflammaging. *FASEB J.* 33, 1605–1616. doi: 10.1096/fj.201800965R

Bär, C., Thum, T., and de Gonzalo-Calvo, D. (2019). Circulating miRNAs as mediators in cell-to-cell communication. *Epigenomics* 11, 111–113. doi: 10.2217/epi-2018-0183

Benjamin, E. J., Larson, M. G., Keyes, M. J., Mitchell, G. F., Vasan, R. S., Keaney, J. F. Jr., et al. (2004). Clinical correlates and heritability of flow-mediated dilation in the community: the Framingham Heart Study. *Circulation* 109, 613–619. doi: 10.1161/01.CIR.0000112565.60887.1E

Benz, F., Roy, S., Trautwein, C., Roderburg, C., and Luedde, T. (2016). Circulating MicroRNAs as Biomarkers for Sepsis. *Int. J. Mol. Sci.* 17:78. doi: 10.3390/ijms17010078

Berglund, L. M., Kotova, O., Osmark, P., Grufman, H., Xing, C., Lydrup, M. L., et al. (2012). NFAT regulates the expression of AIF-1 and IRT-1: yin and yang splice variants of neointima formation and atherosclerosis. *Cardiovasc. Res.* 93, 414–423. doi: 10.1093/cvr/cvr309

Beyer, A. M., Durand, M. J., Hockenberry, J., Gamblin, T. C., Phillips, S. A., and Gutterman, D. D. (2014). An acute rise in intraluminal pressure shifts the mediator of flow-mediated dilation from nitric oxide to hydrogen peroxide in human arterioles. *Am. J. Physiol. Heart Circ. Physiol.* 307, H1587–H1593. doi: 10.1152/ajpheart.00557.2014

Beyer, A. M., Zinkevich, N., Miller, B., Liu, Y., Wittenburg, A. L., Mitchell, M., et al. (2017). Transition in the mechanism of flow-mediated dilation with aging and development of coronary artery disease. *Basic Res. Cardiol.* 112:5. doi: 10.1007/s00395-016-0594-x

Bochkov, V. N., Mechtcheriakova, D., Lucerna, M., Huber, J., Malli, R., Graier, W. F., et al. (2002). Oxidized phospholipids stimulate tissue factor expression in human endothelial cells via activation of ERK/EGR-1 and Ca(++)/NFAT. *Blood* 99, 199–206. doi: 10.1182/blood.V99.1.199

Boss, V., Wang, X., Koppelman, L. F., Xu, K., and Murphy, T. J. (1998). Histamine induces nuclear factor of activated T cell-mediated transcription and cyclosporin A-sensitive interleukin-8 mRNA expression in human umbilical vein endothelial cells. *Mol. Pharmacol.* 54, 264–272. doi: 10.1124/mol.54.2.264

Bottino, D. A., Lopes, F. G., de Oliveira, F. J., Mecenas, A. S., Clapauch, R., and Bouskela, E. (2015). Relationship between biomarkers of inflammation, oxidative stress and endothelial/microcirculatory function in successful aging versus healthy youth: a transversal study. *BMC Geriatr.* 15:41. doi: 10.1186/s12877-015-0044-x

Bretz, C. A., Savage, S. R., Capozzi, M. E., Suarez, S., and Penn, J. S. (2015). NFAT isoforms play distinct roles in TNFalpha-induced retinal leukostasis. *Sci. Rep.* 5:14963. doi: 10.1038/srep14963

Broxterman, R. M., Witman, M. A., Trinity, J. D., Groot, H. J., Rossman, M. J., Park, S. Y., et al. (2019). Strong Relationship Between Vascular Function in the Coronary and Brachial Arteries. *Hypertension* 74, 208–215. doi: 10.1161/HYPERTENSIONAHA.119.12881

Bruning, R. S., Kenney, W. L., and Alexander, L. M. (2015). Altered skin flowmotion in hypertensive humans. *Microvascular. Res.* 97, 81–87. doi: 10.1016/j.mvr.2014.01.001

Bucci, M., Vellecco, V., Cantalupo, A., Brancaleone, V., Zhou, Z., Evangelista, S., et al. (2014). Hydrogen sulfide accounts for the peripheral vascular effects of zofenopril independently of ACE inhibition. *Cardiovasc. Res.* 102, 138–147. doi: 10.1093/cvr/cvu026

Buus, N. H., Jørgensen, C. G., Mulvany, M. J., and Sørensen, K. E. (2007). Large and small artery endothelial function in patients with essential hypertension–effect of ACE inhibition and beta-blockade. *Blood Press.* 16, 106–113. doi: 10.1080/08037050701343688

Cheng, H. S., Njock, M. S., Khyzha, N., Dang, L. T., and Fish, J. E. (2014). Noncoding RNAs regulate NF-κB signaling to modulate blood vessel inflammation. *Front. Genet.* 5:422. doi: 10.3389/fgene.2014.00422

Cockerill, G. W., Bert, A. G., Ryan, G. R., Gamble, J. R., Vadas, M. A., and Cockerill, P. N. (1995). Regulation of granulocyte-macrophage colony-stimulating factor and E-selectin expression in endothelial cells by cyclosporin A and the T-cell transcription factor NFAT. *Blood* 86, 2689–2698. doi: 10.1182/blood.V86.7.2689.2689

Coletta, C., Papapetropoulos, A., Erdelyi, K., Olah, G., Modis, K., Panopoulos, P., et al. (2012). Hydrogen sulfide and nitric oxide are mutually dependent in the regulation of angiogenesis and endothelium-dependent vasorelaxation. *Proc. Natl. Acad. Sci. U S A.* 109, 9161–9166. doi: 10.1073/pnas.1202916109

Craighead, D. H., Freeberg, K. A., and Seals, D. R. (2020). Vascular Endothelial Function in Midlife/Older Adults Classified According to 2017 American College of Cardiology/American Heart Association Blood Pressure Guidelines. *J. Am. Heart Associat.* 9:e016625. doi: 10.1161/JAHA.120.016625

Craighead, D. H., Smith, C. J., and Alexander, L. M. (2017). Blood pressure normalization via pharmacotherapy improves cutaneous microvascular function through NO-dependent and NO-independent mechanisms. *Microcirculation* 24:12382. doi: 10.1111/micc.12382

Craighead, D. H., Wang, H., Santhanam, L., and Alexander, L. M. (2018). Acute lysyl oxidase inhibition alters microvascular function in normotensive but not hypertensive men and women. *Am. J. Physiol. Heart Circ. Physiol.* 314, H424–H433. doi: 10.1152/ajpheart.00521.2017

Crecelius, A. R., Kirby, B. S., Voyles, W. F., and Dinenno, F. A. (2010). Nitric oxide, but not vasodilating prostaglandins, contributes to the improvement of exercise hyperemia via ascorbic acid in healthy older adults. *Am. J. Physiol. Heart Circ. Physiol.* 299, H1633–H1641. doi: 10.1152/ajpheart.00614.2010

Cui, T., Liu, W., Chen, S., Yu, C., Li, Y., and Zhang, J. Y. (2020). Antihypertensive effects of allicin on spontaneously hypertensive rats via vasorelaxation and hydrogen sulfide mechanisms. *Biomed. Pharmacother.* 128:110240. doi: 10.1016/j.biopha.2020.110240

Cupisti, A., Rossi, M., Placidi, S., Fabbri, A., Morelli, E., Vagheggini, G., et al. (2000). Responses of the skin microcirculation to acetylcholine in patients with essential hypertension and in normotensive patients with chronic renal failure. *Nephron* 85, 114–119. doi: 10.1159/000045643

Dillon, G. A., Greaney, J. L., Shank, S., Leuenberger, U. A., and Alexander, L. M. (2020). AHA/ACC-defined stage 1 hypertensive adults do not display cutaneous microvascular endothelial dysfunction. *Am. J. Physiol. Heart Circ. Physiol.* 319, H539–H546. doi: 10.1152/ajpheart.00179.2020

Ding, H., Aljofan, M., and Triggle, C. R. (2007). Oxidative stress and increased eNOS and NADPH oxidase expression in mouse microvessel endothelial cells. *J. Cell Physiol.* 212, 682–689. doi: 10.1002/jcp.21063

Donato, A. J., Eskurza, I., Silver, A. E., Levy, A. S., Pierce, G. L., Gates, P. E., et al. (2007). Direct evidence of endothelial oxidative stress with aging in humans: relation to impaired endothelium-dependent dilation and upregulation of nuclear factor-kappaB. *Circ. Res.* 100, 1659–1666. doi: 10.1161/01.RES.0000269183.13937.e8

Donato, A. J., Pierce, G. L., Lesniewski, L. A., and Seals, D. R. (2009). Role of NFkappaB in age-related vascular endothelial dysfunction in humans. *Aging* 1, 678–680. doi: 10.18632/aging.100080

El Assar, M., Angulo, J., and Rodriguez-Manas, L. (2013). Oxidative stress and vascular inflammation in aging. *Free Radic. Biol. Med.* 65, 380–401. doi: 10.1016/j.freeradbiomed.2013.07.003

Eskurza, I., Monahan, K. D., Robinson, J. A., and Seals, D. R. (2004a). Ascorbic acid does not affect large elastic artery compliance or central blood pressure in

young and older men. *Am. J. Physiol. Heart Circ. Physiol.* 286, H1528–H1534. doi: 10.1152/ajpheart.00879.2003

Eskurza, I., Monahan, K. D., Robinson, J. A., and Seals, D. R. (2004b). Effect of acute and chronic ascorbic acid on flow-mediated dilatation with sedentary and physically active human ageing. *J. Physiol.* 556(Pt 1), 315–324. doi: 10.1113/jphysiol.2003.057042

Farkas, K., Kolossváry, E., Járai, Z., Nemcsik, J., and Farsang, C. (2004). Non-invasive assessment of microvascular endothelial function by laser Doppler flowmetry in patients with essential hypertension. *Atherosclerosis* 173, 97–102. doi: 10.1016/j.atherosclerosis.2003.11.015

Fernández-Hernando, C., and Suárez, Y. (2018). MicroRNAs in endothelial cell homeostasis and vascular disease. *Curr. Opin. Hematol.* 25, 227–236. doi: 10.1097/MOH.0000000000000424

Figueiredo, V. N., Yugar-Toledo, J. C., Martins, L. C., Martins, L. B., de Faria, A. P., de Haro Moraes, C., et al. (2012). Vascular stiffness and endothelial dysfunction: Correlations at different levels of blood pressure. *Blood Press.* 21, 31–38. doi: 10.3109/08037051.2011.617045

Fonkoue, I. T., Le, N. A., Kankam, M. L., DaCosta, D., Jones, T. N., Marvar, P. J., et al. (2019). Sympathoexcitation and impaired arterial baroreflex sensitivity are linked to vascular inflammation in individuals with elevated resting blood pressure. *Physiol. Rep.* 7:e14057. doi: 10.14814/phy2.14057

Friedman, J. K., Nitta, C. H., Henderson, K. M., Codianni, S. J., Sanchez, L., Ramiro-Diaz, J. M., et al. (2014). Intermittent hypoxia-induced increases in reactive oxygen species activate NFATc3 increasing endothelin-1 vasoconstrictor reactivity. *Vascul. Pharmacol.* 60, 17–24. doi: 10.1016/j.vph.2013.11.001

Garcia-Vaz, E., McNeilly, A. D., Berglund, L. M., Ahmad, A., Gallagher, J. R., Dutius Andersson, A. M., et al. (2020). Inhibition of NFAT Signaling Restores Microvascular Endothelial Function in Diabetic Mice. *Diabetes* 69, 424–435. doi: 10.2337/db18-0870

Gokce, N., Holbrook, M., Duffy, S. J., Demissie, S., Cupples, L. A., Biegelsen, E., et al. (2001). Effects of race and hypertension on flow-mediated and nitroglycerin-mediated dilation of the brachial artery. *Hypertension* 38, 1349–1354. doi: 10.1161/hy1201.096575

Gonzalez Bosc, L. V., Wilkerson, M. K., Bradley, K. N., Eckman, D. M., Hill-Eubanks, D. C., and Nelson, M. T. (2004). Intraluminal pressure is a stimulus for NFATc3 nuclear accumulation: role of calcium, endothelium-derived nitric oxide, and cGMP-dependent protein kinase. *J. Biol. Chem.* 279, 10702–10709. doi: 10.1074/jbc.M312920200

Govatati, S., Pichavaram, P., Janjanam, J., Zhang, B., Singh, N. K., Mani, A. M., et al. (2019). NFATc1-E2F1-LMCD1-Mediated IL-33 Expression by Thrombin Is Required for Injury-Induced Neointima Formation. *Arterioscler. Thromb. Vascul. Biol.* 39, 1212–1226. doi: 10.1161/ATVBAHA.119.312729

Grassi, G., Biffi, A., Seravalle, G., Trevano, F. Q., Dell'Oro, R., Corrao, G., et al. (2019). Sympathetic Neural Overdrive in the Obese and Overweight State. *Hypertension* 74, 349–358. doi: 10.1161/HYPERTENSIONAHA.119.12885

Grassi, G., Pisano, A., Bolignano, D., Seravalle, G., D'Arrigo, G., Quarti-Trevano, F., et al. (2018). Sympathetic Nerve Traffic Activation in Essential Hypertension and Its Correlates: Systematic Reviews and Meta-Analyses. *Hypertension* 72, 483–491. doi: 10.1161/HYPERTENSIONAHA.118.11038

Greaney, J. L., Kutz, J. L., Shank, S. W., Jandu, S., Santhanam, L., and Alexander, L. M. (2017). Impaired Hydrogen Sulfide-Mediated Vasodilation Contributes to Microvascular Endothelial Dysfunction in Hypertensive Adults. *Hypertension* 69, 902–909. doi: 10.1161/HYPERTENSIONAHA.116.08964

Greaney, J. L., Matthews, E. L., and Wenner, M. M. (2015). Sympathetic reactivity in young women with a family history of hypertension. *Am. J. Physiol. Heart Circ. Physiol.* 308, H816–H822. doi: 10.1152/ajpheart.00867.2014

Greaney, J. L., Saunders, E. F. H., Santhanam, L., and Alexander, L. M. (2019). Oxidative Stress Contributes to Microvascular Endothelial Dysfunction in Men and Women With Major Depressive Disorder. *Circ. Res.* 124, 564–574. doi: 10.1161/CIRCRESAHA.118.313764

Guzik, T. J., and Touyz, R. M. (2017). Oxidative Stress, Inflammation, and Vascular Aging in Hypertension. *Hypertension* 70, 660–667. doi: 10.1161/HYPERTENSIONAHA.117.07802

Hader, S. N., Zinkevich, N., Norwood Toro, L. E., Kriegel, A. J., Kong, A., Freed, J. K., et al. (2019). Detrimental effects of chemotherapy on human coronary microvascular function. *Am. J. Physiol. Heart Circ. Physiol.* 317, H705–H710. doi: 10.1152/ajpheart.00370.2019

Hemmrich, K., Suschek, C. V., Lerzynski, G., and Kolb-Bachofen, V. (2003). iNOS activity is essential for endothelial stress gene expression protecting against oxidative damage. *J. Appl. Physiol.* 95, 1937–1946. doi: 10.1152/japplphysiol.00419.2003

Hingorani, A. D., Cross, J., Kharbanda, R. K., Mullen, M. J., Bhagat, K., Taylor, M., et al. (2000). Acute systemic inflammation impairs endothelium-dependent dilatation in humans. *Circulation* 102, 994–999. doi: 10.1161/01.CIR.102.9.994

Holwerda, S. W., Luehrs, R. E., DuBose, L., Collins, M. T., Wooldridge, N. A., Stroud, A. K., et al. (2019). Elevated Muscle Sympathetic Nerve Activity Contributes to Central Artery Stiffness in Young and Middle-Age/Older Adults. *Hypertension* 73, 1025–1035. doi: 10.1161/HYPERTENSIONAHA.118.12462

Huang, S.-S., He, S.-L., and Zhang, Y.-M. (2016). The effects of telmisartan on the nuclear factor of activated T lymphocytes signalling pathway in hypertensive patients. *J. Renin Angiotensin Aldosterone Syst.* 17:1470320316655005. doi: 10.1177/1470320316655005

Hughes, W. E., Zinkevich, N., Gutterman, D. D., and Beyer, A. M. (2021b). Hypertension preserves the magnitude of microvascular flow-mediated dilation following transient elevation in intraluminal pressure. *Physiol. Rep.* 9:e14507. doi: 10.14814/phy2.14507

Hughes, W. E., Chabowski, D. S., Ait-Aissa, K., Fetterman, J. L., Hockenberry, J., Beyer, A. M., et al. (2021a). Critical Interaction Between Telomerase and Autophagy in Mediating Flow-Induced Human Arteriolar Vasodilation. *Arterioscler. Thromb. Vascul. Biol.* 41, 446–457. doi: 10.1161/ATVBAHA.120.314944

Hurr, C., Patik, J. C., Kim, K., Christmas, K. M., and Brothers, R. M. (2018). Tempol augments the blunted cutaneous microvascular thermal reactivity in healthy young African Americans. *Exp. Physiol.* 103, 343–349. doi: 10.1113/EP086776

Jacobi, J., Kristal, B., Chezar, J., Shaul, S. M., and Sela, S. (2005). Exogenous superoxide mediates pro-oxidative, proinflammatory, and procoagulatory changes in primary endothelial cell cultures. *Free Radic. Biol. Med.* 39, 1238–1248. doi: 10.1016/j.freeradbiomed.2005.06.010

Ji, H., Kim, A., Ebinger, J. E., Niiranen, T. J., Claggett, B. L., Bairey Merz, C. N., et al. (2020). Sex Differences in Blood Pressure Trajectories Over the Life Course. *JAMA Cardiol.* 5, 19–26. doi: 10.1001/jamacardio.2019.5306

Ji, W., Liu, S., Dai, J., Yang, T., Jiang, X., Duan, X., et al. (2014). Hydrogen sulfide defends against the cardiovascular risk of Nw-nitro-L-argininemethyl ester-induced hypertension in rats via the nitric oxide/endothelial nitric oxide synthase pathway. *Chin. Med. J.* 127, 3751–3757.

Johnson, E. N., Lee, Y. M., Sander, T. L., Rabkin, E., Schoen, F. J., Kaushal, S., et al. (2003). NFATc1 mediates vascular endothelial growth factor-induced proliferation of human pulmonary valve endothelial cells. *J. Biol. Chem.* 278, 1686–1692. doi: 10.1074/jbc.M210250200

Junqueira, C. L. C., Magalhães, M. E. C., Brandão, A. A., Ferreira, E., Junqueira, A. S. M., Neto, J. F. N., et al. (2018). Evaluation of endothelial function by VOP and inflammatory biomarkers in patients with arterial hypertension. *J. Hum. Hypertens.* 32, 105–113. doi: 10.1038/s41371-017-0024-z

Juonala, M., Viikari, J. S., Laitinen, T., Marniemi, J., Helenius, H., Rönnemaa, T., et al. (2004). Interrelations between brachial endothelial function and carotid intima-media thickness in young adults: the cardiovascular risk in young Finns study. *Circulation* 110, 2918–2923. doi: 10.1161/01.CIR.0000147540.88559.00

Kadlec, A. O., Chabowski, D. S., Ait-Aissa, K., Hockenberry, J. C., Otterson, M. F., Durand, M. J., et al. (2017). PGC-1alpha (Peroxisome Proliferator-Activated Receptor gamma Coactivator 1-alpha) Overexpression in Coronary Artery Disease Recruits NO and Hydrogen Peroxide During Flow-Mediated Dilation and Protects Against Increased Intraluminal Pressure. *Hypertension* 70, 166–173. doi: 10.1161/HYPERTENSIONAHA.117.09289

Karbach, S., Wenzel, P., Waisman, A., Munzel, T., and Daiber, A. (2014). eNOS uncoupling in cardiovascular diseases–the role of oxidative stress and inflammation. *Curr. Pharm. Des.* 20, 3579–3594. doi: 10.2174/13816128113196660748

Katulka, E. K., Hirt, A. E., Kirkman, D. L., Edwards, D. G., and Witman, M. A. H. (2019). Altered vascular function in chronic kidney disease: evidence from passive leg movement. *Physiol. Rep.* 7:e14075. doi: 10.14814/phy2.14075

Keir, D. A., Badrov, M. B., Tomlinson, G., Notarius, C. F., Kimmerly, D. S., Millar, P. J., et al. (2020). Influence of Sex and Age on Muscle Sympathetic

Nerve Activity of Healthy Normotensive Adults. *Hypertension* 76, 997–1005. doi: 10.1161/HYPERTENSIONAHA.120.15208

Kiani, A., Rao, A., and Aramburu, J. (2000). Manipulating immune responses with immunosuppressive agents that target NFAT. *Immunity* 12, 359–372. doi: 10.1016/S1074-7613(00)80188-0

Kirkman, D. L., Robinson, A. T., Rossman, M. J., Seals, D. R., and Edwards, D. G. (2021). Mitochondrial contributions to vascular endothelial dysfunction, arterial stiffness, and cardiovascular diseases. *Am. J. Physiol. Heart Circ. Physiol.* 320, H2080–H2100. doi: 10.1152/ajpheart.00917.2020

Kopp, E., and Ghosh, S. (1994). Inhibition of NF-kappa B by sodium salicylate and aspirin. *Science* 265, 956–959. doi: 10.1126/science.8052854

Lee, K. S., Kim, J., Kwak, S. N., Lee, K. S., Lee, D. K., Ha, K. S., et al. (2014). Functional role of NF-κB in expression of human endothelial nitric oxide synthase. *Biochem. Biophys. Res. Communicat.* 448, 101–107. doi: 10.1016/j.bbrc.2014.04.079

Lewington, S., Clarke, R., Qizilbash, N., Peto, R., and Collins, R. (2002). Age-specific relevance of usual blood pressure to vascular mortality: a meta-analysis of individual data for one million adults in 61 prospective studies. *Lancet* 360, 1903–1913. doi: 10.1016/S0140-6736(02)11911-8

Li, L., Sapkota, M., Kim, S. W., and Soh, Y. (2015). Herbacetin inhibits inducible nitric oxide synthase via JNK and nuclear factor-κB in LPS-stimulated RAW264.7 cells. *Eur. J. Pharmacol.* 765, 115–123. doi: 10.1016/j.ejphar.2015.08.032

Lindstedt, I. H., Edvinsson, M. L., and Edvinsson, L. (2006). Reduced responsiveness of cutaneous microcirculation in essential hypertension–a pilot study. *Blood Press.* 15, 275–280.doi:10.1080/08037050600996586

Lipskaia, L., Pourci, M. L., Delomenie, C., Combettes, L., Goudouneche, D., Paul, J. L., et al. (2003). Phosphatidylinositol 3-kinase and calcium-activated transcription pathways are required for VLDL-induced smooth muscle cell proliferation. *Circ. Res.* 92, 1115–1122. doi: 10.1161/01.RES.0000074880.25540.D0

Marin, T., Gongol, B., Chen, Z., Woo, B., Subramaniam, S., Chien, S., et al. (2013). Mechanosensitive microRNAs-role in endothelial responses to shear stress and redox state. *Free Radic. Biol. Med.* 64, 61–68. doi: 10.1016/j.freeradbiomed.2013.05.034

Martens, C. R., Denman, B. A., Mazzo, M. R., Armstrong, M. L., Reisdorph, N., McQueen, M. B., et al. (2018). Chronic nicotinamide riboside supplementation is well-tolerated and elevates NAD(+) in healthy middle-aged and older adults. *Nat. Commun.* 9:1286. doi: 10.1038/s41467-018-03421-7

Martens, C. R., Kirkman, D. L., and Edwards, D. G. (2016). The Vascular Endothelium in Chronic Kidney Disease: A Novel Target for Aerobic Exercise. *Exerc. Sport Sci. Rev.* 44, 12–19. doi: 10.1249/JES.0000000000000065

Matthews, E. L., Greaney, J. L., and Wenner, M. M. (2017). Rapid onset pressor response to exercise in young women with a family history of hypertension. *Exp. Physiol.* 102, 1092–1099. doi: 10.1113/EP086466

McGowan, C. L., Levy, A. S., Millar, P. J., Guzman, J. C., Morillo, C. A., McCartney, N., et al. (2006). Acute vascular responses to isometric handgrip exercise and effects of training in persons medicated for hypertension. *Am. J. Physiol. Heart Circ. Physiol.* 291, H1797–H1802. doi: 10.1152/ajpheart.01113.2005

Mi, S., Zhang, J., Zhang, W., and Huang, R. S. (2013). Circulating microRNAs as biomarkers for inflammatory diseases. *Microrna* 2, 63–71. doi: 10.2174/2211536611302010007

Migrino, R. Q., Truran, S., Gutterman, D. D., Franco, D. A., Bright, M., Schlundt, B., et al. (2011). Human microvascular dysfunction and apoptotic injury induced by AL amyloidosis light chain proteins. *Am. J. Physiol. Heart Circ. Physiol.* 301, H2305–H2312. doi: 10.1152/ajpheart.00503.2011

Mills, K. F., Yoshida, S., Stein, L. R., Grozio, A., Kubota, S., Sasaki, Y., et al. (2016). Long-Term Administration of Nicotinamide Mononucleotide Mitigates Age-Associated Physiological Decline in Mice. *Cell Metab.* 24, 795–806. doi: 10.1016/j.cmet.2016.09.013

Nieves-Cintrón, M., Amberg, G. C., Nichols, C. B., Molkentin, J. D., and Santana, L. F. (2007). Activation of NFATc3 down-regulates the beta1 subunit of large conductance, calcium-activated K+ channels in arterial smooth muscle and contributes to hypertension. *J. Biol. Chem.* 282, 3231–3240. doi: 10.1074/jbc.M608822200

Nilsson, J., Nilsson, L. M., Chen, Y. W., Molkentin, J. D., Erlinge, D., and Gomez, M. F. (2006). High glucose activates nuclear factor of activated T cells in native vascular smooth muscle. *Arterioscler. Thromb. Vascul. Biol.* 26, 794–800. doi: 10.1161/01.ATV.0000209513.00765.13

Nilsson-Berglund, L. M., Zetterqvist, A. V., Nilsson-Ohman, J., Sigvardsson, M., Gonzalez Bosc, L. V., Smith, M. L., et al. (2010). Nuclear factor of activated T cells regulates osteopontin expression in arterial smooth muscle in response to diabetes-induced hyperglycemia. *Arterioscler. Thromb. Vascul. Biol.* 30, 218–224. doi: 10.1161/ATVBAHA.109.199299

Njock, M. S., and Fish, J. E. (2017). Endothelial miRNAs as Cellular Messengers in Cardiometabolic Diseases. *Trends Endocrinol. Metab.* 28, 237–246. doi: 10.1016/j.tem.2016.11.009

Norata, G. D., Grigore, L., Raselli, S., Redaelli, L., Hamsten, A., Maggi, F., et al. (2007). Post-prandial endothelial dysfunction in hypertriglyceridemic subjects: molecular mechanisms and gene expression studies. *Atherosclerosis* 193, 321–327. doi: 10.1016/j.atherosclerosis.2006.09.015

Nowroozpoor, A., Gutterman, D., and Safdar, B. (2021). Is microvascular dysfunction a systemic disorder with common biomarkers found in the heart, brain, and kidneys? - A scoping review. *Microvasc. Res.* 134:104123. doi: 10.1016/j.mvr.2020.104123

On, Y. K., Kim, C. H., Sohn, D. W., Oh, B. H., Lee, M. M., Park, Y. B., et al. (2002). Improvement of endothelial function by amlodipine and vitamin C in essential hypertension. *Korean J. Intern. Med.* 17, 131–137. doi: 10.3904/kjim.2002.17.2.131

Orr, A. W., Lee, M. Y., Lemmon, J. A., Yurdagul, A., Gomez, M. F., Bortz, P. D. S., et al. (2009). Molecular Mechanisms of Collagen Isotype-Specific Modulation of Smooth Muscle Cell Phenotype. *Arterioscl. Throm. Vas.* 29, 225–231. doi: 10.1161/ATVBAHA.108.178749

Ozemek, C., Hildreth, K. L., Groves, D. W., and Moreau, K. L. (2016). Acute ascorbic acid infusion increases left ventricular diastolic function in postmenopausal women. *Maturitas.* 92, 154–161. doi: 10.1016/j.maturitas.2016.08.007

Pang, X., and Sun, N. L. (2009). Calcineurin-NFAT signaling is involved in phenylephrine-induced vascular smooth muscle cell proliferation. *Acta Pharmacol. Sin.* 30, 537–544. doi: 10.1038/aps.2009.28

Park, S. Y., Kwon, O. S., Andtbacka, R. H. I., Hyngstrom, J. R., Reese, V., Murphy, M. P., et al. (2018). Age-related endothelial dysfunction in human skeletal muscle feed arteries: the role of free radicals derived from mitochondria in the vasculature. *Acta physiol.* 222:12893. doi: 10.1111/apha.12893

Phillips, S. A., Hatoum, O. A., and Gutterman, D. D. (2007). The mechanism of flow-induced dilation in human adipose arterioles involves hydrogen peroxide during CAD. *Am. J. Physiol. Heart Circ. Physiol.* 292, H93–H100. doi: 10.1152/ajpheart.00819.2006

Pierce, G. L., Lesniewski, L. A., Lawson, B. R., Beske, S. D., and Seals, D. R. (2009). Nuclear factor-{kappa}B activation contributes to vascular endothelial dysfunction via oxidative stress in overweight/obese middle-aged and older humans. *Circulation* 119, 1284–1292. doi: 10.1161/CIRCULATIONAHA.108.804294

Pierce, J. W., Read, M. A., Ding, H., Luscinskas, F. W., and Collins, T. (1996). Salicylates inhibit I kappa B-alpha phosphorylation, endothelial-leukocyte adhesion molecule expression, and neutrophil transmigration. *J. Immunol.* 156, 3961–3969.

Polhemus, D. J., and Lefer, D. J. (2014). Emergence of hydrogen sulfide as an endogenous gaseous signaling molecule in cardiovascular disease. *Circ. Res.* 114, 730–737. doi: 10.1161/CIRCRESAHA.114.300505

Ratchford, S. M., Clifton, H. L., Gifford, J. R., LaSalle, D. T., Thurston, T. S., Bunsawat, K., et al. (2019a). Impact of acute antioxidant administration on inflammation and vascular function in heart failure with preserved ejection fraction. *Am. J. Physiol. Regul. Integr. Comp. Physiol.* 317, R607–R614. doi: 10.1152/ajpregu.00184.2019

Ratchford, S. M., Broxterman, R. M., La Salle, D. T., Kwon, O. S., Park, S. Y., Hopkins, P. N., et al. (2019b). Salt restriction lowers blood pressure at rest and during exercise without altering peripheral hemodynamics in hypertensive individuals. *Am. J. Physiol. Heart Circ. Physiol.* 317, H1194–H1202.

Richards, J. C., Crecelius, A. R., Larson, D. G., and Dinenno, F. A. (2015). Acute ascorbic acid ingestion increases skeletal muscle blood flow and oxygen

consumption via local vasodilation during graded handgrip exercise in older adults. *Am. J. Physiol. Heart Circ. Physiol.* 309, H360–H368.

Risbano, M. G., and Gladwin, M. T. (2013). Therapeutics targeting of dysregulated redox equilibrium and endothelial dysfunction. *Handb. Exp. Pharmacol.* 218, 315–349. doi: 10.1007/978-3-662-45805-1_13

Rossman, M. J., Santos-Parker, J. R., Steward, C. A. C., Bispham, N. Z., Cuevas, L. M., Rosenberg, H. L., et al. (2018). Chronic Supplementation With a Mitochondrial Antioxidant (MitoQ) Improves Vascular Function in Healthy Older Adults. *Hypertension* 71, 1056–1063. doi: 10.1161/HYPERTENSIONAHA.117.10787

Sapp, R. M., Chesney, C. A., Springer, C. B., Laskowski, M. R., Singer, D. B., Eagan, L. E., et al. (2021). Race-specific changes in endothelial inflammation and microRNA in response to an acute inflammatory stimulus. *Am. J. Physiol. Heart Circ. Physiol.* 320, H2371–H2384. doi: 10.1152/ajpheart.00991.2020

Sapp, R. M., Shill, D. D., Roth, S. M., and Hagberg, J. M. (2017). Circulating microRNAs in acute and chronic exercise: more than mere biomarkers. *J. Appl. Physiol.* 122, 702–717. doi: 10.1152/japplphysiol.00982.2016

Schmitz, B., Breulmann, F. L., Jubran, B., Rolfes, F., Thorwesten, L., Kruger, M., et al. (2019). A three-step approach identifies novel shear stress-sensitive endothelial microRNAs involved in vasculoprotective effects of high-intensity interval training (HIIT). *Oncotarget* 10, 3625–3640. doi: 10.18632/oncotarget.26944

Selemidis, S., Dusting, G. J., Peshavariya, H., Kemp-Harper, B. K., and Drummond, G. R. (2007). Nitric oxide suppresses NADPH oxidase-dependent superoxide production by S-nitrosylation in human endothelial cells. *Cardiovasc. Res.* 75, 349–358. doi: 10.1016/j.cardiores.2007.03.030

Shi, L., Liao, J., Liu, B., Zeng, F., and Zhang, L. (2015). Mechanisms and therapeutic potential of microRNAs in hypertension. *Drug Discov. Today* 20, 1188–1204. doi: 10.1016/j.drudis.2015.05.007

Shiny, A., Regin, B., Mohan, V., and Balasubramanyam, M. (2016). Coordinated augmentation of NFAT and NOD signaling mediates proliferative VSMC phenotype switch under hyperinsulinemia. *Atherosclerosis* 246, 257–266. doi: 10.1016/j.atherosclerosis.2016.01.006

Smith, C. J., Santhanam, L., and Alexander, L. M. (2013). Rho-Kinase activity and cutaneous vasoconstriction is upregulated in essential hypertensive humans. *Microvascul. Res.* 87, 58–64. doi: 10.1016/j.mvr.2013.02.005

Smith, C. J., Santhanam, L., Bruning, R. S., Stanhewicz, A., Berkowitz, D. E., and Holowatz, L. A. (2011). Upregulation of inducible nitric oxide synthase contributes to attenuated cutaneous vasodilation in essential hypertensive humans. *Hypertension* 58, 935–942. doi: 10.1161/HYPERTENSIONAHA.111.178129

Soudani, N., Ghantous, C. M., Farhat, Z., Shebaby, W. N., Zibara, K., and Zeidan, A. (2016). Calcineurin/NFAT Activation-Dependence of Leptin Synthesis and Vascular Growth in Response to Mechanical Stretch. *Front. Physiol.* 7:433. doi: 10.3389/fphys.2016.00433

Sprick, J. D., Downey, R. M., Morison, D. L., Fonkoue, I. T., Li, Y., DaCosta, D., et al. (2019). Functional sympatholysis is impaired in end-stage renal disease. *Am. J. Physiol. Regul. Integr. Comp. Physiol.* 316, R504–R511. doi: 10.1152/ajpregu.00380.2018

Stanhewicz, A. E., Alexander, L. M., and Kenney, W. L. (2015). Folic acid supplementation improves microvascular function in older adults through nitric oxide-dependent mechanisms. *Clin. Sci.* 129, 159–167. doi: 10.1042/CS20140821

Stanhewicz, A. E., and Kenney, W. L. (2017). Role of folic acid in nitric oxide bioavailability and vascular endothelial function. *Nutrit. Rev.* 75, 61–70. doi: 10.1093/nutrit/nuw053

Suzuki, E., Nishimatsu, H., Satonaka, H., Walsh, K., Goto, A., Omata, M., et al. (2002). Angiotensin II induces myocyte enhancer factor 2- and calcineurin/nuclear factor of activated T cell-dependent transcriptional activation in vascular myocytes. *Circ. Res.* 90, 1004–1011. doi: 10.1161/01.RES.0000017629.70769.CC

Takase, B., Hamabe, A., Satomura, K., Akima, T., Uehata, A., Matsui, T., et al. (2006). Comparable prognostic value of vasodilator response to acetylcholine in brachial and coronary arteries for predicting long-term cardiovascular events in suspected coronary artery disease. *Circ. J.* 70, 49–56. doi: 10.1253/circj.70.49

Trinity, J. D., Wray, D. W., Witman, M. A., Layec, G., Barrett-O'Keefe, Z., Ives, S. J., et al. (2016). Ascorbic acid improves brachial artery vasodilation during progressive handgrip exercise in the elderly through a nitric oxide-mediated mechanism. *Am. J. Physiol. Heart Circ. Physiol.* 310, H765–H774. doi: 10.1152/ajpheart.00817.2015

Virani, S. S., Alonso, A., Aparicio, H. J., Benjamin, E. J., Bittencourt, M. S., Callaway, C. W., et al. (2021). Heart Disease and Stroke Statistics-2021 Update: A Report From the American Heart Association. *Circulation* 143, e254–e743. doi: 10.1161/CIR.0000000000000950

Wadley, A. J., Veldhuijzen van Zanten, J. J., and Aldred, S. (2013). The interactions of oxidative stress and inflammation with vascular dysfunction in ageing: the vascular health triad. *Age* 35, 705–718. doi: 10.1007/s11357-012-9402-1

Walker, A. E., Kaplon, R. E., Pierce, G. L., Nowlan, M. J., and Seals, D. R. (2014). Prevention of age-related endothelial dysfunction by habitual aerobic exercise in healthy humans: possible role of nuclear factor κB. *Clin. Sci.* 127, 645–654. doi: 10.1042/CS20140030

Wang, Q., Li, D., Han, Y., Ding, X., Xu, T., and Tang, B. (2017). MicroRNA-146 protects A549 and H1975 cells from LPS-induced apoptosis and inflammation injury. *J. Biosci.* 42, 637–645. doi: 10.1007/s12038-017-9715-4

Wang, Y., Hu, J., Liu, J., Geng, Z., Tao, Y., Zheng, F., et al. (2020). The role of Ca(2+)/NFAT in Dysfunction and Inflammation of Human Coronary Endothelial Cells induced by Sera from patients with Kawasaki disease. *Sci. Rep.* 10:4706. doi: 10.1038/s41598-020-61667-y

Weng, J., Wang, C., Zhong, W., Li, B., Wang, Z., Shao, C., et al. (2017). Activation of CD137 Signaling Promotes Angiogenesis in Atherosclerosis via Modulating Endothelial Smad1/5-NFATc1 Pathway. *J. Am. Heart Assoc.* 6:e004756. doi: 10.1161/JAHA.116.004756

Whelton, P. K., Carey, R. M., Aronow, W. S., Casey, D. E. Jr., Collins, K. J., Dennison Himmelfarb, C., et al. (2018). 2017 ACC/AHA/AAPA/ABC/ACPM/AGS/APhA/ASH/ASPC/NMA/PCNA Guideline for the Prevention, Detection, Evaluation, and Management of High Blood Pressure in Adults: A Report of the American College of Cardiology/American Heart Association Task Force on Clinical Practice Guidelines. *J. Am. Coll. Cardiol.* 71, e127–e248. doi: 10.1161/HYP.0000000000000076

Wray, D. W., Nishiyama, S. K., Harris, R. A., Zhao, J., McDaniel, J., Fjeldstad, A. S., et al. (2012). Acute reversal of endothelial dysfunction in the elderly after antioxidant consumption. *Hypertension* 59, 818–824. doi: 10.1161/HYPERTENSIONAHA.111.189456

Wu, F., Tyml, K., and Wilson, J. X. (2008). iNOS expression requires NADPH oxidase-dependent redox signaling in microvascular endothelial cells. *J. Cell Physiol.* 217, 207–214. doi: 10.1002/jcp.21495

Xue, H., Zhou, S., Xiao, L., Guo, Q., Liu, S., and Wu, Y. (2015). Hydrogen sulfide improves the endothelial dysfunction in renovascular hypertensive rats. *Physiol. Res.* 64, 663–672. doi: 10.33549/physiolres.932848

Yamakuchi, M. (2012). MicroRNA Regulation of SIRT1. *Front. Physiol.* 3:68. doi: 10.3389/fphys.2012.00068

Yamakuchi, M., and Hashiguchi, T. (2018). Endothelial Cell Aging: How miRNAs Contribute? *J. Clin. Med.* 7:170. doi: 10.3390/jcm7070170

Yan, J., Yin, Y., Zhong, W., Wang, C., and Wang, Z. (2015). CD137 Regulates NFATc1 Expression in Mouse VSMCs through TRAF6/NF-κB p65 Signaling Pathway. *Mediat. Inflammat.* 2015:639780. doi: 10.1155/2015/639780

Yang, P., Liu, Y. F., Yang, L., Wei, Q., and Zeng, H. (2010). Mechanism and clinical significance of the prothrombotic state in patients with essential hypertension. *Clin. Cardiol.* 33, E81–E86. doi: 10.1002/clc.20719

Yoshino, J., Mills, K. F., Yoon, M. J., and Imai, S. (2011). Nicotinamide mononucleotide, a key NAD(+) intermediate, treats the pathophysiology of diet- and age-induced diabetes in mice. *Cell Metab.* 14, 528–536. doi: 10.1016/j.cmet.2011.08.014

Zelko, I. N., Mariani, T. J., and Folz, R. J. (2002). Superoxide dismutase multigene family: a comparison of the CuZn-SOD (SOD1), Mn-SOD (SOD2), and EC-SOD (SOD3) gene structures, evolution, and expression. *Free Radic. Biol. Med.* 33, 337–349. doi: 10.1016/S0891-5849(02)00905-X

Zetterqvist, A. V., Berglund, L. M., Blanco, F., Garcia-Vaz, E., Wigren, M., Duner, P., et al. (2014). Inhibition of nuclear factor of activated T-cells (NFAT) suppresses accelerated atherosclerosis in diabetic mice. *PLoS One* 8:e65020. doi: 10.1371/journal.pone.0065020

Zetterqvist, A. V., Blanco, F., Öhman, J., Kotova, O., Berglund, L. M., de Frutos Garcia, S., et al. (2015). Nuclear factor of activated T cells is activated in the endothelium of retinal microvessels in diabetic mice. *J. Diabet. Res.* 2015:428473. doi: 10.1155/2015/428473

Zhang, L., Chen, J., He, Q., Chao, Z., Li, X., and Chen, M. (2019). MicroRNA-217 is involved in the progression of atherosclerosis through regulating inflammatory responses by targeting sirtuin 1. *Mol. Med. Rep.* 20, 3182–3190. doi: 10.3892/mmr.2019.10581

Zhao, W., Zhang, J., Lu, Y., and Wang, R. (2001). The vasorelaxant effect of H(2)S as a novel endogenous gaseous K(ATP) channel opener. *EMBO J.* 20, 6008–6016. doi: 10.1093/emboj/20.21.6008

Zhong, L., Simard, M. J., and Huot, J. (2018). Endothelial microRNAs regulating the NF-kappaB pathway and cell adhesion molecules during inflammation. *FASEB J.* 32, 4070–4084. doi: 10.1096/fj.201701536R

Conflict of Interest: The authors declare that the research was conducted in the absence of any commercial or financial relationships that could be construed as a potential conflict of interest.

frontiers in Physiology

ORIGINAL RESEARCH
published: 22 October 2021
doi: 10.3389/fphys.2021.739185

Treatment Site Does Not Affect Changes in Pulse Wave Velocity but Treatment Length and Device Selection Are Associated With Increased Pulse Wave Velocity After Thoracic Endovascular Aortic Repair

Daijiro Hori, Tomonari Fujimori, Sho Kusadokoro, Takahiro Yamamoto, Naoyuki Kimura and Atsushi Yamaguchi*

Department of Cardiovascular Surgery, Saitama Medical Center, Jichi Medical University, Saitama, Japan

OPEN ACCESS

Edited by:
Jochen Steppan, Johns Hopkins University, United States

Reviewed by:
Viachaslau Barodka, Wayne State University, United States
Lorenzo Carnevale, Istituto Neurologico Mediterraneo Neuromed (IRCCS), Italy
Lee Goeddel, The Johns Hopkins Hospital, Johns Hopkins Medicine, United States

***Correspondence:**
Daijiro Hori
dhori07@jichi.ac.jp

Specialty section:
This article was submitted to Vascular Physiology, a section of the journal Frontiers in Physiology

Received: *10 July 2021*
Accepted: *21 September 2021*
Published: *22 October 2021*

Citation:
Hori D, Fujimori T, Kusadokoro S, Yamamoto T, Kimura N and Yamaguchi A (2021) Treatment Site Does Not Affect Changes in Pulse Wave Velocity but Treatment Length and Device Selection Are Associated With Increased Pulse Wave Velocity After Thoracic Endovascular Aortic Repair. Front. Physiol. 12:739185. doi: 10.3389/fphys.2021.739185

Background: Endovascular treatment of aortic aneurysm is associated with an increase in pulse wave velocity (PWV) after surgery. However, the effect of different types of endovascular devices on PWV at different sites of the thoracic aorta remains unclear.

Objectives: The purposes of this study were (1) to investigate the changes in PWV after endovascular treatment of thoracic aortic aneurysm; (2) to evaluate whether there is a difference in the changes in PWV at different treatment sites; and (3) to evaluate the effect of treatment length on changes in PWV.

Methods: From July 2008 to July 2021, 276 patients underwent endovascular treatment of the true thoracic aortic aneurysm. Of these patients, 183 patients who underwent preoperative and postoperative PWV measurement within 1 year of surgery were included in the study. The treatment length index was calculated by treatment length divided by the height of the patients.

Results: Five different types of endovascular devices were used (Najuta, Kawasumi Laboratories, Inc., Tokyo, Japan; TAG, W.L. Gore & Associates, Inc., AZ, USA; Relay, Bolton Medical, Inc., FL, USA; Talent/Valiant, Medtronic, MN, USA; and Zenith, Cook Medical, IN, USA). There was no significant change in PWV in patients receiving Najuta (Before: 2,040 ± 346.8 cm/s vs. After: 2,084 ± 390.5 cm/s, $p = 0.14$). However, a significant increase was observed in other devices: TAG (Before: 2,090 ± 485.9 cm/s vs. After: 2,300 ± 512.1 cm/s, $p = 0.025$), Relay (Before: 2,102 ± 465.3 cm/s vs. After: 2,206 ± 444.4 cm/s, $p = 0.004$), Valiant (Before: 1,696 ± 330.2 cm/s vs. After: 2,186 ± 378.7 cm/s, $p < 0.001$), and Zenith (Before: 2,084 ± 431.7 cm/s vs. After: 2,321 ± 500.6 cm/s, $p < 0.001$). There was a significant increase in PWV in patients treated from aortic arch (Before: 2,006 ± 333.7 cm/s vs. After: 2,132 ± 423.7 cm/s, $p < 0.001$) and patients treated from descending thoracic aorta (Before: 2,116 ± 460.9 cm/s vs. After: 2,292 ± 460.9 cm/s, $p < 0.001$). Multivariate analysis showed that treatment site was not an independent factor associated with changes in PWV. However, Najuta (Coef −219.43,

95% CI −322.684 to −116.176, $p < 0.001$) and treatment index (Coef 147.57, 95% CI 24.826 to 270.312, $p = 0.019$) were independent factors associated with changes in PWV.

Conclusion: Najuta did not show a significant increase in PWV, while other commercially available devices showed a significant increase. The treatment site did not have a different effect on PWV. However, the treatment length was an independent factor associated with an increase in PWV.

Keywords: pulse wave velocity, endovascular treatment, aortic arch aneurysm, descending thoracic aortic aneurysm, treatment length, Najuta, arterial compliance, TEVAR

INTRODUCTION

Pulse wave velocity (PWV), which is a measure for aortic stiffness, is a well-known factor associated with cardiovascular events (Sutton-Tyrrell et al., 2005; Mattace-Raso et al., 2006; Munakata, 2016; Tomiyama et al., 2016; Ohkuma et al., 2017; Takae et al., 2019). With atherosclerotic changes of the aorta, PWV increases, resulting in reduced diastolic pressure and reduced coronary perfusion. Furthermore, excess volume overload to the peripheral causes end-organ damages (Spadaccio et al., 2016; Tomiyama et al., 2016). Increase in PWV is also observed in patients undergoing graft replacement (Spadaccio et al., 2016). A similar phenomenon was also observed after endovascular treatment of abdominal aortic aneurysms which resulted in cardiac hypertrophy (Takeda et al., 2014). Changes in cardiac dimension have also been reported in patients who underwent endovascular treatment for the thoracic aortic arch aneurysm (Hori et al., 2020).

Meanwhile, *in vitro* study of abdominal aortic endoprostheses on PWV has shown that endoskeleton type stent graft had less effect on PWV compared with other devices (van Noort et al., 2018). Furthermore, medications such as vasodilators and anti-inflammatory drugs have been suggested to reduce PWV (Janic et al., 2014).

Pulse wave velocity is regulated by aortic compliance, and the aortic arch is known to contribute to ∼50% of the total arterial compliance (Kanzaki, 2014). The purposes of this study were (1) to investigate the changes in PWV after endovascular treatment of thoracic aortic aneurysm using commercially available endoprosthesis; (2) to evaluate whether there is a difference in the changes in PWV at different treatment sites of the thoracic aorta; and (3) to evaluate the effect of treatment length on changes in PWV. Our primary hypothesis is that Najuta, which is an endoskeleton type endoprosthesis, has less effect on PWV compared with other commercially available exoskeleton type endoprostheses. The secondary hypothesis is that endoprosthesis placement in the descending thoracic aorta will lead to less increases in postoperative PWV compared with endoprosthesis placement in the aortic arch. Another secondary hypothesis is that longer treatment length would lead to higher increases in postoperative PWV.

Although the main goal of aortic aneurysm repair is to prevent aneurysmal rupture, physiological changes after endovascular treatment should also be considered. Modifying treatment strategy to minimize the changes in PWV may provide better long-term outcomes in patients undergoing endovascular treatment for thoracic aortic aneurysms.

MATERIALS AND METHODS

From July 2008 to July 2021, 276 patients underwent endovascular treatment of the true thoracic aortic aneurysm. Patients with ABI < 0.9 were excluded from the study. Of the remaining patients, 183 patients who underwent PWV measurement within 1 year of surgery were included. Changes in PWV before and after surgery were evaluated for different types of endoprostheses. Furthermore, treatment site and treatment length were evaluated for their effects on the degree of changes in PWV. The study was approved by the institutional review board of Saitama Medical Center, Jichi Medical University (S20-205).

Surgical Strategy

Choice of endoprosthesis was selected by the preference of the surgeon. All endovascular treatments were performed under general anesthesia. For patients receiving Najuta (Kawasumi, Japan), tug of wire technique was prepared from the right brachial artery to the femoral artery (Yuri et al., 2013). Najuta device was introduced from the femoral artery and was guided with a wire to the ascending aorta. The device was deployed without the use of control pacing or mechanical cardiac support. For patients requiring debranching, bypass surgery was performed prior to stent graft deployment. The orifice of each debranched artery was occluded with a coil or a stitch.

For patients receiving other commercially available endoprostheses, the device was guided into the aorta using a stiff wire. Similar to Najuta, the device was deployed without the use of control pacing and mechanical cardiac support.

Pulse Wave Velocity

Brachial-ankle PWV was measured in awake patients, before and after surgery, using a non-invasive device (Omron Colin, Tokyo, Japan) in the physiology laboratory by a trained technician. Two pressure-sensitive transducers were placed on the arm and the ankle. Simultaneous recording of the pulse waves at two different points was performed. The pulse transit time and the distance between the transducers over the body surface were assessed to calculate the PWV [PWV (cm/s) ¼ travel distance (cm) /transit time (s)] (Munakata, 2016). PWV measurements within 1 year

TABLE 1 | Demographics of the patients included in the study.

		Najuta vs. non-Najuta			Non-Najuta device				
	Total	**Najuta**	**Non-Najuta**	***p***	**TAG**	**Relay**	**Valiant**	**Zenith**	***p***
	***n* = 183**	***n* = 66**	***n* = 117**	**Najuta vs. non-Najuta**	***n* = 20**	***n* = 20**	***n* = 30**	***n* = 47**	**All device**
Age (years)	74 ± 7.8	75 ± 7.8	74 ± 7.8	0.71	73 ± 7.4	76 ± 10.2	75 ± 7.3	74 ± 7.3	0.69
Male (%)	139 (76.0%)	53 (80.3%)	86 (73.5%)	0.37	14 (70.0%)	16 (80.0%)	20 (66.7%)	36 (76.6%)	0.61
Creatinine (mg/dl)	0.97 (0.77 to 1.29)	0.87 (0.76–1.16)	1.0 (0.79–1.33)	0.15	0.93 (0.79–1.12)	0.96 (0.74–1.34)	0.89 (0.75–1.30)	1.01 (0.87–1.40)	0.46
Hemoglobin (g/dl)	12.4 ± 1.77	12.4 ± 1.65	12.5 ± 1.84	0.75	12.8 ± 1.68	12.2 ± 1.74	12.4 ± 1.75	12.5 ± 2.04	0.87
Hypertension (%)	173 (94.5%)	63 (95.5%)	110 (94.0%)	1	17 (85.0%)	18 (90.0%)	29 (96.7%)	46 (97.9%)	0.19
Dyslipidemia (%)	85 (46.4%)	32 (48.5%)	53 (45.3%)	0.76	8 (40.0%)	7 (35.0%)	15 (50.0%)	23 (48.9%)	0.79
Diabetes (%)	41 (22.4%)	16 (24.2%)	25 (21.4%)	0.71	5 (25.0%)	1 (5.0%)	8 (26.7%)	11 (23.4%)	0.35
Chronic obstructive pulmonary disease (%)	23 (12.6%)	7 (10.6%)	16 (13.7%)	0.65	3 (15.0%)	2 (10.0%)	6 (20.0%)	5 (10.6%)	0.71
Cerebral vascular disease (%)	28 (15.3%)	11 (16.7%)	17 (14.5%)	0.83	3 (15.0%)	2 (10.0%)	2 (6.7%)	10 (21.3%)	0.5
Ischemic heart disease (%)	44 (24.0%)	18 (27.3%)	26 (22.2%)	0.47	5 (25.0%)	5 (25.0%)	6 (20.0%)	10 (21.3%)	0.94
Tobacco user (%)	137 (74.9%)	51 (77.3%)	86 (73.5%)	0.6	14 (70.0%)	15 (75.0%)	23 (76.7%)	34 (72.3%)	0.95
Angiotensin receptor blocker (%)	69 (37.7%)	18 (27.3%)	51 (43.6%)	0.039	10 (50.0%)	8 (40.0%)	14 (46.7%)	19 (40.4%)	0.22
Calcium channel blocker (%)	128 (69.9%)	45 (68.2%)	83 (70.9%)	0.74	12 (60.0%)	17 (85.0%)	21 (70.0%)	33 (70.2%)	0.52
Beta blocker (%)	78 (42.6%)	25 (37.9%)	53 (45.3%)	0.35	11 (55.0%)	9 (45.0%)	13 (43.3%)	20 (42.6%)	0.75
HMG-CoA inhibitor (%)	92 (50.3%)	31 (47.0%)	61 (52.1%)	0.54	10 (50.0%)	8 (40.0%)	17 (56.7%)	26 (55.3%)	0.73
Arch treatment (%)	107 (58.5%)	59 (89.4%)	48 (41.0%)	<0.001	7 (35.0%)	17 (85.0%)	8 (26.7%)	16 (34.0%)	<0.001
Treatment length (mm)	202.9 ± 55.81	223.1 ± 49.29	192.0 ± 56.28	<0.001	195.5 ± 63.18	198.4 ± 68.86	196.5 ± 60.89	184.5 ± 43.39	0.008
Treatment index (mm/cm)	1.26 ± 0.357	1.38 ± 0.340	1.20 ± 0.350	0.001	1.24 ± 0.434	1.22 ± 0.406	1.22 ± 0.376	1.15 ± 0.259	0.016
Difference in PWV (cm/s)	147 ± 326.0	44 ± 322.0	204 ± 315.1	0.001	210 ± 447.6	104 ± 157.0	217 ± 345.3	237 ± 276.9	0.012
Difference in sBP (mmHg)	−1 ± 14.8	−2 ± 12.2	−1 ± 16.2	0.67	−5 ± 21.0	−9 ± 11.4	1 ± 15.5	4 ± 14.6	0.012

sBP, systolic blood pressure.
p-value for all devices, including Najuta device.

of surgery were collected, and measurements with closest blood pressure before and after surgery were used for the analysis.

Data Analysis

The normal distribution of the data was evaluated using the Kolmogorov–Smirnov test. For continuous variables that were normally distributed, Student's *t*-test (mean ± standard deviation) was used for comparing two groups, paired *t*-test (mean ± standard deviation) was used for comparing paired data, and one-way ANOVA (mean ± standard deviation) was used for comparing more than three groups. For continuous variables that were not normally distributed, Mann–Whitney U test (median, Q1–3) was used for comparing two groups, and Kruskal–Wallis test (median, Q1–3) was used for comparing more than three groups. For categorical variables, Fisher's exact test (*n*, %) was used. Evaluation of correlation between two continuous variables was performed by Pearson's correlation test. Changes in PWV before and after surgery were evaluated for each endoprosthesis using paired *t*-test. Patients were divided into two groups, i.e., those who were treated from the aortic arch and those who were treated from the descending thoracic aorta. Demographics and changes in PWV were evaluated for each group. Factors associated with the degree of changes in PWV were evaluated by multivariate analysis for observed differences in PWV after surgery. Possible confounding factors, such as age, gender, medication for hypertension, diabetes, and dyslipidemia, were included in the linear regression model for the evaluation of the type of endoprosthesis, treatment site, and treatment length in association with an increase in PWV. The treatment length index was calculated by treatment length divided by the height of the patients. The $p < 0.05$ were considered statistically significant. The analysis was performed using Stata (version 13.1, Stata Corp, College Station, TX, USA) and Prism (version 8.0.2, GraphPad Software Inc., La Jolla, CA, USA).

Sample Size

Sample size calculation was performed based on the data from our previous study (Hori et al., 2020). The difference in the mean PWV before and after surgery for patients undergoing endovascular treatment for aortic arch aneurysm was 125 cm/s, while the standard deviation of PWV for both measurements was 421 cm/s. From these data, a sample size of 72 patients would provide a statistical evaluation with $\alpha = 0.05$ and a power of 0.80. A sample size of 66 patients would provide a statistical power of 0.77; and a sample size of 76, 107, and 117 patients would provide a statistical power of 0.82, 0.92, and 0.94, respectively.

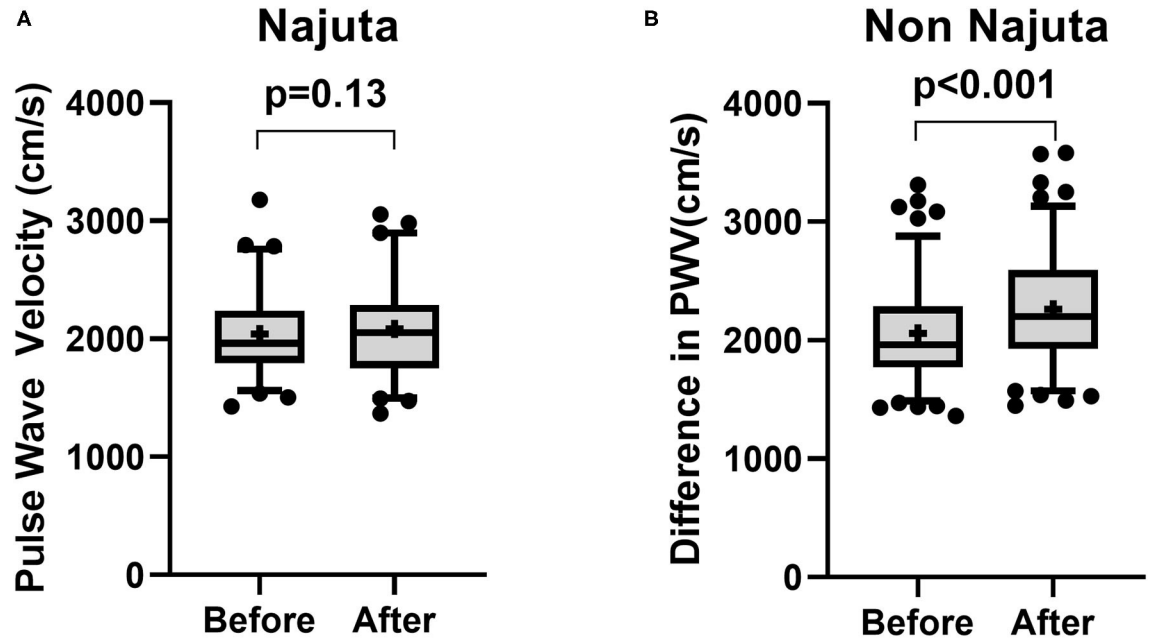

FIGURE 1 | Box and Whisker plot for pulse wave velocity before and after surgery for patients receiving Najuta device **(A)** and non-Najuta device **(B)**. There was no significant difference in pulse wave velocity in patients receiving Najuta device **(A)**. There was a significant increase in pulse wave velocity in patients receiving non-Najuta devices **(B)**. Whisker shows 5–95 percentile range and + shows the mean value.

TABLE 2 | Changes in pulse wave velocity after surgery for each device.

	Before	After	*p*	Mean of difference	SD of difference	95% CI	Cohen's *d*
Najuta	2,040 ± 346.8 cm/s	2,084 ± 390.5 cm/s	0.136	43.83 cm/s	322 cm/s	−35.31 to 123.0 cm/s	0.14
Non-Najuta	2,058 ± 422.1 cm/s	2,263 ± 462.8 cm/s	<0.001	204.4 cm/s	315.1 cm/s	146.7 to 262.1 cm/s	0.65
TAG	2,090 ± 485.9 cm/s	2,300 ± 512.1 cm/s	0.025	209.6 cm/s	447.6 cm/s	0.126 to 419.1 cm/s	0.47
Relay	2,102 ± 465.3 cm/s	2,206 ± 444.4 cm/s	0.004	103.7 cm/s	157 cm/s	30.2 to 177.2 cm/s	0.66
Valiant	1,969 ± 330.2 cm/s	2,186 ± 378.7 cm/s	<0.001	216.9 cm/s	345.3 cm/s	87.94 to 345.8 cm/s	0.63
Zenith	2,084 ± 431.7 cm/s	2,321 ± 500.6 cm/s	<0.001	237.2 cm/s	276.9 cm/s	155.9 to 318.5 cm/s	0.86

RESULTS

Five different types of endovascular devices were used (Najuta, Kawasumi Laboratories, Inc., Tokyo, Japan: $n = 66$; TAG, W.L. Gore & Associates, Inc., AZ, USA: $n = 20$; Relay, Bolton Medical, Inc., FL, USA: $n = 20$; Talent/Valiant, Medtronic, MN, USA: $n = 30$; Zenith, Cook Medical, IN, USA: $n = 47$). Angiotensin receptor blocker was more often used in patient receiving non-Najuta devices (Najuta: 27.3% vs. non-Najuta: 43.6%, $p = 0.039$). Patients treated from aortic arch were more often observed in patients receiving Najuta (Najuta: 89.4% vs. non-Najuta: 41.0%, $p < 0.001$), and the treatment index was longer in patients receiving Najuta (Najuta: 1.38 ± 0.340 vs. non-Najuta: 1.20 ± 0.350, $p = 0.001$) (**Table 1**).

There was no significant change in PWV in patients receiving Najuta (Before: 2,040 ± 346.8 cm/s vs. After: 2,084 ± 390.5 cm/s, $p = 0.14$, $n = 66$) (**Figure 1A**). However, a significant increase was observed in patients receiving non-Najuta devices (Before: 2,058 ± 422.1 cm/s vs. After: 2,263 ± 462.8 cm/s, $p < 0.001$) (**Figure 1B**). Mean values of difference in PWV for Najuta and non-Najuta were 44 ± 322.0 cm/s (95% CI −35.3 to 123.0) and 204 ± 315.1 cm/s (95% CI 146.7 to 262.1), respectively (**Table 2**). Individual analysis for each of the non-Najuta devices also showed a significant increase in PWV after surgery: TAG (Before: 2,090 ± 485.9 cm/s vs. After: 2,300 ± 512.1 cm/s, $p = 0.025$, $n = 20$), Relay (Before: 2,102 ± 465.3 cm/s vs. After: 2,206 ± 444.4 cm/s, $p = 0.004$, $n = 20$), Valiant (Before: 1,696 ± 330.2 cm/s vs. After: 2,186 ± 378.7 cm/s, $p < 0.001$, $n = 30$), and Zenith (Before: 2,084 ± 431.7 cm/s vs. After: 2,321 ± 500.6 cm/s, $p < 0.001$, $n = 47$). Mean values of difference in PWV for TAG, Relay, Valiant, and Zenith were 210 ± 447.6 cm/s, 104 ± 157.0 cm/s, 217 ± 345.3 cm/s, and 237 ± 276.9 cm/s, respectively (**Figures 2A–D**; **Table 2**).

The demographics of patients treated from aortic arch (Arch) and descending thoracic aorta (non-Arch) are shown in **Table 3**. Creatinine was higher in patients receiving endoprosthesis from

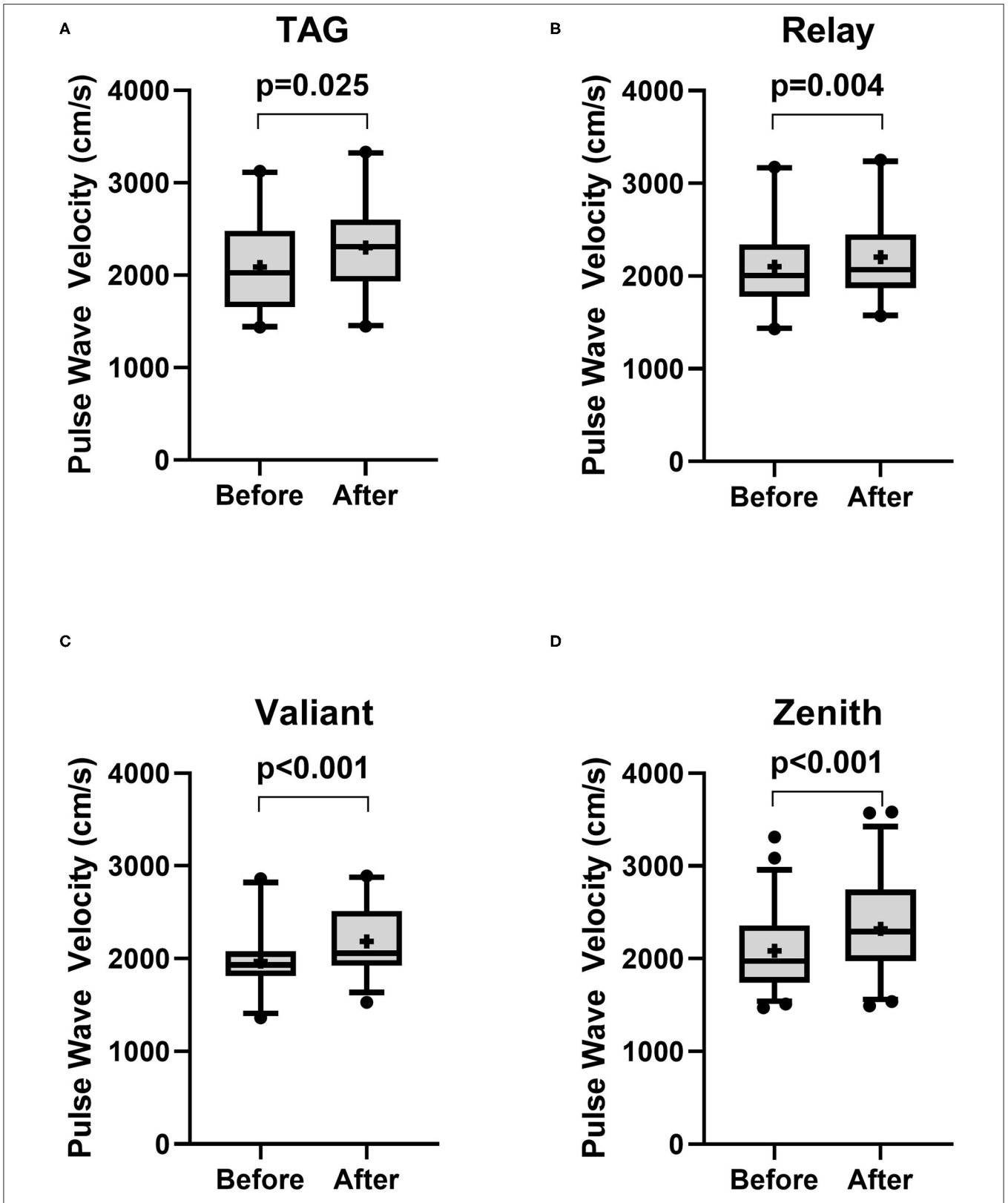

FIGURE 2 | Box and Whisker plot for pulse wave velocity before and after surgery for patients receiving non-Najuta devices. There was a significant difference in pulse wave velocity in patients receiving TAG **(A)**, Relay **(B)**, Valiant **(C)**, and Zenith **(D)**. Whisker shows 5–95 percentile range and + shows the mean value.

the descending thoracic aorta [Arch: 0.87 mg/dl (0.71–1.21) vs. non-Arch: 1.03 mg/dl (0.82–1.31), $p = 0.027$]. Najuta was more often used in patients treated from the aortic arch (Arch: 55.1% vs. non-Arch: 9.2%, $p < 0.001$), and the treatment index was higher in patients treated from the aortic arch (Arch 1.33 ± 0.376 vs. non-Arch: 1.15 ± 0.297, $p < 0.001$). There was a significant increase in PWV in patients treated from aortic arch (Before: 2,006 ± 333.7 cm/s vs. After: 2,132 ± 423.7 cm/s, $p < 0.001$) and patients treated from descending thoracic aorta (Before: 2,116 ± 460.9 cm/s vs. After: 2,292 ± 460.9 cm/s, $p < 0.001$) (**Figures 3A,B**). The mean values of difference in PWV before and after surgery for patients treated from aortic arch and descending thoracic aorta were 126 ± 317 cm/s (95% CI 63.97 to 186.5) and 176 ± 338.2 cm/s (95% CI 98.48 to 253.1), respectively (**Table 4**).

The scatterplot for treatment length index and changes in PWV showed a significant but weak correlation ($r = 0.14$, 95% CI 0.01 to 1.00, $p = 0.038$) (**Figure 4**). Furthermore, there were no significant factors associated with the difference in PWV after surgery (**Table 5**). Multivariate linear regression model for the difference in PWV, including possible confounding factors, showed that angiotensin receptor blocker (Coef 96.28, 95% CI 0.332 to 192.230, $p = 0.049$), use of Najuta (Coef −219.43, 95% CI −322.684 to −116.176, $p < 0.001$), and treatment index (Coef 147.57, 95% CI 24.826 to 270.312, $p = 0.019$) were independent factors associated with changes in PWV ($R^2 = 0.324$). However, the treatment site was not associated with changes in PWV (Coef 26.02, 95% CI −73.596 to 125.627, $p = 0.61$) (**Table 6**).

DISCUSSION

With improvement in endovascular technology, endovascular treatment of aortic aneurysm has currently become a class IIa indication for descending thoracic aortic aneurysm (Hiratzka et al., 2010; Erbel et al., 2014). The outcomes of thoracic endovascular treatment are also promising, especially in high-risk patients. In a study with 579 patients undergoing endovascular treatment of descending thoracic aorta, in-hospital mortality, stroke, and spinal cord injury occurred in 4.7, 2.1, and 0.5% of the patients, respectively. For the long-term outcomes, the aorta-specific survival at 11.8 years was 96.2% (Ranney et al., 2018). Previous reports on commercially available devices have also shown an acceptable outcome with a major advance event rate of 5.6% in patient receiving Relay within 1 year after surgery; 2.8% in patient requiring secondary intervention within 1 year with Cook device; a major adverse event rate of 7.6% in patient receiving cTAG within 4 years after surgery (Bodell et al., 2018). Characterized by its minimal invasiveness and versatility, more young patients are now treated by this technology. Although prevention of aortic rupture is the main goal, physiological changes after implantation of endoprosthesis could be a major concern, especially in young patients with expected long-term survival.

A previous study has shown a significant increase in PWV after thoracic endovascular aortic repair in *ex vivo* porcine model (de Beaufort et al., 2017). In an experiment using a pulsatile mock loop system, cTAG, Relay, Zenith, and Valiant showed a significant increase in PWV after implantation. For the total cohort of 20 aortas, PWV increased by a mean of 600 cm/s or 8.9% of baseline PWV after deployment of a 100-mm endoprosthesis ($p < 0.001$). This change was more profound than that observed in our study. This study showed that in a clinical setting, the treatment length of 192 ± 56.28 mm in patients receiving non-Najuta devices (cTAG, Relay, Valiant, and Zenith) was associated with a mean increase of 204 ± 315.1 cm/s in PWV after surgery. These findings may imply that complex regulation of hemodynamics in humans may be attenuating the effect of implanted endoprosthesis on physiological changes in the aorta.

Previously, we have reported changes in PWV in patients undergoing endovascular treatment of aortic arch aneurysm, which increased from 2,083 ± 454.5 cm/s before surgery to 2,305 ± 479.7 cm/s after surgery ($p = 0.023$) (Hori et al., 2020). Furthermore, an increase in PWV in patients undergoing thoracic endovascular aortic replacement was associated with long-term cardiovascular events and cerebrovascular events in Kaplan–Meyer analysis (Hori et al., 2020). PWV has been reported to be a useful biomarker for major adverse cardiovascular and cerebrovascular events (MACCE) and mortality (Sutton-Tyrrell et al., 2005). A meta-analysis of cohort studies has shown that a 1 m/s increase in PWV was associated with a 12% increase in the risk of cardiovascular events (Munakata, 2016). This study has shown that the mean difference in PWV after surgery was 204 ± 315.1 cm/s (95% CI 146.7 to 262.1) for patients receiving non-Najuta devices. The result from a previous study may indicate that these patients receiving non-Najuta devices may be associated with a 2.4% (12% × 204 cm/s/1,000 cm/s) increase in the risk of cardiovascular events. In contrast, the mean increase in PWV of 44 cm/s in patients receiving Najuta may not be of clinical significance. Medications have also been reported to reduce PWV, which include antihypertensive drugs, statins, peroral antidiabetics, advanced glycation end products (AGE) cross-link breakers, anti-inflammatory drugs, endothelin-A receptor antagonists, and vasopeptidase inhibitors (Janic et al., 2014). Although these medications have shown some effects in reducing PWV, their effects on long-term outcomes are still to be evaluated. Furthermore, their effects on patients receiving endoprosthesis are another factor that should be recognized. In this study, angiotensin receptor blocker was associated with an increase in PWV. This may be due to the background of patients receiving these medications, including hypertension and ischemic heart disease, which are the factors associated with increased PWV (Sutton-Tyrrell et al., 2005; Munakata, 2016; Tomiyama et al., 2016).

This study and previous study from our group have shown that there was no significant change in PWV in patients receiving Najuta (Hori et al., 2017, 2020). There are several types of endovascular devices in the market depending on the differences in the fabric used and stent skeleton design. Comparison of expanded polytetrafluoroethylene (ePTFE) and dacron graft on PWV has shown that ePTFE graft has less effect on the changes in PWV after surgery (Kadoglou et al., 2014). This phenomenon

TABLE 3 | Demographics of the patients receiving endovascular prosthesis from the aortic arch (Arch) and from the descending thoracic aorta (non-Arch).

	Arch	Non-Arch	*p*
	***n* = 107**	***n* = 76**	
Age (years)	75 ± 7.9	74 ± 7.7	0.41
Male (%)	79 (73.8%)	60 (78.9%)	0.49
Creatinine (mg/dl)	0.87 (0.71–1.21)	1.03 (0.82–1.31)	0.027
Hemoglobin (g/dl)	12.4 ± 1.73	12.5 ± 1.84	0.56
Hypertension (%)	102 (95.3%)	71 (93.4%)	0.74
Dyslipidemia (%)	51 (47.7%)	34 (44.7%)	0.76
Diabetes (%)	20 (18.7%)	21 (27.6%)	0.21
Chronic obstructive pulmonary disease (%)	11 (10.3%)	12 (15.8%)	0.27
Cerebral vascular disease (%)	18 (16.8%)	10 (13.2%)	0.54
Ischemic heart disease (%)	23 (21.5%)	21 (27.6%)	0.38
Tobacco user (%)	79 (73.8%)	58 (76.3%)	0.73
Angiotensin receptor blocker (%)	39 (36.4%)	30 (39.5%)	0.76
Calcium channel blocker (%)	79 (73.8%)	49 (64.5%)	0.19
Beta blocker (%)	40 (37.4%)	38 (50.0%)	0.1
HMG-CoA inhibitor (%)	52 (48.6%)	40 (52.6%)	0.65
Najuta (%)	59 (55.1%)	7 (9.2%)	<0.001
Treatment length (mm)	214.7 ± 57.63	186.2 ± 48.82	<0.001
Treatment index (mm/cm)	1.33 ± 0.376	1.15 ± 0.297	<0.001
Difference in PWV (cm/s)	125.7 ± 316.99	175.8 ± 338.24	0.31
Difference in sBP (mmHg)	−0.3 ± 13.83	−1.7 ± 16.21	0.53

sBP, systolic blood pressure.

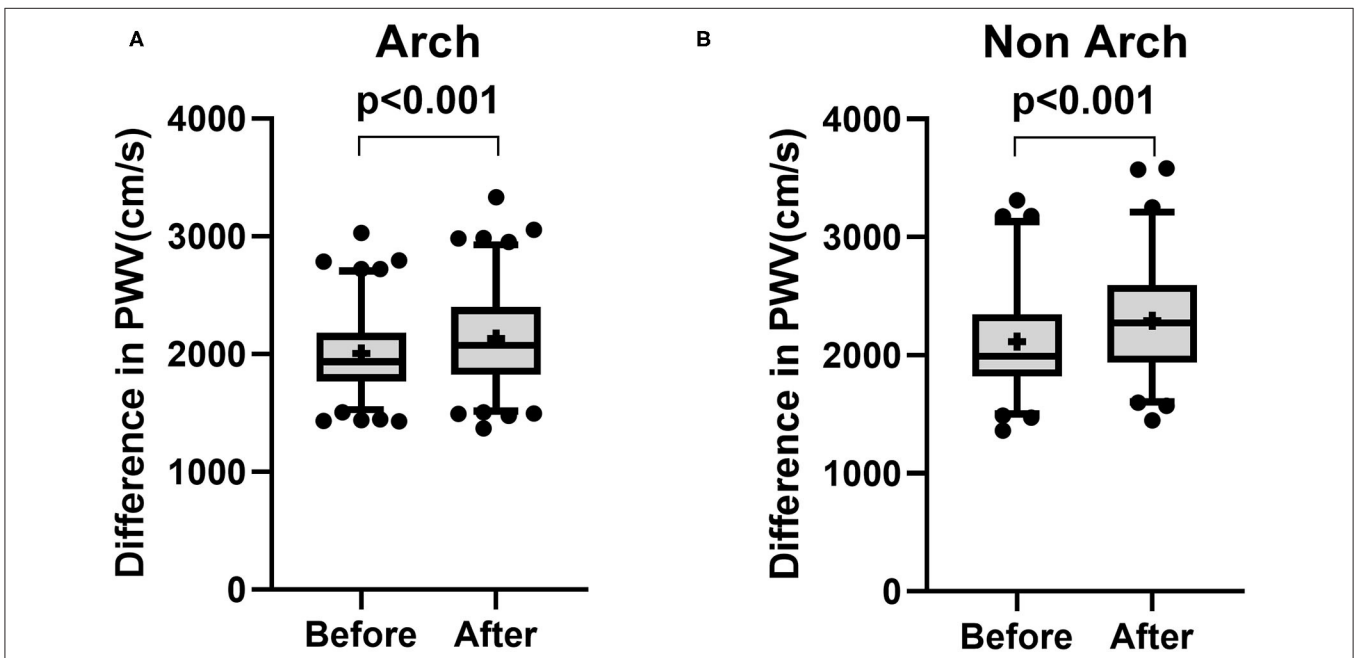

FIGURE 3 | Box and Whisker plot for pulse wave velocity before and after surgery for patients treated from aortic arch (**A**: Arch) and patients treated from descending thoracic aorta (**B**: non-Arch). There was a significant increase in pulse wave velocity in patients treated from aortic arch **(A)** and patients treated from descending thoracic aorta **(B)**. Whisker shows 5–95 percentile range and + shows the mean value.

TABLE 4 | Changes in pulse wave velocity for patients treated for Arch and non-Arch.

	Before	After	*p*	Mean of difference	SD of difference	95% CI	Cohen's *d*
Arch	2,006 ± 337.7 cm/s	2,132 ± 423.7 cm/s	<0.001	125.7 cm/s	317 cm/s	64.97 to 186.5 cm/s	0.40
Non-arch	2,116 ± 460.9 cm/s	2,292 ± 460.9 cm/s	<0.001	175.8 cm/s	338.2 cm/s	98.48 to 253.1 cm/s	0.52

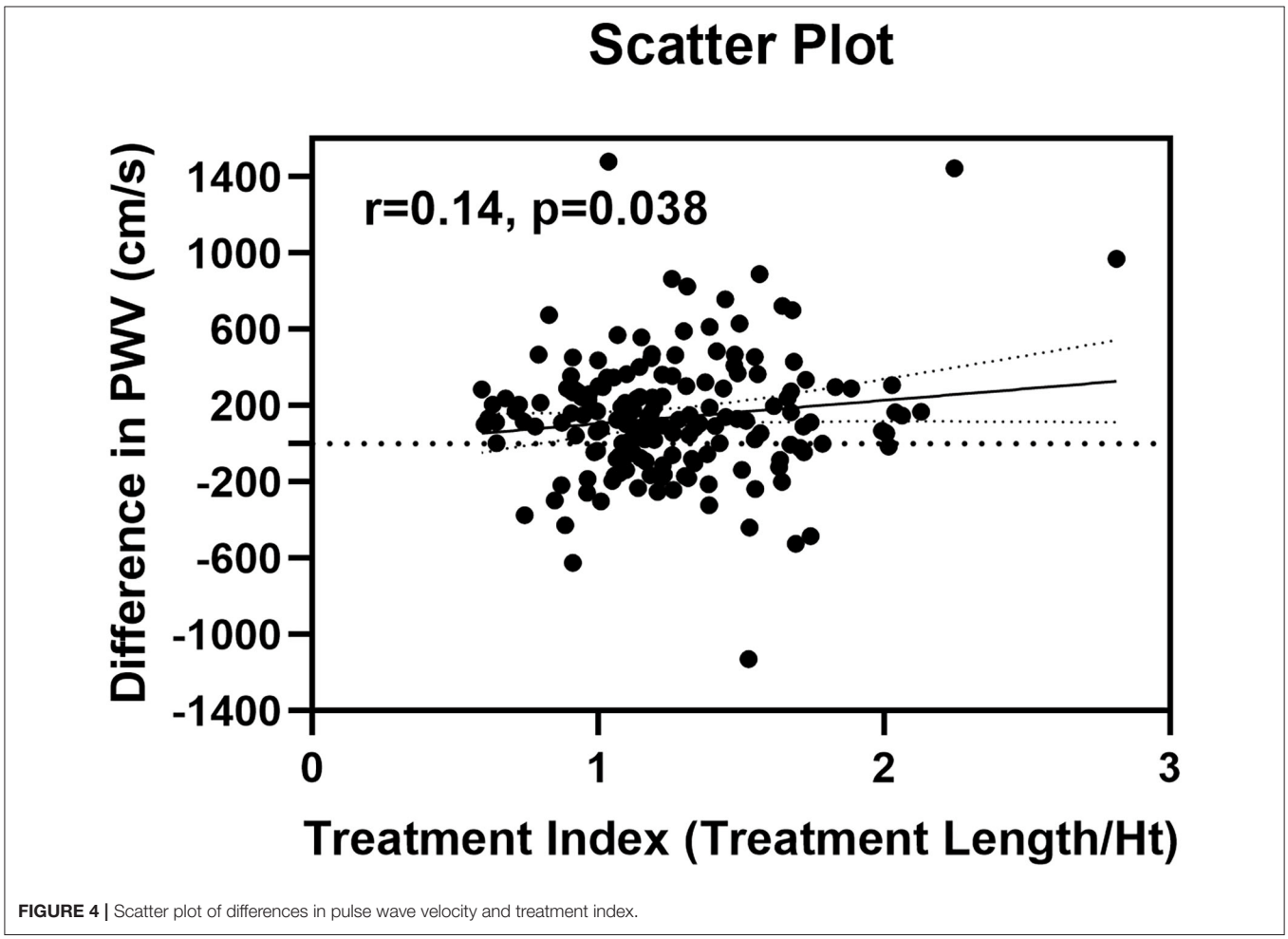

FIGURE 4 | Scatter plot of differences in pulse wave velocity and treatment index.

was also observed in the computational analysis (Kleinstreuer et al., 2008). In a study by Kleinstreuer et al. (2008), the wall distensibility of a stent graft compliance (C) was calculated by the difference in maximum diameter during systolic pressure and diastolic pressure (Δd) over pulse pressure (Δp) and the diastolic diameter of the vessel (d):

$$C = \Delta d / \Delta p d (\%/100\ mmHg)$$

The compliance of a diamond nitinol stent with an ePTFE graft was 1.7%–2.0%/100 mmHg compared with 0.1–0.2%/100 mmHg with a dacron graft. TAG is constructed with an ePTFE, while Relay, Valiant, and Zenith are constructed with a dacron graft. Furthermore, all of these devices are exoskeleton type stent graft in which the graft fabric is covered by stent skeleton. On the contrary, Najuta is characterized by endoskeleton type stent graft with ePTFE graft. The graft is only sutured at the edge of the stent skeleton, and thus, ePTFE graft is able to stretch out with the pulsatile flow. Sail-like effect of the graft fabric in Najuta may have substituted the physiological effect of the aortic compliance, thus reducing the effect on PWV. Furthermore, the stent skeleton of Najuta is rather compliant compared with other devices. Device selection may be an important factor in providing less effect on PWV after surgery. Further advancement in the skeleton design and fabric to accommodate for healthy aortic compliance may provide better long-term outcomes.

Through the Windkessel effect, the aorta stores 50% of left ventricular volume during systole, which is released at diastole by its elastic force (Kanzaki, 2014). This phenomenon allows the constant flow to the peripheral, which reduces mechanical

TABLE 5 | Changes in pulse wave velocity (cm/s) in patient with or without listed variables.

	With Najuta			Without Najuta		
	Without	**With**	***p***	**Without**	**With**	***p***
Hypertension (%)	27.5 ± 302.99	153.4 ± 326.78	0.24	118.6 ± 240.48	209.9 ± 319.34	0.46
Diabetes (%)	142.6 ± 310.36	159.9 ± 379.20	0.77	198.3 ± 284.60	227.2 ± 414.84	0.69
Dyslipidemia (%)	174.7 ± 379.92	114.0 ± 248.21	0.21	232.8 ± 374.62	170.2 ± 221.97	0.29
Chronic obstructive pulmonary disease (%)	153.1 ± 322.57	96.7 ± 358.60	0.44	207.1 ± 323.83	187.4 ± 261.45	0.82
Cerebrovascular disease (%)	141.9 ± 317.20	171.7 ± 376.51	0.66	187.9 ± 293.93	301.9 ± 416.47	0.17
Ischemic heart disease (%)	159.3 ± 328.06	106.3 ± 319.80	0.35	211.5 ± 335.76	179.8 ± 232.43	0.65
Tobacco user (%)	173.7 ± 361.76	137.4 ± 313.99	0.52	263.1 ± 348.46	183.3 ± 301.55	0.23
Postoperative angiotensin converting enzyme inhibitor (%)	142.6 ± 330.73	201.9 ± 253.79	0.54	200.1 ± 319.06	272.7 ± 253.76	0.56
Postoperative angiotensin receptor blocker (%)	128.8 ± 295.47	196.3 ± 399.02	0.22	179.4 ± 245.61	265.6 ± 440.08	0.18
Postoperative calcium channel blocker (%)	153.8 ± 379.58	140.3 ± 274.35	0.78	245.6 ± 354.03	171.5 ± 278.57	0.21
Postoperative beta blocker (%)	144.5 ± 344.50	148.9 ± 305.31	0.93	207.6 ± 309.77	201.4 ± 322.66	0.92
Postoperative HMG-CoA inhibitor (%)	125.8 ± 368.26	166.1 ± 280.84	0.41	165.6 ± 362.67	235.5 ± 270.08	0.24

TABLE 6 | Linear regression model for changes in pulse wave velocity ($R^2 = 0.324$).

	Coef	**95% Confidence interval**	***p***
Age	2.14	−3.247 to 7.528	0.43
Male	−24.96	−124.529 to 74.603	0.62
Angiotensin receptor blocker	96.28	0.332 to 192.230	0.049
Calcium channel blocker	−25.07	−114.348 to 64.215	0.58
Beta blocker	−17.51	−108.373 to 73.348	0.7
HMG-CoA inhibitor	−17.98	−111.145 to 75.183	0.7
Najuta	−219.43	−322.684 to −116.176	<0.001
Treatment index	147.57	24.826 to 270.312	0.019
Arch treatment	26.02	−73.596 to 125.627	0.61
Difference in sBP	10.27	7.355 to 13.188	<0.001

sBP, systolic blood pressure.

stress on the aorta. It has also been reported that the aortic arch contributes ∼50% of the total arterial compliance (Ioannou et al., 2009; Kanzaki, 2014). Therefore, the aortic compliance changes in the aortic arch may have a more profound effect on the changes in PWV compared with other sites of the aorta. However, multivariate analysis of this study has shown that treatment site was not an independent factor associated with an increase in PWV. In contrast, despite the weak correlation between the treatment length index and changes in PWV, the multivariate linear regression model has shown that the treatment length index was an independent factor associated with an increase in PWV after normalizing for possible confounding factors. In a previous study using *ex vivo* porcine model, de Beaufort et al. have shown that an increase in PWV was dependent on the extent of stent coverage, resulting in an increase by a mean of 1,400 cm/s or 23.0% of baseline PWV after an extension of covered length ($p < 0.001$) (de Beaufort et al., 2017). Although these changes were more profound than those observed in our previous study, this study has shown a similar result in the clinical setting, in which the treatment length was associated with the degree of changes in PWV after surgery. The result of this study showed that for a patient with a height of 170 cm, the treatment length of 170 mm would increase PWV by 147.57 cm/s (95% CI 24.826 to 270.312). Adjustment of the treatment length could range from 20 to 40 mm, and thus modification in surgical strategy may not provide clinical significance. However, changes in PWV after endovascular treatment should be recognized as a mean increase in PWV was observed at a range of 44 to 237 cm/s with commercially available endoprostheses.

Limitations

There are several limitations. First, this is a retrospective study with a relatively small sample size. Further study with a larger sample size is recommended to confirm these results. Second, PWV measurement within 1 year of surgery was evaluated in this study. PWV at a longer period after surgery should also be evaluated in which remodeling of the aorta or thrombotic changes in the aneurysm sac may have an effect on PWV. There are few patients with significant aortic remodeling, which shows the disappearance of an aortic aneurysm in long term. The aortic compliance of these patients may be reflected by the characteristics of the implanted endoprosthesis. However, in

patients with residual thrombosed aneurysm sac, the movement of the endoprosthesis with the pulsatile flow may be limited by the thrombosed tissue surrounding the endoprosthesis. Finally, further study with the evaluation of long-term outcomes should be performed to observe whether postoperative changes in PWV reflect long-term outcomes. The present cohort showed a trend toward higher preoperative PWV in patients with ischemic heart disease (IHD: 2,109 ± 466.1 cm/s vs. no IHD: 1,996 ± 449.9 cm/s, $p = 0.15$). This already may imply that patients with higher PWV may be associated with cardiovascular events, and thus an increase in PWV after surgery may put patients at higher risk for cardiovascular events as reported in the previous reports (Vlachopoulos et al., 2012; Tomiyama et al., 2016). In our hospital, every patient is evaluated for coronary artery disease prior to surgery. Patients with significant stenosis of the coronary artery were treated prior to surgery or immediately after the surgery. This could be an important bias that could affect the long-term outcomes in our cohort. Despite these limitations, there are strong evidence that increased PWV is associated with major cardiovascular and cerebral vascular events (Sutton-Tyrrell et al., 2005; Mattace-Raso et al., 2006; Munakata, 2016; Tomiyama et al., 2016; Ohkuma et al., 2017; Takae et al., 2019). Changes in PWV after surgery should be recognized as a possible risk factor for the long-term cardiovascular events.

CONCLUSION

This study showed that the Najuta device may provide less effect on PWV in patients undergoing endovascular treatment of the thoracic aortic aneurysm. There was no significant difference in changes in PWV for different treatment sites. Although modifying endovascular treatment may not provide clinical significance, treatment length was associated with an increase in PWV after implantation of endoprostheses.

DATA AVAILABILITY STATEMENT

The original contributions presented in the study are included in the article/supplementary material, further inquiries can be directed to the corresponding author/s.

ETHICS STATEMENT

The studies involving human participants were reviewed and approved by Institutional review board of Saitama Medical Center, Jichi Medical University. Written informed consent for participation was not required for this study in accordance with the national legislation and the institutional requirements.

AUTHOR CONTRIBUTIONS

DH and TF: had substantial contributions to the conception or design of the work. DH: acquisition. DH, TF, SK, and TY: analysis. DH, NK, and AY: interpretation of data for the work and revision of the work. DH, TF, SK, and TY: drafting of the work. All authors approved the final version of the work.

FUNDING

This work was supported by JSPS KAKENHI [Grant Number JP21K16500 (DH)] from the Ministry of Education, Culture, Sports, Science and Technology, Japan.

REFERENCES

Bodell, B. D., Taylor, A. C., and Patel, P. J. (2018). Thoracic endovascular aortic repair: review of current devices and treatments options. *Tech. Vasc. Interv. Radiol.* 21, 137–145. doi: 10.1053/j.tvir.2018.06.003

de Beaufort, H. W. L., Coda, M., Conti, M., van Bakel, T. M. J., Nauta, F. J. H., Lanzarone, E., et al. (2017). Changes in aortic pulse wave velocity of four thoracic aortic stent grafts in an *ex vivo* porcine model. *PLoS ONE* 12:e0186080. doi: 10.1371/journal.pone.0186080

Erbel, R., Aboyans, V., Boileau, C., Bossone, E., Bartolomeo, R. D., Eggebrecht, H., et al. (2014). 2014 ESC Guidelines on the diagnosis and treatment of aortic diseases: document covering acute and chronic aortic diseases of the thoracic and abdominal aorta of the adult. The Task Force for the Diagnosis and Treatment of Aortic Diseases of the European Society of Cardiology (ESC). *Eur. Heart J.* 35, 2873–2926. doi: 10.1093/eurheartj/ehu281

Hiratzka, L. F., Bakris, G. L., Beckman, J. A., Bersin, R. M., Carr, V. F., Casey, D. E. Jr., et al. (2010). 2010 ACCF/AHA/AATS/ACR/ASA/SCA/SCAI/SIR/STS/SVM Guidelines for the diagnosis and management of patients with thoracic aortic disease. A Report of the American College of Cardiology Foundation/American Heart Association Task Force on Practice Guidelines, American Association for Thoracic Surgery, American College of Radiology,American Stroke Association, Society of Cardiovascular Anesthesiologists, Society for Cardiovascular Angiography and Interventions, Society of Interventional Radiology, Society of Thoracic Surgeons,and Society for Vascular Medicine. *J. Am. Coll. Cardiol.* 55, e27–e129. doi: 10.1161/CIR.0b013e3181d4739e

Hori, D., Akiyoshi, K., Yuri, K., Nishi, S., Nonaka, T., Yamamoto, T., et al. (2017). Effect of endoskeleton stent graft design on pulse wave velocity in patients undergoing endovascular repair of the aortic arch. *Gen. Thorac. Cardiovasc. Surg.* 65, 506–511. doi: 10.1007/s11748-017-0787-8

Hori, D., Yuri, K., Kusadokoro, S., Shimizu, T., Kimura, N., and Yamaguchi, A. (2020). Effect of endoprostheses on pulse wave velocity and its long-term outcomes after thoracic endovascular aortic repair. *Gen. Thorac. Cardiovasc. Surg.* 68, 1134–1141. doi: 10.1007/s11748-020-01343-0

Ioannou, C. V., Morel, D. R., Katsamouris, A. N., Katranitsa, S., Startchik, I., Kalangos, A., et al. (2009). Left ventricular hypertrophy induced by reduced aortic compliance. *J. Vasc. Res.* 46, 417–425. doi: 10.1159/000194272

Janic, M., Lunder, M., and Sabovic, M. (2014). Arterial stiffness and cardiovascular therapy. *Biomed Res. Int.* 2014:621437. doi: 10.1155/2014/621437

Kadoglou, N. P., Moulakakis, K. G., Papadakis, I., Ikonomidis, I., Alepaki, M., Spathis, A., et al. (2014). Differential effects of stent-graft fabrics on arterial stiffness in patients undergoing endovascular aneurysm repair. *J. Endovasc. Ther.* 21, 850–858. doi: 10.1583/14-4772MR.1

Kanzaki, H. (2014). Aortic compliance and left ventricular diastolic function. Do endovascular repairs for aortic aneurysm alter aortic stiffness? *Circul. J.* 78, 307–308. doi: 10.1253/circj.CJ-13-1520

Kleinstreuer, C., Li, Z., Basciano, C. A., Seelecke, S., and Farber, M. A. (2008). Computational mechanics of Nitinol stent grafts. *J. Biomech.* 41, 2370–2378. doi: 10.1016/j.jbiomech.2008.05.032

Mattace-Raso, F. U., van der Cammen, T. J., Hofman, A., van Popele, N. M., Bos, M. L., Schalekamp, M. A., et al. (2006). Arterial stiffness and risk of coronary heart disease and stroke: the Rotterdam Study. *Circulation* 113, 657–663. doi: 10.1161/CIRCULATIONAHA.105.555235

Munakata, M. (2016). Brachial-ankle pulse wave velocity: background, method, and clinical evidence. *Pulse* 3, 195–204. doi: 10.1159/000443740

Ohkuma, T., Ninomiya, T., Tomiyama, H., Kario, K., Hoshide, S., Kita, Y., et al. (2017). Brachial-ankle pulse wave velocity and the risk prediction of cardiovascular disease: an individual participant data meta-analysis. *Hypertension* 69, 1045–1052. doi: 10.1161/HYPERTENSIONAHA.117.09097

Ranney, D. N., Cox, M. L., Yerokun, B. A., Benrashid, E., McCann, R. L., and Hughes, G. C. (2018). Long-term results of endovascular repair for descending thoracic aortic aneurysms. *J. Vasc. Surg.* 67, 363–368. doi: 10.1016/j.jvs.2017.06.094

Spadaccio, C., Nappi, F., Al-Attar, N., Sutherland, F. W., Acar, C., Nenna, A., et al. (2016). Old myths, new concerns: the long-term effects of ascending aorta replacement with Dacron grafts. Not All That Glitters Is Gold. *J. Cardiovasc. Transl. Res.* 9, 334–342. doi: 10.1007/s12265-016-9699-8

Sutton-Tyrrell, K., Najjar, S. S., Boudreau, R. M., Venkitachalam, L., Kupelian, V., Simonsick, E. M., et al. (2005). Elevated aortic pulse wave velocity, a marker of arterial stiffness, predicts cardiovascular events in well-functioning older adults. *Circulation* 111, 3384–3390. doi: 10.1161/CIRCULATIONAHA.104.483628

Takae, M., Yamamoto, E., Tokitsu, T., Oike, F., Nishihara, T., Fujisue, K., et al. (2019). Clinical significance of brachial-ankle pulse wave velocity in patients with heart failure with reduced left ventricular ejection fraction. *Am. J. Hypertens.* 32, 657–667. doi: 10.1093/ajh/hpz048

Takeda, Y., Sakata, Y., Ohtani, T., Tamaki, S., Omori, Y., Tsukamoto, Y., et al. (2014). Endovascular aortic repair increases vascular stiffness and alters cardiac structure and function. *Circul. J.* 78, 322–328. doi: 10.1253/circj.CJ-13-0877

Tomiyama, H., Matsumoto, C., Shiina, K., and Yamashina, A. (2016). Brachial-ankle PWV: current status and future directions as a useful marker in the management of cardiovascular disease and/or cardiovascular risk factors. *J. Atheroscler. Thromb.* 23, 128–146. doi: 10.5551/jat.32979

van Noort, K., Holewijn, S., Schuurmann, R. C. L., Boersen, J. T., Overeem, S. P., Jebbink, E. G., et al. (2018). Effect of abdominal aortic endoprostheses on arterial pulse wave velocity in an *in vitro* abdominal aortic flow model. *Physiol. Meas.* 39:104001. doi: 10.1088/1361-6579/aae195

Vlachopoulos, C., Aznaouridis, K., Terentes-Printzios, D., Ioakeimidis, N., and Stefanadis, C. (2012). Prediction of cardiovascular events and all-cause mortality with brachial-ankle elasticity index: a systematic review and meta-analysis. *Hypertension* 60, 556–562. doi: 10.1161/HYPERTENSIONAHA.112.194779

Yuri, K., Yokoi, Y., Yamaguchi, A., Hori, D., Adachi, K., and Adachi, H. (2013). Usefulness of fenestrated stent grafts for thoracic aortic aneurysms. *Eur. J. Cardiothorac. Surg.* 44, 760–767. doi: 10.1093/ejcts/ezt127

Conflict of Interest: AY serves as a consultant to Japan Lifeline Co. Ltd., which was a distributor for Relay device.

The remaining authors declare that the research was conducted in the absence of any commercial or financial relationships that could be construed as a potential conflict of interest.

Publisher's Note: All claims expressed in this article are solely those of the authors and do not necessarily represent those of their affiliated organizations, or those of the publisher, the editors and the reviewers. Any product that may be evaluated in this article, or claim that may be made by its manufacturer, is not guaranteed or endorsed by the publisher.

frontiers in Physiology

ORIGINAL RESEARCH
published: 25 October 2021
doi: 10.3389/fphys.2021.746796

Comparative Study of Human and Murine Aortic Biomechanics and Hemodynamics in Vascular Aging

*Sara E. Hopper[1], Federica Cuomo[1], Jacopo Ferruzzi[2], Nicholas S. Burris[3], Sara Roccabianca[4], Jay D. Humphrey[5,6] and C. Alberto Figueroa[1,7]**

[1] Department of Biomedical Engineering, University of Michigan, Ann Arbor, MI, United States, [2] Department of Bioengineering, The University of Texas at Dallas, Richardson, TX, United States, [3] Department of Radiology, University of Michigan, Ann Arbor, MI, United States, [4] Department of Mechanical Engineering, Michigan State University, East Lansing, MI, United States, [5] Department of Biomedical Engineering, Yale University, New Haven, CT, United States, [6] Vascular Biology and Therapeutics Program, Yale University, New Haven, CT, United States, [7] Department of Surgery, University of Michigan, Ann Arbor, MI, United States

OPEN ACCESS

Edited by:
Lakshmi Santhanam, Johns Hopkins University, United States

Reviewed by:
Jing Wu, Medical College of Wisconsin, United States
Guillaume Goudot, Institut National de la Santé et de la Recherche Médicale (INSERM), France
Lacolley Patrick, Institut National de la Santé et de la Recherche Médicale (INSERM), France

***Correspondence:**
C. Alberto Figueroa
figueroc@med.umich.edu

Specialty section:
This article was submitted to Vascular Physiology, a section of the journal Frontiers in Physiology

Received: *24 July 2021*
Accepted: *05 October 2021*
Published: *25 October 2021*

Citation:
Hopper SE, Cuomo F, Ferruzzi J, Burris NS, Roccabianca S, Humphrey JD and Figueroa CA (2021) Comparative Study of Human and Murine Aortic Biomechanics and Hemodynamics in Vascular Aging. Front. Physiol. 12:746796. doi: 10.3389/fphys.2021.746796

Introduction: Aging has many effects on the cardiovascular system, including changes in structure (aortic composition, and thus stiffening) and function (increased proximal blood pressure, and thus cardiac afterload). Mouse models are often used to gain insight into vascular aging and mechanisms of disease as they allow invasive assessments that are impractical in humans. Translation of results from murine models to humans can be limited, however, due to species-specific anatomical, biomechanical, and hemodynamic differences. In this study, we built fluid-solid-interaction (FSI) models of the aorta, informed by biomechanical and imaging data, to compare wall mechanics and hemodynamics in humans and mice at two equivalent ages: young and older adults.

Methods: For the humans, 3-D computational models were created using wall property data from the literature as well as patient-specific magnetic resonance imaging (MRI) and non-invasive hemodynamic data; for the mice, comparable models were created using population-based properties and hemodynamics as well as subject-specific anatomies. Global aortic hemodynamics and wall stiffness were compared between humans and mice across age groups.

Results: For young adult subjects, we found differences between species in pulse pressure amplification, compliance and resistance distribution, and aortic stiffness gradient. We also found differences in response to aging between species. Generally, the human spatial gradients of stiffness and pulse pressure across the aorta diminished with age, while they increased for the mice.

Conclusion: These results highlight key differences in vascular aging between human and mice, and it is important to acknowledge these when using mouse models for cardiovascular research.

Keywords: arterial stiffness, pulse wave velocity (PWV), fluid-solid-interaction, hypertension, aortic morphology

INTRODUCTION

Aging is a primary risk factor for numerous cardiovascular diseases (Lakatta et al., 2009; Safar, 2010). Even in the absence of co-morbidities that often arise in aging, natural aging-induced changes in structure and function of the vascular system include pronounced central artery stiffening and associated changes in the peripheral vasculature (Mitchell, 2009; Humphrey et al., 2016). Such structural stiffening results in large part from changes in the composition and thickness of the arterial wall: elastin fibers undergo fatigue-related damage and can begin to degrade naturally despite their long half-life, while proteoglycans and collagen fibers can both remodel and accumulate, also influenced by increased cross-linking (Greenwald, 2007). Whereas loss of elastic fiber integrity can reduce central artery resilience, and thus overall biomechanical functionality, the overall increase in structural stiffness due to accumulating extracellular matrix can compromise hemodynamics, and thus vascular physiology, via increases in the speed at which the pulse pressure travels along the central vessels (Mitchell, 2009; Safar et al., 2020). In particular, this structural stiffening (or loss of compliance) compromises the dampening function of the central arteries, resulting in both augmented central pulse pressures that adversely affect the heart and a deeper penetration of pulsatility into the peripheral vessels that affects end-organ function (Mitchell, 2008, 2009; Boutouyrie et al., 2021).

Direct comprehensive measurement of aortic stiffness, both material and structural, is not possible *in vivo*. Rather, the gold standard method to estimate the structural stiffness of the aorta clinically is to measure the pulse wave velocity (PWV). PWV increases with natural aging as well as with many related co-morbidities and has been linked clinically to hypertension and other cardiovascular diseases (Laurent et al., 2006; Laurent and Boutouyrie, 2015; Townsend et al., 2015). Connecting stiffening to underlying histo-mechanical changes in the vessel wall is difficult in a clinical setting, hence many have turned to mouse models to obtain more information about mechanisms of arterial stiffening and its relation to other conditions, including hypertension (Fleenor et al., 2010; Rammos et al., 2014; Lerman et al., 2019). Benefits of mouse models include rapid maturation and aging, ability of genetic manipulation, low cost, and enhanced experimental control, particularly in biomechanical measurement and computation (Ferruzzi et al., 2013; Cuomo et al., 2015, 2019).

No mouse model phenocopies the human cardiovascular system exactly, hence results should be synthesized across multiple studies of different mouse models and interpreted carefully (Ferruzzi et al., 2016). Obvious differences between humans and mice include their very different lifespans [70+ years versus 2+ years (Hamlin and Altschuld, 2011)] and body size, with adult mice weighing approximately 0.05% that of the adult human (Doevendans et al., 1998). Cardiovascular differences include cardiac output [5 L/min for humans (Brandfonbrener et al., 1955), 15 mL/min for mice (Doevendans et al., 1998)], which reflects the size difference, but also heart rate [60 bpm for humans, 600 bpm for mice (Papadimitriou et al., 2008)]. Blood pressure is yet similar between the species. Notwithstanding the order of magnitude higher heart rate in mice, the expected number of cardiac cycles over a lifetime is still higher in humans (2.2×10^9) than in mice (6.3×10^8), which is expected to impact mechanical fatigue-induced loss of elastic fiber integrity (Greenwald, 2007). Indeed, given that the normal half-life of vascular elastin is many decades (Davis, 1993), it appears that arterial aging in mice can be attributed more to the accumulation of proteoglycans and remodeled collagen (Fleenor et al., 2010; Ferruzzi et al., 2018) than to the loss of elastic fiber integrity that occurs in humans alongside matrix remodeling. It is for this reason that different mouse models of compromised elastic fiber integrity can be useful in arterial aging research (Ferruzzi et al., 2016). Further differences between human and murine vascular aging remain to be established.

Computational simulations, particularly those based on fluid-solid-interactions (FSI), can be used to quantify and compare hemodynamic quantities that are difficult to infer experimentally in humans and mice. In this study, FSI models were built for young and old female adult humans and mice to compare multiple hemodynamic and biomechanical effects of aging on the two species. For the humans, representative computational models for young and old adult subjects were defined using imaging data, non-invasive pressure measurements, and population-specific arterial wall properties. For the mice, representative population-based computational models for young and old adults were obtained using *in vivo* and *in vitro* data on vascular anatomy, hemodynamics, and wall mechanics. Both human and mouse subjects were considered healthy, with no comorbidities, with the ages between species generally equivalent. Structural and hemodynamic results were compared to determine the species- and age-related differences between subjects.

MATERIALS AND METHODS

In setting an age correspondence between mice and humans, the Jax Mice website[1] suggests that a 13–27 weeks old mouse is similar to a 20–30 years old human, and an 81–108 weeks old mouse is similar to a 56–69 years old human. Imaging and brachial cuff pressure data were obtained for young adult (31 years old) and older adult (81 years old) female human subjects. This study was approved by the University of Michigan Board of Review (HUM00041514). *In vivo* imaging and *ex vivo* biomechanical testing data were obtained for young adult (20 weeks old) and older adult (100 weeks old) female mice. All animal procedures were approved by the Institutional Animal Care and Use Committee (IACUC) of Yale University. The mice had a mixed C57BL/6 × 129/SvEv background, generated as $Fbln5^{+/+}$ by breeding $Fbln5^{+/-}$ heterozygous pairs (Yanagisawa et al., 2002). For the young adult mice, data were collected for three cohorts at 20 weeks of age: one for anatomy, one for hemodynamics, and one for wall mechanics. For the old adult mice, data were collected from two cohorts that aged naturally to 100 weeks:

[1] jax.org

one for anatomy and one for both hemodynamics and wall mechanics.

Experimental Methods

Vascular Anatomy

Magnetic resonance angiography (MRA) was performed on human subjects at the University of Michigan Medical Center. These exams were performed on 3T MRI scanners (Ingenia, Philips, Best, Netherlands) using a 32-channel torso coil. A non-contrast MRA was performed spanning the thoraco-abdominal aorta using a 3D balanced turbo field echo sequence with navigator-based respiratory compensation (TE: 1.3 ms, TR: 4.3 ms, resolution: 0.7 × 0.7 × 1.5 mm).

As described previously (Cuomo et al., 2019), mice were anesthetized with 1–2% isoflurane and given a bolus intravenous (jugular vein) injection of nanoemulsion formulation (Fenestra VC, MediLumine Inc., Montreal, QC, Canada), at a dose of 0.2 ml/20 g, as a blood-pool contrast agent for prolonged vascular imaging. The animal was immediately placed prone in a micro-CT scanner (eXplore CT120, GE healthcare) for non-gated whole-body scanning. Images were reconstructed as isotropic 49 μm × 49 μm × 49 μm voxels. A relatively constant heart rate (±10%) was achieved by careful maintenance of isoflurane anesthesia and body temperature.

Hemodynamics

40-phase, 2D phase-contrast MRI (PC-MRI) images were acquired in planes orthogonal to the human aorta at the levels of the mid-ascending aorta and distal descending aorta at the diaphragm (TE: 3.0 ms, TR: 5.0 ms, slice thickness: 8 mm, temporal resolution: 19 ms, velocity encoding value: 150 cm/s). Brachial artery blood pressure was measured with a standard non-invasive cuff method, averaged from patient data dating back 2 years (averaged values of 111/66 mmHg for young adult and 111/55 mmHg for old adult). It is important to note that the older human was considered healthy and free of cardiovascular diseases and medication, except for long-term, low-dose diuretic (hydrochlorothiazide) to control blood pressure which resulted in a reduction of blood pressure from 140/85 mmHg prior to medication to the 111/55 mmHg used in this study.

As described previously (Ferruzzi et al., 2018; Cuomo et al., 2019), mice were laid supine after isoflurane inhalation anesthesia (2–3% for induction, 1.5% for maintenance) and secured on a surgical platform with a recirculating heating pad (TP-500 Heat Therapy Pump, Gaymar Industries Inc., Orchard Park, NY, United States) to maintain body temperature at 37°C. Mean blood velocity and luminal diameters were then acquired via ultrasound (Vevo 2100 system, FUJIFILM VisualSonics) in the ascending thoracic aorta (ATA), infrarenal abdominal aorta (IAA), and a common carotid artery (CCA). Cardiac output (CO) was measured with standard B-mode transthoracic echocardiography and central aortic pressure was measured using a SPR-1000 Millar pressure catheter with a diameter of 1F. Hemodynamic measurements were performed on n = 10 young adult and n = 10 old adult mice.

Aortic Biomechanics

It is the *structural* stiffness, the product of the intrinsic *material* properties and wall thickness, which dictates the hemodynamic response to an artery under pulsatile flow. A four-fiber family constitutive model was used to quantify the biaxial *material* stiffness of the arterial wall, both human and murine. This model contains 8 parameters to capture the macroscopic behavior resulting from the contributions of elastic fibers, collagen fibers, and additional matrix (Ferruzzi et al., 2011, 2013). The strain energy density equation for the four-fiber family model can be seen in Eq. 1.

$$W\left(C, M^i\right) = \frac{c}{2}\left(I_c - 3\right) + \sum_{i=1}^{4} \frac{c_1^i}{4c_2^i}\left\{\exp\left[c_2^i\left(IV_c^i - 1\right)^2\right] - 1\right\} \tag{1}$$

Where $\boldsymbol{C}$ is the right Cauchy-Green tensor, F is the deformation tensor $[F = diag\left(\lambda_r, \lambda_\vartheta, \lambda_z\right)]$,$M^i$ represents the orientation of the fiber families $[M^i = \left(0, \sin\alpha_0^i, \cos\alpha_0^i\right)]$, and $IV_C^i = \lambda_\vartheta^2 \sin^2\alpha_0^i + \lambda_z^2 \cos^2\alpha_0^i$. The 8-material parameters fit for each aortic region are c, c_1^1 c_2^1, c_1^2, c_2^2, $c_1^{3,4}$, $c_2^{3,4}$, and α_0, where c refers to the material parameter for the elastin mass fraction and c_1^1 c_2^1 and c_1^2, c_2^2 refer to the collagen coefficients for the axial and circumferential fiber families, respectively. $c_1^{3,4}$, $c_2^{3,4}$, and α_0 refer to the material parameters and angle for symmetric diagonal collagen fiber families.

For the humans, the 8 model parameters and *in vivo* axial stretch (λ_z) were specified from literature data for three segments of the aorta: ATA, descending thoracic aorta (DTA), and IAA for different age groups (Roccabianca et al., 2014). Material parameters for the young adult were based on data for 31–60 years old subjects, while those for the old adult were based on data for the 61+ years old age group. An iterative approach was then used to adjust the resulting pressure-diameter curves to match patient data on *in vivo* pressure and diameter. The unloaded diameter [and therefore the *in vivo* circumferential stretch (λ_θ)] was iteratively adjusted until the mean pressure [estimated as $P_{mean} = \left(2P_{dias} + P_{sys}\right)/3$ from cuff measurements] corresponded with the *in vivo* mean diameter [estimated as $D_{mean} = \left(2D_{dias} + D_{sys}\right)/3$ from PC-MRI images] on the pressure diameter curve (Roccabianca et al., 2014). Examples of adjusted pressure-diameter curves can be seen in **Figure 1**.

For the mice, *in vitro* mechanical testing was performed on four excised segments of the murine aorta [ATA, DTA, suprarenal abdominal aorta (SAA), and IAA] and a CCA with a computer-controlled custom biaxial testing device (Gleason et al., 2004), as described previously (Cuomo et al., 2019). After standard preconditioning, seven cyclic pressure diameter tests were performed: cyclic pressure diameter tests from 10 to 140 mmHg at three different fixed values of axial stretch (λ_z) (95, 100, and 105% of the *in vivo* value) and cyclic axial extension tests at four fixed values of transmural pressure (10, 60, 100, and 140 mmHg) (Ferruzzi et al., 2013). Best-fit values of the eight model parameters for the same four-fiber family constitutive model were determined for n = 5 young adult and n = 5 old adult mice (Ferruzzi et al., 2013).

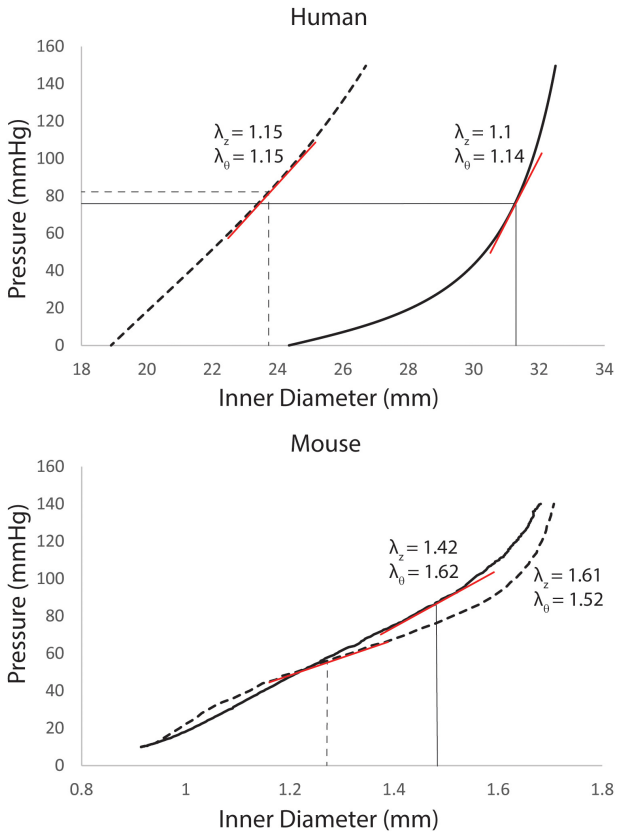

FIGURE 1 | Pressure-diameter curves for the ascending thoracic aorta (ATA) of young (dashed line) and old (solid lines) adult subjects with corresponding values of *in vivo* axial stretch (λ_z, from literature data) and circumferential stretch (λ_θ, iteratively calibrated). Linearized stiffness (red lines) were used in our FSI simulations. For the humans (top), curves are recreated from best-fit values of the 8 material properties from Roccabianca et al. (2014) with *in vivo* circumferential stretches adjusted until *in vivo* mean pressures corresponded with *in vivo* mean diameters. For the mice (bottom), the pressure-diameter curves were measured directly *in vitro*, with best-fit values of the material parameters determined via non-linear regression of the biaxial data.

Computational Modeling

FSI models were built with the open source computational hemodynamics platform CRIMSON (Arthurs et al., 2021). Data from imaging, hemodynamics, and wall mechanics were combined to create FSI models comprised of 3D anatomical models having spatially varying anisotropic wall mechanical properties and external tissue support, with inlet flow waveforms and 3-element Windkessel models on each outflow branch.

Anatomical Models and Finite Element Meshes

The CRIMSON GUI was used to create 3D models of the aorta and main branches. Centerline paths were determined for each vessel of interest and circular contours were added perpendicular to the centerline with discrete spacing to represent the vessel lumen. 3D volumes resulted by lofting between contours and applying a union function to blend the aorta and main branching vessels. For the humans, the 3D representation was based on MRA images. For the mice, the 3D representation was based on μCTA images. Furthermore, for the mice, 9 sets of intercostal arteries were added based on the location of the ribs.

Field-driven mesh adaptation techniques were used to create finite-element meshes refined on regions of high velocity gradients. For the humans, meshes had 1.4×10^6 tetrahedral elements and 2×10^5 nodes for the young adult and 2.6×10^6 tetrahedral elements and 5×10^5 nodes for the old adult. For the mice, meshes had 1.7×10^6 tetrahedral elements and 3×10^5 nodes for the young adult and 2.9×10^6 tetrahedral elements and 5×10^5 nodes for the old adult.

Boundary Conditions

For the humans, available data on pressure and cardiac output for each subject were used to inform computational models. For the mice, allometric scaling (Cuomo et al., 2019) was used to incorporate data from hemodynamics and wall mechanics from multiple mouse cohorts in to the 3D FSI models. Briefly, allometric scaling took the form $\Upsilon = \Upsilon_0 M^b$ with Υ being the quantity of interest (e.g., CO, resistance R_{TOT}, and compliance C_{TOT}), Υ_0 the normalized quantity from experimental data, M the body mass, and b a scaling constant. Linear regression of log-log plots of the quantify of interest versus body mass was used to determine the coefficients (Cuomo et al., 2019).

Inflow boundary condition

For the humans, aortic inflow waveforms were generated from PC-MRI velocity and diameter data using the freely available Medviso software Segment, version 3.0 R8115 (Lee et al., 2008). A semi-automated technique was used to segment the ATA lumen over one cardiac cycle. For the mice, population-averaged flow waveforms from a hemodynamics cohort were used, as described previously (Cuomo et al., 2019). CO was allometrically scaled based on body mass for the old and young subjects, again as before (Cuomo et al., 2015, 2019). ATA flow waveforms and cardiac output can be seen in **Figure 2** for all subjects.

Outflow boundary conditions

A three-element Windkessel model was applied to the outlet of all branches. First, total arterial resistance (R_{TOT}) and total arterial compliance (C_{TOT}) were estimated. R_{TOT} was estimated from P_{mean}/CO for both species. For the humans, C_{TOT} was estimated from $\left(Q_{max} - Q_{\min}/P_{systole} - P_{diastole}\right)^{\Delta t}$ (Xiao et al., 2014). For the mice, C_{TOT} was estimated from the slope of the diastolic decay curve of the experimental ATA pressure waveforms $[P_{diastole}(t) = P_0 \exp\left(-t/R_{TOT}C_{TOT}\right)]$ (Simon et al., 1979). Furthermore, in the mice, R_{TOT} and C_{TOT} were estimated using population data from the hemodynamics and wall mechanics cohort, then allometrically scaled as described previously.

R_{TOT} and C_{TOT} can be separated into 3D (central) and peripheral portions. The 3D portion is set by the anatomy and stiffness of the central vasculature; the peripheral portion can be estimated iteratively. Once R_{TOT} and the distal portion of C_{TOT} are obtained, they must be distributed among the outflow branches of each computational model to ultimately

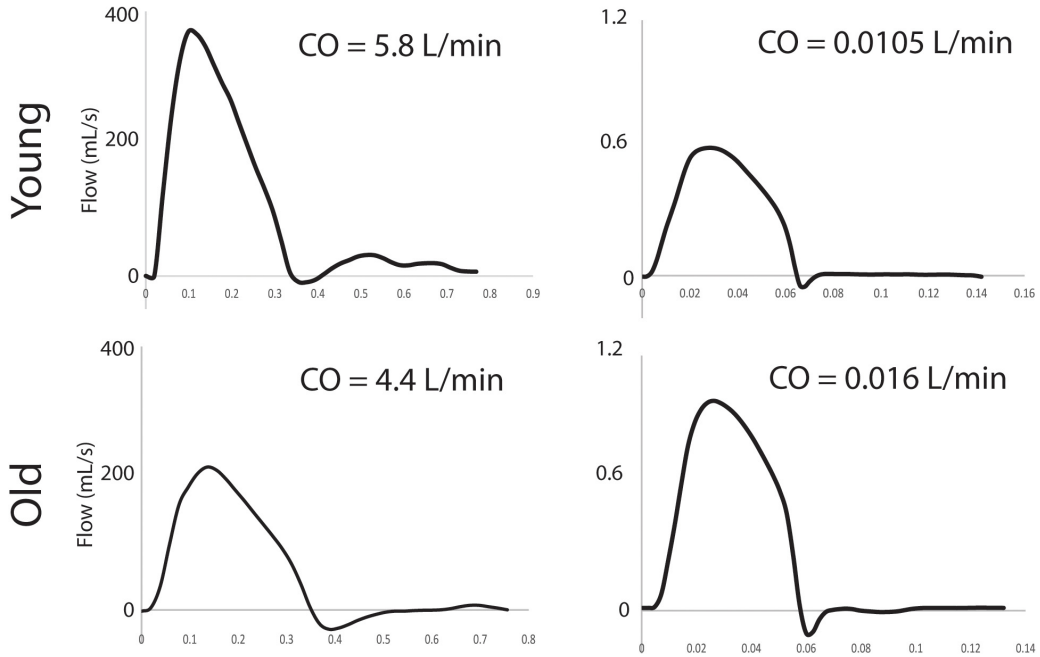

FIGURE 2 | ATA inflow waveforms (mL/s) and associated values of CO (L/min).

specify proximal resistance (R^i_{prox}), compliance (C^i), and distal resistance (R^i_{dist}) for each outlet (i) as described previously (Cuomo et al., 2019).

Wall Mechanics

The FSI simulations were based on a coupled momentum formulation (Figueroa et al., 2006). The vessel walls were modeled as an incompressible, elastic membrane with a 5 × 5 stiffness matrix and wall thickness, h. The theory of small deformations superimposed on large was used to linearize the material stiffness around the mean pressure using *in vivo* axial and circumferential stretches (Baek et al., 2007; Cuomo et al., 2019). For both species, anisotropic stiffness parameters varied spatially for the aorta and main branches.

For the humans, thickness h and *in vivo* axial stretch were adopted from the literature: h was assumed to be 14% of the luminal radius for the young adult and 16% for the old adult (Roccabianca et al., 2014). Spatially varying parameters for the aorta were assigned for the ATA, DTA, and IAA, as described in section "Aortic Biomechanics." Linearization of stiffness occurred at the mean diameter and mean pressure point of the pressure diameter curve. Branching vessels were assigned the stiffness of the closest aortic segment; for example, the upper branches were assigned the stiffness of the ATA.

For the mice, h and *in vivo* axial stretch were determined from *in vitro* testing (Ferruzzi et al., 2013). *In vivo* circumferential stretch was calculated from the unloaded diameter and pressurized diameter from μCT images. Linearization for the mice occurred at *in vivo* axial and circumferential stretches. For the ATA, *in vivo* axial stretch was determined from length in μCT images. Different values of stiffness and thickness were prescribed for six regions of the aorta, the ATA, proximal DTA (pDTA), distal DTA (dDTA), SAA, IAA, and one CCA based on *in vitro* testing. The same values for the four-fiber family parameters were used for both sections of the DTA, but because of differences in diameter, linearization was performed at different *in vivo* circumferential stretch for the proximal and distal portions. Upper branches (both CCAs, left subclavian, and right innominate artery) were assigned the same stiffness and thickness as the tested CCA. Middle branches (mesenteric, celiac, and left and right renal arteries) were assigned the same stiffness matrix as the SAA and the thickness of the CCA. Iliac and tail arteries were assigned the stiffness and thickness of the IAA.

Perivascular support given by stiffness (k_s) and damping (c_s) coefficients were applied to all vessels to represent the pressure (P_{ext}) from tissues surrounding the vasculature (Moireau et al., 2012; Ferruzzi et al., 2018). In the human, different k_s and c_s were applied to the ATA, DTA, and IAA portions of the aorta, as described previously (Cuomo et al., 2017). Branches off the aorta were assigned the same values of perivascular support as the closest aortic segment. For the young adult human, k_s = 200 Pa/mm for the ATA, 100 Pa/mm for the DTA, and 10 Pa/mm for the IAA with c_s = 10 Pa*s/mm for the entirety of the aorta. For the old adult human, k_s = 5,200 Pa/mm for the ATA, 5,050 Pa/mm for the DTA, and 10 Pa/mm for the IAA with c_s = 10 Pa*s/mm for the entirety of the aorta. A similar approach was used for the mice, as described previously for the young adult (Cuomo et al., 2019). This resulted in applied k_s = 13,500 Pa/mm

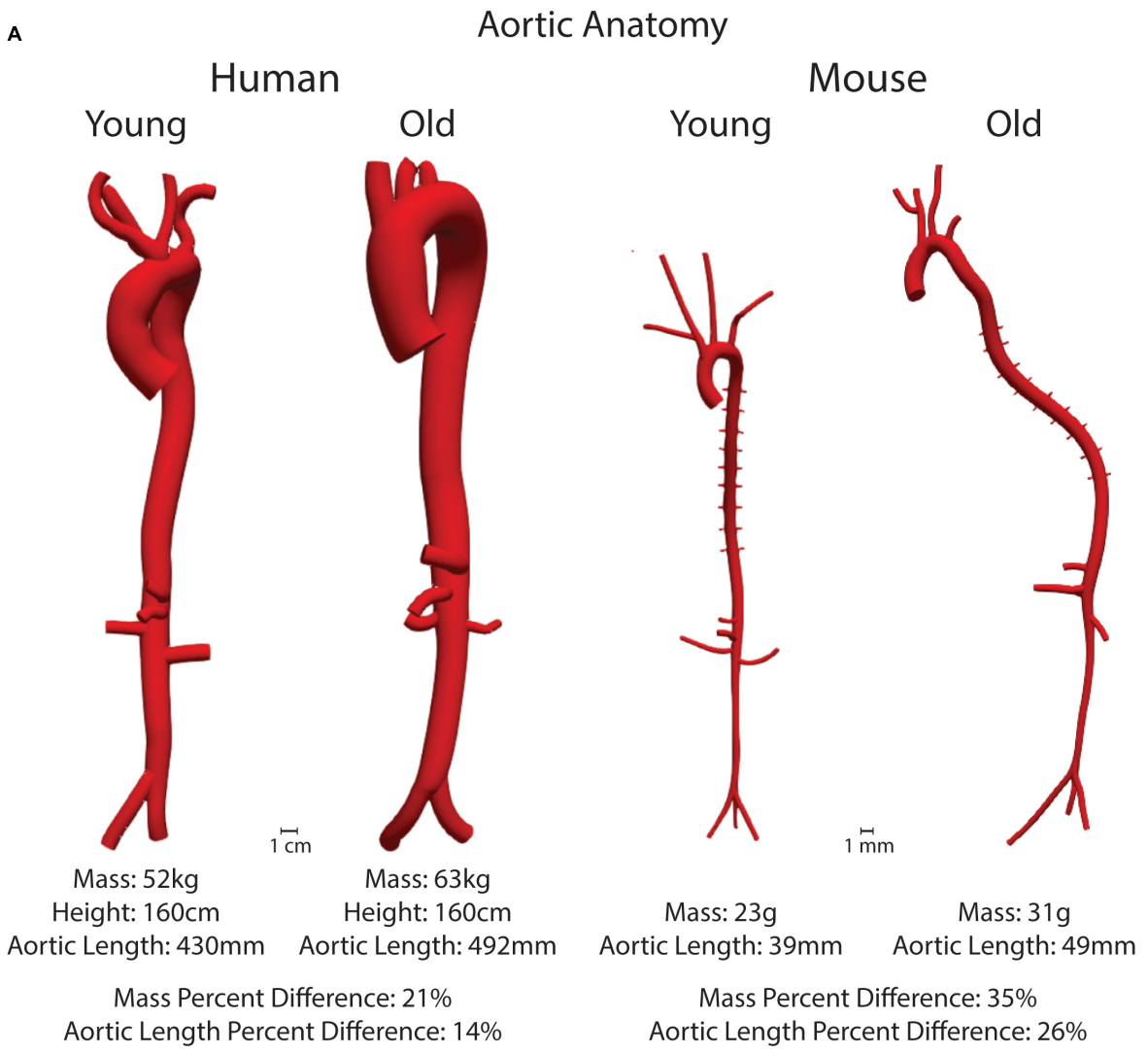

FIGURE 3 | (A) 3D models of the aorta and main branches for each subject along with body mass, height (for humans), and aortic length. Percent differences between young and old adults for each species is shown for mass and aortic length. Anatomical models are shown in the same scale between age groups, but not between species. **(B)** Percent changes in inner diameter by region (pDTA, proximal descending thoracic aorta; dDTA, distal descending thoracic aorta; SAA, suprarenal abdominal aorta; and IAA, infrarenal abdominal aorta) of the aorta in comparison to the young ascending thoracic aorta (ATA_ diameter) for both species.

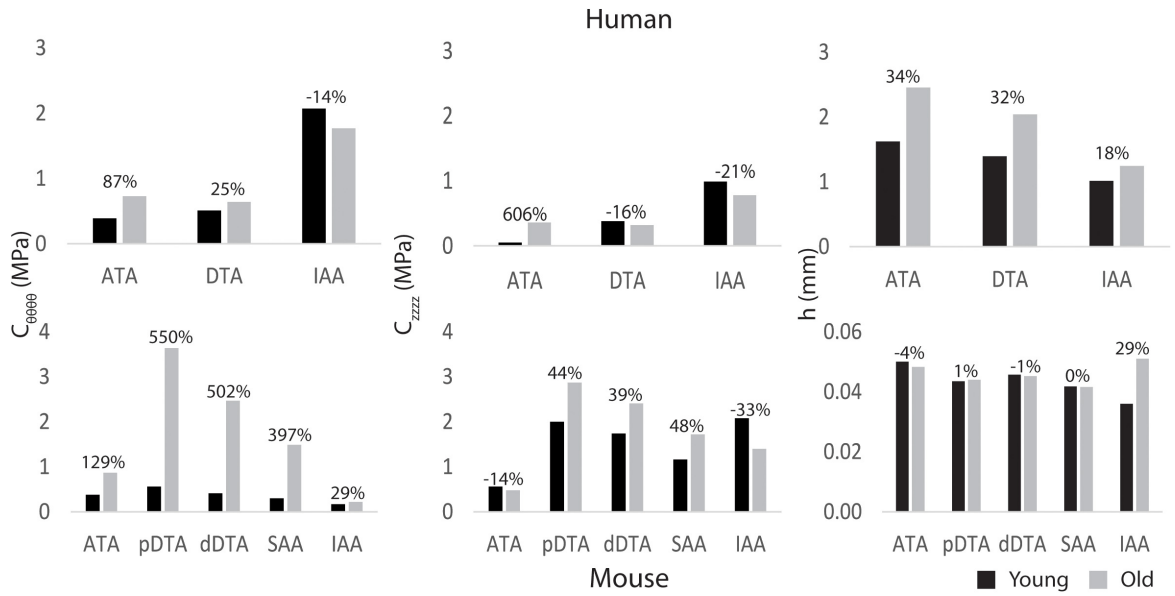

FIGURE 4 | Regional circumferential ($C_{\theta\theta\theta\theta}$) and axial ($C_{zzzz}$) material stiffness and wall thickness h for young adult and old adult humans (top) and mice (bottom) for five locations along the aorta (ATA, ascending thoracic aorta; pDTA, proximal descending thoracic aorta; dDTA, distal descending thoracic aorta; SAA, suprarenal abdominal aorta; and IAA, infrarenal abdominal aorta). The percentages indicate changes with aging relative to the young value. Note that the ATA stiffened the most with aging in humans (cf. Redheuil et al., 2010) whereas the DTA stiffened the most with aging in mice.

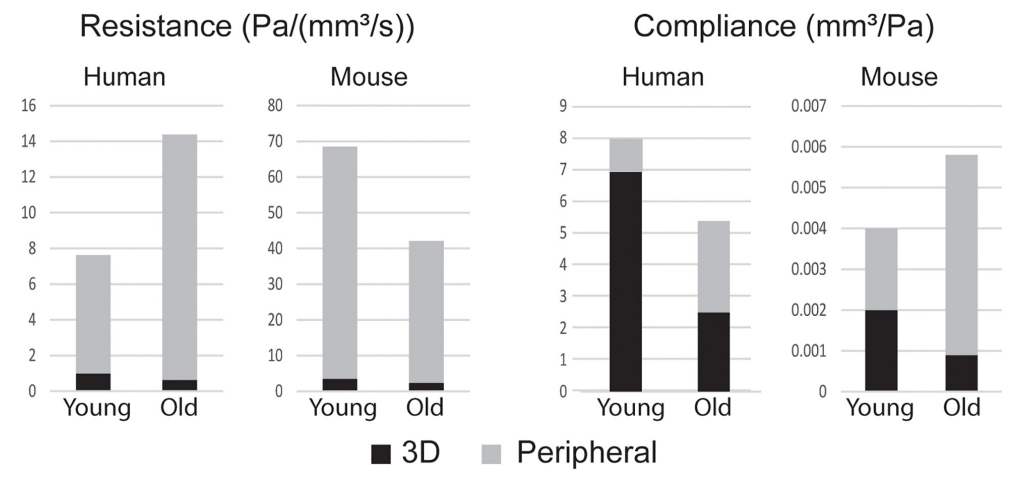

FIGURE 5 | Total resistance R_{TOT} and compliance C_{TOT} broken into components of the central (3D) and peripheral vasculature.

for the ATA, 9,000 Pa/mm for the pDTA, 16,500 Pa/mm for the dDTA, 20,000 Pa/mm for the SAA, 47,000 Pa/mm for the IAA, and 50,000 Pa/mm for the CCAs with c_s = 10 Pa*s/mm for the young adult mouse; global values of k_s = 40 Pa/mm and c_s = 30 Pa*s/mm were prescribed for the old adult mouse.

Pulse Wave Velocity Analysis

Pulse wave velocity was calculated from the ATA (near the aortic root) to the iliac artery (directly after the iliac bifurcation), which is different from the common carotid-femoral PWV (cfPWV) which fails to include the ATA, a region of particular change in aging (Redheuil et al., 2010). PWV was calculated as the ratio of the centerline distance between the ATA and iliac artery and the pulse transient time (PTT). To calculate the PTT, the foot of the pressure waves at each region of interest was calculated based on the "intersecting tangent algorithm" (Gaddum et al., 2013).

RESULTS

Morphology

Anatomical models of the aorta and main branches of humans and mice can be seen in **Figure 3A**. Body mass, height, and aortic length for all subjects along with age-related percent differences

are also presented. Quantitative differences between young adult and old adult aortic inner diameter are shown in the bar plots for **Figure 3B**, which show the percent diameter of each aortic region in comparison to the young ATA diameters. Humans experienced a more dramatic increase in aortic diameter than the mice, especially in the ATA though not in the IAA, noting that the aorta in the young human tapered gradually from the ATA to the IAA. This trend matches previously published work using human population data (Cuomo et al., 2017). Both young and adult mouse geometries revealed the drastic reductions in IAA diameter in relation to the other regions.

Material Properties

Figure 4 shows regional values of circumferential ($C_{\theta\theta\theta\theta}$) and axial ($C_{zzzz}$) material stiffness and wall thickness (h) prescribed based on available data (ATA, DTA, and IAA for humans based on linearized values from literature; ATA, pDTA, dDTA, SAA, and IAA for mice based on biaxial tissue testing). Humans and mice demonstrated differing patterns of aortic stiffness. Human subjects exhibited increased material stiffness down the aorta with peak values occurring in the IAA. In contrast, mice exhibited peak circumferential stiffness in the pDTA that then decreased distally. Nevertheless, both species experienced an increase in circumferential stiffness with age in all aortic regions with the exception of the human IAA. This increase in stiffness was larger in the mouse than the human with the largest increase (550%) occurring in the mouse pDTA. Humans had the greatest increase in circumferential and axial stiffness (87 and 606%, respectively) from young to old in the ATA. For the mouse, axial stiffness increased with age in all aortic regions except for the IAA. Wall thickness increased in the human subjects with age, while in the mouse it remained relatively constant, except for in the IAA.

Central and Peripheral Contributions of Resistance and Compliance

Figure 5 shows the breakdown of R_{TOT} and C_{TOT} between the central (3D) and peripheral components. R_{TOT} was of similar magnitude for mice and humans, but C_{TOT} was three orders of magnitude smaller for the mice. The young adult human had smaller total resistance and larger total compliance than the older. Conversely, mice experienced a decrease in resistance and an increase in compliance with age. Humans had most of their total compliance in the central vasculature, while mice, particularly the older mice, had a majority in the periphery. For both species, there was a decrease in central and increase in peripheral compliance with age.

Hemodynamics

Computational results for peak systolic blood velocity as well as regional (ATA, DTA, and IAA) blood pressure and flow waveforms are shown in **Figure 6** for all four basic models: young and old adult human, young and old adult mouse. The younger human had greater blood velocities than the older subject, consistent with the larger cardiac output (**Figure 2**) and smaller aortic dimensions (**Figure 3**). Conversely, the older mouse had greater blood velocities and higher aortic flows than the younger. Both older subjects show reverse flow in diastole, which is absent in the younger subjects. Human CO decreased 32% from the young to the old subjects, while mouse CO increased 52% with age.

Hemodynamic results were validated against experimental data. For the humans, averaged blood pressure cuff measurements were compared with the simulated (not imposed) left subclavian artery pressure (**Figure 7**), resulting in discrepancies less than 5% for diastolic and systolic pressures for both young and old adult humans. For the mice, simulated ATA pressure waveforms were compared with measured Millar ATA pressure waveforms in terms of pulse pressure, mean pressure, and slope of the diastolic decay (**Figure 7**). Further, simulated IAA and CCA mean flows showed good agreement with their experimental counterparts.

Figure 8 shows the calculated mean arterial pressure for five aortic locations (ATA, pDTA, dDTA, SAA, and IAA) and iliac artery. Mean pressure was similar between species and the pressure gradient down the aorta was small for all subjects. **Figure 9** shows pressure waveforms at the same six locations. Numerical values for pulse pressure are indicated at the ATA and iliac artery. The overall spatial trends of the pressure waveforms differ significantly between species. Humans show an amplification of the pulse pressure down the aorta (31% increase for the young, 9% increase for the old, see table in **Figure 9**), consistent with the increase in material stiffness reported in **Figure 4**. On the other hand, mice show an attenuation of pulse pressure down the aorta (-19% for the young, -36% for the old), consistent with the reported decrease in material stiffness in the descending thoracic and infrarenal aorta (**Figure 4**). Conversely, both species show similar changes in ATA pulse pressure with aging: 33% increase for the old human and 41% increase for the old mouse. These increases in pulse pressure are driven by the similar stiffening of the ATA with age (87% increase in circumferential stiffness for the human, 129% increase for the mice, see **Figure 4**). Lastly, ATA-to-iliac PWV and spatially weighted averages of structural aortic stiffness can be seen in **Figure 10**. The humans had higher values of PWV than the mice. Yet, the mice showed a larger increase in PWV with age than did humans, consistent with the larger increase in structural stiffness.

DISCUSSION

Notwithstanding all that has been learned about vascular biology, mechanics, and physiology via the use of diverse animal models, mice have emerged as the primary model of choice in contemporary vascular research, including studies of the effects of hypertension and aging on the cardiovascular system (Paneni et al., 2017; Lerman et al., 2019). Nevertheless, similarities and differences in central arterial hemodynamics have not been studied in depth between humans and mice, especially in relation to aging. Here, we used consistent biomechanical assessments of central artery mechanical properties (species and age specific four-fiber family constitutive descriptions) and consistent FSI modeling to elucidate possible structurally induced differences in hemodynamics.

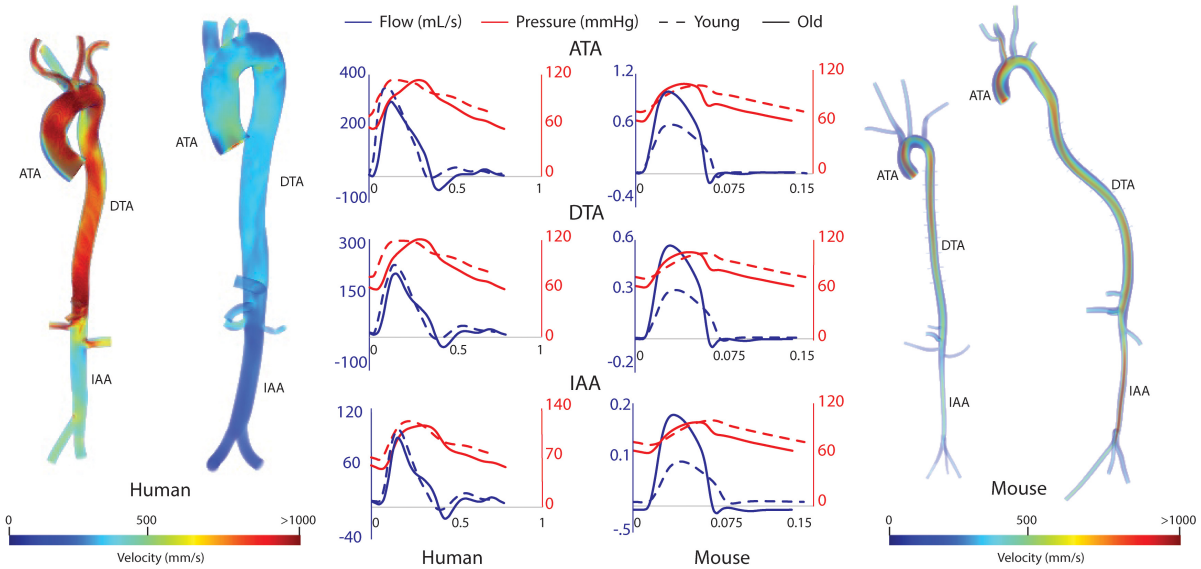

FIGURE 6 | Volume rendering of blood velocity at peak systole for the humans (left) and mice (right), with pressure and flow waveforms at three sites along the aorta (ATA, ascending thoracic aorta; DTA, descending thoracic aorta; and IAA, infrarenal abdominal aorta) (center).

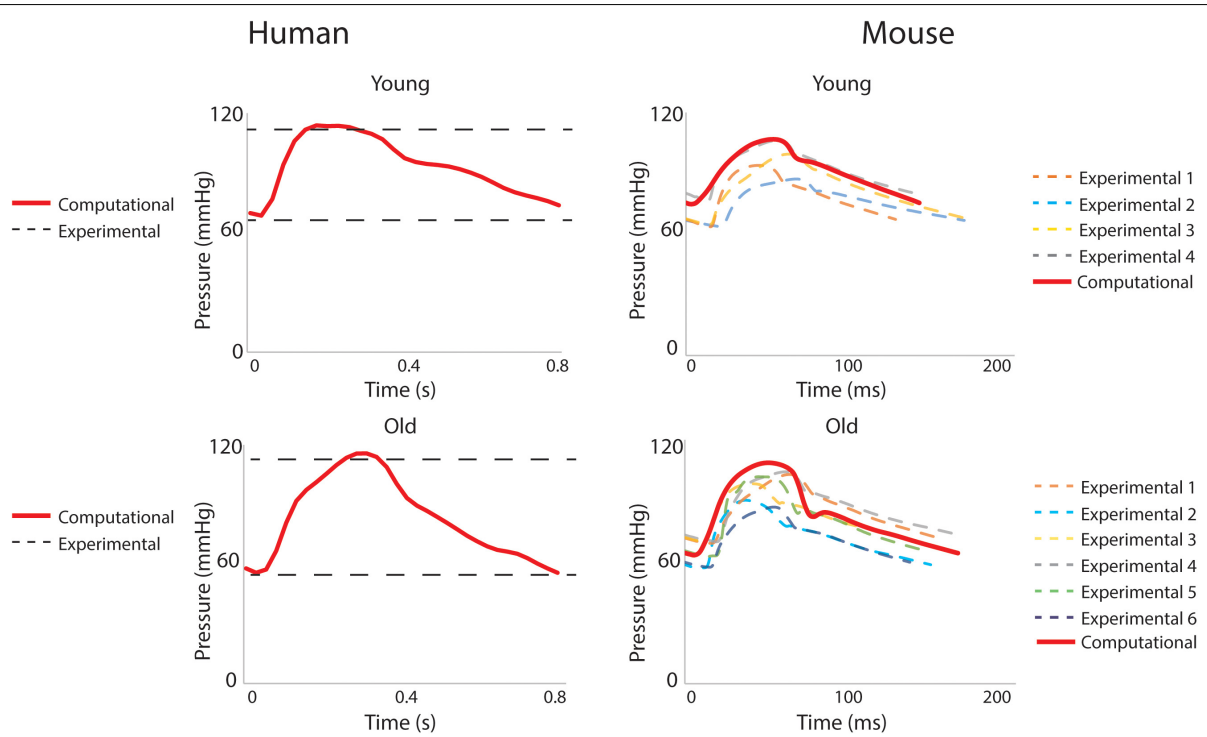

FIGURE 7 | Validation of hemodynamic results using pressure data. For humans, the simulated left subclavian artery pressure (solid red line) compared well with systolic and diastolic pressure cuff values (dashed black lines). For the mice, simulated ascending thoracic aortic (ATA) flow waveforms (solid red lines) compared well with experimental data from multiple subjects (dashed lines).

The representative healthy human subjects in this study showed a decrease in CO with aging, which is consistent with trends found in the literature. Katori (1979) measured resting cardiac output in a cohort of 105 healthy individuals and found a decrease in CO of 0.45 L/min per decade for individuals 20 and older. In contrast, our subjects showed an effective decrease in CO of 0.28 L/min per decade. Consistent reporting of changes in CO and other hemodynamic parameters with age in mice has

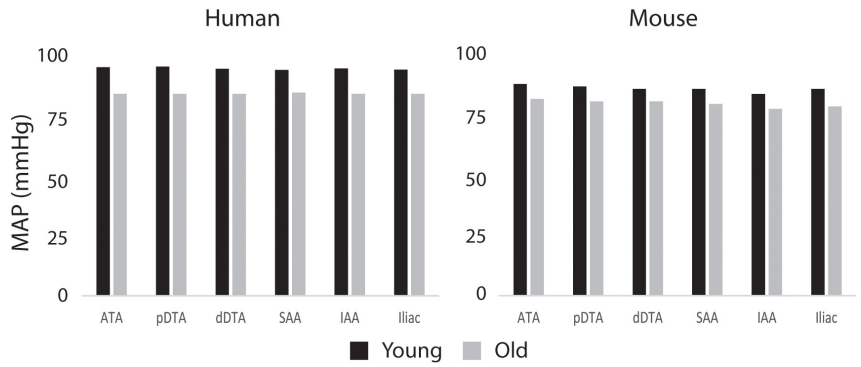

FIGURE 8 | Computed values of mean arterial pressure (MAP) for five aortic locations (ATA, ascending thoracic aorta; pDTA, proximal descending thoracic aorta; dDTA, distal descending thoracic aorta; SAA, suprarenal abdominal aorta; and IAA, infrarenal abdominal aorta) and an iliac artery for all four primary study groups, all showing modest changes proximal to distal.

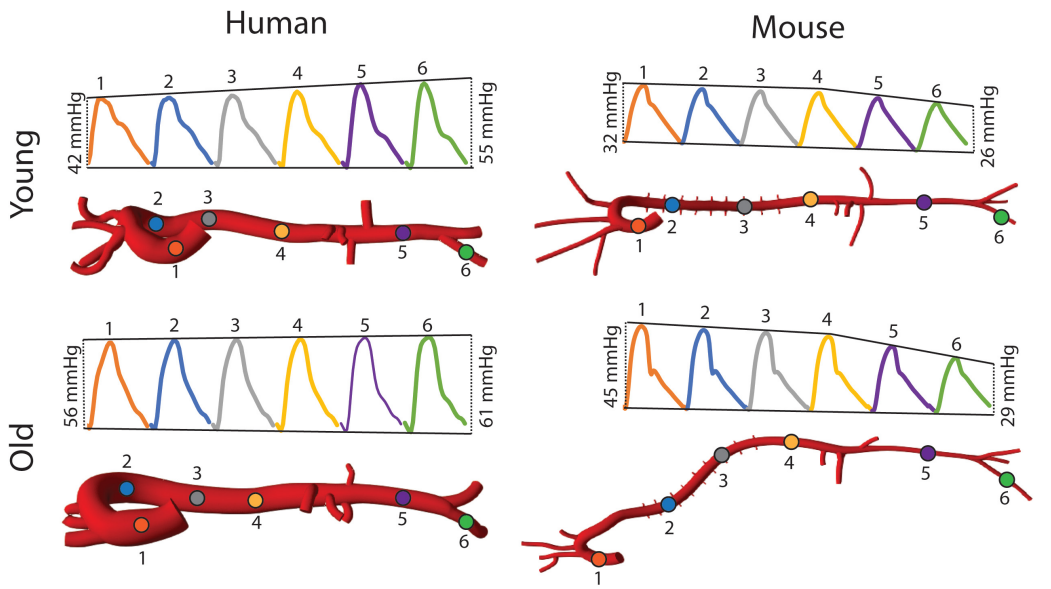

	Human			Mouse		
	Young	Old	% Difference with Age	Young	Old	% Difference with Age
ATA Pulse Pressure (mmHg)	42	56	+33	32	45	+41
Iliac Pulse Pressure (mmHg)	55	61	+11	26	29	+12
Pulse Amplification (%)	+31	+9		-19	-36	

FIGURE 9 | Pulse pressure amplification manifests in the human aorta, but not the mouse.

been challenging due to variations in strains and experimental procedures (Doevendans et al., 1998). Here, mice showed an increase in CO with age which can be explained by the increase in body size (Ferruzzi et al., 2018). Furthermore, both older subjects had reverse flow throughout the aorta, which is absent in the younger subjects. This is of particular importance in the IAA, as reverse flow negatively impacts renal function (Hashimoto and Ito, 2015).

In this study, older subjects showed larger values of aortic length and diameter for both species. In the human, this is consistent with trends found in the literature (Craiem et al., 2012; Rylski et al., 2014). For the representative subjects used herein, aortic length increased more in the mice than in the humans because of the increased aortic tortuosity and body size in the older mouse. Aortic tortuosity often increases with age in humans as well (Cuomo et al., 2017; Ciuricã et al., 2019), although

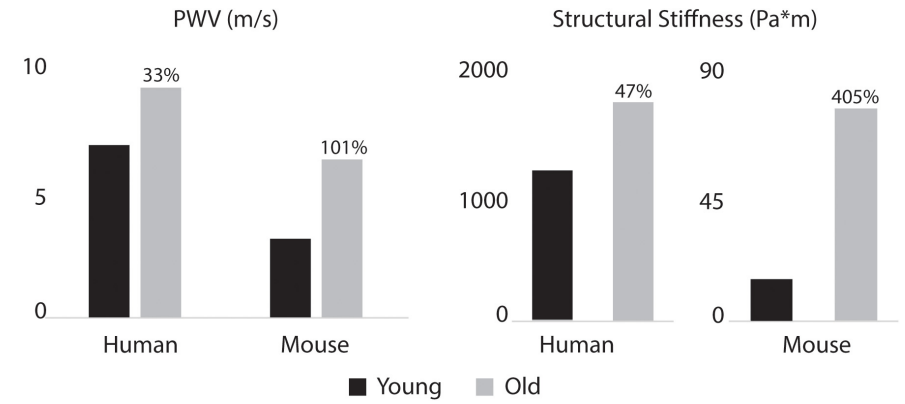

FIGURE 10 | Aorto-iliac PWV **(left)** and spatially weighted averages of structural aortic stiffness **(right)** for the humans and mice. Percent difference from young to old are indicated for both species. Baseline values for the young subjects were 6.9 m/s for human and 3.2 m/s for mouse PWV and 1195.7 and 15.3 for human and mouse structural stiffness.

this was not seen in the old adult human subject in this study. Although not considered here, aortic tortuosity has also been reported to increase in mouse models of compromised elastic fiber integrity (e.g., *Fbln5*$^{-/-}$), which capture some aspects of aortic aging in humans (Weiss et al., 2020). There was a trend toward a decreasing aortic inner diameter along the length of the aorta in both species, which is consistent with results reported in previous studies (Roccabianca et al., 2014; Cuomo et al., 2017).

Humans and mice showed marked differences in both spatial patterns of aortic stiffness and changes in stiffness with aging. Mainly, we see an increase in stiffness down the aorta in humans, which is consistent with trends found in literature (Mitchell, 2009; Roccabianca et al., 2014). In contrast, in mice the circumferential stiffness increases from the ATA to the pDTA, then decreases distally, which is consistent with previous murine studies (Bersi et al., 2017; Cuomo et al., 2019). With age, both species exhibit an increase in aortic stiffness. In the humans, the largest increase in stiffness with age occurs in the ATA. In the mouse, the largest stiffening happens in the DTA and SAA. These age-related changes in stiffness of the two species are most likely determined by different mechanisms: mechanical fatigue-induced loss of elastic fiber integrity over many decades in the human (Davis, 1993; Greenwald, 2007), and accumulation of proteoglycans and remodeled collagen in the mouse (Fleenor et al., 2010; Ferruzzi et al., 2018).

The aforementioned differences in aortic stiffness between species and age groups also resulted in marked hemodynamic differences. Consistent with previously reported findings (Safar and Laurent, 2003; O'Rourke and Hashimoto, 2007), humans present a pulse pressure amplification down the aorta while mice have pulse pressure attenuation down the aorta. However, both species showed an increase in ATA pulse pressure with age, which suggests similar hemodynamic responses to aging. In the humans, ATA and iliac pulse pressures became more similar with age, also consistent with prior findings (Safar and Laurent, 2003; O'Rourke and Hashimoto, 2007), whereas these metrics became more different in the mouse with age. Both species showed an increase in ATA to iliac PWV with age. Despite not commonly being used clinically due to difficulty in measurement, aortoiliac PWV has advantages over cfPWV, mainly that it includes the ATA, an area known for stiffening with age (Mitchell, 2009; Redheuil et al., 2010). For the humans, PWV values were consistent with mean healthy population data (Mattace-Raso et al., 2010) for both age groups: 6.2 $\pm$ 1.5 m/s (compared to our 6.9 m/s) for 30-year-old, and 10.9 $\pm$ 5.4 m/s (compared to our 9.23 m/s) for subjects >70-year-old subjects. While ATA to iliac PWV was directly calculated from our computational models, Mattace-Raso et al. (2010) measured cfPWV and scaled it by 0.8 to represent the ATA to iliac values.

Humans and mice also exhibited different trends in terms of RTOT and compliance. **Figure 5** shows that most of the vascular compliance is in the periphery in mice, as opposed to in the central vasculature in humans (Saouti et al., 2010). The younger human has lower total resistance and larger total compliance than the older, which contradicts the trend seen in the mouse of a decrease in resistance and an increase in compliance with age. These findings in mice are consistent with previous computational FSI studies of hemodynamics in fibulin-5 deficient mice (Cuomo et al., 2019). Despite an overall decrease in vascular resistance and increase in vascular compliance, there is an increase in resistance and decrease in compliance in the central vasculature, which is consistent with our age-related changes in vascular diameter and stiffness.

Despite the importance and advantages of direct comparisons across species and age using consistent methods, limitations herein include the use of subject-specific morphological and hemodynamic data for the humans (noting expectation of considerable differences across subject cohorts) and population-based data for the mice. In this work, we do not present any population-based statistics. Statistical significance would be important to address for different patient cohorts or for different mouse groups, but with greater numbers of subjects. The key focus here is not on group-to-group differences, but rather on similarities and differences between representative subjects of the species, human and murine in particular. Furthermore, in both species, non-linear material properties were population based. All

results were for females, and cardiovascular aging likely differs for males. Similar studies comparing young and old males and contrasting aged males and females would be interesting as well. Because we used population-based data for a particular mouse colony, our results hold for the C57BL/6 × 129/SvEv strain, with expected differences for pure C57BL/6 and 129/SvEv mice (cf. Spronck et al., 2021). Previous work has characterized regional aortic biomechanics in multiple mouse models, though without associated FSI analyses of the central hemodynamics (Ferruzzi et al., 2013; Bersi et al., 2017; Murtada et al., 2020; Spronck et al., 2020). It was beyond the present scope to consider effects of specific genetic mutations or modifiers in either the mice or the humans. Moreover, because we used subject-based data for the human, these results are not indicative of the entire population, although the subjects were selected such that changes in cardiac output, aortic dimensions, and aortic stiffness with age were consistent with reported population data. The only notable difference is the lack of increased tortuosity in the older human subject aorta. Furthermore, the *in vivo* data were collected under resting conditions in the human and under anesthesia in the mice. Finally, because of the ability to use invasive procedures in murine subjects, there are intrinsic differences in the measurement techniques between the species. To mitigate the effects of this, efforts were made to ensure the consistency of data. Particularly, despite not being able to perform biaxial tissue testing in humans, the four-fiber family model was used based on literature values and adapted to simulated biaxial test data (Roccabianca et al., 2014). Computational techniques were consistent between the species.

CONCLUSION

To our knowledge, this study is the first comparison of the differences in hemodynamics, wall properties, and vascular anatomy as a function of age between mice and humans. We identified key differences between the human and murine central vasculature such as patterns in aortic stiffness, pulse amplification, amount and distribution of arterial resistance and compliance, and changes in CO, stiffening, and resistance and compliance with age, which question many uses of naturally aged mouse models for understanding certain aspects of cardiovascular aging in humans. Conversely, there are also key similarities between the species, as, for example, a global increase in aortic stiffness, increase in ATA pulse pressure, decrease in mean arterial pressure, reverse flow in older subjects, and increase in PWV. Furthermore, genetic manipulation of mouse models may lessen the differences by capturing broader population diversity, which is a critical step toward personalized medicine. For example, there are mouse models that effect elastin structure and content (Yanagisawa and Wagenseil, 2020), which may prove to be a more closely related analog for human aging.

DATA AVAILABILITY STATEMENT

The raw data supporting the conclusions of this article will be made available by the authors, without undue reservation.

ETHICS STATEMENT

The studies involving human participants were reviewed and approved by the University of Michigan Board of Review. The patients/participants provided their written informed consent to participate in this study. The animal study was reviewed and approved by the Institutional Animal Care and Use Committee (IACUC) of Yale University, New Haven, CT, United States.

AUTHOR CONTRIBUTIONS

FC, NB, JH, and CF: conceptualization. FC, JF, and NB: data collection. SH, FC, JF, SR, JH, and CF: formal analysis. JH and CF: funding acquisition, supervision, and overall responsibility. SH and CF: writing of original draft. SH, FC, JF, NB, SR, JH, and CF: writing—review and editing and final approval of the manuscript. All authors contributed to the article and approved the submitted version.

FUNDING

This research was supported, in part, by grants from the NIH (R01 HL105297 and U01 HL135842). Computing resources were provided by the National Science Foundation (Grant 1531752): Acquisition of Conflux, A Novel Platform for Data-Driven Computational Physics (Tech. Monitor: Ed Walker).

REFERENCES

Arthurs, C. J., Khlebnikov, R., Melville, A., Marèan, M., Gomez, A., Dillon-Murphy, D., et al. (2021). CRIMSON: an open-source software framework for cardiovascular integrated modelling and simulation. *PLoS Comput. Biol.* 17:e1008881. doi: 10.1371/journal.pcbi.1008881

Baek, S., Gleason, R. L., Rajagopal, K. R., and Humphrey, J. D. (2007). Theory of small on large: potential utility in computations of fluid-solid interactions in arteries. *Comput. Methods Appl. Mech. Eng.* 196, 3070–3078. doi: 10.1016/j.cma.2006.06.018

Bersi, M. R., Khosravi, R., Wujciak, A. J., Harrison, D. G., and Humphrey, J. D. (2017). Differential cell-matrix mechanoadaptations and inflammation drive regional propensities to aortic fibrosis, aneurysm or dissection in hypertension. *J. R. Soc. Interface* 14:0170327. doi: 10.1098/rsif.2017.0327

Boutouyrie, P., Chowienczyk, P., Humphrey, J. D., and Mitchell, G. F. (2021). Arterial stiffness and cardiovascular risk in hypertension. *Circ. Res.* 128, 864–886. doi: 10.1161/circresaha.121.318061

Brandfonbrener, M., Landowne, M., and Shock, N. W. (1955). Changes in cardiac output with age. *Circulation* 12, 557–566. doi: 10.1161/01.cir.12.4.557

Ciuricã, S., Lopez-Sublet, M., Loeys, B. L., Radhouani, I., Natarajan, N., Vikkula, M., et al. (2019). Arterial tortuosity. *Hypertension* 73, 951–960. doi: 10.1161/hypertensionaha.118.11647

Craiem, D., Chironi, G., Redheuil, A., Casciaro, M., Mousseaux, E., Simon, A., et al. (2012). Aging impact on thoracic aorta 3D morphometry in intermediate-risk

subjects: looking beyond coronary arteries with non-contrast cardiac CT. *Ann. Biomed. Eng.* 40, 1028–1038. doi: 10.1007/s10439-011-0487-y

Cuomo, F., Ferruzzi, J., Agarwal, P., Li, C., Zhuang, Z. W., Humphrey, J. D., et al. (2019). Sex-dependent differences in central artery haemodynamics in normal and fibulin-5 deficient mice: implications for ageing. *Proc. R. Soc. A Math. Phys. Eng. Sci.* 475:20180076. doi: 10.1098/rspa.2018.0076

Cuomo, F., Ferruzzi, J., Humphrey, J. D., and Figueroa, C. A. (2015). An experimental–computational study of catheter induced alterations in pulse wave velocity in anesthetized mice. *Ann. Biomed. Eng.* 43, 1555–1570. doi: 10.1007/s10439-015-1272-0

Cuomo, F., Roccabianca, S., Dillon-Murphy, D., Xiao, N., Humphrey, J. D., and Figueroa, C. A. (2017). Effects of age-associated regional changes in human central artery mechanics on systemic hemodynamics revealed by computational modeling. *PLoS One* 12:e0173177. doi: 10.7302/Z24B2Z7Z

Davis, E. C. (1993). Stability of elastin in the developing mouse aorta: a quantitative radioautographic study. *Histochemistry* 100, 17–26. doi: 10.1007/BF00268874

Doevendans, P. A., Daemen, M. J., De Muinck, E. D., and Smits, J. F. (1998). Cardiovascular phenotyping in mice. *Cardiovasc. Res.* 39, 34–49. doi: 10.1016/S0008-6363(98)00073-X

Ferruzzi, J., Bersi, M. R., and Humphrey, J. D. (2013). Biomechanical phenotyping of central arteries in health and disease: advantages of and methods for murine models. *Ann. Biomed. Eng.* 41, 1311–1330. doi: 10.1007/s10439-013-0799-1

Ferruzzi, J., Bersi, M. R., Mecham, R. P., Ramirez, F., Yanagisawa, H., Tellides, G., et al. (2016). Loss of elastic fiber integrity compromises common carotid artery function: implications for vascular aging. *Artery Res.* 14:41. doi: 10.1016/j.artres.2016.04.001

Ferruzzi, J., Madziva, D., Caulk, A. W., Tellides, G., and Humphrey, J. D. (2018). Compromised mechanical homeostasis in arterial aging and associated cardiovascular consequences. *Biomech. Model. Mechanobiol.* 17, 1281–1295. doi: 10.1007/s10237-018-1026-7

Ferruzzi, J., Vorp, D. A., and Humphrey, J. D. (2011). On constitutive descriptors of the biaxial mechanical behaviour of human abdominal aorta and aneurysms. *J. R. Soc. Interface* 8, 435–450. doi: 10.1098/rsif.2010.0299

Figueroa, C. A., Vignon-Clementel, I. E., Jansen, K. E., Hughes, T. J. R., and Taylor, C. A. (2006). A coupled momentum method for modeling blood flow in three-dimensional deformable arteries. *Comput. Methods Appl. Mech. Eng.* 195, 5685–5706. doi: 10.1016/j.cma.2005.11.011

Fleenor, B. S., Marshall, K. D., Durrant, J. R., Lesniewski, L. A., and Seals, D. R. (2010). Arterial stiffening with ageing is associated with transforming growth factor-β1-related changes in adventitial collagen: reversal by aerobic exercise. *J. Physiol.* 588, 3971–3982. doi: 10.1113/jphysiol.2010.194753

Gaddum, N. R., Alastruey, J., Beerbaum, P., Chowienczyk, P., and Schaeffter, T. (2013). A technical assessment of pulse wave velocity algorithms applied to non-invasive arterial waveforms. *Ann. Biomed. Eng.* 41, 2617–2629. doi: 10.1007/s10439-013-0854-y

Gleason, R. L., Gray, S. P., Wilson, E., and Humphrey, J. D. (2004). A multiaxial computer-controlled organ culture and biomechanical device for mouse carotid arteries. *J. Biomech. Eng.* 126, 787–795. doi: 10.1115/1.1824130

Greenwald, S. (2007). Ageing of the conduit arteries. *J. Pathol.* 211, 157–172. doi: 10.1002/path.2101

Hamlin, R. L., and Altschuld, R. A. (2011). Extrapolation from mouse to man. *Circ. Cardiovasc. Imaging* 4, 2–4. doi: 10.1161/circimaging.110.961979

Hashimoto, J., and Ito, S. (2015). Aortic blood flow reversal determines renal function: potential explanation for renal dysfunction caused by aortic stiffening in hypertension. *Hypertension* 66, 61–67. doi: 10.1161/HYPERTENSIONAHA.115.05236

Humphrey, J. D., Harrison, D. G., Figueroa, C. A., Lacolley, P., and Laurent, S. (2016). Central artery stiffness in hypertension and aging a problem with cause and consequence. *Circ. Res.* 118, 379–381. doi: 10.1161/circresaha.115.307722

Katori, R. (1979). Normal cardiac output in relation to age and body size. *Tohoku J. Exp. Med.* 128, 377–387. doi: 10.1620/tjem.128.377

Lakatta, E. G., Wang, M., and Najjar, S. S. (2009). Arterial aging and subclinical arterial disease are fundamentally intertwined at macroscopic and molecular levels. *Med. Clin. North Am.* 93, 583–604. doi: 10.1016/j.mcna.2009.02.008

Laurent, S., and Boutouyrie, P. (2015). The structural factor of hypertension: large and small artery alterations. *Circ. Res.* 116, 1007–1021. doi: 10.1161/circresaha.116.303596

Laurent, S., Cockcroft, J., Van Bortel, L., Boutouyrie, P., Giannattasio, C., Hayoz, D., et al. (2006). Expert consensus document on arterial stiffness: methodological issues and clinical applications. *Eur. Heart J.* 27, 2588–2605. doi: 10.1093/eurheartj/ehl254

Lee, J. T., Munch, K. R., Carlis, J. V., Pardo, J. V., Engblom, H., Arheden, H., et al. (2008). Design and validation of segment–freely available software for cardiovascular image analysis. *BMC Med. Imaging* 8:10. doi: 10.1186/1471-2342-8-10

Lerman, L. O., Kurtz, T. W., Touyz, R. M., Ellison, D. H., Chade, A. R., Crowley, S. D., et al. (2019). Animal models of hypertension: a scientific statement from the american heart association. *Hypertension* 73, e87–e120. doi: 10.1161/HYP.0000000000000090

Mattace-Raso, F. U. S., Hofman, A., Verwoert, G. C., Wittemana, J. C. M., Wilkinson, I., Cockcroft, J., et al. (2010). Determinants of pulse wave velocity in healthy people and in the presence of cardiovascular risk factors: 'Establishing normal and reference values.'. *Eur. Heart J.* 31, 2338–2350. doi: 10.1093/eurheartj/ehq165

Mitchell, G. F. (2008). Effects of central arterial aging on the structure and function of the peripheral vasculature: implications for end-organ damage. *J. Appl. Physiol.* 105, 1652–1660. doi: 10.1152/japplphysiol.90549.2008

Mitchell, G. F. (2009). Arterial stiffness and wave reflection: biomarkers of cardiovascular risk. *Artery Res.* 3, 56–64. doi: 10.1016/j.artres.2009.02.002

Moireau, P., Xiao, N., Astorino, M., Figueroa, C. A., Chapelle, D., Taylor, C. A., et al. (2012). External tissue support and fluid-structure simulation in blood flows. *Biomech. Model. Mechanobiol.* 11, 1–18. doi: 10.1007/s10237-011-0289-z

Murtada, S.-I., Kawamura, Y., Caulk, A. W., Ahmadzadeh, H., Mikush, N., Zimmerman, K., et al. (2020). Paradoxical aortic stiffening and subsequent cardiac dysfunction in Hutchinson–Gilford progeria syndrome. *J. R. Soc. Interface* 17:20200066. doi: 10.1098/rsif.2020.0066

O'Rourke, M. F., and Hashimoto, J. (2007). Mechanical factors in arterial aging. A clinical perspective. *J. Am. Coll. Cardiol.* 50, 1–13. doi: 10.1016/j.jacc.2006.12.050

Paneni, F., Diaz Cañestro, C., Libby, P., Lüscher, T. F., and Camici, G. G. (2017). The aging cardiovascular system: understanding it at the cellular and clinical levels. *J. Am. Coll. Cardiol.* 69, 1952–1967. doi: 10.1016/j.jacc.2017.01.064

Papadimitriou, D., Xanthos, T., Dontas, I., Lelovas, P., and Perrea, D. (2008). The use of mice and rats as animal models for cardiopulmonary resuscitation research. *Lab. Anim.* 42, 265–276. doi: 10.1258/la.2007.006035

Rammos, C., Hendgen-Cotta, U. B., Pohl, J., Totzeck, M., Luedike, P., Schulze, V. T., et al. (2014). Modulation of circulating macrophage migration inhibitory factor in the elderly. *Biomed Res. Int.* 2014:582586. doi: 10.1155/2014/582586

Redheuil, A., Yu, W. C., Wu, C. O., Mousseaux, E., De Cesare, A., Yan, R., et al. (2010). Reduced ascending aortic strain and distensibility: earliest manifestations of vascular aging in humans. *Hypertension* 55, 319–326. doi: 10.1161/hypertensionaha.109.141275

Roccabianca, S., Figueroa, C. A., Tellides, G., and Humphrey, J. D. (2014). Quantification of regional differences in aortic stiffness in the aging human. *J. Mech. Behav. Biomed. Mater.* 29, 618–634. doi: 10.1016/j.jmbbm.2013.01.026

Rylski, B., Desjardins, B., Moser, W., Bavaria, J. E., and Milewski, R. K. (2014). Gender-related changes in aortic geometry throughout life. *Eur. J. Cardio Thorac. Surg.* 45, 805–811. doi: 10.1093/ejcts/ezt597

Safar, M. E. (2010). Arterial aging-hemodynamic changes and therapeutic options. *Nat. Rev. Cardiol.* 7, 442–449. doi: 10.1038/nrcardio.2010.96

Safar, M. E., and Laurent, P. (2003). Pulse pressure and arterial stiffness in rats: comparison with humans. *Am. J. Physiol. Hear. Circ. Physiol.* 285, 1363–1369. doi: 10.1152/ajpheart.00513.2003

Safar, M. E., Regnault, V., and Lacolley, P. (2020). Sex differences in arterial stiffening and central pulse pressure: mechanistic insights? *J. Am. Coll. Cardiol.* 75, 881–883. doi: 10.1016/j.jacc.2019.12.041

Saouti, N., Westerhof, N., Postmus, P. E., and Vonk-Noordegraaf, A. (2010). The arterial load in pulmonary hypertension. *Eur. Respir. Rev.* 19, 197–203. doi: 10.1183/09059180.00002210

Simon, A. C., Safar, M. E., Levenson, J. A., London, G. M., Levy, B. I., Chau, N. P., et al. (1979). An evaluation of large arteries compliance in man. *Am. J. Physiol.* 237, H550–H554.

Spronck, B., Ferruzzi, J., Bellini, C., Caulk, A. W., Murtada, S.-I., and Humphrey, J. D. (2020). Aortic remodeling is modest and sex-independent in mice when hypertension is superimposed on aging. *J. Hypertens* 38, 1312–1321. doi: 10.1097/HJH.0000000000002400

Spronck, B., Latorre, M., Wang, M., Mehta, S., Caulk, A. W., Ren, P., et al. (2021). Excessive adventitial stress drives inflammation-mediated fibrosis in hypertensive aortic remodelling in mice. *J. R. Soc. Interface* 18:20210336. doi: 10.1098/RSIF.2021.0336

Townsend, R. R., Wilkinson, I. B., Schiffrin, E. L., Avolio, A. P., Chirinos, J. A., Cockcroft, J. R., et al. (2015). Recommendations for improving and standardizing vascular research on arterial stiffness: a scientific statement from the american heart association. *Hypertension* 66, 698–722. doi: 10.1161/hyp.0000000000000033

Weiss, D., Cavinato, C., Gray, A., Ramachandra, A. B., Avril, S., Humphrey, J. D., et al. (2020). Mechanics-driven mechanobiological mechanisms of arterial tortuosity. *Sci. Adv.* 6:eabd3574. doi: 10.1126/sciadv.abd3574

Xiao, N., Alastruey, J., and Alberto Figueroa, C. (2014). A systematic comparison between 1-D and 3-D hemodynamics in compliant arterial models. *Int. J. Numer. Method Biomed. Eng.* 30, 204–231. doi: 10.1002/cnm.2598

Yanagisawa, H., Davist, E. C., Startcher, B. C., Ouchi, T., Yanagisawa, M., Richardson, J. A., et al. (2002). Fibulin-5 is an elastin-binding protein essential for elastic fibre development in vivo. *Nature* 415, 168–171. doi: 10.1038/415168a

Yanagisawa, H., and Wagenseil, J. (2020). Elastic fibers and biomechanics of the aorta: insights from mouse studies. *Matrix Biol.* 85–86, 160–172. doi: 10.1016/j.matbio.2019.03.001

Conflict of Interest: The authors declare that the research was conducted in the absence of any commercial or financial relationships that could be construed as a potential conflict of interest.

Publisher's Note: All claims expressed in this article are solely those of the authors and do not necessarily represent those of their affiliated organizations, or those of the publisher, the editors and the reviewers. Any product that may be evaluated in this article, or claim that may be made by its manufacturer, is not guaranteed or endorsed by the publisher.

frontiers in Physiology

REVIEW
published: 07 December 2021
doi: 10.3389/fphys.2021.762437

Vascular Stiffness in Aging and Disease

Stephen F. Vatner[1], Jie Zhang[1], Christina Vyzas[1], Kalee Mishra[1], Robert M. Graham[2] and Dorothy E. Vatner[1]*

[1] Department of Cell Biology and Molecular Medicine, Rutgers University – New Jersey Medical School, Newark, NJ, United States, [2] Victor Chang Cardiac Research Institute, University of New South Wales, Darlinghurst, NSW, Australia

The goal of this review is to provide further understanding of increased vascular stiffness with aging, and how it contributes to the adverse effects of major human diseases. Differences in stiffness down the aortic tree are discussed, a topic requiring further research, because most prior work only examined one location in the aorta. It is also important to understand the divergent effects of increased aortic stiffness between males and females, principally due to the protective role of female sex hormones prior to menopause. Another goal is to review human and non-human primate data and contrast them with data in rodents. This is particularly important for understanding sex differences in vascular stiffness with aging as well as the changes in vascular stiffness before and after menopause in females, as this is controversial. This area of research necessitates studies in humans and non-human primates, since rodents do not go through menopause. The most important mechanism studied as a cause of age-related increases in vascular stiffness is an alteration in the vascular extracellular matrix resulting from an increase in collagen and decrease in elastin. However, there are other mechanisms mediating increased vascular stiffness, such as collagen and elastin disarray, calcium deposition, endothelial dysfunction, and the number of vascular smooth muscle cells (VSMCs). Populations with increased longevity, who live in areas called "Blue Zones," are also discussed as they provide additional insights into mechanisms that protect against age-related increases in vascular stiffness. Such increases in vascular stiffness are important in mediating the adverse effects of major cardiovascular diseases, including atherosclerosis, hypertension and diabetes, but require further research into their mechanisms and treatment.

Keywords: aortic stiffness, aging, cardiovascular diseases, human, non-human primate

OPEN ACCESS

Edited by:
Lakshmi Santhanam, Johns Hopkins University, United States

Reviewed by:
Owen Woodman, Monash University, Australia
Daniel Nyhan, Johns Hopkins University, United States

****Correspondence:***
Stephen F. Vatner
vatnersf@njms.rutgers.edu

Specialty section:
This article was submitted to Vascular Physiology, a section of the journal Frontiers in Physiology

Received: *21 August 2021*
Accepted: *26 October 2021*
Published: *07 December 2021*

Citation:
Vatner SF, Zhang J, Vyzas C, Mishra K, Graham RM and Vatner DE (2021) Vascular Stiffness in Aging and Disease. Front. Physiol. 12:762437. doi: 10.3389/fphys.2021.762437

INTRODUCTION

The goal of this article is to review what is known about changes in vascular stiffness with aging and disease. It is widely accepted that aortic stiffness increases with advancing age. However, most existing research employs measures of aortic stiffness at a single aortic location as an estimate of overall aortic stiffness. This makes it a challenge to understand age-related stiffness along the length of the aortic tree, from the aortic root to its bifurcation into the iliac arteries, and regional vessels. Another goal is to review human and non-human primate data, which is particularly important for understanding sex differences in vascular stiffness with aging and the changes in vascular stiffness before and after menopause in females. Several mechanisms that mediate the increases in vascular stiffness will be reviewed. The most well-studied mechanism involves the extracellular matrix, with increases in vascular collagen and decreases in vascular elastin. There are other mechanisms,

less well studied, that also contribute to the increased vascular stiffness, e.g., collagen and elastin disarray and increased vascular smooth muscle cell stiffness and numbers. Further insight can also be gained from populations with an extended lifespan, living in areas called "Blue Zones," where a healthy diet and exercise ameliorate the increases in vascular stiffness observed with age.

AORTA

Anatomy

The aorta is divided into sections by location; the ascending aorta, aortic arch, and the descending aorta. The descending aorta can be divided into thoracic and abdominal sections. Branches of interest include the left and right coronary arteries, which branch from the aortic root, and the brachiocephalic, left carotid, and left subclavian, which branch from the aortic arch. As the aorta descends there are numerous branches which supply the surrounding muscles and organs including intercostal, celiac, hepatic, gastric, splenic, renal, mesenteric, and gonadal arteries. The abdominal aorta bifurcates into the iliac arteries which extend inferiorly, turning into the femoral arteries, which supply blood flow to each leg.

Morphometry

The morphometric properties of the aorta differ along its length. The aorta tapers, with the average systolic diameter decreasing from the proximal to the distal aortic tree (Hickson et al., 2010). In healthy humans, helical computed tomography showed that maximum aortic diameter is in the ascending aorta, distal to the aortic valve sinus and proximal to the innominate artery (Hager et al., 2002). The aortic diameter then decreases progressively along the thoracic aorta and continues to decrease from the infrarenal abdominal aorta to the lower abdominal aorta (Hager et al., 2002; Rogers et al., 2013). Overall thickness of the aortic wall also decreases down the thoracic aorta, but then remains constant in the abdominal aorta (Sokolis, 2007). In the pig, the tunica media decreases in thickness distally along the thoracic and abdominal aorta, while the tunica adventitia thickness is negligible in the thoracic aorta, but increases down the length of the abdominal aorta (Sokolis, 2007). Aging results in morphometric changes to the diameter, length, and thickness of the aorta. Overall, the diameter and length increase progressively with age (Komutrattananont et al., 2019), with the greatest change in diameter occurring at the level of the ascending aorta (+0.96 mm/decade) (Hickson et al., 2010). The tunica intima and media of the aortic wall thicken with age (Komutrattananont et al., 2019).

AGE-RELATED CHANGES IN AORTIC STIFFNESS

One measure of aortic stiffness, carotid-femoral pulse wave velocity (PWV), is an estimate of the pulse transit-time between the carotid and femoral arteries (O'Rourke et al., 2002; Pannier et al., 2002; Laurent and Boutouyrie, 2020). This is an approximation that averages the many branches of the aortic tree and does not consider the influence of regional differences in stiffness and diameter (Millasseau et al., 2005). With aging, large elastic arteries, such as the aorta, show increases in arterial stiffness, which correlate with histological and biochemical changes within the arterial wall. Several studies have examined both thoracic and abdominal aortic stiffness with aging, *in vivo* (Farrar et al., 1984; Rogers et al., 2001; Nelson et al., 2009; Hickson et al., 2010; Taviani et al., 2011; Westenberg et al., 2011; Devos et al., 2015). In humans, where PWV was measured by cine phase contrast magnetic resonance imaging (PCMRI) in four segments of the aorta, it was found that the greatest age-related increase in aortic stiffness occurred in the abdominal aorta (+0.9 m/s per decade) followed by the thoracic-descending region (+0.7 m/s), the mid-descending region (+0.6 m/s), and aortic arch (+0.4 m/s) (Hickson et al., 2010). Another study, focusing on the ascending, descending, and infrarenal aorta showed increases in stiffness down the aortic tree in humans aged 40, 60, and 75 years (Cuomo et al., 2017). Variation in stiffness down the aortic tree has also been addressed via computational modeling of the human aortic tree using several metrics for stiffness and geometric and hemodynamic data from the literature. *In silico* examination of the effect of aging showed that pulse pressure and stiffness increase down the aortic tree and are most marked with advanced age. PWV may deviate from this pattern when it comes to the most distal sections of the aorta, as these are likely influenced by arterial tapering and branching (Cuomo et al., 2017). Isolated *in vitro* studies have also found that abdominal aortic stiffness is increased more with aging (Haskett et al., 2010).

Although many studies have reported that stiffness increases down the aortic tree, there still is some controversy. Some *in vivo* studies reported that increases in thoracic aortic stiffness with aging were greater than, or similar to those observed in the abdominal aorta (Farrar et al., 1984; Rogers et al., 2001; Nelson et al., 2009; Hickson et al., 2010; Taviani et al., 2011; Westenberg et al., 2011; Devos et al., 2015). Using PCMRI in a single para-sagittal plane to measure PWV in different regions, one study in humans found that participants below 55 years of age had similar PWVs at different aortic locations, but those older than 55 experienced the reverse of what is generally thought, i.e., stiffness decreased down the aortic tree (Rogers et al., 2001). In this study the investigators also suggested that the most significant mechanisms for increasing aortic stiffness with age are fragmentation of elastin, which would primarily affect the proximal aorta due to its higher elastin content, and diminished nitric oxide activity (Rogers et al., 2001). However, it's possible that the changes noted are not statistically significant, since the population studied had a low probability of having atherosclerosis and PWV variability increased markedly with age. Another study in humans found no significant difference in aortic PWV in pre- and post-menopausal women, but significantly lower brachial and femoral PWV values in pre-menopausal women (London et al., 1995).

By comparison with these studies in humans, we found significantly greater increases in stiffness in the abdominal aorta compared to the thoracic aorta in studies of non-human

primates (Zhang et al., 2016; Babici et al., 2020; **Figures 1**, **2**). Recording of aortic dimensions using implanted ultrasonic crystals in monkeys (**Figure 3**) showed that abdominal aortic stiffness was greater than thoracic aortic stiffness in both young and old monkeys (**Figures 1**, **2**; Zhang et al., 2016). These measurements of arterial stiffness using direct and continuous measurements of arterial pressure and diameter are more precise than measurements of stiffness using PWV, since they permit assessment of stiffness at distinct locations in the aorta. Examination of old premenopausal female monkeys also showed that the aortic stiffness index (β) was significantly higher in the abdominal vs. the thoracic aorta, both in older (20 ± 1.8) and younger (8 ± 1.1) monkeys (Babici et al., 2020). In addition, histological correlates of vessel stiffness were greatest in the iliac artery, suggesting iliac artery stiffness was even greater than abdominal aortic stiffness (Babici et al., 2020). Our *in vivo* studies of monkeys clearly indicate that age-related increases in aortic stiffness are greater in the abdominal compared to the thoracic aorta (**Figures 1**, **2**). Our previous studies also found significantly greater aortic stiffness in the abdominal compared to the thoracic aorta, in young monkeys (Zhang et al., 2016; Babici et al., 2020). Similarly, in normal rabbits PWV increased more with age in the abdominal than the thoracic aorta (Katsuda et al., 2014).

As noted above there are several reasons why studies in non-human primates are ideal for understanding vascular stiffness. Although it would be best to conduct these studies in humans there are ethical limitations to those studies and it is challenging to study changes in vascular stiffness in the absence of other disease states that normally evolve in older patients. The non-human primate is closest to humans on the evolutionary tree and therefore has the closest changes in genomics to humans among animal models, which occur with age. Moreover, sex-specific changes with aging, particularly the similarity between menopause in humans and non-human primates, is another important feature. On the other hand, there are features that make it considerably more difficult to study non-human primates than other animal models. First of all cost: there is a difference of thousands of dollars in purchasing non-human primates compared to other laboratory animals. Secondly, their supply is limited. Thirdly, care for these animals is more complex and most vivariums do not have the appropriate veterinary staff and facilities to house primates. Finally, there is increasing criticism for the use on non-human primates on an ethical basis. Whereas,

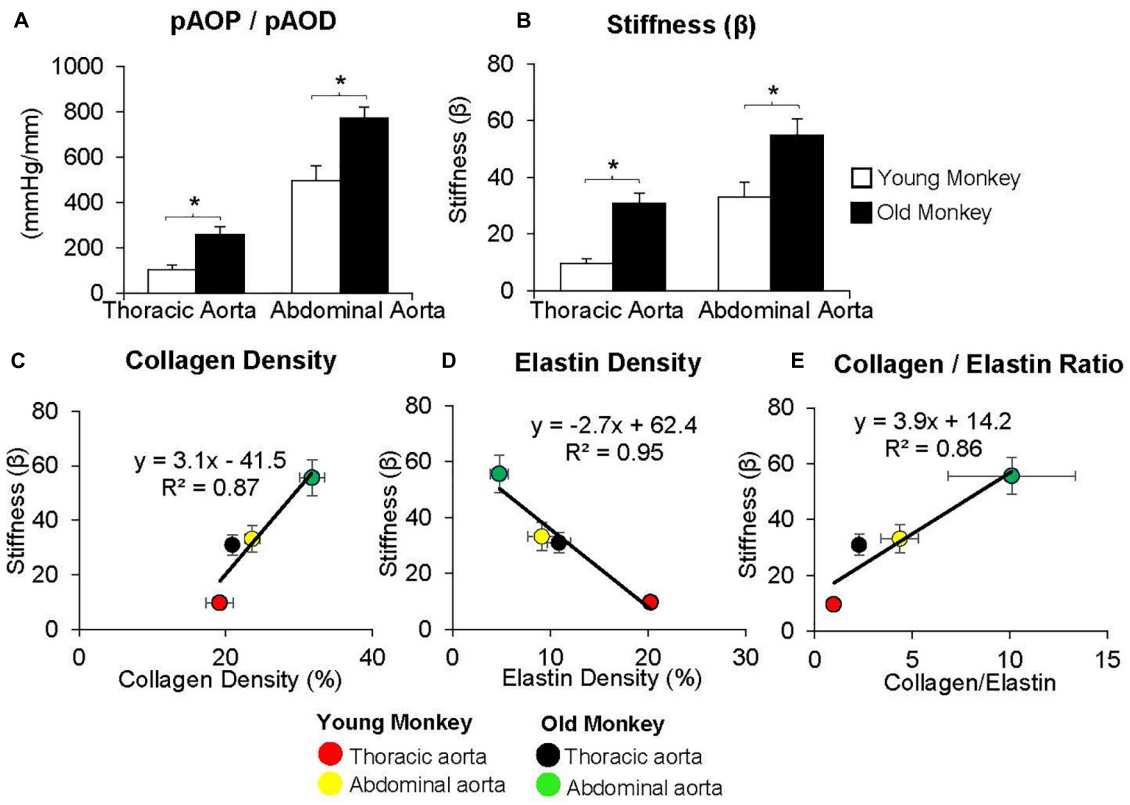

FIGURE 1 | (A) Measurements of the ratio of pulse aortic pressure (pAoP) to pulse aortic diameter (pAoD) are compared in young and old male monkeys both in the thoracic aorta and the abdominal aorta. The pAOP/pAOD ratio was significantly increased in old male monkeys, both in the thoracic and abdominal aorta. **(B)** Aortic stiffness was significantly increased in both the thoracic and abdominal aorta in old (26 ± 1 years) compared to young (9 ± 1 years) male monkeys. Correlation between aortic stiffness and collagen density **(C)**, elastin density **(D)**, and the collagen/elastin ratio **(E)** show linear relationships with aortic stiffness. Aortic stiffness was higher in the abdominal aorta than in the thoracic aorta in both young and old male monkeys and was higher in old vs. young male monkeys in both the thoracic and abdominal aorta. *$p < 0.05$ vs. corresponding young animals (reprint from Zhang et al., 2016).

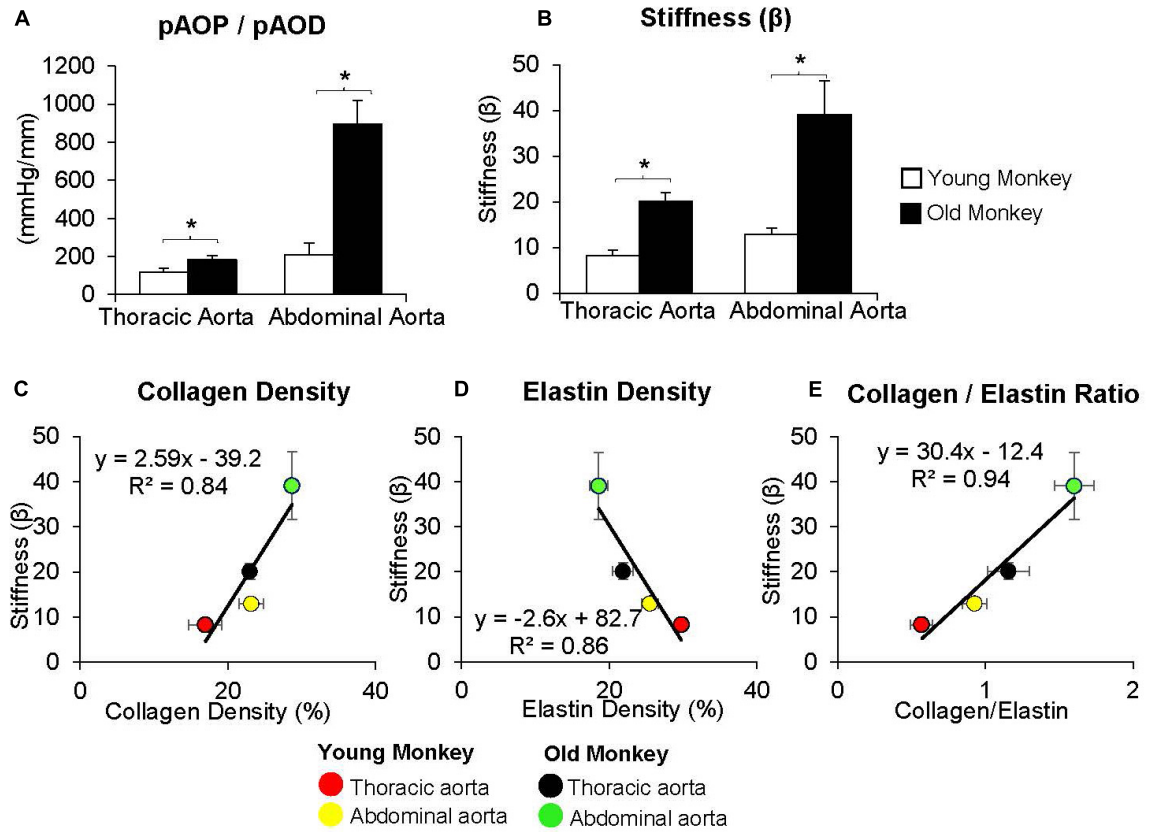

FIGURE 2 | (A) Measurements of the ratio of pulse aortic pressure (pAoP) to pulse aortic diameter (pAoD) are compared in young and old female monkeys both in the thoracic aorta and the abdominal aorta. The pAOP/pAOD ratio was significantly increased in old female monkeys, both in the thoracic and abdominal aorta. **(B)** Aortic stiffness was significantly increased in both the thoracic and abdominal aorta in old (24 ± 0.7 years) compared to younger (7 ± 0.7 years) monkeys. Correlation between aortic stiffness and collagen density **(C)**, elastin density **(D)**, and the collagen/elastin ratio **(E)** show linear relationships with aortic stiffness. Aortic stiffness was higher in the abdominal aorta than in the thoracic aorta in both old and young monkeys and was higher in old vs. young monkeys in both the thoracic and abdominal aorta. *$p < 0.05$ vs. corresponding young animals (reprint from Babici et al., 2020).

there are some groups that do not condone any animal research, there are others that specifically oppose primate research.

Most interest in age-related vascular stiffness has focused on the changes observed between midlife and older age in adults. However, it would also be of interest to know if changes in vascular stiffness occur between birth and midlife. To this end, we examined fetal, newborn and adult sheep, chronically instrumented for measurements of aortic diameter and pressure. At baseline levels of arterial pressure the elastic modulus of the aorta of young adult sheep was higher than that of the newborn lamb or the fetus, associated with a higher stress level (Pagani et al., 1979). However, when data were evaluated at common levels of stress, the aorta of the adult had a lower elastic modulus, than either the newborn or fetal animals (**Figure 4**). Furthermore, in the adult, a marked shift in the pressure-diameter and stress-radius relationships were observed in response to alpha-adrenergic mediated vasoconstriction. In contrast, no shift was observed in the newborn or fetal lambs (Pagani et al., 1979). The mechanism could either be at the level of either alpha adrenergic receptor signaling development or the inability of the aortic smooth muscle to constrict.

PERIPHERAL AND REGIONAL VESSELS

In comparison to the aorta, peripheral arteries are less elastic, more muscular, and inherently stiffer (Yu and Mceniery, 2020). In humans, the femoral artery has a more rigid wall, a greater diastolic diameter, and a twofold lower distensibility coefficient than the carotid artery (Benetos et al., 1993). The diastolic diameter of the carotid artery increases with age, while in the femoral artery, arterial diameter only increases slightly with age (Benetos et al., 1993). Carotid artery distensibility decreases linearly with aging, and cross-sectional compliance also decreases (Benetos et al., 1993). Although stiffness of peripheral arteries prior to the age of 50 is higher than that of central arteries, the increases in stiffness with aging is less in peripheral arteries than in central arteries (Mitchell et al., 2004). A study of static mechanical properties using an ultrasonic phase locked echo tracking system showed that the common carotid, femoral, and brachial arteries all increase in diameter with age (Kawasaki et al., 1987). Stiffness increases in all arteries as well; however, this was only significant in the common carotid and changes in stiffness of the brachial and femoral arteries varies greatly among individuals

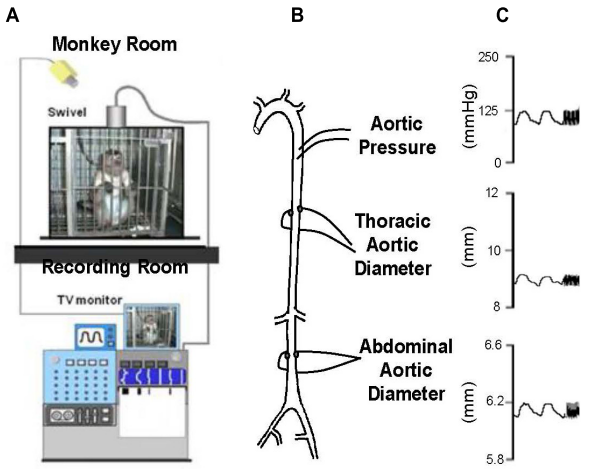

FIGURE 3 | (A) Chronically instrumented, conscious monkeys were connected to a tether to record data, but otherwise unrestrained in their cage during recording. **(B)** The animals were instrumented with thoracic aortic catheters for measurement of aortic pressure and ultrasonic dimension crystals, on opposing surfaces of the thoracic and abdominal aorta, for measurement of aortic diameters. **(C)** Examples of phasic measurements of aortic pressure and diameters in a young adult monkey (reprint from Zhang et al., 2016).

(Kawasaki et al., 1987). As with the aging aorta, it is believed that collagen content in the pulmonary and carotid arteries increases, while elastin content and the number of vascular smooth muscle cells (VSMCs) decrease with age (Greenwald, 2007). However, aging likely impacts large conduit arteries, such as the aorta and carotid, differently than small resistance vessels, which have fewer layers of VSMC and less matrix (Trache et al., 2020).

In non-human primates, as noted above, stiffness increases from the thoracic to the abdominal aorta and even distally to the iliac artery in both male and female monkeys (Zhang et al., 2016; Babici et al., 2020). However, most other studies have not measured stiffness directly but have examined the histological properties at different vessel levels. For example, the canine femoral artery has a higher content of collagen and lower content of elastin when compared to the ascending aorta, which would correlate to increases in stiffness physiologically (Fischer and Llaurado, 1966). However, stiffness was not directly measured in this study at any of the sites analyzed (Fischer and Llaurado, 1966).

MECHANISMS OF AGE-RELATED INCREASES IN VASCULAR STIFFNESS

The mechanisms of increased stiffness in aging are both extracellular and cellular (**Figure 5**). The three main aortic wall components, elastin, collagen, and smooth muscle cells, vary along the length of the aortic tree. With aging, these components of the aortic wall are altered. The number of elastic fibers and smooth muscle cells in the tunica media decrease, while collagen fibers increase with advancing age (Maurel et al., 1987). The number of smooth muscle cells in the tunica media decreases with age and vascular smooth muscle cell migration from the tunica media thickens the intima (Collins et al., 2014).

Extracellular Matrix Remodeling

The most important mechanism studied as a cause of age-related increases in vascular stiffness is alteration in the extracellular matrix (ECM), resulting from an increase in collagen and decrease in elastin. The ECM is composed of a complex network of different matrix proteins, metalloproteases, and glycosaminoglycans, which are also responsible for the structural integrity of the vasculature, and therefore contribute to its stiffness (Ma et al., 2020). Collagen is a very stiff protein with the function of limiting vessel elasticity and distension (Briones et al., 2010), and is therefore fundamental to defining the stiffness of the arterial wall. Collagen deposition throughout the vasculature increases with age, which alters the normal ECM network (Kohn et al., 2015). This has been shown to occur in the intima, media, and adventitia of the vessel wall leading to substantial changes in its morphology and function (Greenberg, 1986; Fleenor et al., 2010, 2012). In addition to increased collagen deposition, there is also increased non-enzymatic glycation. This is also responsible for age-related increases in arterial stiffness (Schleicher et al., 1997), as it induces collagen cross-linking, which increases stiffness (Reddy, 2004).

Unlike collagen, elastin, the other major ECM protein, provides flexibility and extensibility of the vessel wall (Wagenseil and Mecham, 2012). Elastin fibers are mainly found in the medial layer of large elastic arteries and are oriented around smooth muscle cells and collagen. Elastin content decreases, while collagen content increases from the proximal to distal aorta (Fischer and Llaurado, 1966; Sokolis, 2007). The elastin/collagen ratio is highest in the thoracic aorta and decreases distally (Hager et al., 2002), whereas the reverse is found in the collagen/elastin ratio (**Figures 1**, **2**). Smooth muscle cell content remains similar throughout the length of the aorta, but increases with aging and is another mechanism for increased aortic stiffness. Degradation of elastin fibers with aging is mediated by the increases of proteolytic enzymes, e.g., matrix metalloproteases (MMP), which degrade elastin fibers, resulting in an increase in collagen/elastin ratio, which in turn increase vessel wall stiffness (Wolinsky, 1970). Nevertheless, the extent to which increases in collagen and decreases in elastin contribute to increased vascular stiffness with aging remains controversial.

Using old world monkeys, we previously found that collagen density in the thoracic aorta did not change with age, whereas that in the abdominal aorta increased. In contrast, we found that elastin in both the thoracic and abdominal aorta decreased with age (Zhang et al., 2016; Babici et al., 2020; **Figures 1**, **2**, **6**). Relatively few studies have examined changes in both thoracic and abdominal aortic stiffness with age, *in vivo* (Farrar et al., 1984; Rogers et al., 2001; Nelson et al., 2009; Hickson et al., 2010; Taviani et al., 2011; Westenberg et al., 2011; Devos et al., 2015). Some studies measured collagen and elastin with aging, but did not measure aortic stiffness, *in vivo*. Interestingly, the results of these studies are controversial, with some studies finding an increase (Faber and Oller-Hou, 1952; Chamiot-Clerc et al., 2001;

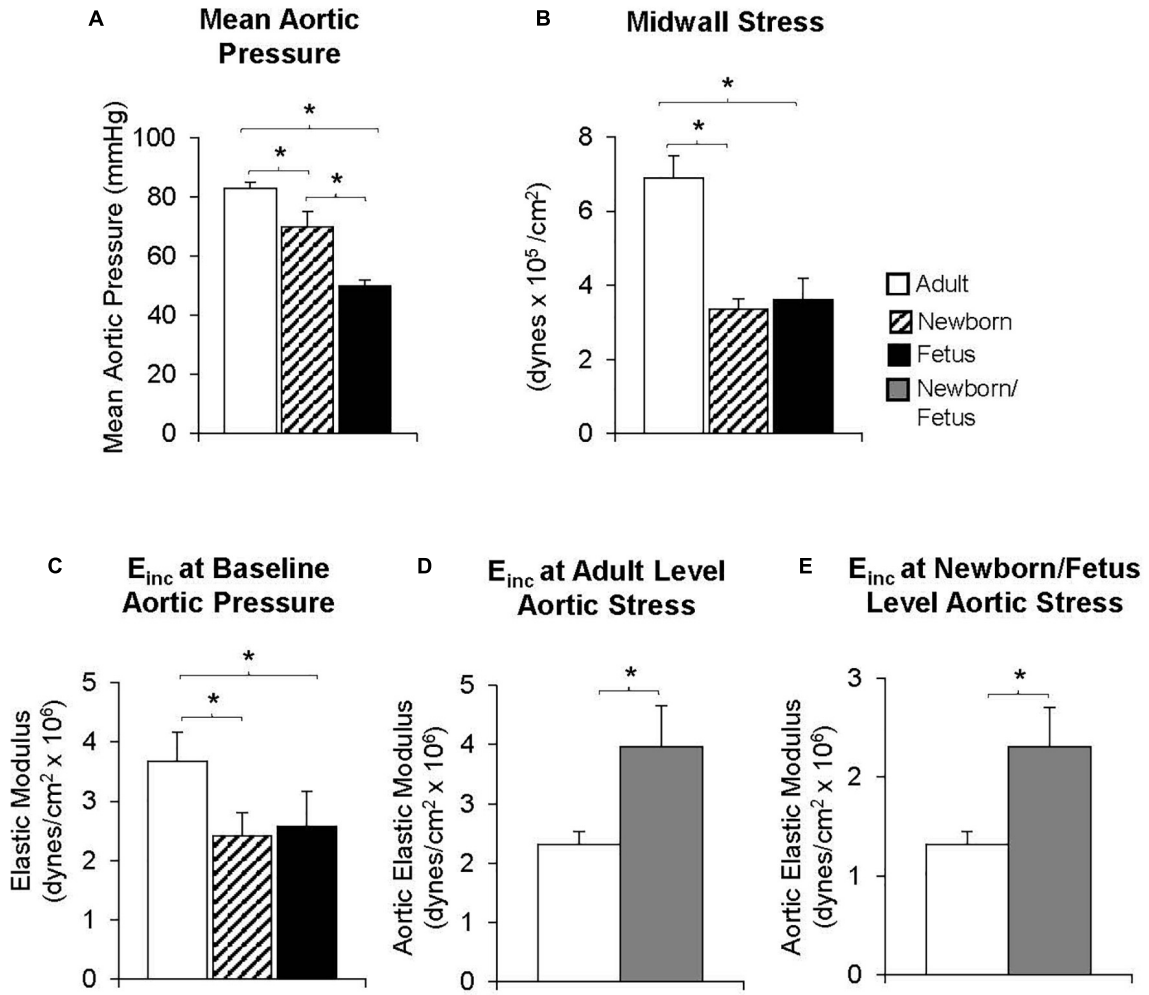

FIGURE 4 | Both **(A)** mean aortic pressure and **(B)** midwall stress were lower in fetal or newborn lambs than in adult sheep. **(C)** The elastic modulus was lower in fetal and newborn lambs, compared with adult sheep at baseline levels of aortic pressure, but surprisingly, the reverse was observed when the elastic modulus was compared at equal levels of aortic stress in fetal and newborn lambs and adult sheep **(D)** or when compared at the fetal/newborn levels of aortic stress **(E)**. Moreover, values were similar in fetal and newborn lambs suggesting that increases in aortic stiffness occur well after birth. *$p < 0.05$ (replot from Pagani et al., 1979).

Aronson, 2003; Nosaka et al., 2003; Astrand et al., 2011; Taviani et al., 2011; Wheeler et al., 2015) and others finding no change in collagen (Hosoda et al., 1984) or a decrease in collagen (Nosaka et al., 2003; Qiu et al., 2007a; Astrand et al., 2011; Taviani et al., 2011; Atanasova et al., 2012) or no change in elastin (Wheeler et al., 2015).

In contrast to the thoracic aorta, collagen content rose by 34% in the abdominal aorta with aging, which was a significantly greater increase than that observed in the thoracic aorta (Zhang et al., 2016). Elastin was decreased in the abdominal compared to the thoracic aorta in young animals, and decreased to even lower levels with aging (Zhang et al., 2016). Consistent with our finding that stiffness in the abdominal aorta of young monkeys equaled or was greater than that of the thoracic aorta in old monkeys, the collagen and elastin levels in the abdominal aortas of young monkeys equaled the values observed in the thoracic aorta for old monkeys (Zhang et al., 2016; Babici et al., 2020), emphasizing the importance for studying regional aortic stiffness changes with aging. However, basal levels of collagen and elastin are not the only mechanism accounting for greater stiffness observed in the abdominal compared to the thoracic aorta both in young and old monkeys. From our previous studies, we also observed marked disarray of both collagen and elastin; a finding that was more prominent with aging and in the abdominal vs. thoracic aorta. In fact, the marked disarray of elastin and collagen in the young abdominal aorta is likely responsible for the unexpected more severe stiffness than even in the old thoracic aorta (Zhang et al., 2016; Babici et al., 2020). The elastin and

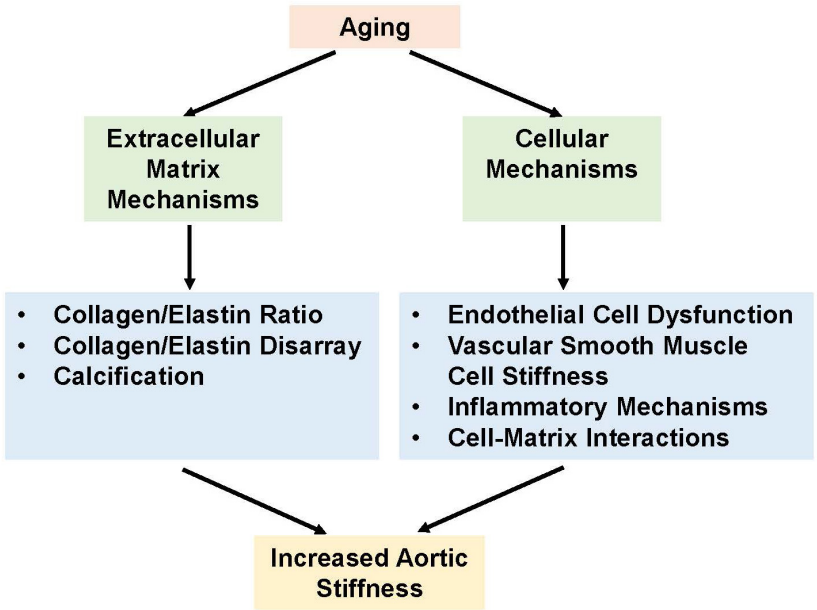

FIGURE 5 | Increased arterial stiffness develops from both extracellular and cellular mechanisms.

collagen disarray correlated better with stiffness than did elastin and collagen content (**Figure 6**). Another study also found elastic tissue in the abdominal aorta is most affected by aging (Maurel et al., 1987). Elastic fibers become damaged and thicken the tunica intima. Within the tunica media, elastic lamellae become damaged and elastic fibers become fragmented and disarrayed (Maurel et al., 1987). It is surprising that this marked architectural disarray we observed in the aging aorta with increased stiffness has not been noted extensively in the past, even though isolated observations have previously found disarray in aortae related to aneurysms (Hofmann Bowman et al., 2010; Pezzini et al., 2012; Lee et al., 2014), hypertension (Sans and Moragas, 1993), and aging (Fornieri et al., 1992).

Other important mechanisms mediating increased vascular stiffness, include increases in calcium deposition, endothelial dysfunction, and increases in the stiffness of vascular smooth muscle cells.

Calcium Deposition

Calcification of the vessel wall occurs with normal aging, reducing the vessel wall's distensibility (London et al., 2003). In humans there is a direct correlation between aortic calcification and arterial stiffness (Guo et al., 2017). Calcinosis of arterial walls with aging has been associated with increased cholesterol content in the elderly, suggesting a relationship between these processes (Kanabrocki et al., 1960). However, it is unknown which process occurs first, although some have speculated that calcinosis increases interaction with cholesterol molecules in the arterial wall (Hornebeck and Partridge, 1975). Another explanation for the increase in calcium deposition within the arterial wall is via an increase in inflammation and oxidative stress, both of which occur with normal aging. Increases in oxidative stress that occur with aging, mainly due to decreases in mitophagy and autophagy (Pescatore et al., 2019), stimulate vascular calcification by activating several signaling cascades (Byon et al., 2008). One of the best studied signaling pathways involves the upregulation of bone morphogenetic proteins due to increases in oxidative stress, which results in increased vascular calcification (Sorescu et al., 2004; Johnson et al., 2006).

The relationship between calcification and aortic stiffness differs depending on the location of the calcification. Carotid artery stiffness was more strongly associated with thoracic aorta calcification than calcification of the coronary arteries (Blaha et al., 2009). This may be because calcification of the coronary arteries usually involves only the intimal layer, while in large arteries calcification involves both the intima and media (Blaha et al., 2009); with medial calcification being more strongly associated with aging, diabetes, and severe renal disease (Iribarren et al., 2000). In addition, structural features may be involved: carotid arteries, being more elastic, are more similar to the aorta than to coronary arteries, which are non-elastic, predominantly conduit vessels.

Endothelial Dysfunction

The vascular endothelium is the innermost, monolayer of cells in blood vessels. When the endothelium is healthy, vascular tone is regulated by a balance of vasoconstriction and vasodilation; the latter controlled by nitric oxide (NO) release (Furchgott and Zawadzki, 1980). Reduced bioavailability of nitric oxide leads to endothelial dysfunction, resulting

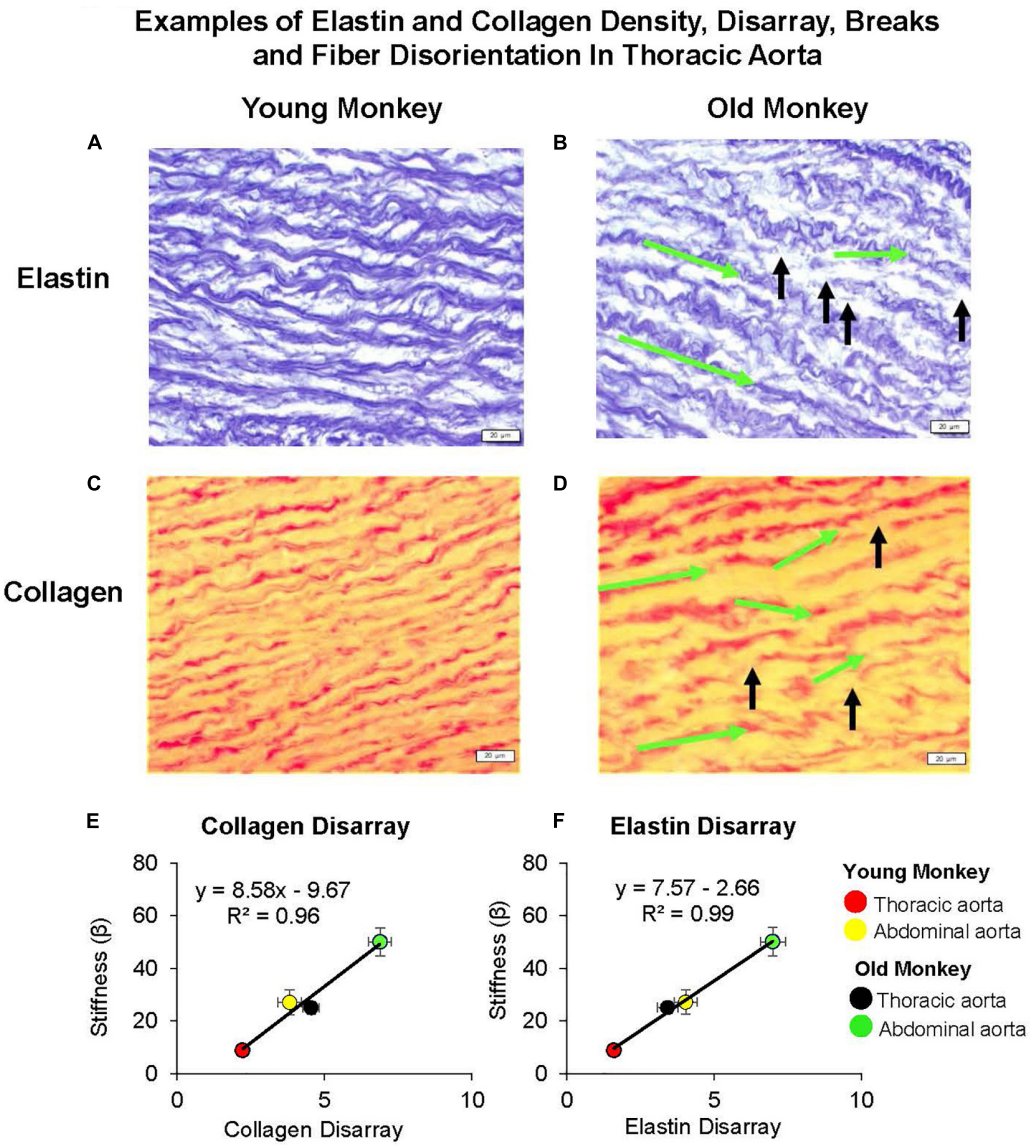

FIGURE 6 | Examples of elastin and collagen fiber disarray, breaks, and fiber disorientation in the thoracic aorta of young **(A,C)** as compared to those of old premenopausal females **(B,D)**. In old premenopausal monkeys, elastin and collagen disarray, fiber breaks, and fiber disorientation were increased compared to the young females. The green arrows indicate the change of fiber angle from the starting point of a fiber toward the end point of a fiber, and the black arrows indicate the fiber breaks. A linear correlation between stiffness and extracellular matrix was found for both **(E)** collagen disarray and **(F)** elastin disarray. Disarray was greater in the abdominal vs. the thoracic aorta in both old and young female monkeys and both were greater in old female vs. young female monkeys (reprint from Babici et al., 2020).

in impaired vasodilation, which increases arterial stiffness (Mceniery et al., 2006). Endothelium impairment and decreased NO bioavailability occur with normal aging, ultimately leading to a proinflammatory, vasoconstrictive state, resulting in increased vascular fibrosis and arterial stiffness (Santhanam et al., 2010; Santos-Parker et al., 2014). Furthermore, endothelial dysfunction leads to an increase in oxidative stress through an increase in the production of superoxide causing damage to the vessels leading to changes in hemodynamics (Donato et al., 2018). Recently, it has also been proposed that autophagy, the cellular housekeeping mechanism that maintains cellular homeostasis, decreases in the aging endothelium, further leading to increases in oxidative stress (Larocca et al., 2012). This was further confirmed with the use of a pro-autophagy treatment, which reduced arterial stiffness and oxidative stress in aged mice (Larocca et al., 2013).

Age-related endothelial dysfunction may affect the arterial network differently based on location and vessel type. Aging results in endothelial dysfunction in the aorta but not in the femoral artery (Barton et al., 1997). The anatomic variation in the influence of age on endothelial function may be related to increased pulse pressure and reduced eNOS mRNA expression in the aorta (Barton et al., 1997). In rats, acetylcholine-induced

vasorelaxation is impaired in large conduit arteries (abdominal aorta and iliac arteries) but not in smaller conduit (femoral arteries) or resistance arteries (Luttrell et al., 2020).

Vascular Smooth Muscle Cells

Vascular smooth muscle cells have recently been discovered as important contributors to age-related increases in arterial stiffness (Trache et al., 2020). This mechanism, which we named "Vascular Smooth Muscle Cell Stiffness Syndrome" (Sehgel et al., 2015b), was elucidated in aged non-human primates that displayed an increase in VSMC stiffness in large arterial vessels (Qiu et al., 2010; Sehgel et al., 2015a; **Figure 7**). This increased VSMC stiffness is due to the direct relationship between VSMCs and endothelial cells. Endothelial cells regulate vascular tone mainly through the release of nitric oxide. This reduces active tone of VSMCs (Furchgott and Zawadzki, 1980; Van Bussel et al., 2015), which counteracts the increase in wall shear stress that occurs with both aging and high blood pressure (Boutouyrie et al., 1995; Van Bussel et al., 2015; Jaminon et al., 2019; **Figure 8**). However, aging also leads to a decrease in the number of cells within the vascular wall due to a decrease in cell proliferation with age (Greenwald, 2007; Chi et al., 2019). Multiple mechanisms mediate the decrease of VSMCs with age, but most notably inflammation and calcification, which increase VSMC apoptosis (Lacolley et al., 2012). In humans, the VSMCs lost with aging are replaced by collagen fibers in the media of the arterial wall, resulting in increased vascular stiffness (Schlatmann and Becker, 1977). Interestingly, when the stiffness

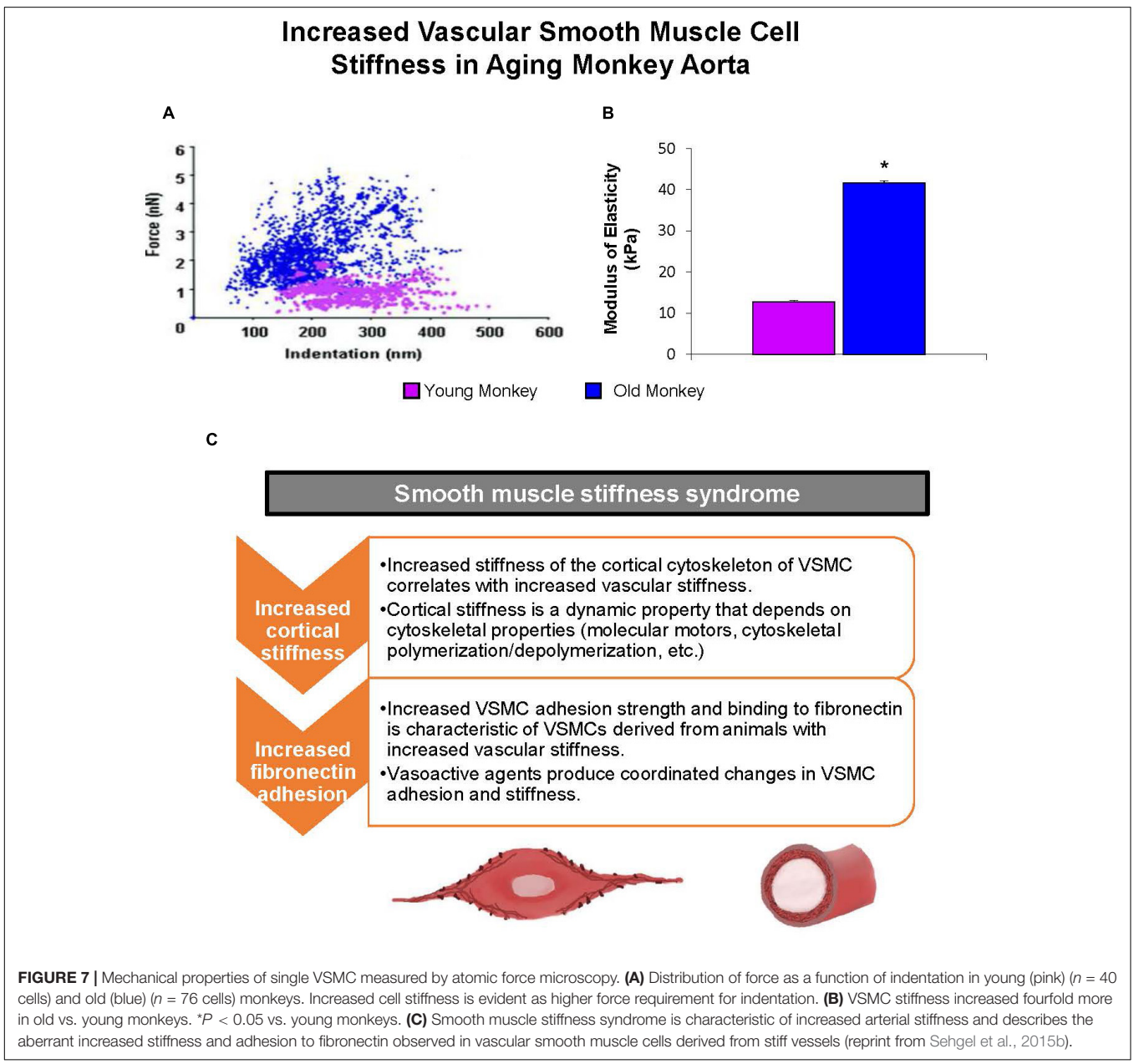

FIGURE 7 | Mechanical properties of single VSMC measured by atomic force microscopy. **(A)** Distribution of force as a function of indentation in young (pink) (n = 40 cells) and old (blue) (n = 76 cells) monkeys. Increased cell stiffness is evident as higher force requirement for indentation. **(B)** VSMC stiffness increased fourfold more in old vs. young monkeys. *P < 0.05 vs. young monkeys. **(C)** Smooth muscle stiffness syndrome is characteristic of increased arterial stiffness and describes the aberrant increased stiffness and adhesion to fibronectin observed in vascular smooth muscle cells derived from stiff vessels (reprint from Sehgel et al., 2015b).

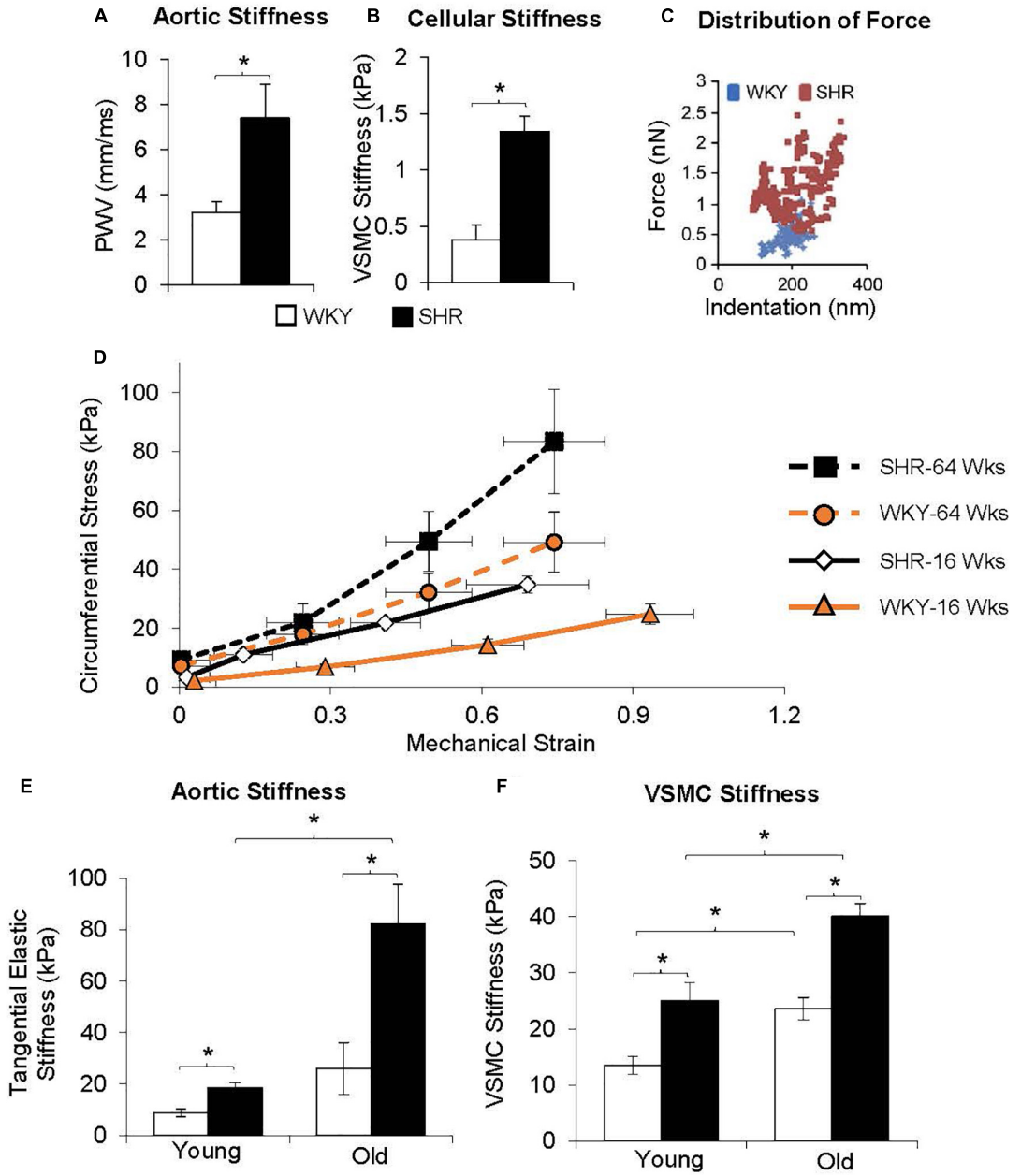

FIGURE 8 | Aortic stiffness was increased in *in vivo* **(A)** and in vascular smooth muscle cells **(B)** in spontaneously hypertensive rats (SHRs) compared with Wistar-Kyoto (WKY) rats. **(C)** Distribution of force was also higher at all levels of indentation in old vs. young SHR. **(D)** Excised aortic rings from young (16 weeks old) and old (64 weeks old) WKY and SHR were mechanically stretched, and their stiffness was determined from the stress-strain relationship, as shown for representative rings. Stress was greater in old vs. young SHR and WKY rats at any level of strain. **(E)** Aortic stiffness was increased in the SHR more than WKY in young rats, and was further increased in old SHR. **(F)** VSMC stiffness was also increased more in SHR than WKY at both young and old ages, and with greater increases observed in old age. *$p < 0.05$ (reprint from Sehgel et al., 2013, 2015a).

of isolated VSMCs was measured with atomic force microscopy, it did not differ with age between the thoracic and abdominal aorta (Zhang et al., 2016). This suggests that VSMC stiffness is not the mechanism by which stiffness varies regionally within the aorta, unless it is related to differences in VSMC function as a result of altered endothelial cell function, inflammation or calcium mechanisms that occur variably along the aortic tree with aging.

EXTENDED AND ABBREVIATED LIFESPAN MODELS

As emphasized in this review, increased aortic stiffness is mainly associated with aging. Interestingly, children with Hutchinson-Gilford progeria syndrome, a premature aging syndrome with a mean lifespan of 13 years, experience severe arterial stiffening from a young age. Patients aged 7 years have the aortic stiffness of a 60–69-year old without additional diseases (Gordon et al., 2005). This is thought to be related to abnormal elastin production (Sloop et al., 2015). These patients die prematurely, primarily of atherosclerotic disease and its complications. Since increased vascular stiffness, particularly in coronary arteries is linked to atherosclerosis, this provides further support for the concept that vascular stiffness is an important determinant of longevity.

Studying populations and animal models that experience longevity without cardiovascular decline and consequent increases in vascular stiffness could provide new insights into delaying vascular aging and promoting vascular health. Populations with extended lifespan live in areas known as Blue Zones (Vatner et al., 2020). They are geographically widespread, and include locations in the United States, Costa Rica, the Mediterranean, and East-Asia, Loma Linda, United States; the Nicoya peninsula in Costa Rica; Sardinia, Italy; Ikaria, Greece; Okinawa, Japan (Buettner and Skemp, 2016; Huang and Mark Jacquez, 2017). In these areas the number of centenarians, i.e., those reaching the age of 100, is 10 times greater than the average in the United States. The inhabitants share general features leading to healthful aging, e.g., frequent ambulation, healthy social relationships and psychological wellbeing, and diets that prevent weight gain, as opposed to Western diets, which are associated with increased vascular stiffness (Dupont et al., 2019). As noted above, protection against vascular stiffness plays a role in extended lifespan. Data supporting this can be found in a study in one of these Blue Zone populations, people living on the island of Ikaria, where aortic stiffness increases gradually with age, but then begins to decelerate at 50 years of age, with PWV being significantly lower than that in normal lifespan populations (Pietri et al., 2015). In the Ikaria population, habitual physical exercise, which is known to ameliorate the effects of vascular aging (Siasos et al., 2013), is associated with increased endothelial function, also known to protect against vascular stiffness (Anderson, 2006). It has also been shown that body fat-percentage is directly associated with arterial stiffness in long-lived populations, consistent with individuals with more lean muscle having more elastic arteries (Melo et al., 2021). Exercise also preserves muscle mass and a healthy diet can promote anti-inflammatory and anti-oxidative pathways (Redei and Mehta, 2015). Another interesting population are the Yanomami Indians of South America, whose diets are low in fat and salt, and high in fiber, plantains, cassavas (a root vegetable), and fruit. Vascular stiffness has not been studied in Yanomami Indians, but their blood pressure remains largely unchanged from age 1 to 60 years (Mueller et al., 2018).

Obesity, one of the most common worldwide problems, is associated with almost all cardiovascular diseases, including increased vascular stiffness (Dupont et al., 2019). Conversely, caloric restriction has also been reported to increase lifespan, both in humans and animal models, and protects against obesity, diabetes, hypertension, cancer, and cardiovascular disease (Trepanowski et al., 2011; Yan et al., 2012, 2013; Ravussin et al., 2015; Redman et al., 2018; Vatner et al., 2020). Caloric restriction also protects against arterial stiffness. In rats, this is evidenced by increased aortic distensibility and decreased PWV (Ahmet et al., 2011). Less collagen builds up, more elastin remains, and vascular smooth muscle is preserved in the aorta (Fornieri et al., 1999). A major mechanism by which caloric restriction is protective and prolongs longevity is through increased eNOS levels, which increase nitric oxide bioavailability, and protect against oxidative stress (Wilkinson et al., 2002).

However, vascular stiffness has not been evaluated in most studies of animal models with an extended lifespan. Whales, for example, are some of the longest living mammals but not much is known about the aging of their vasculature. They have a vastly different structure to their aortic tree with an anatomy representing arterial adaptation by diving mammals (Shadwick and Gosline, 1994). Of interest, Japanese women, who are lifelong pearl divers, demonstrate significantly lower arterial stiffness in proximal and elastic arteries and lower carotid artery impedance modulus compared with non-diving residents in the same village (Sugawara et al., 2018). Vascular stiffness, however, has not been studied in other long-lived animal models, such as, bats (Podlutsky et al., 2005), and tortoises (living over 100 years) (Quesada et al., 2019).

An exception to this is the naked mole-rat, which is the longest-lived rodent known (Dammann and Burda, 2006; Grimes et al., 2014). This rodent does not display the age-related pathology seen in other mammalian species, including shorter living rodents. In naked mole-rats, systolic, mean, and pulse pressure as well as PWV remain unchanged with age (Grimes et al., 2014). Additionally, they maintain normal cardiovascular structure and function at 24 years of age, which is 8 times the lifespan of normal rats, an age physiologically equivalent to a 92-year-old human (Grimes et al., 2014). Studies suggest that their youthful vasculature may be attributed to sustained nitric oxide availability and protection against oxidative stress (Csiszar et al., 2007). Further studies of vascular stiffness in animal models with extended or abbreviated lifespan are warranted as they might provide novel therapeutic targets for the prevention of age-related increases in vascular stiffness.

SEX DIFFERENCES

Aging-related vascular stiffening is sexually dimorphic, a topic that has not been studied extensively. Although arterial stiffness increases from young adulthood to older ages in both men and women, the increases in stiffness in women before menopause are less than those in age-matched men (Ogola et al., 2018). This pattern reverses after menopause (Nethononda et al., 2015; Babici et al., 2020). This may partly explain why women tend

to live longer than men but are in worse health at older ages when compared to men (Hagg and Jylhava, 2021). In humans, postmenopausal women have a higher carotid-femoral PWV than premenopausal women; a step-up in PWV that is not observed in age-adjusted men (Staessen et al., 2001). This finding suggests that investigations into sex-specific gene regulation and sex hormones, may provide new insights into the mechanisms mediating these patterns.

Much of the previous experimental work on vascular stiffness has been performed in rodent models, which have a short lifespan and do not experience menopause. Because of this, the most relevant studies are those in non-human primates and humans. Non-human primates have a longer lifespan (>30 years), and undergo menopause like humans but are exempt from diseases, such as atherosclerosis, hypertension and diabetes, which are confounding factors when studying age-related changes in vascular stiffness in humans (Qiu et al., 2007a).

The studies considered here, on sex differences in arterial stiffness in humans, will focus predominantly on primary measures of arterial stiffness, namely, PWV, pulse pressure, and aortic distensibility; PWV and pulse pressure increasing and aortic distensibility decreasing as age and stiffness increases. In a study involving 777 people aged 21–85 years, aortic distensibility and aortic PWV were assessed using cardiovascular MRI, with age-related differences examined in successive deciles in each sex (Nethononda et al., 2015). In the first age group (20–29 years), aortic distensibility was significantly higher in women than men. This pattern was reversed in older aged groups, the sex differences being most marked in those aged around 60 years. In both sex groups, aortic distensibility decreased with increasing age in all regions studied, namely, the ascending, proximal aorta, and abdominal aorta. In both men and women, the greatest decreases in aortic distensibility occurred between those aged 50–59 and 60–69 years, although the decrease between these age groups was larger in women (47–61%) than in men (31–45%). These findings indicate that the decline in aortic distensibility is sex-independent, although the steepest decline occurs in women between the pre- to the postmenopausal periods. Surprisingly, however, these aortic distensibility changes were not mirrored by commensurate steep increases in PWV in the peri-menopausal period (Nethononda et al., 2015). One mechanism that may contribute to the rapid decline in aortic distensibility in females between these age groups is body weight changes that accompany menopause. Greater weight gain and an increase in the waist:hip ratio, suggesting increased abdominal fat, are seen in women compared to the increases in correspondingly aged men (Nethononda et al., 2015). Interestingly, other studies have also noted similar age-related but sex-independent PWV increases (Smulyan et al., 2001; Hickson et al., 2010). It is possible that no sex differences are observed in aortic PWV because despite distensibility decreasing rapidly after menopause, blood viscosity increases with menopause (Schillaci et al., 1998). The mathematical relationship between PWV and distensibility is demonstrated by the Bramwell-Hill equation; PWV ($\rho \times$ Distensibility)1/2, with (ρ being blood density, Nethononda et al., 2015). Given that blood viscosity increases greatly with menopause, the equation aids us in understanding why a large decrease in distensibility does not correlate with an increase in PWV of the same magnitude (Nethononda et al., 2015). However, in contrast, the Baltimore Longitudinal Study of Aging identified a steeper longitudinal increase of PWV in men compared to age-matched women (Alghatrif et al., 2013).

It is important to note that, although aortic stiffness is more severe in males than females prior to menopause, pre-menopausal women also exhibit age-dependent increases in aortic stiffness, as observed in primates (Babici et al., 2020). An aortic pressure catheter and ultrasonic diameter transducers implanted in young (7 ± 0.7 years old) and aging premenopausal female monkeys (24 ± 0.7 years old) found that the aortic pulse pressure was increased in old premenopausal monkeys (48 ± 2.7 mmHg) compared to young monkeys (33 ± 2.5 mmHg) (Babici et al., 2020). The aortic stiffness index, a function of aortic pressure and aortic strain, was increased in the old vs. young subjects in both the thoracic and abdominal aortas. Furthermore, the collagen/elastin ratio increased down the aortic tree and was consistently higher in the old premenopausal monkeys (Babici et al., 2020). Elastin and collagen showed progressively more disarray down the aortic tree (quantitation of disarray is described in the section on Mechanisms). Twice as much disarray was noted in the older group compared to the younger group in the thoracic aorta, abdominal aorta, and iliac artery (Babici et al., 2020). Elastin- and collagen-fiber disarray and breaks also increased down the aortic tree and were more marked in premenopausal monkeys. In a previous study, elastin and collagen disarray correlated better with stiffness than elastin and collagen content (Zhang et al., 2016). Studies on these structural proteins also identified sex differences in the specific characteristics of elastin and collagen. In the human abdominal aorta, elastin content decreased but the stiffness of elastin and collagen increased with age in men (Astrand et al., 2011). There was a much lesser age-related change in aortic elastin- and collagen-stiffness between young, middle-aged, and elderly women (Astrand et al., 2011). Collagen and elastin seem less affected in the female aortic wall due to the influence of sex hormones.

The mechanisms underlying age-related and regional differences in aortic stiffness are also sexually dimorphic. In non-human primate models, aging-related changes in gene expression have been shown to be sex-dependent and to involve key contributors of vascular stiffness, such as ECM composition, VSMC phenotype, cell signaling pathways, resistance to apoptosis, metabolism, protein synthesis, and transcription factors. Aging male, but not female monkeys, show downregulation of collagen type III protein expression and upregulation of collagen type VIII transcript levels. Collagen type III decreases collagen bundle size and increases vascular elasticity while collagen type VIII promotes VSMC migration into the intima (Qiu et al., 2007b). This may explain the finding that elastin stiffness increases with age in men, but not in women (Astrand et al., 2011). Similar protein and gene expression changes have also been observed in another study of a non-human primate model, in which female premenopausal animals were compared with their aged-matched male counterparts (Qiu et al., 2007a). In addition

to changes in gene regulation, sex hormones are also potential contributors to sex-specific differences in age-related increases in vascular stiffness.

Role of Sex Related Hormones

The greater increases in vascular stiffness in aged-matched men, than in women prior to menopause, is reversed, so that after menopause women show more severe increases in vascular stiffness. The difference in vascular stiffness between pre- and postmenopausal women is primarily ascribed to proposed protective roles of estrogen, which reduces increased stiffness with age. Estrogen levels rapidly decrease just before menopause and continue to fall after menopause (Moreau and Hildreth, 2014). This coincides with the timing of the accelerated age-associated vascular stiffness seen in women after menopause, when compared to age-matched men and premenopausal women. Animal studies have found that estrogen can increase elastin content, inhibit collagen deposition, and prevent abnormal VSMC proliferation and migration (Dubey et al., 2000a,b; Yoon et al., 2001). In other words, estrogen appears to counteract many of the mechanisms associated with age-dependent vascular stiffening. Furthermore, hormonal therapy with estrogen, initiated around the time of menopause, decreases arterial stiffening in postmenopausal women when compared to non-hormonal therapy-treated postmenopausal women (Moreau and Hildreth, 2014). Arterial stiffening is also associated with increased vascular tone and increased oxidative stress. Estrogen is also a potent antioxidant and prevents scavenging of nitric oxide (NO) by reactive oxygen species (Moreau and Hildreth, 2014). Thus, prolonged estrogen deficiency in postmenopausal women, by limiting availability of estrogen as an antioxidant and of NO, may contribute to an increase in vascular tone, and in susceptibility to oxidative stress. Nevertheless, it is of interest that despite the evidence for a protective role of estrogen with respect to arterial stiffness during the fertile period, epidemiological evidence suggests that there is no sudden increase in the rate of cardiovascular disease in women at the time of menopause, but this is observed rather after menopause (Woodward, 2019). Furthermore, clinical trials have found no overall cardiovascular benefit of exogenous estrogen in postmenopausal women (Boardman et al., 2015).

In mice, NO bioavailability has been directly linked to the mechanical properties of the vessel wall, corroborating that the effect of estrogen is mediated by NO. Female ovariectomized mice display increased circumferential elastic modulus in all arteries, suggesting stiffening, as well as decreased eNOS protein expression, and reduced endogenous NO production (Guo et al., 2006). Female mice lacking the endothelial NO synthase gene displayed increases in circumferential modulus in the aorta and decreased NO production in the femoral and carotid arteries (Guo et al., 2006). This supports the idea that estrogen works to reduce stiffness by stimulating NO production, which maintains structural and mechanical properties of arteries. When rodent models were given an NO synthase inhibitor, either acutely or chronically, PWV increased compared to that in controls. In fact, chronic administration showed an additional 8% increase in PWV when compared to the control experimental group (Fitch et al., 2001).

Administration of BH_4 (tetrahydrobiopterin), a critical cofactor for NO production, increased carotid artery compliance and brachial artery flow-mediated dilatation in postmenopausal, but not premenopausal women (Moreau et al., 2012). This increase in carotid compliance was also seen when estradiol was administered to postmenopausal women (Moreau et al., 2012). However, no additional improvement was seen when BH_4 and estradiol were co-administered (Moreau et al., 2012). Therefore, reduced BH_4 may contribute to arterial stiffness in postmenopausal women and estrogen may increase BH_4 bioavailability.

These varying trends between men and women significantly impact their cardiovascular disease susceptibility (Dupont et al., 2019). Heart failure with preserved ejection fraction (HFpEF) is observed twice as commonly in women than men. This increased incidence of HFpEF in women may be associated with the increased proximal aortic stiffness in post-menopausal women, when compared to men (Coutinho et al., 2013). The mean age in this study was 65 years for post-menopausal women and 67 for men (Coutinho et al., 2013). Women also exhibit more pronounced age-related increases in aortic flow impedance than men (Coutinho et al., 2013). These pathophysiological changes may have a cascade effect whereby lower aortic compliance leads to greater impedance to flow. In turn, this increases hemodynamic load on the left ventricle, resulting in an enhanced propensity for women to develop heart failure.

The enhanced arterial stiffness of older postmenopausal women, compared to their male counterparts, is an issue that warrants greater research not only to better understand the mechanisms behind this phenomenon, but also to develop more targeted and effective therapies for postmenopausal women. Isolated systolic hypertension is more common in older women and these women are less likely to achieve optimal blood pressure control than age-matched men (Dupont et al., 2019).

As mentioned previously, findings from studies of vascular aging in rodents are limited, as rodents have a shorter lifespan than monkeys or humans, and do not go through menopause. This may explain why one study of aging in rats showed similar levels of aortic stiffness at 6, 12, and 24 months of age in males and females (Mitchell et al., 2004). One rodent species that does live over 20 years, the naked mole rat, has been found to be better protected against aging-induced oxidative stress and apoptotic cell death than its shorter-living counterparts; differences that likely contribute to their exceptional longevity (Csiszar et al., 2007). This provides insight into the key roles oxidative stress may have on age-related arterial stiffness. Further studies may also be warranted of male and female naked mole rats to determine if, like human and monkeys, they also display sex-specific differences in longevity.

Sexually dimorphic longevity is observed in many mammalian species, with females living longer than males (Hagg and Jylhava, 2021). Despite differences in cardiac physiology and anatomy, rodent models have been helpful in beginning to understand mechanisms underlying sex-specific differences in vascular aging (Blenck et al., 2016). However, monkey models are more

applicable to humans than rodents because they live longer and have a menstrual cycle. But with the availability of non-human primate models, more research is required to fully elucidate the key drivers of sex-specific differences in vascular aging.

Vascular Stiffness in Prepubescent Years

Sex differences in arterial stiffening have been found even in prepubescent human subjects and may be attributed to both sex steroids and intrinsic differences. Prepubescent girls, for example, have less compliant arteries and higher central and peripheral PWV than their male counterparts (Ahimastos et al., 2003). However, after puberty, central PWV falls in females but increases in male (Ahimastos et al., 2003). Interestingly, prepubescent and postmenopausal arterial stiffness are both likely due to the same mechanism, namely, low levels of sex steroids.

DISEASES STATES

Hypertension

Aortic stiffness and arterial pressure are strongly correlated in hypertension with vascular stiffness being both a cause and a consequence of hypertension (Humphrey et al., 2016). High blood pressure may cause vascular damage and elastin fragmentation, leading to increased stiffness. On the other hand, aortic stiffness widens pulse pressure which affects systolic blood pressure. Hypertension and aging may have an additive effect evidenced by elderly hypertensive patients having stiffer arteries than age-matched normotensive patients (Verwoert et al., 2014). However, these differences may be attributed to hypertension, rather than intrinsic vascular changes associated with increased stiffness (Bavishi et al., 2016).

Vascular stiffness is linearly related to age both in normotensive and severely hypertensive subjects (**Figure 9**; Safar et al., 2018). Interestingly the slope of these linear relationships is not that different (**Figure 9**); arterial stiffness rising in normotensive people almost as much as in those who are hypertensive. Aortic stiffness is also increased in spontaneously hypertensive rats, even at a young age, but much more in older rats (Sehgel et al., 2013, 2015a,b; **Figure 8**). As discussed above, elastin breakdown, due to matrix metallopeptidases and serum elastase, is a major mediator of increased vascular stiffness (4). Serum MMP-9 and MMP-2 levels, and serum elastase activity, which degrade elastin degradation and increase aortic and brachial PWV, are increased in subjects with isolated systolic hypertension (Yasmin et al., 2005).

Isolated systolic hypertension, defined as systolic blood pressure > 140 mmHg and diastolic blood pressure < 90 mm Hg (Mancia et al., 2013), is the predominant form of hypertension in the elderly, and is associated with increased arterial stiffness (Franklin et al., 1997; Yasmin et al., 2005; Bavishi et al., 2016). Interestingly, in older patients, systolic arterial pressure continues to increase along with aortic stiffness, but diastolic hypertension declines, further demonstrating the important relationship between systolic arterial hypertension and aortic stiffness (Franklin et al., 1997). Systolic-diastolic hypertension due to elevation of both systolic and diastolic arterial pressures is less common in older adults (Tsimploulis et al., 2017), but is associated with an increased incidence of heart failure and cardiovascular mortality (Tsimploulis et al., 2017). Also, pre-eclampsia, which induces hypertension during pregnancy, is associated with increased vascular stiffness (Hausvater et al., 2012).

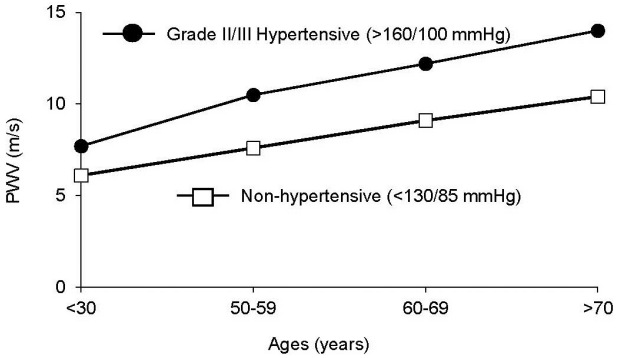

FIGURE 9 | Interaction between hypertension and arterial stiffness in patients. There were similar linear relationships in hypertensive patients vs. non-hypertensive patients, but with stiffness greater in hypertensive patients at all ages (reprint from Safar et al., 2018).

Salt intake, a key mechanism mediating hypertension, is positively correlated with carotid-femoral P; the slope of the linear regression line linking these two parameters was steeper in women than in men (0.0199 ± 0.0045 vs. 0.0326 ± 0.0052 m/s per gram of salt, respectively, $P < 0.05$). However, after adjustment in the data of outliers, the association remained significant only in men (Baldo et al., 2019).

Calcium deposition in the aorta is another mechanism mediating the increase in arterial stiffness in hypertension (Guo et al., 2017). Interestingly, it was most pronounced in subjects who were resistant to anti-hypertensive therapy, suggesting that arterial stiffness not only contributes to isolated systolic hypertension development, but may also be involved in resistance to hypertension treatment (Mceniery et al., 2009).

Another important mechanism of aortic stiffness in hypertension is vascular smooth muscle stiffness (Sehgel et al., 2013, 2015a,b). Changes to the intrinsic stiffness of VSMCs and to their adhesion properties are observed in hypertension. Using atomic force microscopy and a reconstituted aortic tissue model, it was found that spontaneously hypertensive rats had increased aortic VSMC stiffness as well as different temporal oscillations in VSMC stiffness compared to normotensive control rats (Sehgel et al., 2013). In a later study in which VSMC stiffness and adhesions to the ECM were also found to be increased in hypertensive rats (Sehgel et al., 2015a), hypertension did not increase the amount of collagen in the thoracic aorta, suggesting that increased vascular stiffness associated with hypertension is

likely not exclusively mediated by altered collagen and elastin content, but by increased VSMC stiffness and adhesion (Sehgel et al., 2015a). VSMC changes with aging are augmented when hypertension is superimposed on aging.

Atherosclerosis

Atherosclerosis, which is more common with aging, is a chronic inflammatory disease in which atheromatous plaques form, resulting in arterial narrowing. Many studies, such as the Rotterdam study (Van Popele et al., 2001), show that stiffness of the aorta increases with plaque burden and conclude that arterial stiffness is strongly associated with atherosclerosis. However, these conclusions must be tempered by the fact that increased vascular stiffness is also a feature of aging in the absence of atherosclerosis (Sun, 2015). Atherosclerosis can occur at an earlier age in a condition known as Pediatric atherosclerosis (Wilson, 2000). Also, as discussed above the autosomal recessive premature aging disorder, Hutchison-Gilford Progeria syndrome, is characterized by precocious atherosclerosis and stiffening of the arteries, which cause early death in affected individuals (Keay et al., 1955). Consistent with the arterial stiffness found in these children, their carotid-femoral PWV is also markedly increased (Gerhard-Herman et al., 2012; Gordon et al., 2012). One way to address the question of mechanisms of atherosclerosis in a younger population is to examine atherosclerosis mechanisms in animal models that develop disease at a young age. Our laboratory has begun to study aortic stiffness in Watanabe rabbits, an animal model of atherosclerosis (Aliev and Burnstock, 1998). Our preliminary data suggest that aortic stiffness is increased even in relatively young Watanabe rabbits, as compared to aged-matched New Zealand White rabbit controls. In hypercholesterolemia Kurosawa and Kusanagi rabbits, PWV reflecting the atherosclerotic regions found that vascular stiffness was increased more in these regions and more in the abdominal vs. the thoracic aorta (Katsuda et al., 2014).

Many different mechanisms have been implicated in the stiffening of arteries associated with atherosclerosis. Hypercholesterolemia is most commonly implicated in the pathogenesis of atherosclerosis in humans and animal models, ranging from rodents to rabbits, pigs and monkeys (Linton et al., 2000; Getz and Reardon, 2012). Extracellular matrix proteins are also involved in the development of increased vascular stiffness in atherosclerosis. Elastin degradation is increased by the build-up of atheromatous plaques. Non-atherosclerotic arteries contain MMP-2 as well as inhibitors of MMP, such as TIMP 1 and 2 (Galis et al., 1994). In contrast, atheromatous plaques also contain macrophages that secrete MMP-1, MMP-9, and MMP-3, smooth muscle cells, lymphocytes, and endothelium (Galis et al., 1994). Based on SDS-PAGE zymography, plaques have been found to contain activated forms of MMP-2 and MMP-9 (Galis et al., 1994). In addition, patients with hypercholesterolemia exhibit more circulating $CD31^{+}/CD42^{-}$ microparticles, less endothelial progenitors (EPCs), and have stiffer aortae than controls. The ratio of $CD31^{+}/CD42^{-}$ microparticles to EPCs was found to be directly associated with arterial PWV (aPWV) (Pirro et al., 2006). This suggests that hypercholesterolemia contributes to large artery stiffness by increasing microparticle release and by reducing the number of circulating EPCs (Pirro et al., 2006). In addition, the extracellular matrix protein, fibrillin-1, has been found to modulate large-artery stiffness and pulse pressure (Medley et al., 2002).

Elevated oxidative stress also plays a role in increased arterial stiffening in patients with atherosclerosis. A study examining patients with peripheral arterial disease found an independent association of aPWV with serum levels of osteopontin and oxidized low-density lipoprotein, which are involved in oxidative stress, thus supporting the role for oxidative stress in mediating arterial stiffness in patients with atherosclerosis (Zagura et al., 2012).

Intimal arterial calcification within atherosclerotic plaques may also be responsible for increased vascular stiffness (Mackey et al., 2007). A study in the Twins United Kingdom population suggests that it is the propensity of plaques to calcify rather than the amount of plaque that determines arterial stiffness (Cecelja et al., 2013). Aortic stiffness was correlated with calcified plaques in the carotid and femoral arteries detected by ultrasound and with total aortic calcification measured by computed tomography (Cecelja et al., 2013).

Diabetes

Diabetes predisposes to cardiovascular disease and accelerated arterial stiffness. The magnitude of the effect of diabetes on central stiffness has been compared to the equivalent of 6–15 years of chronological aging on vessels (Cameron and Cruickshank, 2007; Loehr et al., 2016). It has been suggested that vascular stiffness in diabetic patients may be attributed more to the role of diabetes and metabolism, than to aging, *per se* (Cameron et al., 2003). One major metabolic mechanism is the non-enzymatic advanced glycation of proteins observed in diabetes. The accelerated production of advanced glycation end-products (AGEs) is implicated in diabetes-associated increasing stiffness. AGEs form in hyperglycemic environments, accumulate in the vessel wall, and form cross-links with collagen and elastin fibers, decreasing arterial wall distensibility (Goldin et al., 2006). The incidence of atherosclerosis is also increased in diabetic patients (Poznyak et al., 2020) and, thus, increased vascular stiffening due to accelerated atherosclerosis also contributes to the increase vascular stiffness in diabetic patients (Stehouwer et al., 2008; Prenner and Chirinos, 2015). Patients with type 2 diabetes also displayed endothelial dysfunction and a reduced contractile response to endothelin-1, suggesting these mechanisms factor into the development of vascular stiffness, due to the role of vasoconstriction in mediating vascular stiffness (Rizzoni et al., 2001). For example, endothelium-dependent dilation has shown to be abnormal in patients with type 2 diabetes attributed mainly to dyslipidemia (Schofield et al., 2002).

It has been shown that vascular stiffness increases as glucose tolerance deteriorates. Impaired glucose metabolism and type 2 diabetes (DM-2) are associated with decreased total systemic arterial compliance and increased aortic augmentation index, indicating increased central artery stiffness (Schram et al., 2004). Central artery stiffness is greater and carotid-femoral transit time is decreased in patients with DM-2 (Schram et al., 2004). It has also been shown that stiffness of the peripheral arteries

increases with deteriorating glucose tolerance (Henry et al., 2003). Together, these studies suggest that stiffness due to impaired glucose metabolism and DM-2 are worse in peripheral than central arteries (Henry et al., 2003; Schram et al., 2004). Interestingly, in children with type 1 diabetes, especially males, stiffness of peripheral arteries is more common than of central arteries (Urbina et al., 2010).

As noted throughout this review, an important mechanism mediating increased vascular stiffness is increased oxidative stress (Giacco and Brownlee, 2010; Pasupuleti et al., 2020). It is well known that diabetes leads to increased oxidative stress, involving mitochondrial superoxide overproduction in the vasculature and in in the myocardium (Giacco and Brownlee, 2010; Pasupuleti et al., 2020). It is also recognized that increased intracellular reactive oxygen species cause defective angiogenesis in response to ischemia, and activate a number of proinflammatory pathways in diabetes and mediate the atherosclerosis and cardiomyopathy associated with diabetes (Giacco and Brownlee, 2010; Pasupuleti et al., 2020).

Even patients with prediabetes experience increased arterial stiffness. In one study, diabetes was associated with higher aortic PWV and prediabetes was associated with higher brachial-ankle PWV, a measure of composite stiffness (Loehr et al., 2016). Similarly, it has been shown that higher baPWV is associated with an increased risk of developing diabetes and that arterial stiffness may precede the increase in fasting blood glucose (Zheng et al., 2020). Arterial stiffness is also increased in patients with impaired fasting glucose but no other cardiovascular complications (Rerkpattanapipat et al., 2009). That study found that total vascular stiffness, but not thoracic aortic stiffness, is increased in patients with impaired fasting glucose compared to control subjects (Rerkpattanapipat et al., 2009).

CONCLUSION

One of the most important effects of aging on the cardiovascular system is a progressive increase in vascular stiffness. Understanding the extent to which vascular stiffness increases with aging and the mechanisms involved are important, since vascular stiffness is a critical factor in mediating the adverse effects of most cardiovascular diseases, including atherosclerosis, hypertension and diabetes. Many prior studies are limited in defining changes in vascular stiffness down the aortic tree, because only one section of the aorta was studied. We found that abdominal aortic stiffness is greater than thoracic aortic stiffness. However, this topic warrants further investigation as there are major sex differences. In men vascular stiffness increases progressively from young adulthood to old age. In women vascular stiffness increases, but to a lesser extent up to menopause, and then increases at a rate exceeding that for males after menopause. Less data are available on sex differences in animals, since the most commonly studied species are rodents, where females do not go through menopause, Their relevance for understanding human disease, therefore, is limited. Studies of sex differences in the changes in vascular stiffness associated with age are best carried out in humans without associated cardiovascular diseases, and in non-human primates that live over 30 years and, like human females, go through menopause. Several mechanisms mediate the protection in females, with the most significant one being the female hormone, estrogen, which is present up to menopause and then declines. Other important mechanisms of increased vascular stiffness include changes in the extracellular matrix, with increases in vascular collagen and decreases in vascular elastin. It is also known that calcium deposition and endothelial dysfunction in the vessels contribute to increased vascular stiffness. Less well studied mechanisms may also contribute, such as collagen and elastin disarray, and increased vascular smooth muscle cell stiffness and numbers. Additional insights come from studies in populations with an extended lifespan that live in areas known as "Blue Zones." People in these areas maintain a healthy diet and daily exercise and have lesser increases in vascular stiffness with age. Understanding how these environmental factors influence the progression of vascular stiffness may provide critical insights into retarding its progression and, thereby reducing cardiovascular disease.

FUTURE DIRECTIONS

As elucidated in this review, considerable progress has been made in understanding the role of vascular stiffness in normal biology and aging as well as in mediating changes in disease states. However, considerably more work needs to be done in this field. Differences in stiffness down the aortic tree in regional arteries and veins and arterial resistance vessels requires further research, since most prior work only examined the aorta. More work is also required to understand the divergent effects of increased aortic stiffness in males and females, and the role of sex hormones in mediating those differences. There is much more to be learned about the molecular mechanisms mediating changes in arterial stiffness. There is also much more clarification needed to understand the relationship between disease states in affecting changes in vascular stiffness, and conversely, how vascular stiffness mediates disease states. An important example is atherosclerosis, where it is needed to understand the extent to which changes in vascular function in atherosclerosis are due to changes in vascular stiffness vs. changes due to atheroma.

AUTHOR CONTRIBUTIONS

SV: conceptualization. SV, JZ, CV, KM, and DV: writing—original draft. SV, JZ, CV, KM, RG, and DV: writing—review and editing. All authors contributed to the article and approved the submitted version.

FUNDING

This study was supported by the National Institutes of Health grants: R01HL137368 and R01HL137405.

REFERENCES

Ahimastos, A. A., Formosa, M., Dart, A. M., and Kingwell, B. A. (2003). Gender differences in large artery stiffness pre- and post puberty. *J. Clin. Endocrinol. Metab.* 88, 5375–5380. doi: 10.1210/jc.2003-030722

Ahmet, I., Tae, H. J., De Cabo, R., Lakatta, E. G., and Talan, M. I. (2011). Effects of calorie restriction on cardioprotection and cardiovascular health. *J. Mol. Cell Cardiol.* 51, 263–271. doi: 10.1016/j.yjmcc.2011.04.015

Alghatrif, M., Strait, J. B., Morrell, C. H., Canepa, M., Wright, J., Elango, P., et al. (2013). Longitudinal trajectories of arterial stiffness and the role of blood pressure: the Baltimore Longitudinal Study of Aging. *Hypertension* 62, 934–941. doi: 10.1161/HYPERTENSIONAHA.113.01445

Aliev, G., and Burnstock, G. (1998). Watanabe rabbits with heritable hypercholesterolaemia: a model of atherosclerosis. *Histol. Histopathol.* 13, 797–817.

Anderson, T. J. (2006). Arterial stiffness or endothelial dysfunction as a surrogate marker of vascular risk. *Can. J. Cardiol.* 22(Suppl. B), 72B–80B.

Aronson, D. (2003). Cross-linking of glycated collagen in the pathogenesis of arterial and myocardial stiffening of aging and diabetes. *J. Hypertens.* 21, 3–12.

Astrand, H., Stalhand, J., Karlsson, J., Karlsson, M., Sonesson, B., and Lanne, T. (2011). In vivo estimation of the contribution of elastin and collagen to the mechanical properties in the human abdominal aorta: effect of age and sex. *J. Appl. Physiol.* 110, 176–187. doi: 10.1152/japplphysiol.00579.2010

Atanasova, M., Dimitrova, A., Ruseva, B., Stoyanova, A., Georgieva, M., and Konova, E. (2012). "Quantification of elastin, collagen and advanced glycation end products as functions of age and hypertension," in *Agriculture and Biological Sciences, Senescence*, ed. T. Nagata (London: InTechOpen).

Babici, D., Kudej, R. K., Mcnulty, T., Zhang, J., Oydanich, M., Berkman, T., et al. (2020). Mechanisms of increased vascular stiffness down the aortic tree in aging, premenopausal female monkeys. *Am. J. Physiol. Heart Circ. Physiol.* 319, H222–H234. doi: 10.1152/ajpheart.00153.2020

Baldo, M. P., Brant, L. C. C., Cunha, R. S., Molina, M., Griep, R. H., Barreto, S. M., et al. (2019). The association between salt intake and arterial stiffness is influenced by a sex-specific mediating effect through blood pressure in normotensive adults: the ELSA-Brasil study. *J. Clin. Hypertens.* 21, 1771–1779. doi: 10.1111/jch.13728

Barton, M., Cosentino, F., Brandes, R. P., Moreau, P., Shaw, S., and Lüscher, T. F. (1997). Anatomic heterogeneity of vascular aging. *Hypertension* 30, 817–824. doi: 10.1161/01.hyp.30.4.817

Bavishi, C., Goel, S., and Messerli, F. H. (2016). Isolated systolic hypertension: an update after SPRINT. *Am. J. Med.* 129, 1251–1258. doi: 10.1016/j.amjmed.2016.08.032

Benetos, A., Laurent, S., Hoeks, A. P., Boutouyrie, P. H., and Safar, M. E. (1993). Arterial alterations with aging and high blood pressure. A noninvasive study of carotid and femoral arteries. *Arterioscler. Thromb.* 13, 90–97.

Blaha, M. J., Budoff, M. J., Rivera, J. J., Katz, R., O'leary, D. H., Polak, J. F., et al. (2009). Relationship of carotid distensibility and thoracic aorta calcification: multi-ethnic study of atherosclerosis. *Hypertension* 54, 1408–1415. doi: 10.1161/HYPERTENSIONAHA.109.138396

Blenck, C. L., Harvey, P. A., Reckelhoff, J. F., and Leinwand, L. A. (2016). The importance of biological sex and estrogen in rodent models of cardiovascular health and disease. *Circ. Res.* 118, 1294–1312.

Boardman, H. M., Hartley, L., Eisinga, A., Main, C., Roque, I., Figuls, M., et al. (2015). Hormone therapy for preventing cardiovascular disease in post-menopausal women. *Cochrane Database Syst. Rev.* 10:CD002229.

Boutouyrie, P., Laurent, S., Girerd, X., Benetos, A., Lacolley, P., Abergel, E., et al. (1995). Common carotid artery stiffness and patterns of left ventricular hypertrophy in hypertensive patients. *Hypertension* 25, 651–659. doi: 10.1161/01.hyp.25.4.651

Briones, A. M., Arribas, S. M., and Salaices, M. (2010). Role of extracellular matrix in vascular remodeling of hypertension. *Curr. Opin. Nephrol. Hypertens.* 19, 187–194. doi: 10.1097/mnh.0b013e328335eec9

Buettner, D., and Skemp, S. (2016). Blue zones: lessons from the world's longest lived. *Am. J. Lifestyle Med.* 10, 318–321. doi: 10.1177/1559827616637066

Byon, C. H., Javed, A., Dai, Q., Kappes, J. C., Clemens, T. L., Darley-Usmar, V. M., et al. (2008). Oxidative stress induces vascular calcification through modulation of the osteogenic transcription factor Runx2 by AKT signaling*. *J. Biol. Chem.* 283, 15319–15327. doi: 10.1074/jbc.M800021200

Cameron, J. D., Bulpitt, C. J., Pinto, E. S., and Rajkumar, C. (2003). The aging of elastic and muscular arteries: a comparison of diabetic and nondiabetic subjects. *Diabetes Care* 26, 2133–2138. doi: 10.2337/diacare.26.7.2133

Cameron, J. D., and Cruickshank, J. K. (2007). Glucose, insulin, diabetes and mechanisms of arterial dysfunction. *Clin. Exp. Pharmacol. Physiol.* 34, 677–682.

Cecelja, M., Hussain, T., Greil, G., Botnar, R., Preston, R., Moayyeri, A., et al. (2013). Multimodality imaging of subclinical aortic atherosclerosis: relation of aortic stiffness to calcification and plaque in female twins. *Hypertension* 61, 609–614. doi: 10.1161/HYPERTENSIONAHA.111.00024

Chamiot-Clerc, P., Renaud, J. F., and Safar, M. E. (2001). Pulse pressure, aortic reactivity, and endothelium dysfunction in old hypertensive rats. *Hypertension* 37, 313–321.

Chi, C., Li, D. J., Jiang, Y. J., Tong, J., Fu, H., Wu, Y. H., et al. (2019). Vascular smooth muscle cell senescence and age-related diseases: State of the art. *Biochim. Biophys. Acta Mol. Basis Dis.* 1865, 1810–1821. doi: 10.1016/j.bbadis.2018.08.015

Collins, J. A., Munoz, J.-V., Patel, T. R., Loukas, M., and Tubbs, R. S. (2014). The anatomy of the aging aorta. *Clin. Anat.* 27, 463–466. doi: 10.1002/ca.22384

Coutinho, T., Borlaug, B. A., Pellikka, P. A., Turner, S. T., and Kullo, I. J. (2013). Sex differences in arterial stiffness and ventricular-arterial interactions. *J. Am. Coll. Cardiol.* 61, 96–103.

Csiszar, A., Labinskyy, N., Orosz, Z., Xiangmin, Z., Buffenstein, R., and Ungvari, Z. (2007). Vascular aging in the longest-living rodent, the naked mole rat. *Am. J. Physiol. Heart Circ. Physiol.* 293, H919–H927.

Cuomo, F., Roccabianca, S., Dillon-Murphy, D., Xiao, N., Humphrey, J. D., and Figueroa, C. A. (2017). Effects of age-associated regional changes in aortic stiffness on human hemodynamics revealed by computational modeling. *PLoS One* 12:e0173177. doi: 10.1371/journal.pone.0173177

Dammann, P., and Burda, H. (2006). Sexual activity and reproduction delay ageing in a mammal. *Curr. Biol.* 16, R117–R118. doi: 10.1016/j.cub.2006.02.012

Devos, D. G., Rietzschel, E., Heyse, C., Vandemaele, P., Van Bortel, L., Babin, D., et al. (2015). MR pulse wave velocity increases with age faster in the thoracic aorta than in the abdominal aorta. *J. Magn. Reson. Imaging* 41, 765–772. doi: 10.1002/jmri.24592

Donato, A. J., Machin, D. R., and Lesniewski, L. A. (2018). Mechanisms of dysfunction in the aging vasculature and role in age-related disease. *Circ. Res.* 123, 825–848. doi: 10.1161/circresaha.118.312563

Dubey, R. K., Gillespie, D. G., Zacharia, L. C., Rosselli, M., Korzekwa, K. R., Fingerle, J., et al. (2000a). Methoxyestradiols mediate the antimitogenic effects of estradiol on vascular smooth muscle cells via estrogen receptor-independent mechanisms. *Biochem. Biophys. Res. Commun.* 278, 27–33. doi: 10.1006/bbrc.2000.3755

Dubey, R. K., Jackson, E. K., Gillespie, D. G., Zacharia, L. C., Imthurn, B., and Keller, P. J. (2000b). Clinically used estrogens differentially inhibit human aortic smooth muscle cell growth and mitogen-activated protein kinase activity. *Arterioscler. Thromb. Vasc. Biol.* 20, 964–972. doi: 10.1161/01.atv.20.4.964

Dupont, J. J., Kenney, R. M., Patel, A. R., and Jaffe, I. Z. (2019). Sex differences in mechanisms of arterial stiffness. *Br. J. Pharmacol.* 176, 4208–4225. doi: 10.1111/bph.14624

Faber, M., and Oller-Hou, G. (1952). The human aorta. V. Collagen and elastin in the normal and hypertensive aorta. *Acta Pathol. Microbiol. Scand.* 31, 377–382.

Farrar, D. J., Bond, M. G., Sawyer, J. K., and Green, H. D. (1984). Pulse wave velocity and morphological changes associated with early atherosclerosis progression in the aortas of cynomolgus monkeys. *Cardiovasc. Res.* 18, 107–118. doi: 10.1093/cvr/18.2.107

Fischer, G. M., and Llaurado, J. G. (1966). Collagen and elastin content in canine arteries selected from functionally different vascular beds. *Circ. Res.* 19, 394–399. doi: 10.1161/01.res.19.2.394

Fitch, R. M., Vergona, R., Sullivan, M. E., and Wang, Y.-X. (2001). Nitric oxide synthase inhibition increases aortic stiffness measured by pulse wave velocity in rats. *Cardiovasc. Res.* 51, 351–358. doi: 10.1016/s0008-6363(01)00299-1

Fleenor, B. S., Marshall, K. D., Durrant, J. R., Lesniewski, L. A., and Seals, D. R. (2010). Arterial stiffening with ageing is associated with transforming growth factor-β1-related changes in adventitial collagen: reversal by aerobic exercise. *J. Physiol.* 588, 3971–3982. doi: 10.1113/jphysiol.2010.194753

Fleenor, B. S., Marshall, K. D., Rippe, C., and Seals, D. R. (2012). Replicative aging induces endothelial to mesenchymal transition in human aortic endothelial

cells: potential role of inflammation. *J. Vasc. Res.* 49, 59–64. doi: 10.1159/000329681

Fornieri, C., Quaglino, D. Jr., and Mori, G. (1992). Role of the extracellular matrix in age-related modifications of the rat aorta. Ultrastructural, morphometric, and enzymatic evaluations. *Arterioscler. Thromb.* 12, 1008–1016. doi: 10.1161/01.atv.12.9.1008

Fornieri, C., Taparelli, F., Quaglino, D. Jr., Contri, M. B., Davidson, J. M., Algeri, S., et al. (1999). The effect of caloric restriction on the aortic tissue of aging rats. *Connect. Tissue Res.* 40, 131–143. doi: 10.3109/03008209909029109

Franklin, S. S., Gustin, W. T., Wong, N. D., Larson, M. G., Weber, M. A., Kannel, W. B., et al. (1997). Hemodynamic patterns of age-related changes in blood pressure. The Framingham Heart Study. *Circulation* 96, 308–315. doi: 10.1161/01.cir.96.1.308

Furchgott, R. F., and Zawadzki, J. V. (1980). The obligatory role of endothelial cells in the relaxation of arterial smooth muscle by acetylcholine. *Nature* 288, 373–376. doi: 10.1038/288373a0

Galis, Z. S., Sukhova, G. K., Lark, M. W., and Libby, P. (1994). Increased expression of matrix metalloproteinases and matrix degrading activity in vulnerable regions of human atherosclerotic plaques. *J. Clin. Invest.* 94, 2493–2503. doi: 10.1172/JCI117619

Gerhard-Herman, M., Smoot, L. B., Wake, N., Kieran, M. W., Kleinman, M. E., Miller, D. T., et al. (2012). Mechanisms of premature vascular aging in children with Hutchinson-Gilford progeria syndrome. *Hypertension* 59, 92–97.

Getz, G. S., and Reardon, C. A. (2012). Animal models of atherosclerosis. *Arterioscler. Thromb. Vasc. Biol.* 32, 1104–1115.

Giacco, F., and Brownlee, M. (2010). Oxidative stress and diabetic complications. *Circ. Res.* 107, 1058–1070.

Goldin, A., Beckman, J. A., Schmidt, A. M., and Creager, M. A. (2006). Advanced glycation end products. *Circulation* 114, 597–605.

Gordon, L. B., Harten, I. A., Patti, M. E., and Lichtenstein, A. H. (2005). Reduced adiponectin and HDL cholesterol without elevated C-reactive protein: clues to the biology of premature atherosclerosis in Hutchinson-Gilford Progeria Syndrome. *J. Pediatr.* 146, 336–341. doi: 10.1016/j.jpeds.2004.10.064

Gordon, L. B., Kleinman, M. E., Miller, D. T., Neuberg, D. S., Giobbie-Hurder, A., Gerhard-Herman, M., et al. (2012). Clinical trial of a farnesyltransferase inhibitor in children with Hutchinson-Gilford progeria syndrome. *Proc. Natl. Acad. Sci. U.S.A.* 109, 16666–16671.

Greenberg, S. R. (1986). The association of medial collagenous tissue with atheroma formation in the aging human aorta as revealed by a special technique. *Histol. Histopathol.* 1, 323–326.

Greenwald, S. E. (2007). Ageing of the conduit arteries. *J. Pathol.* 211, 157–172. doi: 10.1002/path.2101

Grimes, K. M., Reddy, A. K., Lindsey, M. L., and Buffenstein, R. (2014). And the beat goes on: maintained cardiovascular function during aging in the longest-lived rodent, the naked mole-rat. *Am. J. Physiol. Heart Circ. Physiol.* 307, H284–H291. doi: 10.1152/ajpheart.00305.2014

Guo, J., Fujiyoshi, A., Willcox, B., Choo, J., Vishnu, A., Hisamatsu, T., et al. (2017). Increased aortic calcification is associated with arterial stiffness progression in multiethnic middle-aged men. *Hypertension* 69, 102–108. doi: 10.1161/HYPERTENSIONAHA.116.08459

Guo, X., Lu, X., Ren, H., Levin, E. R., and Kassab, G. S. (2006). Estrogen modulates the mechanical homeostasis of mouse arterial vessels through nitric oxide. *Am. J. Physiol. Heart Circ. Physiol.* 290, H1788–H1797. doi: 10.1152/ajpheart.01070.2005

Hager, A., Kaemmerer, H., Rapp-Bernhardt, U., Blücher, S., Rapp, K., Bernhardt, T. M., et al. (2002). Diameters of the thoracic aorta throughout life as measured with helical computed tomography. *J. Thorac. Cardiovasc. Surg.* 123, 1060–1066. doi: 10.1067/mtc.2002.122310

Hagg, S., and Jylhava, J. (2021). Sex differences in biological aging with a focus on human studies. *eLife* 10:e63425.

Haskett, D., Johnson, G., Zhou, A., Utzinger, U., and Vande Geest, J. (2010). Microstructural and biomechanical alterations of the human aorta as a function of age and location. *Biomech. Model. Mechanobiol.* 9, 725–736. doi: 10.1007/s10237-010-0209-7

Hausvater, A., Giannone, T., Sandoval, Y. H., Doonan, R. J., Antonopoulos, C. N., Matsoukis, I. L., et al. (2012). The association between preeclampsia and arterial stiffness. *J. Hypertens.* 30, 17–33.

Henry, R. M. A., Kostense, P. J., Spijkerman, A. M. W., Dekker, J. M., Nijpels, G., Heine, R. J., et al. (2003). Arterial stiffness increases with deteriorating glucose tolerance status. *Circulation* 107, 2089–2095. doi: 10.1161/01.cir.0000065222.34933.fc

Hickson, S. S., Butlin, M., Graves, M., Taviani, V., Avolio, A. P., Mceniery, C. M., et al. (2010). The relationship of age with regional aortic stiffness and diameter. *JACC Cardiovasc Imaging* 3, 1247–1255. doi: 10.1016/j.jcmg.2010.09.016

Hofmann Bowman, M., Wilk, J., Heydemann, A., Kim, G., Rehman, J., Lodato, J. A., et al. (2010). S100A12 mediates aortic wall remodeling and aortic aneurysm. *Circ. Res.* 106, 145–154. doi: 10.1161/CIRCRESAHA.109.209486

Hornebeck, W., and Partridge, S. M. (1975). Conformational changes in fibrous elastin due to calcium ions. *Eur. J. Biochem.* 51, 73–78. doi: 10.1111/j.1432-1033.1975.tb03908.x

Hosoda, Y., Kawano, K., Yamasawa, F., Ishii, T., Shibata, T., and Inayama, S. (1984). Age-dependent changes of collagen and elastin content in human aorta and pulmonary artery. *Angiology* 35, 615–621. doi: 10.1177/000331978403501001

Huang, Y., and Mark Jacquez, G. (2017). Identification of a blue zone in a typical chinese longevity region. *Int. J. Environ. Res. Public Health* 14:571. doi: 10.3390/ijerph14060571

Humphrey, J. D., Harrison, D. G., Figueroa, C. A., Lacolley, P., and Laurent, S. (2016). Central artery stiffness in hypertension and aging. *Circ. Res.* 118, 379–381. doi: 10.1161/circresaha.115.307722

Iribarren, C., Sidney, S., Sternfeld, B., and Browner, W. S. (2000). Calcification of the aortic archrisk factors and association with coronary heart disease, stroke, and peripheral vascular disease. *JAMA* 283, 2810–2815. doi: 10.1001/jama.283.21.2810

Jaminon, A., Reesink, K., Kroon, A., and Schurgers, L. (2019). The role of vascular smooth muscle cells in arterial remodeling: focus on calcification-related processes. *Int. J. Mol. Sci.* 20:5694. doi: 10.3390/ijms20225694

Johnson, R. C., Leopold, J. A., and Loscalzo, J. (2006). Vascular calcification: pathobiological mechanisms and clinical implications. *Circ. Res.* 99, 1044–1059. doi: 10.1161/01.res.0000249379.55535.21

Kanabrocki, E. L., Fels, I. G., and Kaplan, E. (1960). Calcium, cholesterol, and collagen levels in human aortas. *J. Gerontol.* 15, 383–387.

Katsuda, S.-I., Takazawa, K., Miyake, M., Kobayashi, D., Kusanagi, M., and Hazama, A. (2014). Local pulse wave velocity directly reflects increased arterial stiffness in a restricted aortic region with progression of atherosclerotic lesions. *Hypertens. Res.* 37, 892–900. doi: 10.1038/hr.2014.96

Kawasaki, T., Sasayama, S., Yagi, S., Asakawa, T., and Hirai, T. (1987). Non-invasive assessment of the age related changes in stiffness of major branches of the human arteries. *Cardiovasc. Res.* 21, 678–687. doi: 10.1093/cvr/21.9.678

Keay, A. J., Oliver, M. F., and Boyd, G. S. (1955). Progeria and atherosclerosis. *Arch. Dis. Child.* 30, 410–414. doi: 10.1136/adc.30.153.410

Kohn, J. C., Lampi, M. C., and Reinhart-King, C. A. (2015). Age-related vascular stiffening: causes and consequences. *Front. Genet.* 6:112.

Komutrattananont, P., Mahakkanukrauh, P., and Das, S. (2019). Morphology of the human aorta and age-related changes: anatomical facts. *Anat. Cell Biol.* 52, 109–114. doi: 10.5115/acb.2019.52.2.109

Lacolley, P., Regnault, V., Nicoletti, A., Li, Z., and Michel, J. B. (2012). The vascular smooth muscle cell in arterial pathology: a cell that can take on multiple roles. *Cardiovasc. Res.* 95, 194–204.

Larocca, T. J., Gioscia-Ryan, R. A., Hearon, C. M., and Seals, D. R. (2013). The autophagy enhancer spermidine reverses arterial aging. *Mech. Ageing Dev.* 134, 314–320. doi: 10.1016/j.mad.2013.04.004

Larocca, T. J., Henson, G. D., Thorburn, A., Sindler, A. L., Pierce, G. L., and Seals, D. R. (2012). Translational evidence that impaired autophagy contributes to arterial ageing. *J. Physiol.* 590, 3305–3316. doi: 10.1113/jphysiol.2012.229690

Laurent, S., and Boutouyrie, P. (2020). Arterial stiffness and hypertension in the elderly. *Front. Cardiovasc. Med.* 7:544302. doi: 10.3389/fcvm.2020.544302

Lee, J., Shen, M., Parajuli, N., Oudit, G. Y., Mcmurtry, M. S., and Kassiri, Z. (2014). Gender-dependent aortic remodelling in patients with bicuspid aortic valve-associated thoracic aortic aneurysm. *J. Mol. Med.* 92, 939–949. doi: 10.1007/s00109-014-1178-6

Linton, M. R. F., Yancey, P. G., Davies, S. S., Jerome, W. G., Linton, E. F., Song, W. L., et al. (eds) (2000). "The role of lipids and lipoproteins in atherosclerosis," in *Endotext*, (South Dartmouth, MA: MDText.com, Inc).

Loehr, L. R., Meyer, M. L., Poon, A. K., Selvin, E., Palta, P., Tanaka, H., et al. (2016). Prediabetes and diabetes are associated with arterial stiffness in older adults: the ARIC Study. *Am. J. Hypertens.* 29, 1038–1045.

London, G. M., Guérin, A. P., Marchais, S. J., Métivier, F., Pannier, B., and Adda, H. (2003). Arterial media calcification in end-stage renal disease: impact on all-cause and cardiovascular mortality. *Nephrol. Dial. Transplant.* 18, 1731–1740. doi: 10.1093/ndt/gfg414

London, G. M., Guerin, A. P., Pannier, B., Marchais, S. J., and Stimpel, M. (1995). Influence of sex on arterial hemodynamics and blood pressure. Role of body height. *Hypertension* 26, 514–519.

Luttrell, M., Kim, H., Shin, S. Y., Holly, D., Massett, M. P., and Woodman, C. R. (2020). Heterogeneous effect of aging on vasorelaxation responses in large and small arteries. *Physiol. Rep.* 8:e14341.

Ma, Z., Mao, C., Jia, Y., Fu, Y., and Kong, W. (2020). Extracellular matrix dynamics in vascular remodeling. *Am. J. Physiol. Cell Physiol.* 319, C481–C499.

Mackey, R. H., Venkitachalam, L., and Sutton-Tyrrell, K. (2007). Calcifications, arterial stiffness and atherosclerosis. *Adv. Cardiol.* 44, 234–244. doi: 10.1159/000096744

Mancia, G., Fagard, R., Narkiewicz, K., Redon, J., Zanchetti, A., Böhm, M., et al. (2013). 2013 ESH/ESC guidelines for the management of arterial hypertension: the Task Force for the management of arterial hypertension of the European Society of Hypertension (ESH) and of the European Society of Cardiology (ESC). *Eur. Heart J.* 34, 2159–2219.

Maurel, E., Shuttleworth, C. A., and Bouissou, H. (1987). Interstitial collagens and ageing in human aorta. *Virchows Arch. A Pathol. Anat. Histopathol.* 410, 383–390. doi: 10.1007/bf00712757

Mceniery, C. M., Mcdonnell, B. J., So, A., Aitken, S., Bolton, C. E., Munnery, M., et al. (2009). Aortic calcification is associated with aortic stiffness and isolated systolic hypertension in healthy individuals. *Hypertension* 53, 524–531. doi: 10.1161/HYPERTENSIONAHA.108.126615

Mceniery, C. M., Wallace, S., Mackenzie, I. S., Mcdonnell, B., Yasmin, Newby, D. E., et al. (2006). Endothelial function is associated with pulse pressure, pulse wave velocity, and augmentation index in healthy humans. *Hypertension* 48, 602–608. doi: 10.1161/01.hyp.0000239206.64270.5f

Medley, T. L., Cole, T. J., Gatzka, C. D., Wang, W. Y., Dart, A. M., and Kingwell, B. A. (2002). Fibrillin-1 genotype is associated with aortic stiffness and disease severity in patients with coronary artery disease. *Circulation* 105, 810–815. doi: 10.1161/hc0702.104129

Melo, E. S. F. V., Almonfrey, F. B., Freitas, C. M. N., Fonte, F. K., Sepulvida, M. B. C., Almada-Filho, C. M., et al. (2021). Association of body composition with arterial stiffness in long-lived people. *Arq. Bras. Cardiol.* 117, 457–462. doi: 10.36660/abc.20190774

Millasseau, S. C., Stewart, A. D., Patel, S. J., Redwood, S. R., and Chowienczyk, P. J. (2005). Evaluation of carotid-femoral pulse wave velocity. *Hypertension* 45, 222–226.

Mitchell, G. F., Parise, H., Benjamin, E. J., Larson, M. G., Keyes, M. J., Vita, J. A., et al. (2004). Changes in arterial stiffness and wave reflection with advancing age in healthy men and women. *Hypertension* 43, 1239–1245. doi: 10.1161/01.HYP.0000128420.01881.aa

Moreau, K. L., and Hildreth, K. L. (2014). Vascular aging across the menopause transition in healthy women. *Adv. Vasc. Med.* 2014:204390.

Moreau, K. L., Meditz, A., Deane, K. D., and Kohrt, W. M. (2012). Tetrahydrobiopterin improves endothelial function and decreases arterial stiffness in estrogen-deficient postmenopausal women. *Am. J. Physiol. Heart Circ. Physiol.* 302, H1211–H1218. doi: 10.1152/ajpheart.01065.2011

Mueller, N. T., Noya-Alarcon, O., Contreras, M., Appel, L. J., and Dominguez-Bello, M. G. (2018). Association of age with blood pressure across the lifespan in isolated yanomami and yekwana villages. *JAMA Cardiol.* 3, 1247–1249. doi: 10.1001/jamacardio.2018.3676

Nelson, A. J., Worthley, S. G., Cameron, J. D., Willoughby, S. R., Piantadosi, C., Carbone, A., et al. (2009). Cardiovascular magnetic resonance-derived aortic distensibility: validation and observed regional differences in the elderly. *J. Hypertens.* 27, 535–542.

Nethononda, R. M., Lewandowski, A. J., Stewart, R., Kylinterias, I., Whitworth, P., Francis, J., et al. (2015). Gender specific patterns of age-related decline in aortic stiffness: a cardiovascular magnetic resonance study including normal ranges. *J. Cardiovasc. Magn. Reson.* 17:20. doi: 10.1186/s12968-015-0126-0

Nosaka, T., Tanaka, H., Watanabe, I., Sato, M., and Matsuda, M. (2003). Influence of regular exercise on age-related changes in arterial elasticity: mechanistic insights from wall compositions in rat aorta. *Can. J. Appl. Physiol.* 28, 204–212. doi: 10.1139/h03-016

Ogola, B. O., Zimmerman, M. A., Clark, G. L., Abshire, C. M., Gentry, K. M., Miller, K. S., et al. (2018). New insights into arterial stiffening: does sex matter? *Am. J. Physiol. Heart Circ. Physiol.* 315, H1073–H1087. doi: 10.1152/ajpheart.00132.2018

O'Rourke, M. F., Staessen, J. A., Vlachopoulos, C., Duprez, D., and Plante, G. ÉE. (2002). Clinical applications of arterial stiffness; definitions and reference values. *Am. J. Hypertens.* 15, 426–444. doi: 10.1016/s0895-7061(01)02319-6

Pagani, M., Mirsky, I., Baig, H., Manders, W. T., Kerkhof, P., and Vatner, S. F. (1979). Effects of age on aortic pressure-diameter and elastic stiffness-stress relationships in unanesthetized sheep. *Circ. Res.* 44, 420–429. doi: 10.1161/01.res.44.3.420

Pannier, B. M., Avolio, A. P., Hoeks, A., Mancia, G., and Takazawa, K. (2002). Methods and devices for measuring arterial compliance in humans. *Am. J. Hypertens.* 15, 743–753. doi: 10.1016/s0895-7061(02)02962-x

Pasupuleti, V. R., Arigela, C. S., Gan, S. H., Salam, S. K. N., Krishnan, K. T., Rahman, N. A., et al. (2020). A review on oxidative stress, diabetic complications, and the roles of honey polyphenols. *Oxid. Med. Cell Longev.* 2020:8878172. doi: 10.1155/2020/8878172

Pescatore, L. A., Gamarra, L. F., and Liberman, M. (2019). Multifaceted mechanisms of vascular calcification in aging. *Arterioscler. Thromb. Vasc. Biol.* 39, 1307–1316. doi: 10.1161/ATVBAHA.118.311576

Pezzini, A., Del Zotto, E., Giossi, A., Volonghi, I., Costa, P., and Padovani, A. (2012). Transforming growth factor beta signaling perturbation in the Loeys-Dietz syndrome. *Curr. Med. Chem.* 19, 454–460.

Pietri, P., Vlachopoulos, C., Chrysohoou, C., Lazaros, G., Masoura, K., Ioakeimidis, N., et al. (2015). Deceleration of age-related aortic stiffening in a population with high longevity rates: the IKARIA study. *J. Am. Coll. Cardiol.* 66, 1842–1843. doi: 10.1016/j.jacc.2015.07.070

Pirro, M., Schillaci, G., Paltriccia, R., Bagaglia, F., Menecali, C., Mannarino, M. R., et al. (2006). Increased ratio of CD31+/CD42- microparticles to endothelial progenitors as a novel marker of atherosclerosis in hypercholesterolemia. *Arterioscler. Thromb. Vasc. Biol.* 26, 2530–2535. doi: 10.1161/01.ATV.0000243941.72375.15

Podlutsky, A. J., Khritankov, A. M., Ovodov, N. D., and Austad, S. N. (2005). A new field record for bat longevity. *J. Gerontol. A Biol. Sci. Med. Sci.* 60, 1366–1368. doi: 10.1093/gerona/60.11.1366

Poznyak, A., Grechko, A. V., Poggio, P., Myasoedova, V. A., Alfieri, V., and Orekhov, A. N. (2020). The diabetes mellitus-atherosclerosis connection: the role of lipid and glucose metabolism and chronic inflammation. *Int. J. Mol. Sci.* 21:1835. doi: 10.3390/ijms21051835

Prenner, S. B., and Chirinos, J. A. (2015). Arterial stiffness in diabetes mellitus. *Atherosclerosis* 238, 370–379.

Qiu, H., Depre, C., Ghosh, K., Resuello, R. G., Natividad, F. F., Rossi, F., et al. (2007a). Mechanism of gender-specific differences in aortic stiffness with aging in nonhuman primates. *Circulation* 116, 669–676. doi: 10.1161/CIRCULATIONAHA.107.689208

Qiu, H., Tian, B., Resuello, R. G., Natividad, F. F., Peppas, A., Shen, Y. T., et al. (2007b). Sex-specific regulation of gene expression in the aging monkey aorta. *Physiol. Genomics* 29, 169–180. doi: 10.1152/physiolgenomics.00229.2006

Qiu, H., Zhu, Y., Sun, Z., Trzeciakowski, J. P., Gansner, M., Depre, C., et al. (2010). Short communication: vascular smooth muscle cell stiffness as a mechanism for increased aortic stiffness with aging. *Circ. Res.* 107, 615–619. doi: 10.1161/CIRCRESAHA.110.221846

Quesada, V., Freitas-Rodriguez, S., Miller, J., Perez-Silva, J. G., Jiang, Z. F., Tapia, W., et al. (2019). Giant tortoise genomes provide insights into longevity and age-related disease. *Nat. Ecol. Evol.* 3, 87–95. doi: 10.1038/s41559-018-0733-x

Ravussin, E., Redman, L. M., Rochon, J., Das, S. K., Fontana, L., Kraus, W. E., et al. (2015). A 2-year randomized controlled trial of human caloric restriction: feasibility and effects on predictors of health span and longevity. *J. Gerontol. A Biol. Sci. Med. Sci.* 70, 1097–1104. doi: 10.1093/gerona/glv057

Reddy, G. K. (2004). Cross-linking in collagen by nonenzymatic glycation increases the matrix stiffness in rabbit achilles tendon. *Exp. Diabesity Res.* 5, 143–153.

Redei, E. E., and Mehta, N. S. (2015). Blood transcriptomic markers for major depression: from animal models to clinical settings. *Ann. N. Y. Acad. Sci.* 1344, 37–49. doi: 10.1111/nyas.12748

Redman, L. M., Smith, S. R., Burton, J. H., Martin, C. K., Il'yasova, D., and Ravussin, E. (2018). Metabolic slowing and reduced oxidative damage with sustained caloric restriction support the rate of living and oxidative damage theories of aging. *Cell Metab.* 27, 805.e4–815.e4. doi: 10.1016/j.cmet.2018.02.019

Rerkpattanapipat, P., D'agostino, R. B. Jr., Link, K. M., Shahar, E., Lima, J. A., Bluemke, D. A., et al. (2009). Location of arterial stiffening differs in those with impaired fasting glucose versus diabetes: implications for left ventricular hypertrophy from the Multi-Ethnic Study of Atherosclerosis. *Diabetes Metab. Res. Rev.* 58, 946–953. doi: 10.2337/db08-1192

Rizzoni, D., Porteri, E., Guelfi, D., Muiesan, M. L., Valentini, U., Cimino, A., et al. (2001). Structural alterations in subcutaneous small arteries of normotensive and hypertensive patients with non–insulin-dependent diabetes mellitus. *Circulation* 103, 1238–1244.

Rogers, I. S., Massaro, J. M., Truong, Q. A., Mahabadi, A. A., Kriegel, M. F., Fox, C. S., et al. (2013). Distribution, determinants, and normal reference values of thoracic and abdominal aortic diameters by computed tomography (from the Framingham Heart Study). *Am. J. Cardiol.* 111, 1510–1516. doi: 10.1016/j.amjcard.2013.01.306

Rogers, W. J., Hu, Y. L., Coast, D., Vido, D. A., Kramer, C. M., Pyeritz, R. E., et al. (2001). Age-associated changes in regional aortic pulse wave velocity. *J. Am. Coll. Cardiol.* 38, 1123–1129. doi: 10.1016/s0735-1097(01)01504-2

Safar, M. E., Asmar, R., Benetos, A., Blacher, J., Boutouyrie, P., Lacolley, P., et al. (2018). Interaction between hypertension and arterial stiffness. *Hypertension* 72, 796–805. doi: 10.1161/hypertensionaha.118.11212

Sans, M., and Moragas, A. (1993). Mathematical morphologic analysis of the aortic medial structure. Biomechanical implications. *Anal. Quant. Cytol. Histol.* 15, 93–100.

Santhanam, L., Tuday, E. C., Webb, A. K., Dowzicky, P., Kim, J. H., Oh, Y. J., et al. (2010). Decreased S-nitrosylation of tissue transglutaminase contributes to age-related increases in vascular stiffness. *Circ. Res.* 107, 117–125. doi: 10.1161/CIRCRESAHA.109.215228

Santos-Parker, J. R., Larocca, T. J., and Seals, D. R. (2014). Aerobic exercise and other healthy lifestyle factors that influence vascular aging. *Adv. Physiol. Educ.* 38, 296–307.

Schillaci, G., Verdecchia, P., Borgioni, C., Ciucci, A., and Porcellati, C. (1998). Early cardiac changes after menopause. *Hypertension* 32, 764–769.

Schlatmann, T. J. M., and Becker, A. E. (1977). Histologic changes in the normal aging aorta: implications for dissecting aortic aneurysm. *Am. J. Cardiol.* 39, 13–20.

Schleicher, E. D., Wagner, E., and Nerlich, A. G. (1997). Increased accumulation of the glycoxidation product N(epsilon)-(carboxymethyl)lysine in human tissues in diabetes and aging. *J. Clin. Invest.* 99, 457–468.

Schofield, I., Malik, R., Izzard, A., Austin, C., and Heagerty, A. (2002). Vascular structural and functional changes in type 2 diabetes mellitus. *Circulation* 106, 3037–3043.

Schram, M. T., Henry, R. M., van Dijk, R. A., Kostense, P. J., Dekker, J. M., Nijpels, G., et al. (2004). Increased central artery stiffness in impaired glucose metabolism and type 2 diabetes. *Hypertension* 43, 176–181. doi: 10.1161/01.hyp.0000111829.46090.92

Sehgel, N. L., Sun, Z., Hong, Z., Hunter, W. C., Hill, M. A., Vatner, D. E., et al. (2015a). Augmented vascular smooth muscle cell stiffness and adhesion when hypertension is superimposed on aging. *Hypertension* 65, 370–377. doi: 10.1161/HYPERTENSIONAHA.114.04456

Sehgel, N. L., Vatner, S. F., and Meininger, G. A. (2015b). "Smooth muscle cell stiffness syndrome"-revisiting the structural basis of arterial stiffness. *Front. Physiol.* 6:335. doi: 10.3389/fphys.2015.00335

Sehgel, N. L., Zhu, Y., Sun, Z., Trzeciakowski, J. P., Hong, Z., Hunter, W. C., et al. (2013). Increased vascular smooth muscle cell stiffness: a novel mechanism for aortic stiffness in hypertension. *Am. J. Physiol. Heart Circ. Physiol.* 305, H1281–H1287.

Shadwick, R. E., and Gosline, J. M. (1994). Arterial mechanics in the fin whale suggest a unique hemodynamic design. *Am. J. Physiol.* 267, R805–R818. doi: 10.1152/ajpregu.1994.267.3.R805

Siasos, G., Chrysohoou, C., Tousoulis, D., Oikonomou, E., Panagiotakos, D., Zaromitidou, M., et al. (2013). The impact of physical activity on endothelial function in middle-aged and elderly subjects: the Ikaria study. *Hellenic J. Cardiol.* 54, 94–101.

Sloop, G. D., Weidman, J. J., and Shecterle, L. M. (2015). The interplay of aging, aortic stiffness, and blood viscosity in atherogenesis. *J. Cardiol. Ther.* 2, 350–354.

Smulyan, H., Asmar, R. G., Rudnicki, A., London, G. M., and Safar, M. E. (2001). Comparative effects of aging in men and women on the properties of the arterial tree. *J. Am. Coll. Cardiol.* 37, 1374–1380. doi: 10.1016/s0735-1097(01)01166-4

Sokolis, D. P. (2007). Passive mechanical properties and structure of the aorta: segmental analysis. *Acta Physiol.* 190, 277–289. doi: 10.1111/j.1748-1716.2006.01661.x

Sorescu, G. P., Song, H., Tressel, S. L., Hwang, J., Dikalov, S., Smith, D. A., et al. (2004). Bone morphogenic protein 4 produced in endothelial cells by oscillatory shear stress induces monocyte adhesion by stimulating reactive oxygen species production from a nox1-based NADPH oxidase. *Circ. Res.* 95, 773–779. doi: 10.1161/01.RES.0000145728.22878.45

Staessen, J. A., Van Der Heijden-Spek, J. J., Safar, M. E., Den Hond, E., Gasowski, J., Fagard, R. H., et al. (2001). Menopause and the characteristics of the large arteries in a population study. *J. Hum. Hypertens.* 15, 511–518.

Stehouwer, C. D. A., Henry, R. M. A., and Ferreira, I. (2008). Arterial stiffness in diabetes and the metabolic syndrome: a pathway to cardiovascular disease. *Diabetologia* 51:527. doi: 10.1007/s00125-007-0918-3

Sugawara, J., Tomoto, T., Lin, H.-F., Chen, C.-H., and Tanaka, H. (2018). Aortic reservoir function of Japanese female pearl divers. *J. Appl. Physiol.* 125, 1901–1905. doi: 10.1152/japplphysiol.00466.2018

Sun, Z. (2015). Aging, arterial stiffness, and hypertension. *Hypertension* 65, 252–256.

Taviani, V., Hickson, S. S., Hardy, C. J., Mceniery, C. M., Patterson, A. J., Gillard, J. H., et al. (2011). Age-related changes of regional pulse wave velocity in the descending aorta using Fourier velocity encoded M-mode. *Magn. Reson. Med.* 65, 261–268. doi: 10.1002/mrm.22590

Trache, A., Massett, M. P., and Woodman, C. R. (2020). "Chapter Six - Vascular smooth muscle stiffness and its role in aging," in *Current Topics in Membranes*, eds I. Levitan and A. Trache (Cambridge, MA: Academic Press), 217–253. doi: 10.1016/bs.ctm.2020.08.008

Trepanowski, J. F., Canale, R. E., Marshall, K. E., Kabir, M. M., and Bloomer, R. J. (2011). Impact of caloric and dietary restriction regimens on markers of health and longevity in humans and animals: a summary of available findings. *Nutr. J.* 10:107. doi: 10.1186/1475-2891-10-107

Tsimploulis, A., Sheriff, H. M., Lam, P. H., Dooley, D. J., Anker, M. S., Papademetriou, V., et al. (2017). Systolic-diastolic hypertension versus isolated systolic hypertension and incident heart failure in older adults: insights from the Cardiovascular Health Study. *Int. J. Cardiol.* 235, 11–16.

Urbina, E. M., Wadwa, R. P., Davis, C., Snively, B. M., Dolan, L. M., Daniels, S. R., et al. (2010). Prevalence of increased arterial stiffness in children with type 1 diabetes mellitus differs by measurement site and sex: the SEARCH for diabetes in youth Study. *J. Pediatr.* 156, 731.e1–737.e1. doi: 10.1016/j.jpeds.2009.11.011

Van Bussel, F. C., Van Bussel, B. C., Hoeks, A. P., Op 'T Roodt, J., Henry, R. M., Ferreira, I., et al. (2015). A control systems approach to quantify wall shear stress normalization by flow-mediated dilation in the brachial artery. *PLoS One* 10:e0115977. doi: 10.1371/journal.pone.0115977

Van Popele, N. M., Grobbee, D. E., Bots, M. L., Asmar, R., Topouchian, J., Reneman, R. S., et al. (2001). Association between arterial stiffness and atherosclerosis: the Rotterdam Study. *Stroke* 32, 454–460. doi: 10.1161/01.str.32.2.454

Vatner, S. F., Zhang, J., Oydanich, M., Berkman, T., Naftalovich, R., and Vatner, D. E. (2020). Healthful aging mediated by inhibition of oxidative stress. *Ageing Res. Rev.* 64:101194. doi: 10.1016/j.arr.2020.101194

Verwoert, G. C., Franco, O. H., Hoeks, A. P., Reneman, R. S., Hofman, A., Cm, V. D., et al. (2014). Arterial stiffness and hypertension in a large population of untreated individuals: the Rotterdam Study. *J. Hypertens.* 32, 1606–1612. doi: 10.1097/HJH.0000000000000237

Wagenseil, J. E., and Mecham, R. P. (2012). Elastin in large artery stiffness and hypertension. *J. Cardiovasc. Transl. Res.* 5, 264–273. doi: 10.1007/s12265-012-9349-8

Westenberg, J. J., Scholte, A. J., Vaskova, Z., Van Der Geest, R. J., Groenink, M., Labadie, G., et al. (2011). Age-related and regional changes of aortic stiffness in the Marfan syndrome: assessment with velocity-encoded MRI. *J. Magn. Reson. Imaging* 34, 526–531. doi: 10.1002/jmri.22646

Wheeler, J. B., Mukherjee, R., Stroud, R. E., Jones, J. A., and Ikonomidis, J. S. (2015). Relation of murine thoracic aortic structural and cellular changes with aging to passive and active mechanical properties. *J. Am. Heart Assoc.* 4:e001744. doi: 10.1161/JAHA.114.001744

Wilkinson, I. B., Qasem, A., Mceniery, C. M., Webb, D. J., Avolio, A. P., and Cockcroft, J. R. (2002). Nitric oxide regulates local arterial distensibility in vivo. *Circulation* 105, 213–217. doi: 10.1161/hc0202.101970

Wilson, D. P. (2000). "Is atherosclerosis a pediatric disease?," in *Endotext*, eds K. R. Feingold, B. Anawalt, A. Boyce, G. Chrousos, W. W. De Herder, K. Dhatariya, et al. (South Dartmouth, MA: MDText.com, Inc).

Wolinsky, H. (1970). Response of the rat aortic media to hypertension. Morphological and chemical studies. *Circ. Res.* 26, 507–522. doi: 10.1161/01.res.26.4.507

Woodward, M. (2019). Cardiovascular disease and the female disadvantage. *Int. J. Environ. Res. Public Health* 16:1165.

Yan, L., Gao, S., Ho, D., Park, M., Ge, H., Wang, C., et al. (2013). Calorie restriction can reverse, as well as prevent, aging cardiomyopathy. *Age* 35, 2177–2182. doi: 10.1007/s11357-012-9508-5

Yan, L., Park, J. Y., Dillinger, J. G., De Lorenzo, M. S., Yuan, C., Lai, L., et al. (2012). Common mechanisms for calorie restriction and adenylyl cyclase type 5 knockout models of longevity. *Aging Cell* 11, 1110–1120. doi: 10.1111/acel.12013

Yasmin, Wallace, S., Mceniery, C. M., Dakham, Z., Pusalkar, P., Maki-Petaja, K., et al. (2005). Matrix metalloproteinase-9 (MMP-9), MMP-2, and serum elastase activity are associated with systolic hypertension and arterial stiffness. *Arterioscler. Thromb. Vasc. Biol.* 25, 372–378. doi: 10.1161/01.ATV.0000151373.33830.41

Yoon, B. K., Oh, W. J., Kessel, B., Roh, C. R., Choi, D., Lee, J. H., et al. (2001). 17Beta-estradiol inhibits proliferation of cultured vascular smooth muscle cells induced by lysophosphatidylcholine via a nongenomic antioxidant mechanism. *Menopause* 8, 58–64. doi: 10.1097/00042192-200101000-00010

Yu, S., and Mceniery, C. M. (2020). Central versus peripheral artery stiffening and cardiovascular risk. *Arterioscler. Thromb. Vasc. Biol.* 40, 1028–1033. doi: 10.1161/atvbaha.120.313128

Zagura, M., Kals, J., Serg, M., Kampus, P., Zilmer, M., Jakobson, M., et al. (2012). Structural and biochemical characteristics of arterial stiffness in patients with atherosclerosis and in healthy subjects. *Hypertens. Res.* 35, 1032–1037. doi: 10.1038/hr.2012.88

Zhang, J., Zhao, X., Vatner, D. E., Mcnulty, T., Bishop, S., Sun, Z., et al. (2016). Extracellular matrix disarray as a mechanism for greater abdominal versus thoracic aortic stiffness with aging in primates. *Arterioscler. Thromb. Vasc. Biol.* 36, 700–706. doi: 10.1161/atvbaha.115.306563

Zheng, M., Zhang, X., Chen, S., Song, Y., Zhao, Q., Gao, X., et al. (2020). Arterial stiffness preceding diabetes. *Circ. Res.* 127, 1491–1498. doi: 10.1161/circresaha.120.317950

Conflict of Interest: The authors declare that the research was conducted in the absence of any commercial or financial relationships that could be construed as a potential conflict of interest.

Publisher's Note: All claims expressed in this article are solely those of the authors and do not necessarily represent those of their affiliated organizations, or those of the publisher, the editors and the reviewers. Any product that may be evaluated in this article, or claim that may be made by its manufacturer, is not guaranteed or endorsed by the publisher.

frontiers in Physiology

ORIGINAL RESEARCH
published: 17 December 2021
doi: 10.3389/fphys.2021.763444

Upregulation of Aquaporin 1 Mediates Increased Migration and Proliferation in Pulmonary Vascular Cells From the Rat SU5416/Hypoxia Model of Pulmonary Hypertension

*Xin Yun, Nicolas M. Philip, Haiyang Jiang, Zion Smith, John C. Huetsch†, Mahendra Damarla, Karthik Suresh and Larissa A. Shimoda**

Division of Pulmonary and Critical Care Medicine, Johns Hopkins School of Medicine, Baltimore, MD, United States

OPEN ACCESS

Edited by:
Lakshmi Santhanam, Johns Hopkins University, United States

Reviewed by:
Elena Goncharova, University of California, Davis, United States
Zhiyu Dai, University of Arizona, United States

***Correspondence:**
Larissa A. Shimoda
lshimod1@jhmi.edu

†Present address:
John C. Huetsch, Arrowhead Pharmaceuticals, Pasadena, CA, United States

Specialty section:
This article was submitted to Vascular Physiology, a section of the journal Frontiers in Physiology

Received: *23 August 2021*
Accepted: *01 November 2021*
Published: *17 December 2021*

Citation:
Yun X, Philip NM, Jiang H, Smith Z, Huetsch JC, Damarla M, Suresh K and Shimoda LA (2021) Upregulation of Aquaporin 1 Mediates Increased Migration and Proliferation in Pulmonary Vascular Cells From the Rat SU5416/Hypoxia Model of Pulmonary Hypertension. Front. Physiol. 12:763444. doi: 10.3389/fphys.2021.763444

Pulmonary arterial hypertension (PAH) is a progressive disorder characterized by exuberant vascular remodeling leading to elevated pulmonary arterial pressure, maladaptive right ventricular remodeling, and eventual death. The factors controlling pulmonary arterial smooth muscle cell (PASMC) and endothelial cell hyperplasia and migration, hallmark features of the vascular remodeling observed in PAH, remain poorly understood. We previously demonstrated that hypoxia upregulates the expression of aquaporin 1 (AQP1), a water channel, in PASMCs, and that this upregulation was required for hypoxia-induced migration and proliferation. However, whether the same is true in a model of severe PAH and in pulmonary microvascular endothelial cells (MVECs) is unknown. In this study, we used the SU5416 plus hypoxia (SuHx) rat model of severe pulmonary hypertension, which mimics many of the features of human PAH, to determine whether AQP1 levels were altered in PASMCs and MVECs and contributed to a hyperproliferative/hypermigratory phenotype. Rats received a single injection of SU5416 (20 mg/kg) and then were placed in 10% O_2 for 3 weeks, followed by a return to normoxic conditions for an additional 2 weeks. We found that AQP1 protein levels were increased in both PASMCs and MVECs from SuHx rats, even in the absence of sustained hypoxic exposure, and that in MVECs, the increase in protein expression was associated with upregulation of AQP1 mRNA levels. Silencing of AQP1 had no significant effect on PASMCs from control animals but normalized enhanced migration and proliferation observed in cells from SuHx rats. Loss of AQP1 also reduced migration and proliferation in MVECs from SuHx rats. Finally, augmenting AQP1 levels in MVECs from control rats using forced expression was sufficient to increase migration and proliferation. These results demonstrate a key role for enhanced AQP1 expression in mediating abnormal migration and proliferation in pulmonary vascular cells from a rodent model that reflects many of the features of human PAH.

Keywords: smooth muscle cells, pulmonary arterial hypertension, microvascular endothelial cells, lung, remodeling

INTRODUCTION

Pulmonary hypertension (PH) is a devastating, progressive condition of varying etiology leading to eventual right heart failure. Clinically diagnosed as a mean pulmonary arterial pressure >20 mmHg, PH can be divided into five categories based on clinical manifestations, hemodynamics, inciting cause, and response to therapies (Simonneau et al., 2019). PH associated with hypoxia (Group 3) is common in individuals with chronic lung disease or non-adapted individuals who live at high altitudes, whereas the most severe form of PH is disease predominating in the pre-capillary circulation, classified as pulmonary arterial hypertension (PAH; Group 1). Mortality with PAH is unacceptably high, with 5-year survival at approximately 50% (Benza et al., 2012). Vascular remodeling is a prominent feature of all forms of PH, but is especially robust in PAH, with thickening of all layers of the vascular wall and development of occlusive lesions that obstruct blood flow in the small arteries (Tuder, 2009; Hemnes and Humbert, 2017; Humbert et al., 2019). While vascular remodeling is a known contributor to the elevation in pulmonary vascular resistance and pressure during PH, no current therapies are available that directly target remodeling, partly because the cellular mechanisms governing this process remain poorly understood.

In previous work, we demonstrated that hypoxia upregulates the protein expression of the water channel, aquaporin 1 (AQP1), in pulmonary arterial smooth muscle cells (PASMCs) and identified a role for this protein in mediating proliferation and migration in response to hypoxia (Leggett et al., 2012). Following this initial study, other labs confirmed the role of AQP1 in governing PASMC growth during hypoxia and showed that targeting AQP1 *in vivo* reduced the development of hypoxia-induced PH in rodents (Schuoler et al., 2017; Liu et al., 2019). While these studies appear to cement a role for AQP1 in hypoxia-induced PH, the role of AQP1 in pulmonary vascular cell growth and migration in PAH, where sustained hypoxia is not an inciting or complicating factor, is unknown. At present, no preclinical model perfectly recreates human PAH; however, the model produced by injecting rats with a vascular endothelial growth factor receptor inhibitor (SU5416) combined with hypoxic exposure followed by a return to normoxic conditions for several weeks recapitulates several important features of human PAH, including severe elevations in pulmonary arterial pressure and robust vascular remodeling including vaso-occlusive lesions (Taraseviciene-Stewart et al., 2001; Abe et al., 2010; Huetsch et al., 2016). We have previously shown that PASMCs and pulmonary microvascular endothelial cells (MVECs) isolated from this model exhibit several abnormalities, including enhanced migratory and proliferative capacity (Huetsch et al., 2016; Suresh et al., 2018, 2019). The current study tested the hypothesis that AQP1 is upregulated in PASMCs and MVECs from the SuHx rat model and contributes to the abnormal growth and migration observed in these cells.

MATERIALS AND METHODS

Ethical Approval

All procedures and protocols in this study were conducted in accordance with NIH guidelines for the proper care and use of animals in research and were approved by the Johns Hopkins University Animal Care and Use Committee.

Sugen/Hypoxia Model

To induce PH, adult male Wistar rats (150–200 g) received a subcutaneous injection of SU5416 (20 mg/kg) prepared in a carboxymethylcellulose (CMC)-containing diluent as described previously (Taraseviciene-Stewart et al., 2001; Huetsch et al., 2016) and were exposed to 10% O_2 (hypoxia) for 3 weeks. During this time, the rats were exposed to normoxic conditions for <5 min twice a week to change cages and replenish food and water. At the end of 3 weeks, rats were returned to room air (normoxia) for an additional 2 weeks. Control rats were injected with vehicle and maintained in room air for 5 weeks. All animals were kept in the same room and exposed to the same light-dark cycle and ambient temperature and were housed in standard rat cages (three rats/cage) with free access to food and water. At the end of exposures, rats were anesthetized (Ketamine, 75 mg/kg; Xylazine, 7.5 mg/kg). Depth of anesthesia was confirmed *via* paw pinch prior to measurement of the right ventricular systolic pressure (RVSP) *via* transdiaphragmatic right heart puncture with a heparinized 23 gauge needle attached to a pressure transducer as previously described (Huetsch et al., 2016; Suresh et al., 2018). Animals were euthanized *via* exsanguination after hemodynamic measurements and the heart and lungs removed and transferred to a dissecting dish filled with cold N-[2-hydroxyethyl]piperazine-N′-[2-ethanesulfonic acid] HEPES-buffered salt solution (HBSS) containing (in mmol/L): 130 NaCl, 5 KCl, 1.2 $MgCl_2$, 1.5 $CaCl_2$, 10 HEPES, and 10 glucose, with pH adjusted to 7.2 with 5 mol/L NaOH. Under a microscope, the atria and large conduit vessels were removed, and the right ventricular (RV) wall was carefully separated from the left ventricle and the septum (LV + S). Both portions were blotted dry and weighed.

Isolation of Smooth Muscle Cells

Pulmonary arterial smooth muscle cells were isolated as described previously (Shimoda et al., 1998). Lungs were placed in cold HBSS and intrapulmonary arteries (PAs; 200–600 μm outer diameter) were isolated under a dissecting microscope and cleaned of adventitia and endothelium. The arteries were allowed to recover for at least 30 min on ice before being transferred to reduced-Ca^{2+} (20 μM $CaCl_2$) HBSS at room temperature for at least 20 min. The tissue was digested for 20–25 min at 37°C in reduced-Ca^{2+} HBSS containing collagenase (type I; 1,750 U/ml), papain (9.5 U/ml), bovine serum albumin (2 mg/ml) and dithiothreitol (1 mM). PASMCs were obtained by gentle trituration in Ca^{2+}-free HBSS using a modified P1000 pipette tip and cultured in Smooth Muscle Cell Medium supplemented with SmGM™-2 bullet kit (Lonza). PASMC phenotype and purity were validated by assessing the presence of smooth

muscle-specific actin (SMA) using immunofluorescence in cells incubated with anti-SMA (1:1,000, Sigma) primary antibody and counterstained with DAPI. PASMCs were used at passages 0–3.

Isolation of Endothelial Cells

Microvascular endothelial cells were isolated, grown to confluence, and phenotyped as described previously (Suresh et al., 2018, 2019). Peripheral strips of rat lung were dissected and digested in reduced Ca^{2+} HBSS containing collagenase type 1 (357 U/ml for 30 min). Following digestion, cells were incubated for 30 min with CD31-conjugated dynabeads (1:40, #11155D, Invitrogen) and then CD31+ cells magnetically selected, plated in DMEM media containing non-essential amino acids, endothelial growth factor supplement (Millipore), and 20% fetal bovine serum (FBS; Hyclone) and 1% penicillin/streptomycin as described previously (Suresh et al., 2018, 2019) and grown to confluence. Cells were then subjected to a second selection using *Griffonia simplicifolia*-conjugated beads (1:2,000, #B-1105, Vector; or 1:40, #11047, Invitrogen). Following dual selection, cells were used or frozen at passage 3. All experiments were performed on cells at passages 3–4. MVECs were routinely phenotyped for lack or presence of smooth muscle (SMA; 1:200, FITC-conjugated smooth muscle-specific α-actin; # F3777, Sigma) and EC (von Willebrand factor, vWF; 1:100, #SARTW-1G, Affinity Biologicals and Donkey anti-sheep Alexa Fluor, 1:100, #A21436, Invitrogen) markers, respectively. Cells were counterstained with DAPI (1 μg/ml in PBS, #62247, ThermoFisher Scientific) to visualize nuclei.

Real-Time RT-PCR

Total RNA was extracted from PAs, PASMCs, and MVECs *via* the RNeasy Plus Mini kit (Qiagen). Reverse transcription was performed using 500 ng of RNA and the iScript cDNA synthesis kit (Bio-Rad). Real-time PCR was performed using 1,000 ng of cDNA with QuantiTect SYBR Green PCR Master Mix (Qiagen) in an iCycler IQ real-time PCR detection system (Bio-Rad). The specific primer pairs for real-time PCR are listed in **Table 1**. Confirmation of correct PCR products was achieved by observation of a single peak in the melt curve and visualization of a single band of the correct size when products were run on an agarose gel. Finally, bands were excised and sequenced. Relative amounts of each gene were calculated using the Pfaffl (2001) method, and data are expressed as a power ratio of the gene of interest to the housekeeping gene (Cyclophilin B; CpB) within a sample using the efficiency for each gene calculated from efficiency curves run on the same plate as samples. For each experiment, the values were normalized to the value of the control sample.

Forced Expression of AQP1

An adenoviral construct containing wild-type AQP1 with an N-terminal hemagglutinin (HA)-tag (AdAQP1) was created as described previously (Lai et al., 2014). The same adenoviral construct containing GFP (AdGFP) was used as a control for infection. MVECs were infected with 100 ifu/cell of virus in low serum (1% FBS) media for 6 h after which media was replaced and cells allowed to incubate an additional 24 h before being used in experiments.

siRNA Transfection

Depletion of endogenous AQP1 was achieved using siRNA targeting AQP1 and non-targeting siRNA (control) obtained as a "smart pool" (Dharmacon) as previously described (Leggett et al., 2012). PASMCs and MVECs were incubated with 100 nM of siRNA for 6 h in serum- and antibiotic-free media, after which serum was added to media for a total concentration of 0.3% (PASMCs) or 5% (MVECs) FBS. Cells were incubated under these conditions for 24 h, and then media was replaced, and cells were incubated for an additional 24 h prior to experiments.

Western Blotting

Total protein was extracted from PAs, PASMCs, and MVECs in ice-cold T-PER buffer containing protease inhibitors (Roche Diagnostics). Quantification of proteins was performed using BCA protein assay (Pierce) and 10 μg (PAs and PASMCs) or 25 μg (MVECs) total protein per lane was separated by electrophoresis through a 12% SDS-PAGE gel and transferred onto polyvinylidene difluoride membranes. Membranes were incubated in 5% non-fat dry milk in Tris-buffered saline containing 0.2% Tween 20 to block nonspecific binding sites before being probed with primary antibody against AQP1 (1:1,000; # AQP11-A, Alpha Diagnostic Intl. Inc.) or HA (1:500; #sc-7392, Santa Cruz Biotechnology. Inc). Bound antibody was probed with horseradish peroxidase-conjugated anti-rabbit or anti-mouse secondary antibody (1:10,000; #5220-0336 and 5220-0341; KPL) and detected by enhanced chemiluminescence. Membranes were then stripped and re-probed for β-tubulin (1:10,000, #T7816, Sigma) as a housekeeping protein. Protein levels were quantified by densitometry using ImageJ.

Cell Migration

Fifty-thousand cells in low FBS media (0.3% for PASMCs or 5% for MVECs) were added to the top chamber of a polycarbonate transwell insert (8 μm pores) inserted into 6-well plates. Cells were allowed to migrate in low serum media for 16 h (MVECs) or 24 h (PASMCs), after which the cells were fixed in 95% ethanol for 10 min, stained with Brilliant

TABLE 1 | Real-time PCR primers.

Gene name	Accession Number	Forward	Reverse	Product size (kB)
AQP1	NM 012778	5'-CCGAGACTTAGGTGGCTCAG-3'	5'-TTGATCCCACAGCCAGTGTA-3'	118
Cyclophilin B	NM 022536	5'-GGACGAGTGACCTTTGGACT-3'	5'-TGACACGATGGAACTTGCTG-3'	93

TABLE 2 | Hemodynamic and physiological measurements in Control and SuHx rats.

Condition	Weight (g)	RVSP (mmHg)	RV/LV + S	Heart Rate (bpm)
Control ($n = 16$)	398.5 ± 21.4	21.1 ± 3.1	0.243 ± 0.04	341.3 ± 55.1
SuHx ($n = 16$)	309.9 ± 42.2*	68.9 ± 13.3*	0.442 ± 0.09*	316.5 ± 41.3

*RVSP, right ventricular systolic pressure; RV, right ventricle; LV + S, left ventricle plus septum; bmp, beats per minute. *$p < 0.001$.*

Blue (Pierce) for 5 min, and visualized *via* a microscope-mounted camera. For each filter, five fields were randomly chosen and imaged with Q-capture software (total cells). Unmigrated cells were then scraped off from the top of the filter, and the bottom layer was re-imaged (migrated cells). Migration rate was calculated as the percent of cells remaining on the filter after scraping normalized to the total amount of cells.

Cell Proliferation Assay

Five-thousand cells were seeded into low FBS media (0.3% for PASMCs or 5% for MVECs) in wells of a 96-well plate in triplicate for every sample. After incubating for 2–3 h to allow cells to adhere, BrdU (Amersham Biosciences) was added to each well for 16 h (MVECs) or 24 h (PASMCs), after which the media was removed, and cells were fixed. Proliferation was estimated from the detection of peroxidase- labeled anti-BrdU in newly synthesized cells. The developed color was measured at 450 nm in a microtitre plate spectrophotometer. Proliferation rate is shown as the percent of the absorbance values normalized to the control cells on the same plate, with control values set to 100%.

In vitro Exposure to Hypoxia

Microvascular endothelial cells were grown to 60% confluence in tissue culture plates and placed in low serum media for 4–6 h before beginning experiments. Cells were treated with vehicle (1:100 DMSO) or TC-S 7009 (10 μM) an inhibitor of hypoxia-inducible factor 2 (HIF-2) immediately prior to placing the culture plates in a modular chamber (Billups-Rothberg) gassed with 4% O_2; 5% CO_2 as previously described (Leggett et al., 2012). The chamber containing cells was placed in a room air incubator maintained at 37°C and 5% CO_2. Correct oxygen levels inside the hypoxic chamber were confirmed using a hand-held oxygen monitor (model 5,577; Hudson RCI). Culture plates containing non-hypoxic control cells were placed in the same incubator on the shelf next to the modular hypoxia incubator.

Electric Cell-Substrate Impedance Sensing

Endothelial cell barrier function was measured using electric cell-substrate impedance sensing (ECIS; ZTheta system, Applied Biophysics) as previously described (Suresh et al., 2015). MVECs (25,000 cells per well) were plated on gold electrodes in 0.5-ml electrode wells (Applied BioPhysics) and grown to confluence (48 h) in media containing 5% FCS. Baseline resistance for all wells was measured for an additional hour and an average resistance over this time was calculated.

Statistical Analysis

Data are expressed as means ± SD, where "*n*" refers to the sample size. Since all experimental runs were performed on arteries/cells from different animals, "*n*" also refers to the number of animals. Statistical comparisons were performed using parametric or non-parametric tests as appropriate. Differences between groups were assessed by Student's *t*-test, one-sample *t*-test, Mann-Whitney Rank Sum test, or two-way ANOVA with Holm-Sidak post-test. The specific statistical tests used in each experiment are detailed in the Figure legends. Differences were considered to be significant when $p < 0.05$.

RESULTS

Model Validation

At the end of the 5 weeks exposure, SuHx animals weighed less than controls (**Table 2**). As expected, exposure to the SuHx protocol resulted in elevated RVSP (**Figure 1A**) and increased right ventricular mass, reflected in the higher RV/LV + S weight ratio (**Figure 1B**). While PAs in lungs from control animals are thin-walled structures, an inspection of lung sections confirmed substantial thickening of the wall of PAs in lungs from SuHx rats (**Figure 1C**, top). Further examination of small diameter (<100 μm) vessels revealed near occlusion of the vascular lumen in many vessels (**Figure 1C**, bottom). These results are indicative of the development of severe PH and marked vascular remodeling in these animals. Isolation of PASMCs and MVECs was confirmed by immunofluorescence staining. PASMCs exhibited robust staining for SMA, as seen in **Figure 1D**. In contrast, MVECs isolated from control rats lacked SMA expression and instead exhibited staining for vWF, indicative of normal EC function/phenotype.

AQP1 Expression in Pulmonary Cells From SuHx Model

We previously demonstrated upregulated expression of AQP1 in PASMCs from chronically hypoxic rats and in PASMCs exposed to hypoxia *in vitro* (Leggett et al., 2012). To determine whether hypoxia could also increase AQP1 expression in MVECs, we exposed cells from control rats to 4% hypoxia for 48 h *in vitro*. Compared to MVECs kept in non-hypoxic conditions, MVECs exposed to hypoxia exhibited a modest increase in AQP1 protein levels (**Figure 2**). Since the AQP1 promoter had previously been demonstrated to contain a binding site for the oxygen-sensitive transcription factor, hypoxia-inducible factor (HIF; Abreu-Rodriguez et al.,

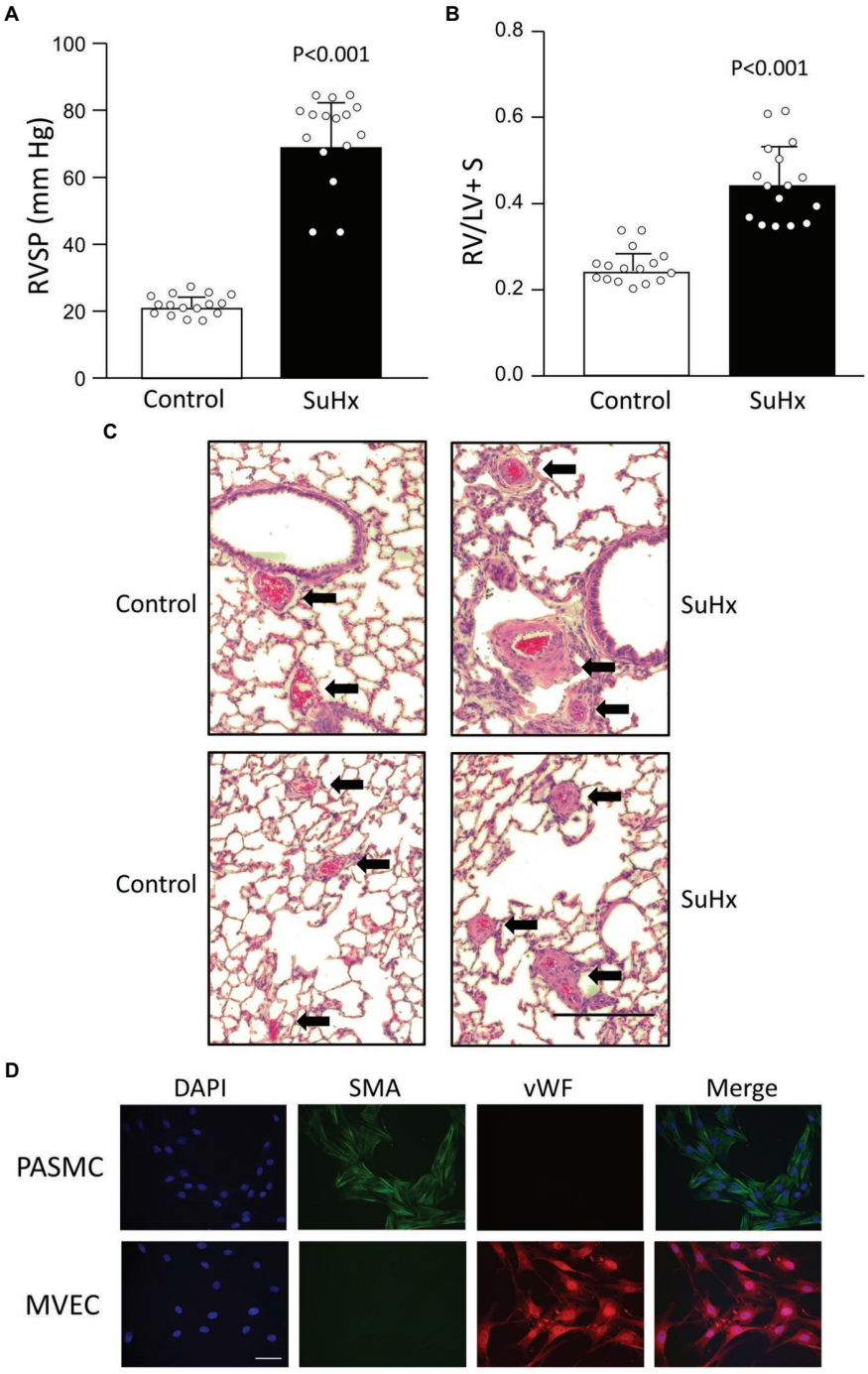

FIGURE 1 | Validation of model. Bar graphs showing mean ± SD values for **(A)** right ventricular systolic pressure (RVSP) and **(B)** right ventricle (RV) to left ventricle plus septum (LV + S) weight ratio in control and SuHx rats. Each dot represents a single animal. Value of *p* determined by *t*-test. **(C)** Representative histology images (H&E staining) illustrating vascular remodeling in SuHx rats. Dark red blood cells are clearly evident within vessels. Arrows point to arteries (top) and small vessels (bottom); bar indicates 200 μm. **(D)** Representative images showing immunofluorescence for DAPI (nuclei), smooth muscle-specific α-actin (SMA), von Willebrand factor (vWF), and the merged image for pulmonary arterial smooth muscle cells (PASMCs) and MVECs isolated from control rats. Scale bar indicates 50 μm. Results representative of those obtained in at least 10 isolates.

2011; Tanaka et al., 2011), we also tested whether the upregulation of AQP1 by hypoxia in MVECs was HIF-dependent. Incubation with an inhibitor to HIF-2, the family member primarily expressed in endothelium, had no significant effect on AQP1 levels under non-hypoxic conditions but prevented the upregulation of AQP1 in MVECs exposed

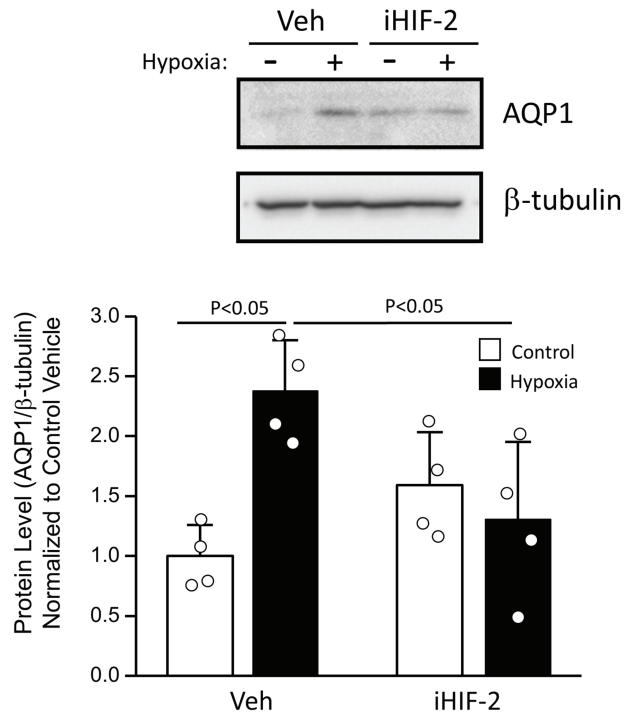

FIGURE 2 | Effect of exposure to *in vitro* hypoxia on aquaporin 1 (AQP1) protein levels in MVECs. Representative immunoblot showing AQP1 and β-tubulin protein expression in MVECs exposed to 4% O_2 for 48 h. Cells were treated with vehicle (Veh; 1:1,000 DMSO) or TC-S 7009 (10 μM), a hypoxia-inducible factor-2 (HIF-2) inhibitor (iHIF-2) prior to hypoxic challenge. Bar graphs show mean ± SD values for the ratio of AQP1 to β-tubulin protein levels, normalized to Control + Veh group. Value of *p* determined from two-way ANOVA with Holm-Sidak post-test. Each dot represents samples from different animals.

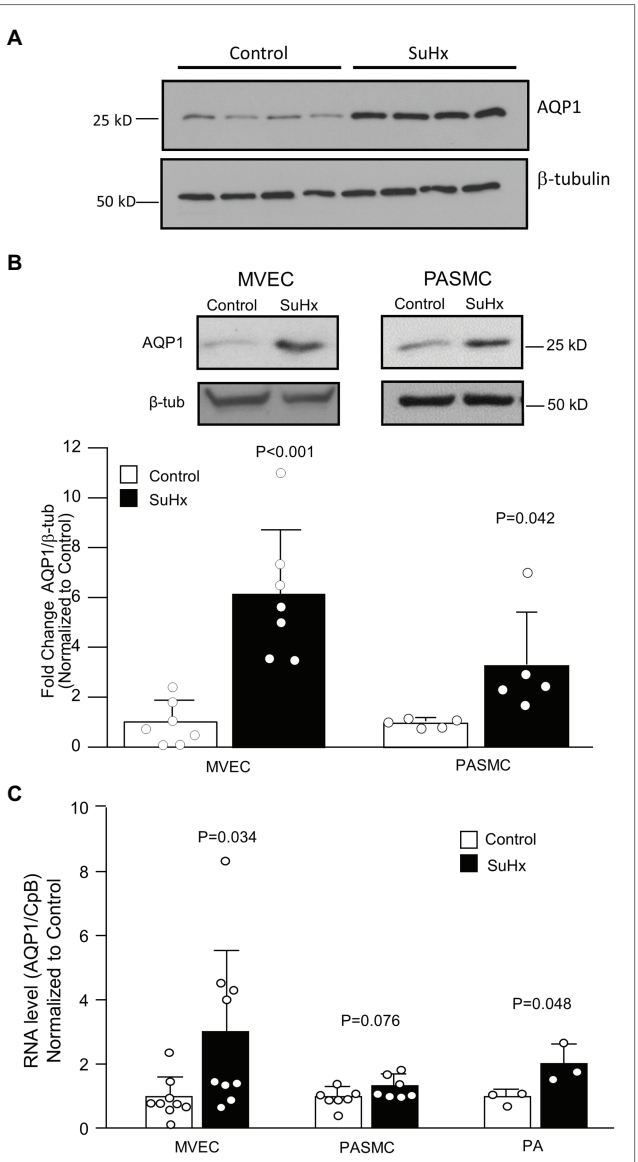

FIGURE 3 | Pulmonary vascular AQP1 expression. **(A)** Immunoblot image showing AQP1 protein levels in pulmonary arteries (PA) from control and SuHx rats. **(B)** Representative images and bar graphs (mean ± SD values) for AQP1 protein levels in microvascular endothelial cell (MVEC) and PASMCs isolated from control and SuHx rats. **(C)** Bar graphs (mean ± SD values) for mRNA levels of AQP1 relative to cyclophilin B (CpB; housekeeping) and normalized to values in Control rat samples. For all graphs, each dot represents samples from different animals and values of *p* determined by *t*-test.

to hypoxia. We next determined whether AQP1 was upregulated in the vasculature of SuHx rats, we initially performed immunoblot analysis on whole PAs. Resistance level PAs from SuHx rats exhibited increased AQP1 protein levels compared to arteries from control rats (**Figure 3A**). We next assessed AQP1 expression in PASMCs and MVECs isolated from these animals. In both PASMCs and MVECs, AQP1 protein levels were significantly higher in cells from SuHx rats than controls (**Figures 3B**,**C**), although AQP1 expression in control MVECs was quite low and required loading more than double the amount of protein (25 μg) as loaded from PASMCs (10 μg) to see comparable levels of basal expression. Even in this case, AQP1 protein was nearly undetectable in several MVEC samples. In contrast to the protein expression findings, MVECs exhibited substantial AQP1 mRNA at baseline, with C_t values for AQP1 in control MVECs (mean $C_t = 24.26$) similar to values measured for AQP1 in control PASMCs ($C_t = 22.9$) in the same experiment. RT-PCR also revealed an increase in AQP1 mRNA levels in MVECs and PAs from normoxic and SuHx rats (**Figure 3C**), whereas AQP1 mRNA levels in PASMCs from control and SuHx rats were not significantly different.

Migration and Proliferation in PASMCs and MVECs

Compared to cells from control rats, PASMCs and MVECs from SuHx rats exhibited greater proliferative (**Figure 4A**) and migratory potential (**Figure 4B**), as expected based on results reported in our previous studies (Huetsch et al., 2016; Suresh et al., 2018). Using siRNA approaches, we were able to achieve a substantial reduction in AQP1 protein levels in both PASMCs

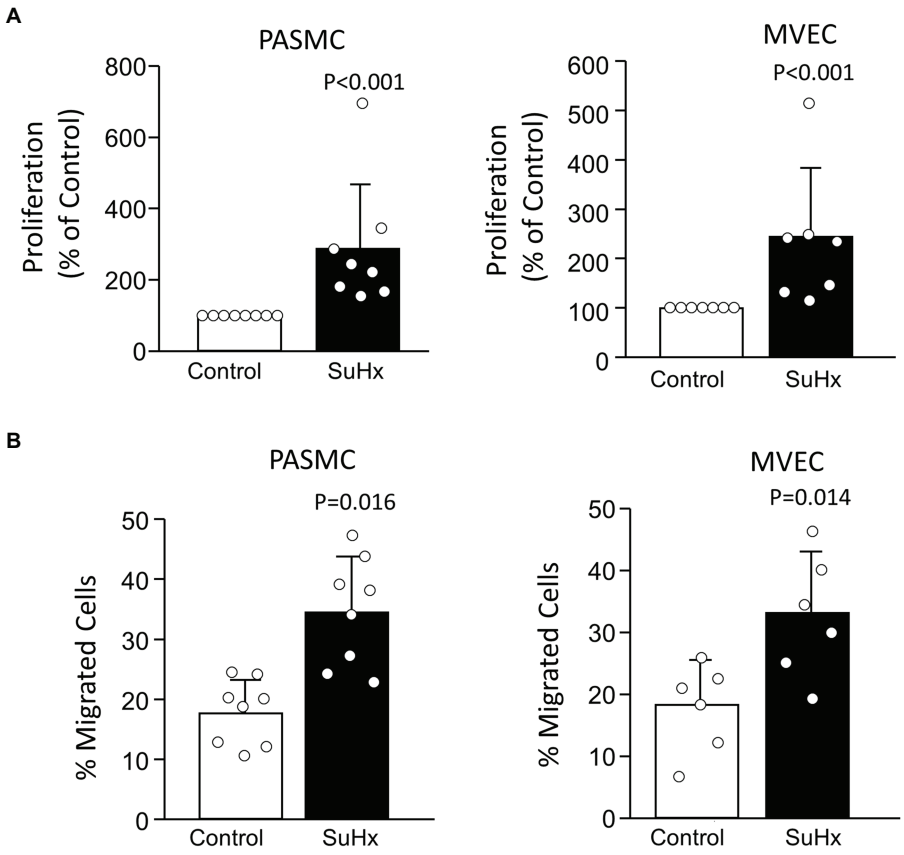

FIGURE 4 | Proliferation and migration in cells from Control and SuHx rats. **(A)** Bar graphs (mean ± SD values) for proliferation, measured by BrdU incorporation normalized to Control value, in PASMC and MVEC isolated from control and SuHx rats. Values of *p* were determined from Mann-Whitney Rank Sum test. **(B)** Bar graphs (mean ± SD values) for migrated cells (% of total) were assessed by transwell assay using PASMCs and MVECs from control and SuHx rats. Values of *p* determined by *t*-test. For all graphs, each dot represents samples from different animals.

and MVECs from SuHx rats (**Figure 5A**). Compared to cells transfected with non-targeting siRNA (siNT), depleting AQP1 reduced proliferation and migration in SuHx PASMCs (**Figure 5B**) but had no effect on migration or proliferation in control PASMCs. Since baseline levels of AQP1 protein were very low and often undetectable in control MVEC, we only performed depletion experiments in cells from SuHx rats. In SuHx MVECs, silencing AQP1 reduced proliferation by 33% and migration to ~15% (**Figure 5C**), very close to levels measured in MVECs from control rats as seen in **Figure 4**.

Effect of Augmenting AQP1 on MVECs Migration and Proliferation

We have previously demonstrated that enhancing AQP1 expression in PASMCs from control rats was sufficient to induce migration and proliferation (Lai et al., 2014; Yun et al., 2017). To test whether the same holds true for MVECs, we increased AQP1 levels in normal cells using adenoviral forced expression of wild-type AQP1. We previously demonstrated that HA-tagged AQP1 transduced by this viral construct is functionally intact and exhibits appropriate surface expression (Lai et al., 2014). Infecting MVECs with AdAQP1 resulted in a significant increase in HA-tagged (expressed) AQP1 protein levels (**Figure 6A**). Compared to cells infected with AdGFP, cells infected with AdAQP1 exhibited increased proliferation (**Figure 6B**) and migration (**Figure 6C**).

Effect of Augmenting AQP1 on MVEC Barrier Function

The main function of the endothelium is to provide a tight vascular barrier. Maintenance of appropriate barrier function and low permeability requires coordination between the cytoskeleton, cell-cell junction complexes, and cell attachments to the extracellular matrix and basement membrane. However, during periods of migration and proliferation, the stability of cell-cell junctions may be reduced to allow cell movement. To assess whether MVECs from SuHx rats exhibited reduced monolayer barrier function, we measured transendothelial resistance using ECIS. Comparison of baseline resistance between MVECs from Control and SuHx rats revealed no significant loss of barrier function (**Figure 7A**). We also tested the effect of augmenting AQP1 levels in control MVECs. Infection with AdGFP appeared to have no appreciable effect on baseline resistance, as levels measured in these cells (**Figure 7B**) were

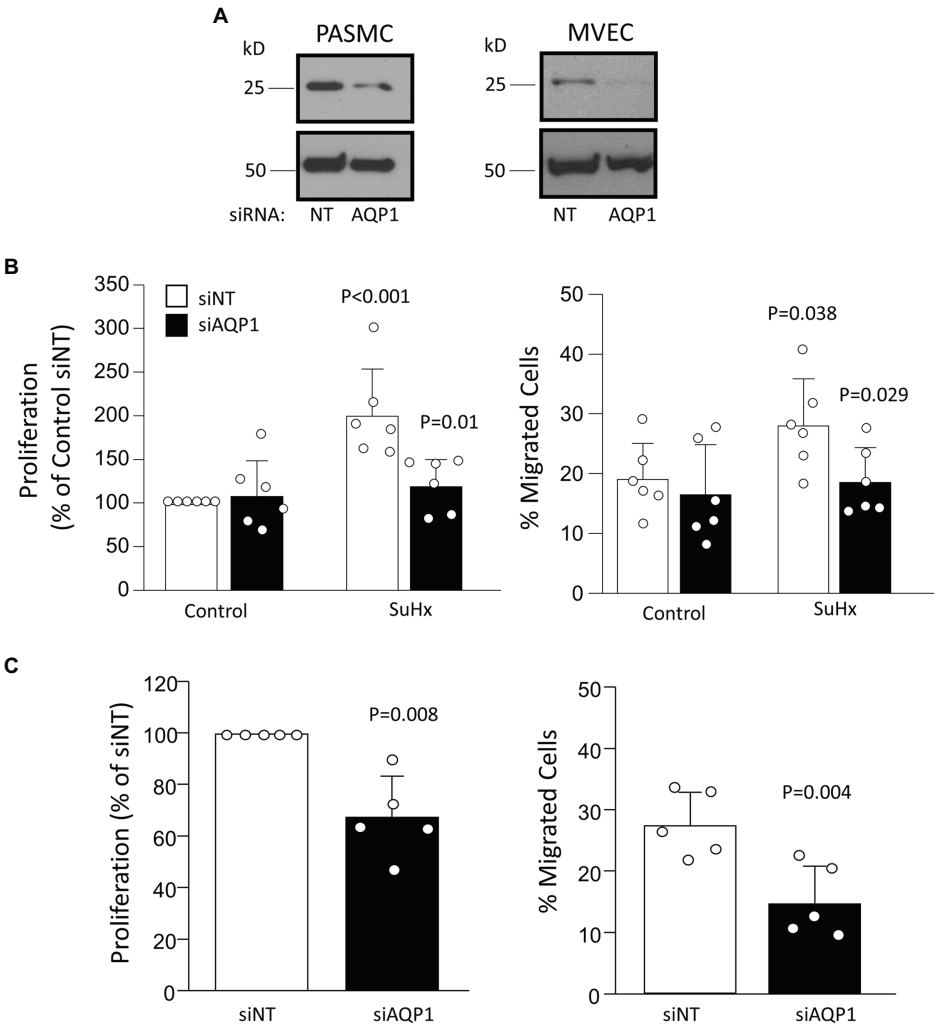

FIGURE 5 | Effect of depleting AQP1 on proliferation and migration. **(A)** Representative images demonstrating level of protein knockdown achieved using siRNA directed against AQP1 (siAQP1) compared to non-targeting siRNA (siNT). Result representative of at least five experiments for each cell type performed on cells from different animals. **(B)** Bar graphs (mean ± SD values) for proliferation, measured by BrdU incorporation and normalized to control, and migration, measured *via* transwell assay, in PASMCs isolated from control and SuHx rats. Values of *p* for proliferation and migration in PASMCs were determined from two-way ANOVA with Holm-Sidak post test to determine differences between specific groups. **(C)** Bar graphs (mean ± SD values) for proliferation and migrated cells in MVEC from SuHx rats. Values of *p* determined by *t*-test (migration) or one-sample *t*-test (proliferation) against a mean of 100. For all graphs, each dot represents samples from different animals.

similar to those observed in uninfected control MVECs. However, cells infected with AdAQP1 consistently exhibited lower baseline resistance, suggesting that these cells had reduced ability to form a tight monolayer.

DISCUSSION

In this study, we explored the role of AQP1 in modulating pulmonary vascular cell migration and proliferation in a severe model of PH that captures many of the features of human PAH. We found that both PASMCs and MVECs from SuHx rats have enhanced expression of AQP1 that was associated with a more robust migratory and proliferative phenotype. We further showed that depleting AQP1 protein reduced migration and proliferation in these cells, whereas augmenting AQP1 expression in control cells was sufficient to mimic the SuHx phenotype. These results indicate an important role for AQP1 in controlling cell growth and movement during severe PH.

We previously demonstrated that exposure to chronic hypoxia upregulated AQP1 expression in PASMCs and contributed to hypoxia-induced migration and proliferation in this cell type (Leggett et al., 2012). This finding was confirmed in other labs (Schuoler et al., 2017; Liu et al., 2019), who also demonstrated that loss of AQP1 in the rodent lung, induced by antisense oligonucleotide (Schuoler et al., 2017) or transgenic approaches (Liu et al., 2019), reduced the development of hypoxia-induced PH. However, these studies have not evaluated the role of

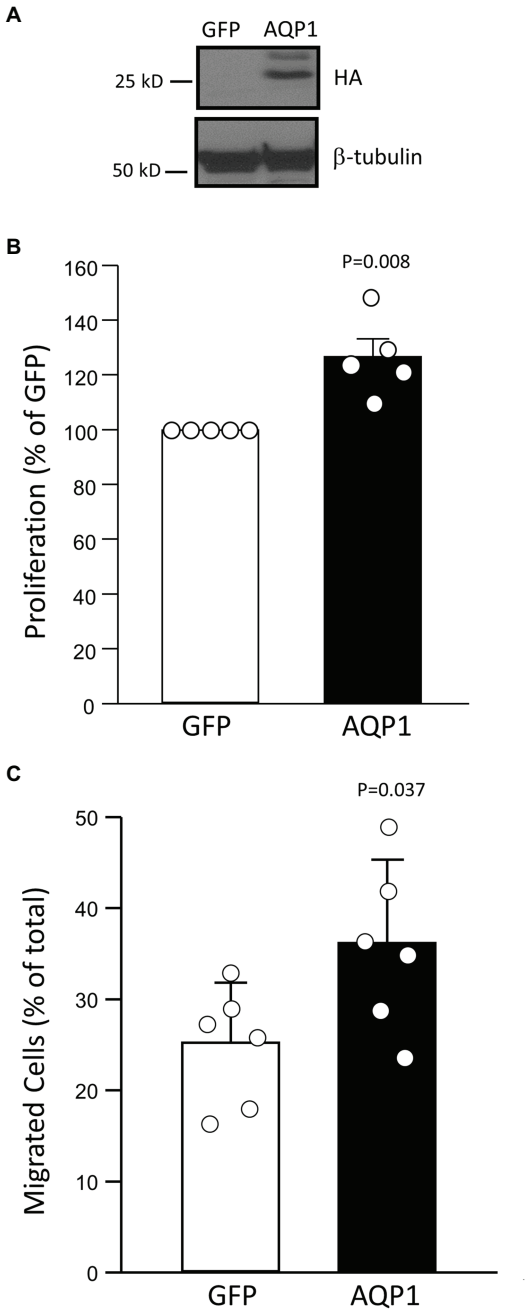

FIGURE 6 | Effect of increasing AQP1 on proliferation and migration. **(A)** Representative images demonstrate a level of HA-tagged AQP1 protein expressed following infection with an adenovirus containing GFP or AQP1 compared to β-tubulin (loading control). **(B)** Bar graph (mean ± SD values) for proliferation, measured by BrdU incorporation and normalized to control, in pulmonary MVECs isolated from control rats and infected with GFP- or AQP1-containing virus. Value of *p* determined from Mann Whitney Rank Sum Test. **(C)** Bar graph (mean ± SD values) for migrated cells in MVECs from control rats infected with virus-containing GFP or AQP1. Values of *p* determined by *t*-test. For all graphs, each dot represents samples from different animals.

AQP1 in non-hypoxia-mediated PH. While the chronic hypoxia model captures features associated with Group 3 PH, it does not include the severe elevations in pulmonary arterial pressure, robust vascular remodeling, and development of vaso-occlusive lesions characteristic of human PAH. PAH is also not typically associated with hypoxia, except perhaps in late disease. Compared to chronic hypoxia and murine models, the SuHx rat model better recapitulates the features of human PAH; while hypoxia is necessary for model initiation, PH progresses after return to normoxic conditions, allowing separation of the direct effects of hypoxia from mechanisms likely to be involved in the maintenance and progression of PAH. In this model, despite a prolonged period of normoxia following the hypoxic exposure, we found that intralobar PAs had greater AQP1 protein expression than that measured in PAs from control rats (**Figure 3**) reminiscent of results published for the chronically hypoxic rat (Leggett et al., 2012).

The development of severe pulmonary vascular remodeling and occlusive lesions may be due to hyperproliferation/migration of PASMCs and/or MVECs, as positive staining for both SMC and EC markers in the cells forming occlusions has been reported (Taraseviciene-Stewart et al., 2001; Abe et al., 2010; Huetsch et al., 2016). Thus, we isolated both PASMCs and MVECs from control and SuHx rats to assess AQP1 expression. To our surprise, AQP1 protein expression in MVECs was remarkably low and often undetectable in control MVECs. Indeed, compared to PASMCs, we needed to load much larger amounts of protein per lane (25 μg vs. 10 μg) to be able to detect AQP1 protein in control MVECs. AQP1 protein expression has been demonstrated in pulmonary vascular ECs *in vivo* (King et al., 1996; Effros et al., 1997) or freshly isolated from the lung (Schnitzer and Oh, 1996), suggesting that in the native environment, these cells express some level of the protein constitutively. One possibility to explain this discrepancy is the potential for differential expression of AQP1 between MVECs and those from larger arteries, as has been demonstrated for other membrane channels (Stevens, 2011). Interestingly, we found that MVECs from control rats expressed ample mRNA transcript, with levels similar to those in PASMCs. Thus, the low levels of AQP1 protein measured in MVECs cannot be attributed to a lack of mRNA. Whether the discrepancy between AQP1 mRNA and protein levels measured in control MVECs reflects the loss of AQP1 protein expression due to culture conditions, removal of mechanical stimuli (i.e., shear stress), and/or differences in post-transcriptional synthesis or degradation pathways remains to be determined.

Despite differences in basal AQP1 levels in control cells, AQP1 protein levels were increased in both cell types from SuHx rats. The increase in AQP1 protein levels observed in MVECs from SuHx rats appears to be due, at least in part, to transcriptional upregulation, likely accounting for the increase in AQP1 mRNA observed in intact PAs. The mechanism by which AQP1 mRNA levels were augmented in MVECs from the SuHx rats is not presently known. The AQP1 promoter has been shown to contain a hypoxia response element and is directly regulated by HIFs (Abreu-Rodriguez et al., 2011; Tanaka et al., 2011), transcription factors that are stabilized during hypoxia and rapidly degraded with a return to normoxia (Semenza, 2012). Consistent with these previous findings, we found that exposure of MVECs from control rats to *in*

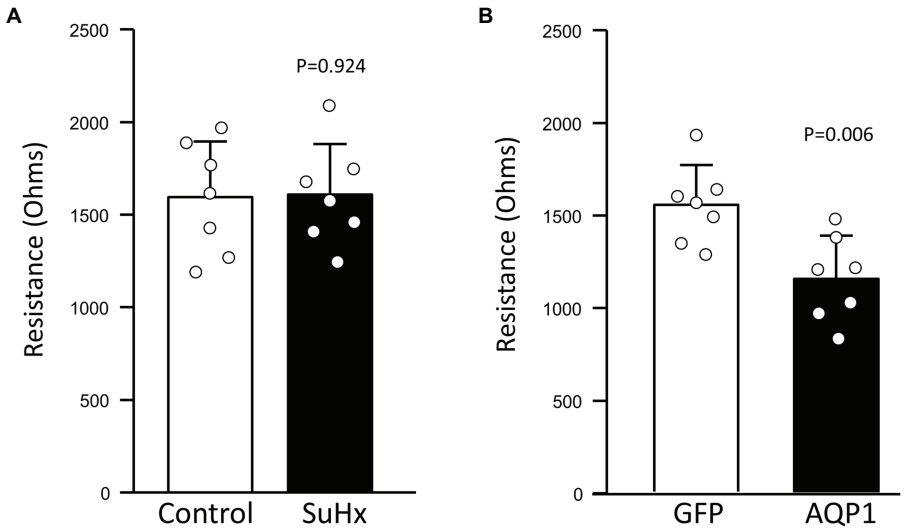

FIGURE 7 | Effect of increasing AQP1 expression on endothelial barrier function. Bar graphs show mean ± SD values for baseline transendothelial resistance measured by electric cell-substrate impedance sensing (ECIS) in MVECs from **(A)** Control and SuHx rats and **(B)** from normal rats infected with adenovirus containing GFP (control) or AQP1. Values of *p* determined by *t*-test. For all graphs, each dot represents independent experiments with cells from different animals.

vitro hypoxia induced a HIF-2-dependent increase in AQP1 protein expression. However, the durable increase in AQP1 mRNA levels in MVECs from SuHx rats, remaining evident 2 weeks after return to normoxia, suggests either a non-hypoxic stabilization of HIFs, perhaps secondary to mitochondrial dysfunction (Archer et al., 2008; Suresh et al., 2019), or could suggest that other factors aside from HIF activation maintain elevated AQP1 mRNA levels. Consistent with the former possibility, HIF levels are increased in PAECs from humans with PAH (Fijalkowska et al., 2010) and in the lungs of SuHx rats, although the cell type(s) involved was not explored (Dai et al., 2018). Whether the upregulation of AQP1 mRNA in MVECs from SuHx rats is due to HIF activation, or induction by another mechanism, also remains to be determined.

In contrast to the findings in MVECs, AQP1 mRNA levels were not statistically increased in PASMCs from SuHx rats despite augmented protein levels, reflecting apparent cell-type-specific regulation. This result is consistent with our previous findings showing hypoxia-induced increases in AQP1 protein were not accompanied by increased mRNA levels (Leggett et al., 2012). Others have shown a modest increase in AQP1 mRNA levels in PASMCs induced by *in vitro* exposure to hypoxia, although protein levels under these conditions were not examined (Abreu-Rodriguez et al., 2011). The lack of statistically significant induction of AQP1 mRNA levels in PASMCs from SuHx rats argues for the potential of post-transcriptional regulation, perhaps *via* enhanced translation or protein stabilization.

Our results indicate that elevated AQP1 protein levels are required for the hyperproliferative/hypermigatory phenotype observed in PASMCs and MVECs from the SuHx rat model. Moreover, using a viral construct to augment AQP1 levels in control MVECs demonstrated that elevations in AQP1 are sufficient to induce these changes in the absence of other stimuli, suggesting an increase in AQP1 levels could be an inciting event to modify cell function. Although we did not test the effect of loss of AQP1 protein *in vivo*, due to lack of appropriate inhibitors to reduce protein expression or availability of AQP1-null rats, in hypoxia-induced PH loss of AQP1 was shown to blunt the development of PH (Schuoler et al., 2017; Liu et al., 2019). Taken together with the findings from the SuHx rat, we speculate that upregulated AQP1 protein in PASMCs and MVECs during PAH may promote vascular remodeling through enhanced growth and migration of these cells.

It should be noted that the previous studies exploring the effect of deleting AQP1 on hypoxia-induced PH did not do so in a cell-type-specific manner, and various cells within the lung have been shown to express AQP1. For example, AQP1 expression has been reported in human and rat PASMCs (Leggett et al., 2012; Schuoler et al., 2017), macrophages (Rabolli et al., 2014; Tyteca et al., 2015), human activated T and B cells (Moon et al., 2004) and human and mouse type II pneumocytes (Effros et al., 1997; Galan-Cobo et al., 2018); however, staining for AQP1 was not observed in rat alveolar epithelium (Nielsen et al., 1997) or mouse type I cells (Effros et al., 1997). Thus, while the reduced development of hypoxia-induced PH in the previous studies could have resulted from the loss of AQP1 in PASMCs or MVECs, a role for AQP1 in other cell types cannot be ruled out at this point.

The main function of the endothelium is to create a tight barrier to prevent protein and fluid leakage into the tissue. AQP1 has been previously shown to play a role in regulating water permeability across the lung endothelium (Bai et al., 1999), although this was thought to be due to transcellular water transport. A hyperproliferative/hypermigratory phenotype,

as observed in MVECs from SuHx rats or with AdAQP1 infection, might be expected to be associated with reduced cell-cell contact, or junction formation, to allow cell movement and thus increased paracellular permeability. To test this possibility, we measured basal transendothelial electrical resistance, a surrogate for paracellular permeability, and found no difference between MVEC isolated from Control and SuHx rats. This finding is consistent with a lack of reports of lung edema formation in SuHx rats or in PAH patients. On the other hand, increasing AQP1 in normal cells significantly reduced monolayer resistance, suggesting reduced cell-cell contact and increased paracellular permeability. This finding contrasts with recent work using human lung MVECs, where depletion of AQP1 was associated with increased monolayer permeability and reduced VE-cadherin expression (Gao et al., 2012). The reason for the discrepancy between our results and those of this previous study is unclear and suggests that further work is needed to fully delineate the role of AQP1 in maintaining endothelial barrier function. Similarly, the difference in our results between acute increases in AQP1 and those induced in cells from SuHx rats also warrants further study, perhaps pointing to compensatory mechanisms activated in PAH to prevent changes in paracellular permeability.

In summary, we found that AQP1 protein was upregulated in a model of PAH and contributed to enhanced migration and proliferation of pulmonary vascular cells. Similar to previous findings in hypoxia-induced PH (Schuoler et al., 2017; Liu et al., 2019), it is likely that AQP1 also mediates remodeling in the rat PAH model and points to a possible role for AQP1 in human PAH. Interestingly, the presence of a variant of AQP1 is associated with PAH in humans (Graf et al., 2018), although the effect of this variant on protein function/expression is currently not known. While these findings are intriguing, additional work will be needed to determine whether AQP1 could be a target for therapeutic intervention to treat human disease.

DATA AVAILABILITY STATEMENT

The raw data supporting the conclusions of this article will be made available by the authors, without undue reservation.

ETHICS STATEMENT

The animal study was reviewed and approved by Johns Hopkins Animal Care and Use Committee.

AUTHOR CONTRIBUTIONS

LS and XY conceived of the experiments. LS, XY, JH, and KS designed the experiments. XY, JH, ZS, HJ, and NP performed the experiments. LS, XY, JH, KS, MD, and ZS analyzed the data and interpreted the results. LS and XY drafted the manuscript. LS, XY, JH, KS, HJ, NP, ZS, and MD revised the manuscript and approved the final version. All authors contributed to the article and approved the submitted version.

FUNDING

This work was funded by grants from the National Institutes of Health (K08HL133475 to JH; K08HL132055 to KS; R01HL073859 and R01HL126514 to LS; and HL159906 to LS and MD) and the American Heart Association (18POST34030262 to XY).

REFERENCES

Abe, K., Toba, M., Alzoubi, A., Ito, M., Fagan, K. A., Cool, C. D., et al. (2010). Formation of plexiform lesions in experimental severe pulmonary arterial hypertension. *Circulation* 121, 2747–2754. doi: 10.1161/CIRCULATIONAHA.109.927681

Abreu-Rodriguez, I., Sanchez Silva, R., Martins, A. P., Soveral, G., Toledo-Aral, J. J., Lopez-Barneo, J., et al. (2011). Functional and transcriptional induction of aquaporin-1 gene by hypoxia; analysis of promoter and role of Hif-1α. *PLoS One* 6:e28385. doi: 10.1371/journal.pone.0028385

Archer, S. L., Gomberg-Maitland, M., Maitland, M. L., Rich, S., Garcia, J. G., and Weir, E. K. (2008). Mitochondrial metabolism, redox signaling, and fusion: a mitochondria-ROS-HIF-1α-Kv1.5 O_2-sensing pathway at the intersection of pulmonary hypertension and cancer. *Am. J. Physiol. Heart Circ. Physiol.* 294, H570–H578. doi: 10.1152/ajpheart.01324.2007

Bai, C., Fukuda, N., Song, Y., Ma, T., Matthay, M. A., and Verkman, A. S. (1999). Lung fluid transport in aquaporin-1 and aquaporin-4 knockout mice. *J. Clin. Invest.* 103, 555–561. doi: 10.1172/JCI4138

Benza, R. L., Miller, D. P., Barst, R. J., Badesch, D. B., Frost, A. E., and McGoon, M. D. (2012). An evaluation of long-term survival from time of diagnosis in pulmonary arterial hypertension from the REVEAL registry. *Chest* 142, 448–456. doi: 10.1378/chest.11-1460

Dai, Z., Zhu, M. M., Peng, Y., Machireddy, N., Evans, C. E., Machado, R., et al. (2018). Therapeutic targeting of vascular remodeling and right heart failure in PAH with HIF-2α inhibitor. *Am. J. Respir. Crit. Care Med.* 198, 1423–1434. doi: 10.1164/rccm.201710-2079OC

Effros, R. M., Darin, C., Jacobs, E. R., Rogers, R. A., Krenz, G., and Schneeberger, E. E. (1997). Water transport and the distribution of aquaporin-1 in pulmonary air spaces. *J. Appl. Physiol. (1985)* 83, 1002–1016. doi: 10.1152/jappl.1997.83.3.1002

Fijalkowska, I., Xu, W., Comhair, S. A., Janocha, A. J., Mavrakis, L. A., Krishnamachary, B., et al. (2010). Hypoxia inducible-factor1α regulates the metabolic shift of pulmonary hypertensive endothelial cells. *Am. J. Pathol.* 176, 1130–1138. doi: 10.2353/ajpath.2010.090832

Galan-Cobo, A., Arellano-Orden, E., Sanchez Silva, R., Lopez-Campos, J. L., Gutierrez Rivera, C., Gomez Izquierdo, L., et al. (2018). The expression of AQP1 IS modified in lung of patients with idiopathic pulmonary fibrosis: addressing a possible new target. *Front. Mol. Biosci.* 5:43. doi: 10.3389/fmolb.2018.00043

Gao, C., Tang, J., Li, R., and Huan, J. (2012). Specific inhibition of AQP1 water channels in human pulmonary microvascular endothelial cells by small interfering RNAs. *J. Trauma Acute Care Surg.* 72, 150–161. doi: 10.1097/TA.0b013e318230e25d

Graf, S., Haimel, M., Bleda, M., Hadinnapola, C., Southgate, L., Li, W., et al. (2018). Identification of rare sequence variation underlying heritable pulmonary arterial hypertension. *Nat. Commun.* 9:1416. doi: 10.1038/s41467-018-03672-4

Hemnes, A. R., and Humbert, M. (2017). Pathobiology of pulmonary arterial hypertension: understanding the roads less travelled. *Eur. Respir. Rev.* 26:170093. doi: 10.1183/16000617.0093-2017

Huetsch, J. C., Jiang, H., Larrain, C., and Shimoda, L. A. (2016). The Na^+/H^+ exchanger contributes to increased smooth muscle proliferation and migration

in a rat model of pulmonary arterial hypertension. *Physiol. Rep.* 4:e12729. doi: 10.14814/phy2.12729

Humbert, M., Guignabert, C., Bonnet, S., Dorfmuller, P., Klinger, J. R., Nicolls, M. R., et al. (2019). Pathology and pathobiology of pulmonary hypertension: state of the art and research perspectives. *Eur. Respir. J.* 53:1801887. doi: 10.1183/13993003.01887-2018

King, L. S., Nielsen, S., and Agre, P. (1996). Aquaporin-1 water channel protein in lung: ontogeny, steroid-induced expression, and distribution in rat. *J. Clin. Invest.* 97, 2183–2191. doi: 10.1172/JCI118659

Lai, N., Lade, J., Leggett, K., Yun, X., Baksh, S., Chau, E., et al. (2014). The aquaporin 1 C-terminal tail is required for migration and growth of pulmonary arterial myocytes. *Am. J. Respir. Cell Mol. Biol.* 50, 1010–1020. doi: 10.1165/rcmb.2013-0374OC

Leggett, K., Maylor, J., Undem, C., Lai, N., Lu, W., Schweitzer, K. S., et al. (2012). Hypoxia-induced migration in pulmonary arterial smooth muscle cells requires calcium-dependent upregulation of aquaporin 1. *Am. J. Physiol. Lung Cell. Mol. Physiol.* 303, L343–L353. doi: 10.1152/ajplung.00130.2012

Liu, M., Liu, Q., Pei, Y., Gong, M., Cui, X., Pan, J., et al. (2019). Aqp-1 gene knockout attenuates hypoxic pulmonary hypertension of mice. *Arterioscler. Thromb. Vasc. Biol.* 39, 48–62. doi: 10.1161/ATVBAHA.118.311714

Moon, C., Rousseau, R., Soria, J. C., Hoque, M. O., Lee, J., Jang, S. J., et al. (2004). Aquaporin expression in human lymphocytes and dendritic cells. *Am. J. Hematol.* 75, 128–133. doi: 10.1002/ajh.10476

Nielsen, S., King, L. S., Christensen, B. M., and Agre, P. (1997). Aquaporins in complex tissues. II. Subcellular distribution in respiratory and glandular tissues of rat. *Am. J. Phys.* 273, C1549–C1561.

Pfaffl, M. W. (2001). A new mathematical model for relative quantification in real-time RT-PCR. *Nucleic Acids Res.* 2:e45. doi: 10.1093/nar/29.9.e45

Rabolli, V., Wallemme, L., Lo Re, S., Uwambayinema, F., Palmai-Pallag, M., Thomassen, L., et al. (2014). Critical role of aquaporins in interleukin 1beta (IL-1beta)-induced inflammation. *J. Biol. Chem.* 289, 13937–13947. doi: 10.1074/jbc.M113.534594

Schnitzer, J. E., and Oh, P. (1996). Aquaporin-1 in plasma membrane and caveolae provides mercury-sensitive water channels across lung endothelium. *Am. J. Phys.* 270, H416–H422. doi: 10.1152/ajpheart.1996.270.1.H416

Schuoler, C., Haider, T. J., Leuenberger, C., Vogel, J., Ostergaard, L., Kwapiszewska, G., et al. (2017). Aquaporin 1 controls the functional phenotype of pulmonary smooth muscle cells in hypoxia-induced pulmonary hypertension. *Basic Res. Cardiol.* 112:30. doi: 10.1007/s00395-017-0620-7

Semenza, G. L. (2012). Hypoxia-inducible factors in physiology and medicine. *Cell* 148, 399–408. doi: 10.1016/j.cell.2012.01.021

Shimoda, L. A., Sylvester, J. T., and Sham, J. S. (1998). Inhibition of voltage-gated K^+ current in rat intrapulmonary arterial myocytes by endothelin-1. *Am. J. Phys.* 274, L842–L853.

Simonneau, G., Montani, D., Celermajer, D. S., Denton, C. P., Gatzoulis, M. A., Krowka, M., et al. (2019). Haemodynamic definitions and updated clinical classification of pulmonary hypertension. *Eur. Respir. J.* 53:1801913. doi: 10.1183/13993003.01913-2018

Stevens, T. (2011). Functional and molecular heterogeneity of pulmonary endothelial cells. *Proc. Am. Thorac. Soc.* 8, 453–457. doi: 10.1513/pats.201101-004MW

Suresh, K., Servinsky, L., Jiang, H., Bigham, Z., Yun, X., Kliment, C., et al. (2018). Reactive oxygen species induced Ca^{2+} influx via TRPV4 and microvascular endothelial dysfunction in the SU5416/hypoxia model of pulmonary arterial hypertension. *Am. J. Physiol. Lung Cell. Mol. Physiol.* 314, L893–L907. doi: 10.1152/ajplung.00430.2017

Suresh, K., Servinsky, L., Jiang, H., Bigham, Z., Zaldumbide, J., Huetsch, J. C., et al. (2019). Regulation of mitochondrial fragmentation in microvascular endothelial cells isolated from the SU5416/hypoxia model of pulmonary arterial hypertension. *Am. J. Physiol. Lung Cell. Mol. Physiol.* 317, L639–L652. doi: 10.1152/ajplung.00396.2018

Suresh, K., Servinsky, L., Reyes, J., Baksh, S., Undem, C., Caterina, M., et al. (2015). Hydrogen peroxide-induced calcium influx in lung microvascular endothelial cells involves TRPV4. *Am. J. Physiol. Lung Cell. Mol. Physiol.* 309, L1467–L1477. doi: 10.1152/ajplung.00275.2015

Tanaka, A., Sakurai, K., Kaneko, K., Ogino, J., Yagui, K., Ishikawa, K., et al. (2011). The role of the hypoxia-inducible factor 1 binding site in the induction of aquaporin-1 mRNA expression by hypoxia. *DNA Cell Biol.* 30, 539–544. doi: 10.1089/dna.2009.1014

Taraseviciene-Stewart, L., Kasahara, Y., Alger, L., Hirth, P., Mc Mahon, G., Waltenberger, J., et al. (2001). Inhibition of the VEGF receptor 2 combined with chronic hypoxia causes cell death-dependent pulmonary endothelial cell proliferation and severe pulmonary hypertension. *FASEB J.* 15, 427–438. doi: 10.1096/fj.00-0343com

Tuder, R. M. (2009). Pathology of pulmonary arterial hypertension. *Semin. Respir. Crit. Care Med.* 30, 376–385. doi: 10.1055/s-0029-1233307

Tyteca, D., Nishino, T., Debaix, H., Van Der Smissen, P., N'Kuli, F., Hoffmann, D., et al. (2015). Regulation of macrophage motility by the water channel aquaporin-1: crucial role of M0/M2 phenotype switch. *PLoS One* 10:e0117398. doi: 10.1371/journal.pone.0117398

Yun, X., Jiang, H., Lai, N., Wang, J., and Shimoda, L. A. (2017). Aquaporin 1-mediated changes in pulmonary arterial smooth muscle cell migration and proliferation involve β-catenin. *Am. J. Physiol. Lung Cell. Mol. Physiol.* 313, L889–L898. doi: 10.1152/ajplung.00247.2016

Conflict of Interest: JH is currently employed by Arrowhead Pharmaceutical. However, his participation in this study was conducted while he was employed by Johns Hopkins.

The remaining authors declare that the research was conducted in the absence of any commercial or financial relationships that could be construed as a potential conflict of interest.

Publisher's Note: All claims expressed in this article are solely those of the authors and do not necessarily represent those of their affiliated organizations, or those of the publisher, the editors and the reviewers. Any product that may be evaluated in this article, or claim that may be made by its manufacturer, is not guaranteed or endorsed by the publisher.

Advantages of publishing in Frontiers

OPEN ACCESS
Articles are free to read for greatest visibility and readership

FAST PUBLICATION
Around 90 days from submission to decision

HIGH QUALITY PEER-REVIEW
Rigorous, collaborative, and constructive peer-review

TRANSPARENT PEER-REVIEW
Editors and reviewers acknowledged by name on published articles

Frontiers
Avenue du Tribunal-Fédéral 34
1005 Lausanne | Switzerland

Visit us: www.frontiersin.org
Contact us: frontiersin.org/about/contact

REPRODUCIBILITY OF RESEARCH
Support open data and methods to enhance research reproducibility

DIGITAL PUBLISHING
Articles designed for optimal readership across devices

FOLLOW US
@frontiersin

IMPACT METRICS
Advanced article metrics track visibility across digital media

EXTENSIVE PROMOTION
Marketing and promotion of impactful research

LOOP RESEARCH NETWORK
Our network increases your article's readership